

Improving the Fatigue Life of Weldments with Longitudinal Attachments

by

Stamati D. Dimitrakis

B.S., Lehigh University, 1992

M.S., University of Illinois at Urbana-Champaign, 1994

THESIS

Submitted in partial fulfillment of the requirements
for the degree of Doctor of Philosophy in Civil Engineering
in the Graduate College of the
University of Illinois at Urbana-Champaign, 1999

Urbana, Illinois

UNIVERSITY OF ILLINOIS AT URBANA-CHAMPAIGN
THE GRADUATE COLLEGE

APRIL 1999

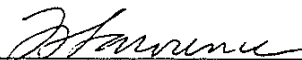
(date)

WE HEREBY RECOMMEND THAT THE THESIS BY

STAMATI D. DIMITRAKIS

ENTITLED IMPROVING THE FATIGUE LIFE OF WELDMENTS WITH
LONGITUDINAL ATTACHMENTS

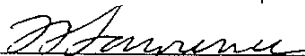
BE ACCEPTED IN PARTIAL FULFILLMENT OF THE REQUIREMENTS FOR
THE DEGREE OF DOCTOR OF PHILOSOPHY



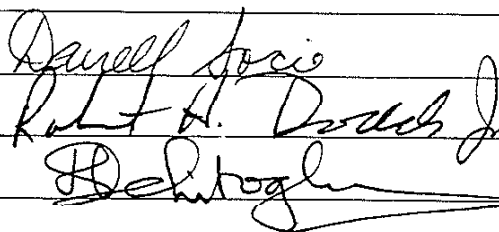
Director of Thesis Research

Head of Department

Committee on Final Examination†



Chairperson



† Required for doctor's degree but not for master's.

IMPROVING THE FATIGUE LIFE OF WELDMENTS WITH LONGITUDINAL ATTACHMENTS

Stamati D. Dimitrakis, Ph.D.
Department of Civil Engineering
University of Illinois at Urbana-Champaign, 1999
Dr. F. V. Lawrence, Advisor

The poor fatigue performance of fillet welded terminations was studied. A review of the literature, an experimental study of mild-steel weldments with longitudinal attachments, and a companion FEM analytical study all indicated that the poor fatigue performance of weldments with longitudinal attachments is due to the combination of a very high 3-D stress concentration, very high tensile residual stresses, and the existence of serious weld-toe stress concentrators such as small weld toe radii or defects such as undercut or cold lap. Cold-lap defects were found to occur at the weld toes when gravitational and/or short circuit transfer gas-metal-arc-welding (GMAW) was used; whereas, the higher heat-input, spray transfer GMAW was found to eliminate these weld toe defects.

A specially designed stress-concentration-reducing part termed "stress diffuser" was developed which was incorporated in the wrap-around welds at the ends of the longitudinal attachments. For longitudinal attachments with a fatigue life of $2E+06$ cycles, increases of 360% in fatigue life and 32% in fatigue strength were obtained with the use of the stress diffuser. The stress diffuser increased the fatigue strength of longitudinal attachments to equal that of transverse attachments. The use of a stress diffuser in a beam-to-column connection was found to eliminate the high stress concentration at the weld access hole and to reduce the maximum principal stresses in the region of the intersection of the bottom beam flange and column flange by 31%.

Fatigue life predictions made using the FEM results of this study were in good agreement with the experimental results. Cold-lap defects were predicted to eliminate the fatigue crack initiation life but to affect the fatigue crack propagation life very little.

DEDICATION

To my wife and parents.

ACKNOWLEDGMENTS

I wish to express my deep gratitude to my advisor, Professor Frederick V. Lawrence, for his guidance. His input and support have been invaluable in this study.

I would like to thank the Fracture Control Program for funding this study.

I would like to thank Assistant Professor Gary T. Fry for funding part of the beam-to-column connection study. The stimulating conversations with him have been appreciated.

I would like to thank Professor W. H. Munse for allowing me to use his database information and references. I would like to thank Dr. Grzegorz Banas for his help in the experimental testing program and his assistance in retrieving the UIUC database. The drawings of the weld details in Fig A1.1 were provided by Dr. Banas.

I would like to thank Professor R. H. Dodds and his group for providing guidance on the FEM modeling used in this study.

The help of Dr. W. C. Mohr of the Edison Welding Institute in obtaining some of the data for this study is greatly appreciated. I would also like to acknowledge Dr. G. Marquis, Dr. T. Dahle, Dr. A. Hobbacher, and Prof. S. D. Thurlbeck for their cooperation. The conversations with members of the FCP advisory committee have been appreciated.

TABLE OF CONTENTS

CHAPTER

1. THE FATIGUE STRENGTH OF WELD TERMINATIONS	1
1.1 INTRODUCTION: THE FATIGUE OF WELDMENTS	1
1.2 NATURE OF THE LONGITUDINAL ATTACHMENT	2
1.2.1 Experimental Studies	2
1.2.2 Theoretical Studies.....	3
1.3 SUMMARY	5
2. EXPERIMENTAL STUDY OF LONGITUDINAL ATTACHMENTS.....	9
2.1 INTRODUCTION	9
2.2 PROCEDURES.....	9
2.2.1 Specimen Fabrication.....	9
2.2.2 Testing Procedure	10
2.3 EXAMINATION OF SPECIMENS	10
2.3.1 Weld Toe Geometry.....	10
2.3.2 Residual Stresses.....	11
2.4 THE FATIGUE STRENGTH OF LONGITUDINAL ATTACHMENTS	11
2.5 POST-TEST EXAMINATION OF SPECIMENS	11
2.5.1 Cold-Lap Defects	11
2.5.2 Crack Paths	12
2.5.3 SEM Evaluation	12
2.6 SUMMARY	12
3. FINITE ELEMENT ANALYSIS OF LONGITUDINAL ATTACHMENTS	25
3.1 INTRODUCTION	25
3.2 PROCEDURES.....	25
3.2.1 Finite Element Analysis Software.....	25
3.2.2 Superposition Method.....	25
3.2.3 Modeling of the Longitudinal Attachment in 3-D	27
3.3 RESULTS.....	28
3.3.1 The Effect of Geometry on the Fatigue Life of Longitudinal Attachments	28

3.3.2 Effects of Bending Load	30
3.3.3 Effects of One-Sided Longitudinal Attachments	30
3.4 SUMMARY	30
4. IMPROVING THE FATIGUE LIFE OF LONGITUDINAL ATTACHMENTS WITH THE USE OF STRESS DIFFUSERS.....	45
4.1 INTRODUCTION	45
4.2 IMPROVING THE FATIGUE LIFE OF LONGITUDINAL ATTACHMENTS.....	45
4.2.1 Simple Modifications of Weld Detail Geometry	45
4.2.2 Development of "Stress Diffusers"	46
4.3 FEM RESULTS OF STRESS DIFFUSERS	47
4.4 SUMMARY	48
5. EXPERIMENTAL STUDY OF LONGITUDINAL ATTACHMENTS WITH STRESS DIFFUSERS.....	57
5.1 INTRODUCTION	57
5.2 PROCEDURES.....	57
5.2.1 Specimen Fabrication.....	57
5.2.2 Testing Procedure	57
5.3 EXAMINATION OF SPECIMENS	58
5.3.1 Weld Toe Geometry.....	58
5.3.2 Residual Stresses.....	58
5.4 THE FATIGUE STRENGTH OF LONGITUDINAL ATTACHMENTS WITH STRESS DIFFUSERS	59
5.5 POST-TEST EXAMINATION OF SPECIMENS: COLD-LAP DEFECTS.....	59
5.6 SUMMARY	60
6. APPLICATION OF STRESS DIFFUSERS TO A BEAM-TO-COLUMN CONNECTION.....	66
6.1 INTRODUCTION	66
6.1.1 Northridge Beam-to Column Connections	66
6.2 PROCEDURES.....	66
6.2.1 Beam-to-Column Connection Modeling.....	66
6.3 FEM RESULTS	67
6.3.1 Beam-to-Column Connection	67
6.3.2 Modeling of the Stress Diffuser.....	68
6.4 SUMMARY	69

7. INFLUENCE OF "COLD-LAP" DEFECTS.....	79
7.1 INTRODUCTION	79
7.2 PROCEDURES.....	79
7.2.1 Superposition Method.....	79
7.3 INFLUENCE OF "COLD-LAP" DEFECTS ON LONGITUDINAL ATTACHMENTS	80
7.3.1 2-D FEM Analyses of Cold-Lap Defects.....	80
7.3.2 3-D FEM Analyses of Cold-Lap Defects.....	82
7.4 INFLUENCE OF "COLD-LAP" DEFECTS ON LONGITUDINAL ATTACHMENTS WITH STRESS DIFFUSERS	83
7.5 SUMMARY	84
8. FATIGUE LIFE PREDICTIONS	99
8.1 INTRODUCTION	99
8.2 PROCEDURES.....	99
8.3 FATIGUE LIFE PREDICTIONS OF SPECIMENS WITHOUT COLD-LAP DEFECTS	99
8.3.1 Longitudinal Attachments.....	99
8.3.2 Longitudinal Attachments with Stress Diffusers	100
8.4 FATIGUE LIFE PREDICTIONS OF SPECIMENS WITH COLD-LAP DEFECTS	100
8.4.1 Longitudinal Attachments.....	100
8.4.2 Longitudinal Attachments with Stress Diffusers	101
8.5 SUMMARY	101
9. DISCUSSION	107
9.1 WELD CLASSIFICATION BY CRACK INITIATION SITE	107
9.2 THE FATIGUE BEHAVIOR OF LONGITUDINAL ATTACHMENTS	108
9.2.1 Significance of Welding Process on Defect Distribution	108
9.2.2 The Poor Fatigue Behavior of Longitudinal Attachments.....	108
9.3 THE USE OF STRESS DIFFUSERS.....	110
9.3.1 Stress Diffusers	110
9.3.2 Comparison with Transverse Attachments	111
9.3.3 Applicability and Limitations of Stress Diffusers.....	111
9.4 MODELING ISSUES	112
9.4.1 Cold-Lap Defects	112
9.4.2 Crack Shape Development.....	113

9.5 FUTURE WORK.....	113
10. CONCLUSIONS.....	118
APPENDIX 1: EXPERIMENTAL INDICATION OF THE POOR FATIGUE BEHAVIOR OF FILLET WELD TERMINATIONS	119
APPENDIX 2: STRESS INTENSITY FACTOR FOR WELDMENTS	137
APPENDIX 3: VERIFICATION OF THE SUPERPOSITION METHOD	139
APPENDIX 4: EVALUATION OF THE SUPERPOSITION METHOD IN ESTIMATING M_k FOR GEOMETRIES WITH COLD-LAP DEFECTS.....	154
REFERENCES.....	157
VITA	161

LIST OF SYMBOLS

a	Crack Length
a_0	Initial Crack Length
a/c	Crack Aspect Ratio
α	Macrogeometry Coefficient
B	Main Plate Width
C', m	Modifies Paris Law Material Constants
D	Cold-Lap Defect Depth
ΔS	Remote Stress Range
ϕ	Azimuth Angle
K_{pp}	Stress Intensity Factor for surface cracks in plain plate
K_I	Mode I Stress Intensity Factor
K_{II}	Mode II Stress Intensity Factor
K_t	Elastic Stress Concentration Factor
K_{weld}	Stress intensity factor of a weldment
$K_{weld CG}$	Stress Intensity Factor of a Weldment Determined From the Cracked Geometry
L	Attachment Plate Length
λ	Geometry Exponent
LOP	Lack of Penetration
M_K	Weld Geometry Correction Factor
$M_{K CG}$	Weld Geometry Correction Factor Determined From the Cracked Geometry
$M_{K s}$	Weld Geometry Correction Factor Determined by Superposition Method
N_I	Fatigue Crack Initiation Life
N_P	Fatigue Crack Propagation Life

N_T	Total Fatigue Life
r	Weld Toe Radius
r_{cl}	Weld Root Radius of a Cold-Lap Defect
R	Load Ratio
ρ	Correlation coefficient
S	Applied Remote Stress
S_y	Base Metal Yield Strength
S_u	Base Metal Ultimate Strength
θ	Weld Toe Angle
t	Attachment Plate Thickness
T	Main Plate Thickness
V	Attachment Plate Height
W	Weld Leg Length
Y	Geometry Correction Factor

CHAPTER 1

THE FATIGUE STRENGTH OF WELD TERMINATIONS

1.1 INTRODUCTION: THE FATIGUE OF WELDMENTS

A selection of 53 details¹ typical of those contained in current design codes are shown in Fig. A1.1 in Appendix 1. If these details are categorized by fatigue crack initiation site, it is found that there are four usual sites (see Fig. 1.1):

- Weld ripple
- Weld toes
- Weld terminations
- Weld roots²

These general categories lead to five common weldment fatigue crack initiation scenarios:

- Initiation at weld RIPPLE of longitudinally loaded groove or fillet welds
- Initiation at the weld toes of transversely loaded GROOVE welds
- Initiation at the weld toes of transversely loaded NON-LOAD-CARRYING FILLET welds
- Initiation at the weld toes of transversely loaded LOAD-CARRYING FILLET welds
- Initiation at the weld toes of longitudinally loaded welds (TERMINATIONS)

Figure 1.2 shows that the S-N curves for ripple, groove, non-load-carrying fillet, and load-carrying fillet scenarios are similar and that the S-N curves for fillet weld terminations scenarios are lower than all others. Fillet weld terminations are frequently encountered in welded construction³ and have the lowest fatigue strength at long lives. It is for these reasons that terminations represent one of the most severe fatigue problems encountered in welded construction. The improvement of the fatigue performance of such fillet welded terminations is the subject of this study.

¹ The weld details of the UIUC fatigue database are described in SSC-318 [1]. The fatigue data was screened and corrected for weldment size prior to re-evaluation. The details of the analysis can be found in Appendix 1.

² Only failures at the welds exterior were considered in this study. Root failures were not considered.

³ The fatigue behavior of Details 15, 32A, 17, 17A, 18, 30, 30B, 31, and 33 in Fig. A1.1 must be considered to be limited by fillet weld terminations.

1.2 NATURE OF THE LONGITUDINAL ATTACHMENT

Fillet weld terminations have frequently been investigated using weldments having longitudinal non-load-carrying fillet welded attachments: see inset of Fig. 1.3. This specimen is frequently used because it is symmetrical (bending effects associated with welding distortions can thus be nearly eliminated) and because it is a simple way of creating a severe notch of reproducible severity [2]. In this study, weldments having longitudinal non-load-carrying fillet welded attachments will be referred to as longitudinal attachments.

1.2.1 Experimental Studies

Database Information: Experimental test results [3-17] for longitudinal attachments have been collected. The majority of the longitudinal attachment test data comes from test programs which investigate methods for improving the fatigue strength or studying the fatigue behavior of high strength steel weldments. Therefore, much of the fatigue data for the longitudinal attachment deals with improvement techniques or the effects of base metal strength. Consequently, there is not much data for mild steel specimens tested in the as-welded state.

The available data for mild steel longitudinal attachments tested in the as-welded condition under pulsating tension are plotted in Fig. 1.3. Some of the scatter can be attributed to the fact that these specimens have similar but not exactly the same dimensions. In order to examine the effects of improvement methods, as-welded and treated specimens with exactly the same dimensions were compared in Fig. 1.4. Small increases in fatigue strength can be obtained through stress relief, but greater improvements occur when favorable residual stresses are induced in the specimens; however, these improvement techniques are usually considered impractical [18] because they are expensive and sometimes unreliable.

Residual Stresses: Gurney [2] reported that the residual stresses in the longitudinal direction of a weld approach the yield strength of the base metal and that the residual stresses in the transverse direction are considerably lower; therefore, the residual stresses in the direction of applied loading in the longitudinal attachment are very high. Berge et al. [19] measured the residual stresses of longitudinal attachments and found that the residual stresses near the weld toe approach the yield strength of the base metal ($S_y = 300$ MPa).

Maddox [12] investigated the residual stresses in longitudinal attachments fabricated from many different strength steels. The specimens were spot-heated after welding to ensure the presence of high tensile residual stresses. The specimens made of mild steels (S_y approx. 350 MPa) were found to have residual stresses of approximately 400 MPa while the higher strength steels (S_y approx. 700 MPa) were found to have residual stresses of approximately 300 MPa. The mild steel specimens actually showed the highest residual stresses. The welds were made using SMAW with AWS E6013 and E7016 electrodes. However, the residual stresses were reported for locations 10 mm away from the weld toe. Maddox recognized that the residual stresses at the weld toe could be higher than the residual stresses induced by the heated spots 10 mm away from the weld toe. Maddox found these results to be inconsistent with those of Satoh [20] who found the residual stresses of 400 to 500 MPa (60 to 70 percent of yield) for specimens of high strength steel. Maddox found that residual stresses introduced by spot heating on a wider specimen produced residual stresses of 400 to 500 MPa ($S_y = 824$).

Bogren et al. [17] also measured the residual stresses in the longitudinal direction of longitudinal attachments tested in the Nordic program. They measured the residual stresses at approximately 2 mm from the weld toe and 0.1 to 0.2 mm below the surface to be in the range of the base metal yield strength.

Initial Defects: Smith et al. [21] inspected longitudinal attachments fabricated using SMAW to determine the initial defects that exist at the wrap-around welds. They found that weld toe undercuts existed at every location inspected. Martinez et al. [22] inspected the longitudinal attachments tested in the Nordic project fabricated with the GMAW process using short-circuit transfer. They found that cold-lap defects commonly occur at the weld toe. Inspection of the fracture surfaces revealed the cold-lap defects to be the sites of fatigue crack initiation. Thus, the initial defects found in these two test programs which used two different welding procedures were completely different.

1.2.2 Theoretical Studies

Smith and Gurney: Smith et al. [23] found that, unlike transverse attachments in which a 2-D FEM analysis is sufficient, longitudinal attachments require a 3-D FEM analysis to estimate the stress concentration factor (K_t). Smith and Gurney [24] characterized fatigue crack growth in longitudinal attachments using linear elastic fracture mechanics and calculated the stress intensity factor for the weldment:

$$K_{\text{weld}} = M_K Y S \sqrt{\pi a}. \quad (1.1)$$

where:

- K_{weld} = Stress intensity factor for the weldment
- M_K = Weld geometry correction factor
- Y = Geometry correction factor
- S = Applied remote stress
- a = Crack length

The weld geometry correction factor, M_K , was determined by the superposition method of Albrecht et al. [25] using the stress distribution of the uncracked plate from a 3-D FEM analysis and the stress intensity factor solution for a plain plate. A review of the weld geometry correction factor and the superposition method can be found in Appendix 2.

Despite the acknowledged inaccuracy in their predictions of fatigue life, Smith and Gurney [24] were able to study the influence of joint geometry on the longitudinal attachment by examining trends in the results. They suggested that fatigue life can be increased by:

1. Decreasing the attachment length below 152.4 mm.
2. Decreasing the attachment height below 50.8 mm.
3. Decreasing the attachment thickness below 12.7 mm.
4. Increasing the weld leg length.
5. Decreasing the main plate width below 127 mm.
6. Increasing the main plate thickness.

Suggestion 6 is confusing because it contradicts the finding that increases in main plate thickness reduces the fatigue life of transverse non-load-carrying fillet welded attachments [2] (transverse attachments).

Hobbacher: Hobbacher [26] also used the approximate superposition method of Albrecht et al. [25] along with 3-D FEM analyses to determine the weld geometry correction factor (M_K). Hobbacher evaluated the effects that variations in weldment geometry would have on M_K .

Hobbacher found that the plate thicknesses, attachment length, plate width, and weld angle were the principal parameters which affect M_K . Hobbacher developed a parametric equation for M_K :

$$M_K = C \left(\frac{a}{T} \right)^K, \quad M_K \geq 1 \quad (1.2)$$

where:

$$C = 0.9809 - 0.2357 \left(\frac{t}{T} \right) + 0.0249 \left(\frac{L}{T} \right) + 0.00038 \left(\frac{L}{T} \right)^2 + 0.0186 \left(\frac{B}{T} \right) - 0.1414 \left(\frac{\theta}{45^\circ} \right)$$

$$K = -0.02285 + 0.0167 \left(\frac{t}{T} \right) - 0.3863 \left(\frac{\theta}{45^\circ} \right) + 0.1230 \left(\frac{\theta}{45^\circ} \right)^2$$

Nordic Project: Dahle et al. [27] also used the superposition method of Albrecht et al. [25] along with 3-D FEM analyses to determine the weld geometry correction factor (M_K). Unlike previous studies of the longitudinal attachment, Dahle et al. performed a limited number of calculations of M_K with a finite weld toe radius. Dahle et al. also modeled the cold-lap defects as a crack with 2-D FEM analyses to determine a weighted (mixed-mode) stress intensity factor. They defined an “equivalent vertical crack” to be an idealized straight crack running perpendicular to the load (mode I) and emanating from the weld toe with a stress intensity factor equal to that of the weighted stress intensity factor. The equivalent vertical crack depth was found to be the same order of size as a “lack of fusion” defect commonly found in SMAW joints; therefore, they used this equivalent vertical crack depth as the initial crack depth in their fatigue life estimations.

1.3 SUMMARY

Weldments with fillet weld terminations exhibit the shortest fatigue lives of all weldments, especially at long lives (high stresses). Fillet weld terminations have frequently been investigated with weldments having longitudinal non-load-carrying fillet welded attachments, termed herein “longitudinal attachments.” Fillet weld terminations are frequently encountered in welded construction and have the lowest fatigue strength at long lives. The improvement of the fatigue performance of fillet welded terminations is the subject of this study because terminations represent one of the most severe fatigue problems encountered in welded construction.

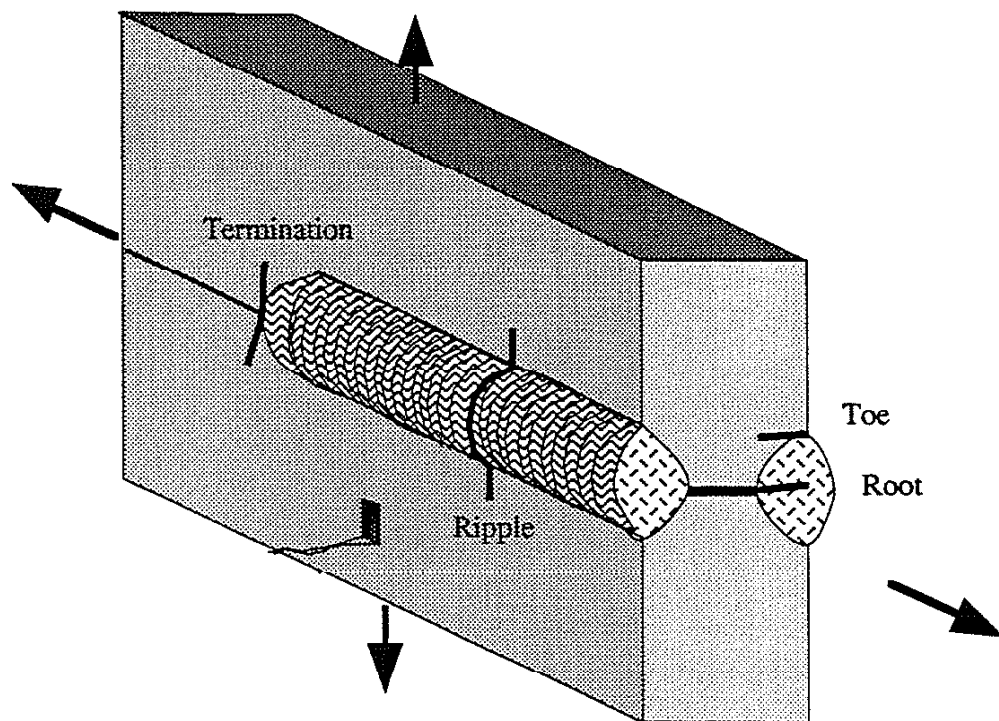


Fig. 1.1 Fatigue crack initiation sites in weldments: ripple, toe, root, or weld termination.

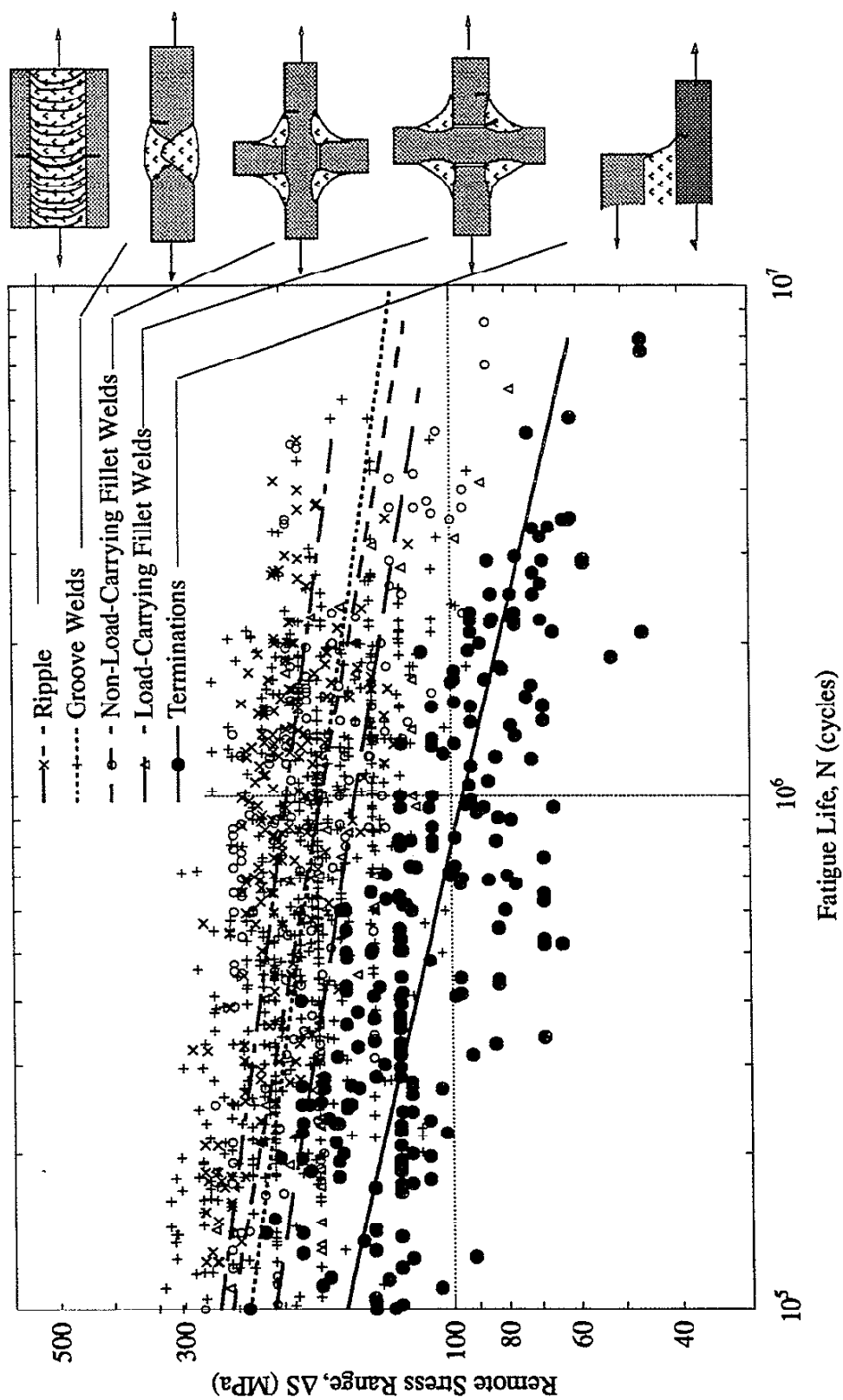


Fig. 1.2 Comparison of the fatigue behavior of weldments with different fatigue crack initiation sites. The weldment describing each initiation site in its purest form is shown.

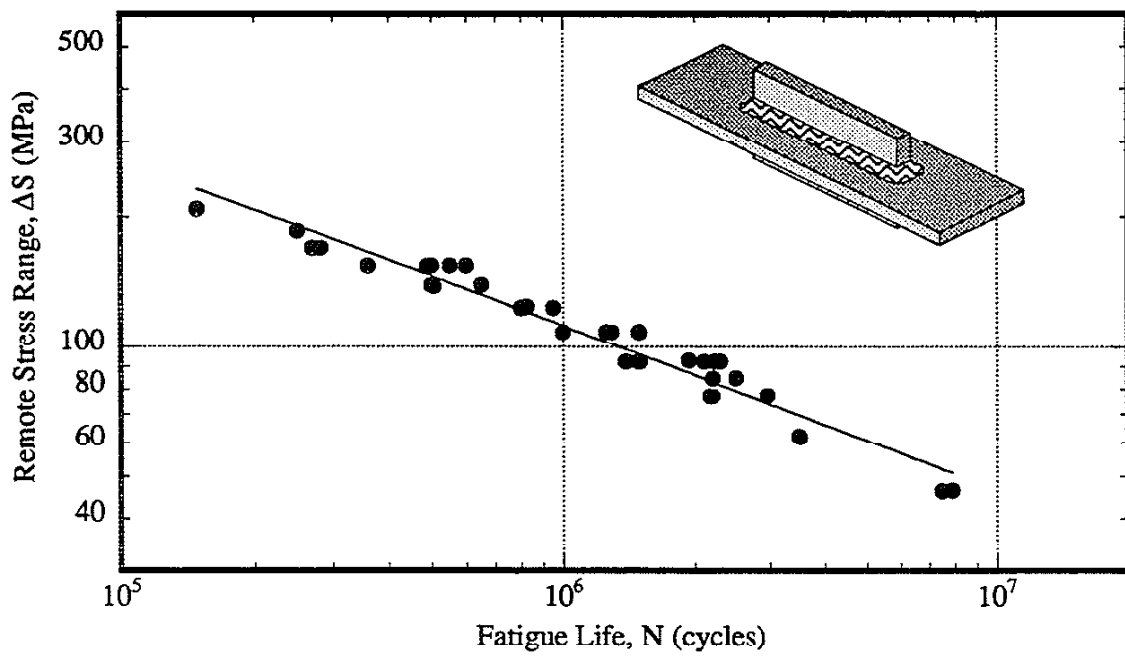


Fig. 1.3 The screened data for mild steel longitudinal attachments in the database.

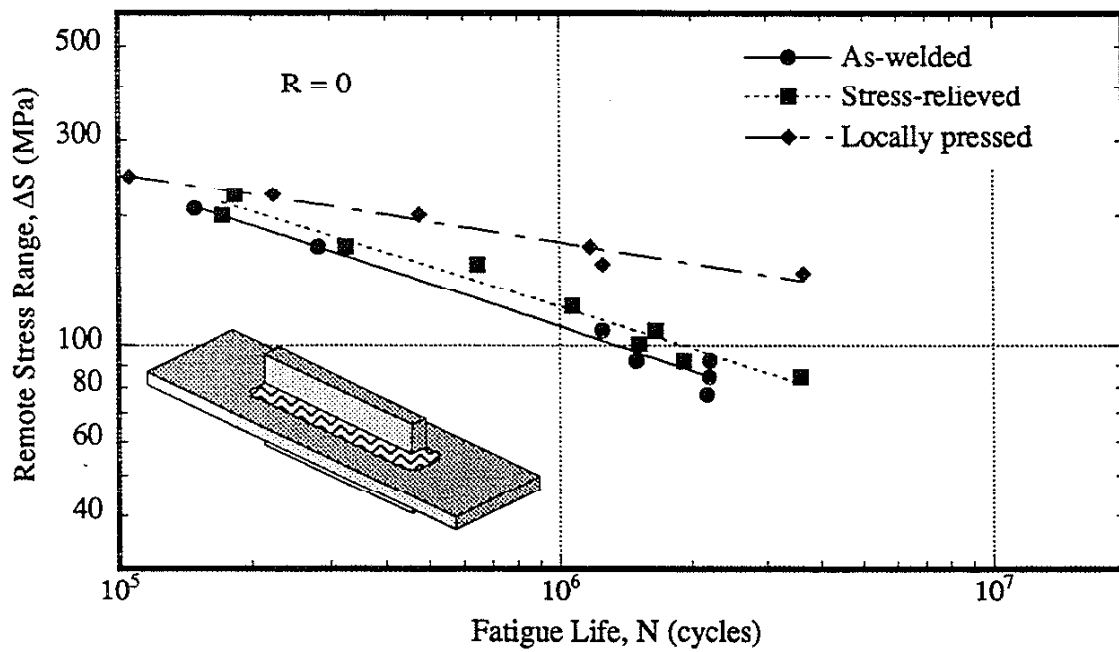


Fig. 1.4 The effect of improvement techniques on the fatigue strength of longitudinal attachments.

CHAPTER 2

EXPERIMENTAL STUDY OF LONGITUDINAL ATTACHMENTS

2.1 INTRODUCTION

Experiments were performed to check the reported fatigue behavior of the longitudinal attachment and to obtain a consistent set of data to permit comparisons with the improvement techniques developed.

2.2 PROCEDURES

2.2.1 Specimen Fabrication

Specimens were fabricated from a SAE/AISI 1020 mild steel to the dimensions shown in Fig 2.1. The composition and mechanical properties of the steel are listed in Tables 2.1 and 2.2. The plates were saw cut keeping the loading direction parallel to the rolling direction. Prior to welding, most mill scale was removed from the intended locations of fillet weld terminations with a grinder. Small particles of mill scale remained that were not completely removed.

All specimens were welded using the gas metal arc welding (GMAW) process. The welding parameters used for the three different series of specimens fabricated are given in Table 2.3. All welds were created in the horizontal position (2F) and laid down in a single pass.

- Series 1 employed both of gravitational and short circuiting transfer,
- Series 2 used short circuiting transfer, and
- Series 3 used spray transfer.

• Series 1 was fabricated in Talbot Laboratory and Series 2 and 3 were fabricated at a later date at Newmark Civil Engineering Laboratory by a different welder. Weld sequencing was employed as shown in Fig. 2.2 to limit the weld distortions. All of the wrap-around welds were executed first, and then the longitudinal fillet welds were made. Starts and stops were not permitted at the end of the attachments to avoid introducing serious weld defects in these locations.

The first series of specimens made (Series 1) had large welding distortions, so additional precautions were undertaken to limit these distortions in Series 2 and 3: the plates were straightened prior to welding by straightening them in tension; the plate was restrained with clamps at the ends and quarter points during the welding process; and the weld leg lengths were reduced in length from 12.7 to 9.52 mm to reduce the volume of weld metal deposited [28].

2.2.2 Testing Procedure

To determine the magnitude of bending stresses induced during testing, four strain gauges were mounted on each specimen as shown in Fig. 2.2. The strain gages were placed at a distance of $2T$ from the weld toe so that the stress concentrating effects of the weld itself would not be measured.

All of the specimens were tested in a 100 kip MTS testing frame. All of the specimens were subjected to cyclic, constant-amplitude axial loads, $R = 0.1$. All tests were carried out in load control at a frequency which varied from 5 to 7.5 Hz. depending on the load level employed. Failure was defined as the separation of the specimen.

2.3 EXAMINATION OF SPECIMENS

2.3.1 Weld Toe Geometry

The weld toe geometry of untested specimens from Series 1, 2, and 3 were examined by sectioning the specimens through the wrap-around weld at the end of the attachment. All sections of the specimens from Series 1 and 2 revealed the presence of cold-lap defects; therefore, the weld toe radius and angle were not measured for these specimens¹. A typical cold-lap defect observed for the longitudinal attachments of Series 1 and 2 can be seen in Fig. 2.3. The measurements of the sections of specimens for Series 3 are listed in Table 2.4. A typical weld toe of a Series 3 longitudinal attachment can be seen in Fig. 2.3 which shows the weld toe radius and local weld toe angle. The average weld toe radius (r) was found to be 0.08 mm. The mean was found to 0.10 mm with a standard deviation of the log r of 0.52². The average overall and local weld toe angles were found to be 36° and 40° with standard deviations of 3.2° and 9.3° , respectively.

¹ With the presence of a cold-lap defect, the weld toe radius and angle do not affect the stresses at the root of the cold-lap defect.

² The distribution of weld toe radius was characterized by a log normal distribution.

2.3.2 Residual Stresses

A Series 3 longitudinal attachment was sent to Lambda Research [29] for the determination of residual stresses using the X-ray diffraction technique in accordance with SAE J784a. The measurements were made adjacent to the weld toe at the surface and at 0.28 mm below the surface. The residual stress measurement at the surface and 0.28 mm below the surface were found to be 595 and 421 MPa, respectively: see Table 2.5. The residual stress measured at the surface exceeds the ultimate strength of the base metal (510 MPa). The measured surface residual stress of 595 MPa is higher than the values reported elsewhere. This higher value may be due to the high yield strength of the weld metal used in the fabrication process.

2.4 THE FATIGUE STRENGTH OF LONGITUDINAL ATTACHMENTS

The fatigue test results for Series 1, 2, and 3 are listed in Table 2.6 and plotted in Fig. 2.3. Large bending stresses were measured during testing and are listed in Table 2.6. No difference can be seen between the fatigue test results of Series 1 and 2. A slight increase in fatigue life can be seen for the fatigue results of Series 3 at long lives.

The fatigue test results of this study are plotted with data for longitudinal attachments from the fatigue database in Fig. 2.4. As seen in Fig. 2.4, the fatigue test results of this study are consistent with the results of past studies.

2.5 POST-TEST EXAMINATION OF SPECIMENS

2.5.1 Cold-Lap Defects

Inspection of Series 1 and 2 specimens reveals that fatigue cracks initiated from cold-lap defects: see Fig. 2.6. The depth(s) of the cold-lap defect(s) at the failure location are listed in Table 2.6. The depth of the cold-lap defects are much larger for Series 1 specimens than for Series 2. The average depth of the largest cold-lap defect found in each specimen for Series 1 and 2 was 2.1 mm and 0.9 mm, respectively. The smaller cold-lap defect depth for Series 2 was expected since a high heat input welding procedure was employed³.

³ The weld of Series 2 was smaller allowing the welder to maintain a steady path and thus better control of the weld path. The larger weld size was very difficult to lay down with one pass and the welder tried to stretch the weld out causing a deeper cold lap defect; b) short-circuiting transfer was used with Series 2 which allowed the welder to move slower and maintain a steadier pace.

Despite the reduction in cold-lap defect depth from Series 1 to Series 2, no increase in fatigue life was observed. Possible explanations for this observed lack of improvement in the fatigue life of longitudinal attachments with decreased defect size will be explored in Chapter 7.

2.5.2 Crack Paths

Specimens were sectioned to investigate the crack path and the initial trajectory of the crack path. A Series 3 (without cold-lap defects) and Series 1 (with cold-lap defects) longitudinal attachment were sectioned and the crack paths were photographed as seen in Figs. 2.7 and 2.8, respectively. In both cases, the crack path was curved.

2.5.3 SEM Evaluation

Crack Shape Development: The fracture surfaces of longitudinal attachments were examined using the Scanning Electron Microscope (SEM) to observe the early stages of crack shape development. The measured values of crack aspect ratio are plotted in Fig. 2.9 as a function of crack length.

Cold-Lap Defects: The fracture surface of specimens initiating fatigue cracks at cold-lap defects was studied using the Scanning Electron Microscope (SEM) to observe the early stages of crack shape development. The aspect ratio for cracks growing from cold-lap defects was found to be the same as that of cracks growing from the weld toe. Typical SEM images of cold-lap defect can be seen in Fig. 2.10 which shows the growth of cracks from fatigue crack initiation sites at the depth of the cold-lap defect.

2.6 SUMMARY

The poor fatigue behavior of longitudinal attachments was experimentally verified. Very high tensile residual stresses were measured adjacent to the weld toe of the wrap-around welds. The presence of cold-lap defects was observed for specimens fabricated with the GMAW process using gravitational and/or short circuit transfer. The use of a higher heat input (spray transfer) in the GMAW process was found to eliminate the cold-lap defects. Eliminating the cold-lap defects did not significantly increase the fatigue lives of the longitudinal attachments.

Table 2.1 The chemical composition of the SAE/AISI 1020 mild steel used in the testing program.

Element	wt %
C	0.200
Mn	0.620
P	0.009
S	0.023
Si	0.230
Ni	0.080
Mo	< 0.010
Cu	0.260

Table 2.2 The mechanical properties of the SAE/AISI 1020 mild steel used in the testing program.

	MPa
Yield Strength (S_y)	333
Ultimate Strength (S_u)	510

Table 2.3 The welding parameters used to fabricate the longitudinal attachments.

Series	1	2	3
Gas	75 % Ar + 25% CO ₂	CO ₂	98 % Ar + 2 % O
Electrode	ER70S-6	ER70S-6	ER70S-6
Electrode Size (mm)	0.90	1.20	0.90
Weld Leg Length (mm)	12.7	9.52	9.52
Current (A)	NA	185	190
Voltage (V)	NA	24	23.5
Metal Transfer	Gravitational / Short Circuit	Short Circuit	Spray

Table 2.4 The weld toe geometry of the longitudinal attachments of Series 3.

	Average	Mean	s.d.	Mean + 2 s.d.	Mean - 2 s.d.
Radius, r (mm)	0.08	0.10	0.52*	1.10	.009
Overall Weld Toe Angle (°)	36	37	3.2	43	31
Local Weld Toe Angle (°)	44	47	9.3	66	28

* The standard deviation for the radius is in log (r).

Table 2.5 Residual stress measurements made on the longitudinal attachments of Series 3.

Depth (mm)	a/T	Residual Stress (MPa)	Error (MPa)	Peak Width (°)
0.00	0.000	+595	± 11	2.48
0.28	0.022	+421	± 42	2.07

Table 2.6 The fatigue test results for Series 1, Series 2, and Series 3.

Series 1:

Specimen	Corrected Stress Range (MPa)	Fatigue Life (cycles)	Bending Stress at Failure Location (%)	Cold Lap Defect Depth(s) (mm)
LA-1-1	109.0	1.063E+06	23.2	1.5, 2.0
LA-1-2	69.1	3.049E+06	-8.4	0.8, 0.8, 2.0
LA-1-3	219.4	1.142E+05	3.4	1.8, 2.4

Series 2:

Specimen	Corrected Stress Range (MPa)	Fatigue Life (cycles)	Bending Stress at Failure Location (%)	Cold Lap Defect Depth(s) (mm)
LA-2-1	77.5	1.346E+06	-15.7	0.5
LA-2-2	227.4	1.070E+05	4.6	1.0, 0.5, 0.5
LA-2-3	81.2	2.679E+06	2.6	0.25
LA-2-4	81.2	2.297E+06	2.7	1.0, 1.0
LA-2-5	95.2	1.508E+06	2.3	1.75, 1.0, 0.5

Series 3:

Specimen	Corrected Stress Range (MPa)	Fatigue Life (cycles)	Bending Stress at Failure Location (%)	Cold Lap Defect Depth(s) (mm)
LA-3-1	242.8	9.759E+04	12.9	-
LA-3-2	154.8	3.857E+05	10.3	-
LA-3-3	95.0	3.318E+06	4.5	-
LA-3-4	195.9	1.711E+05	10.2	-
LA-3-5	101.7	1.312E+06	10.1	-
LA-3-6	98.0	1.124E+06	5.7	-

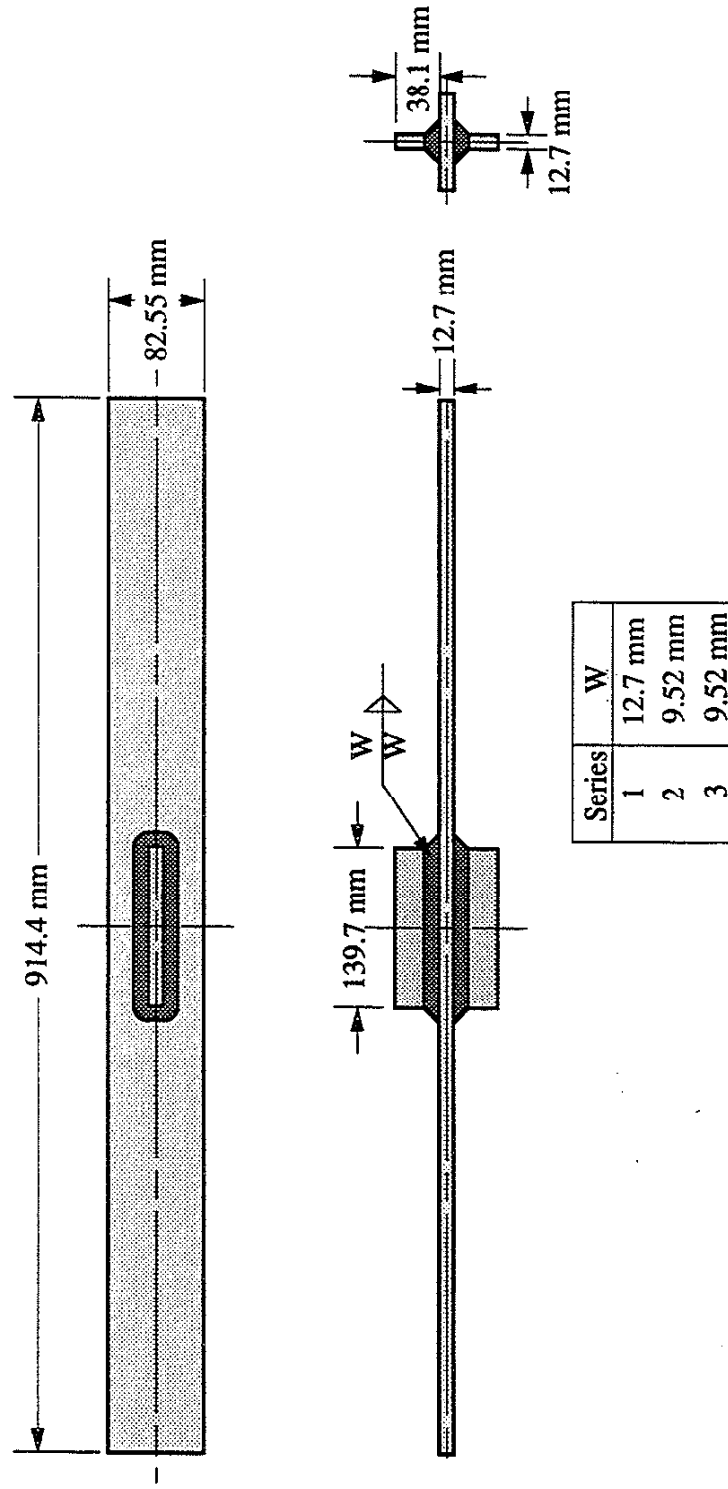


Fig. 2.1 The specimen dimensions for the longitudinal attachment. The weld leg length (W) for the three series of specimens fabricated is listed.

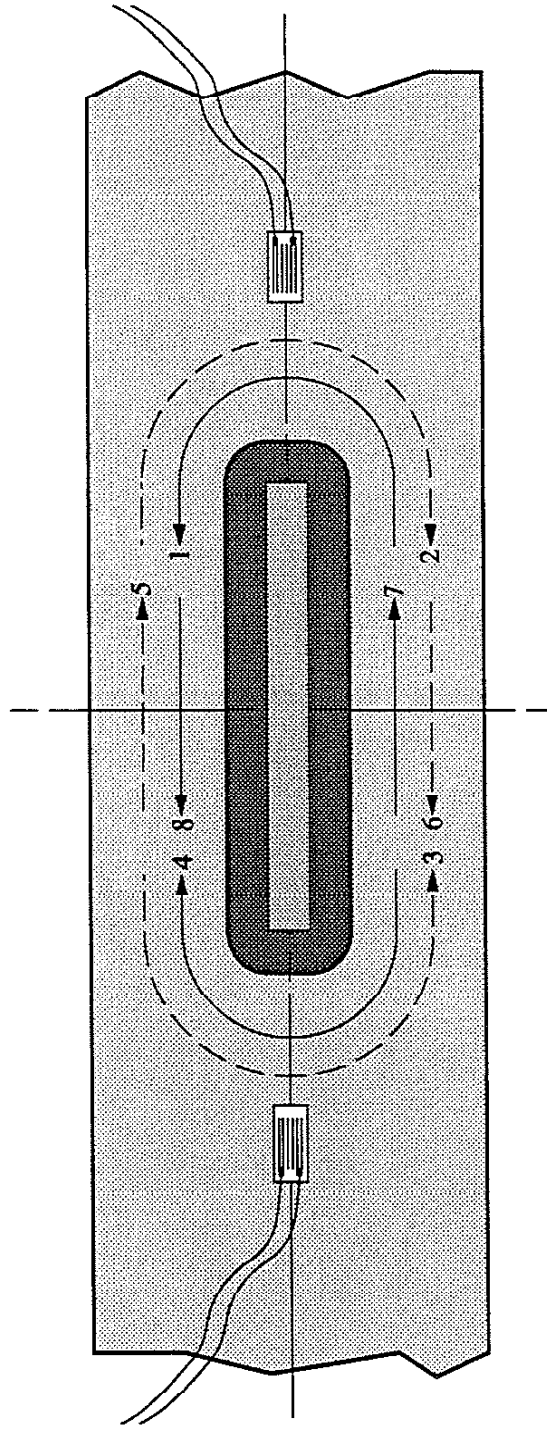
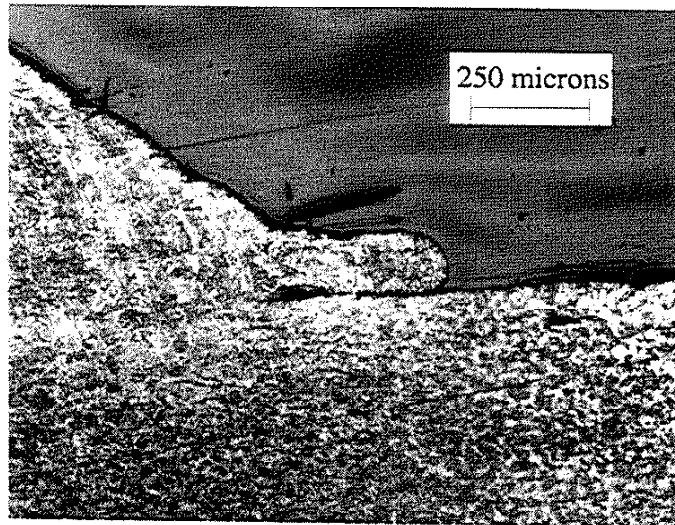
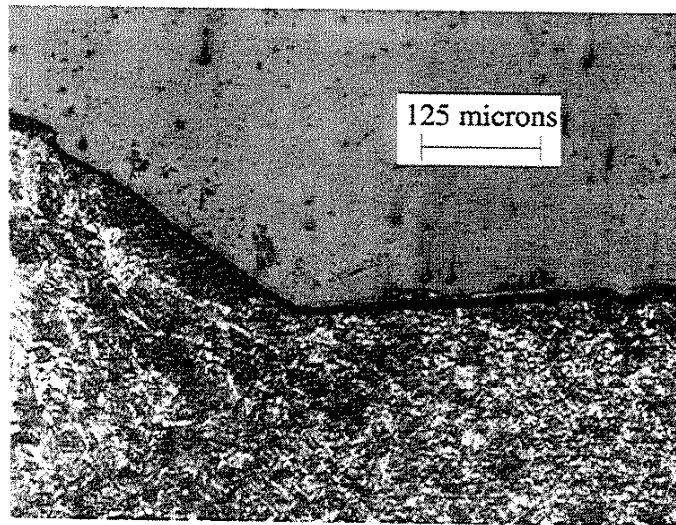


Fig. 2.2 Weld sequencing and strain gauging of the specimens. The solid arrows indicate the welds on top of the specimen and the dashed arrows indicate the welds below the specimen. The strain gages were placed at a distance $2T$ from the toe.



Series 1 and Series 2



Series 3

Fig. 2.3 (Above) A typical cold-lap defect observed for the longitudinal attachments of Series 1 and Series 2 (65X). (Below) A typical weld toe for the longitudinal attachments of Series 3 (125X). The spray transfer GMAW process of Series 3 eliminated the cold-lap defects.

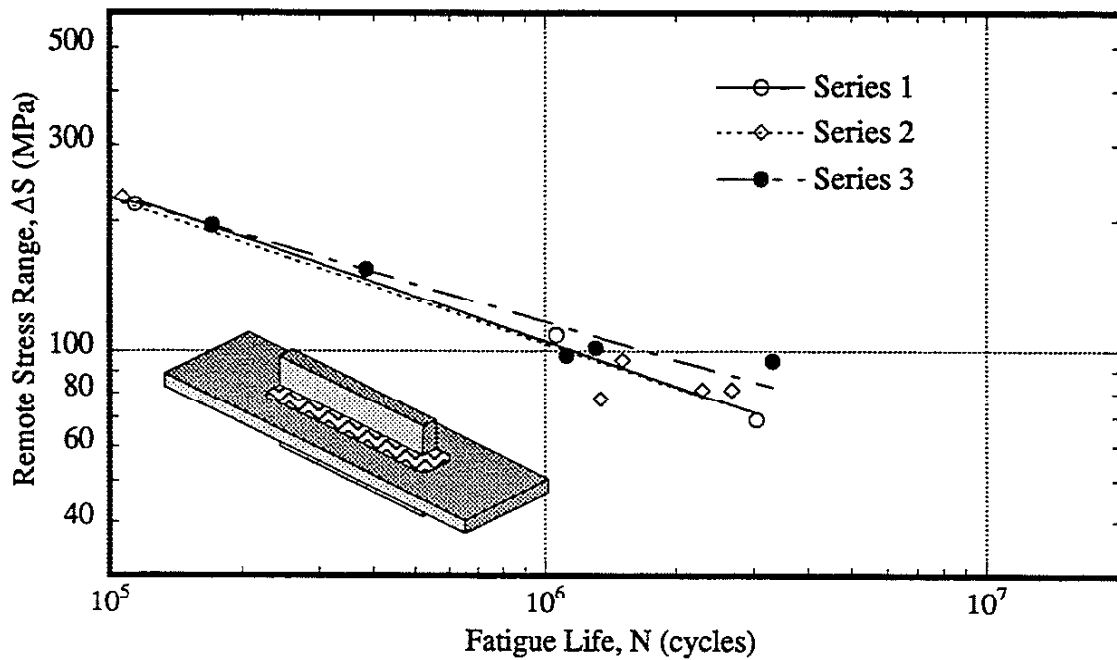


Fig. 2.4 The effect of welding procedure on the fatigue life of longitudinal attachments. Series 1 (gravitational and short circuit transfer), Series 2 (short circuit transfer) and Series 3 (spray transfer). The data has been corrected for bending stresses.

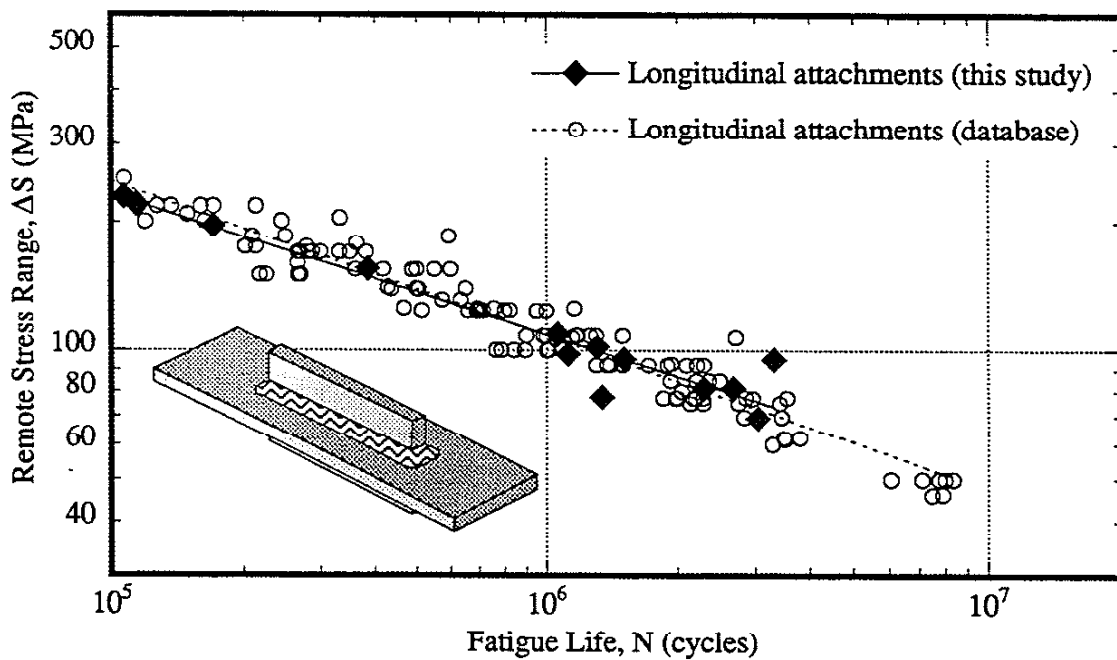
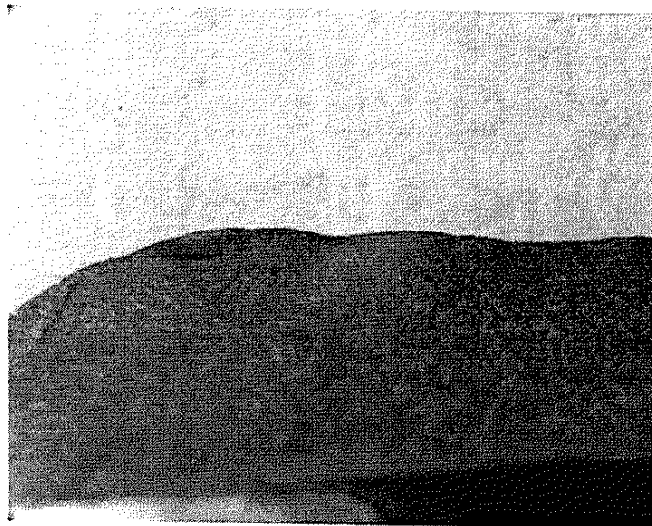


Fig. 2.5 Comparison of the fatigue life of longitudinal attachments of this study and those of the database. The data of this study has been corrected for bending stresses.



Series 1 and 2



Series 3

Fig. 2.6 (Above) A fracture surface typical of the longitudinal attachments of Series 1 and 2 showing the presence of cold-lap defects. (Below) A fracture surface typical of the longitudinal attachments of Series 3 showing the elimination of cold-lap defects.

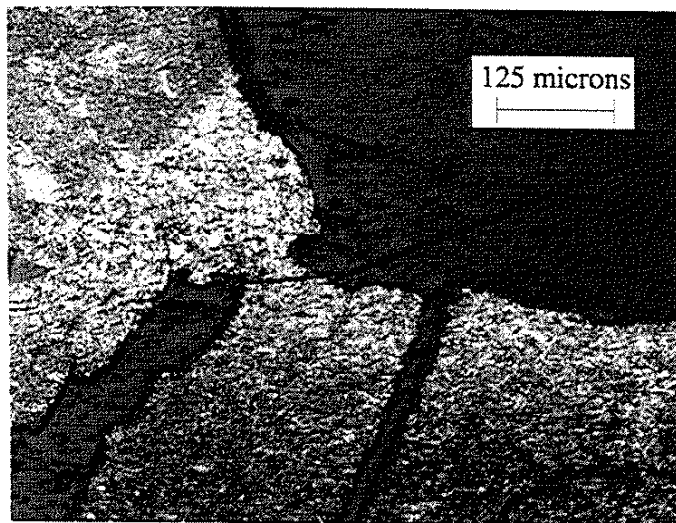
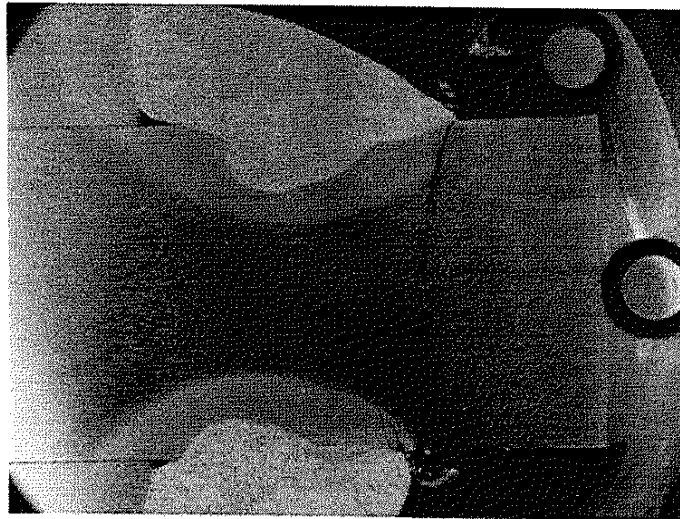


Fig. 2.7 (Above) The shape of the crack path emanating from the weld toe (3.5X). (Below) Enlarged view of the initial trajectory of the crack path (125X).

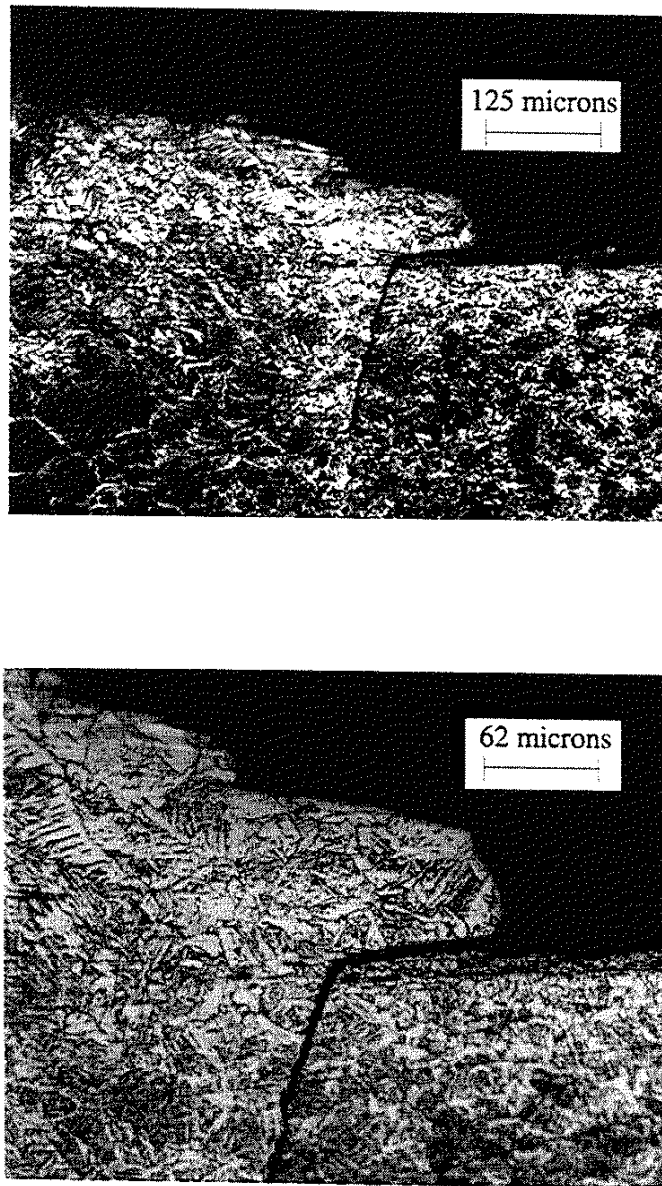


Fig. 2.8 Fatigue crack emanating from a cold-lap defect shown at a magnification of 125X (Above) and 262.5X (Below).

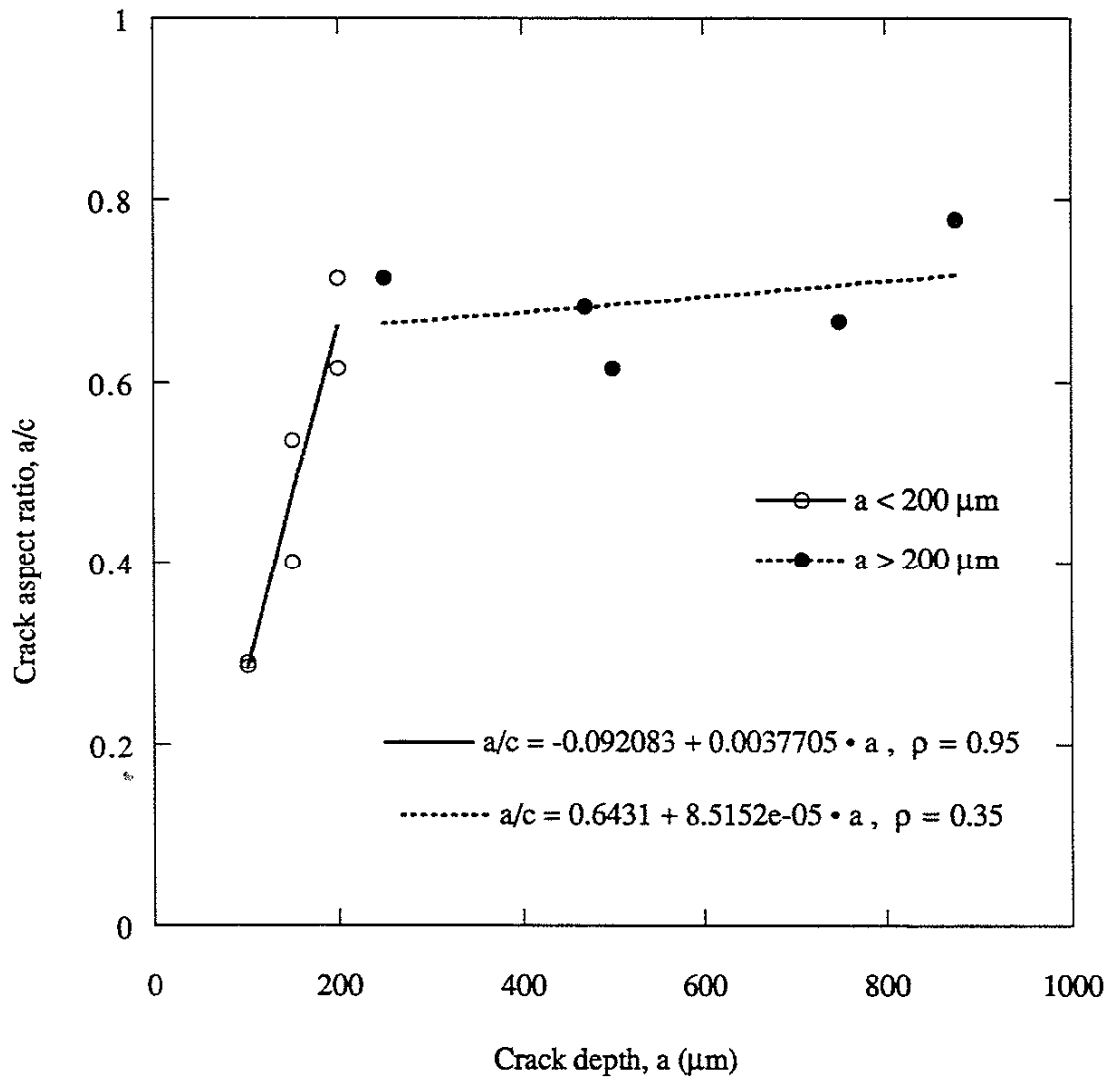


Fig. 2.9 Crack shape development for short cracks measured using the scanning electron microscope.

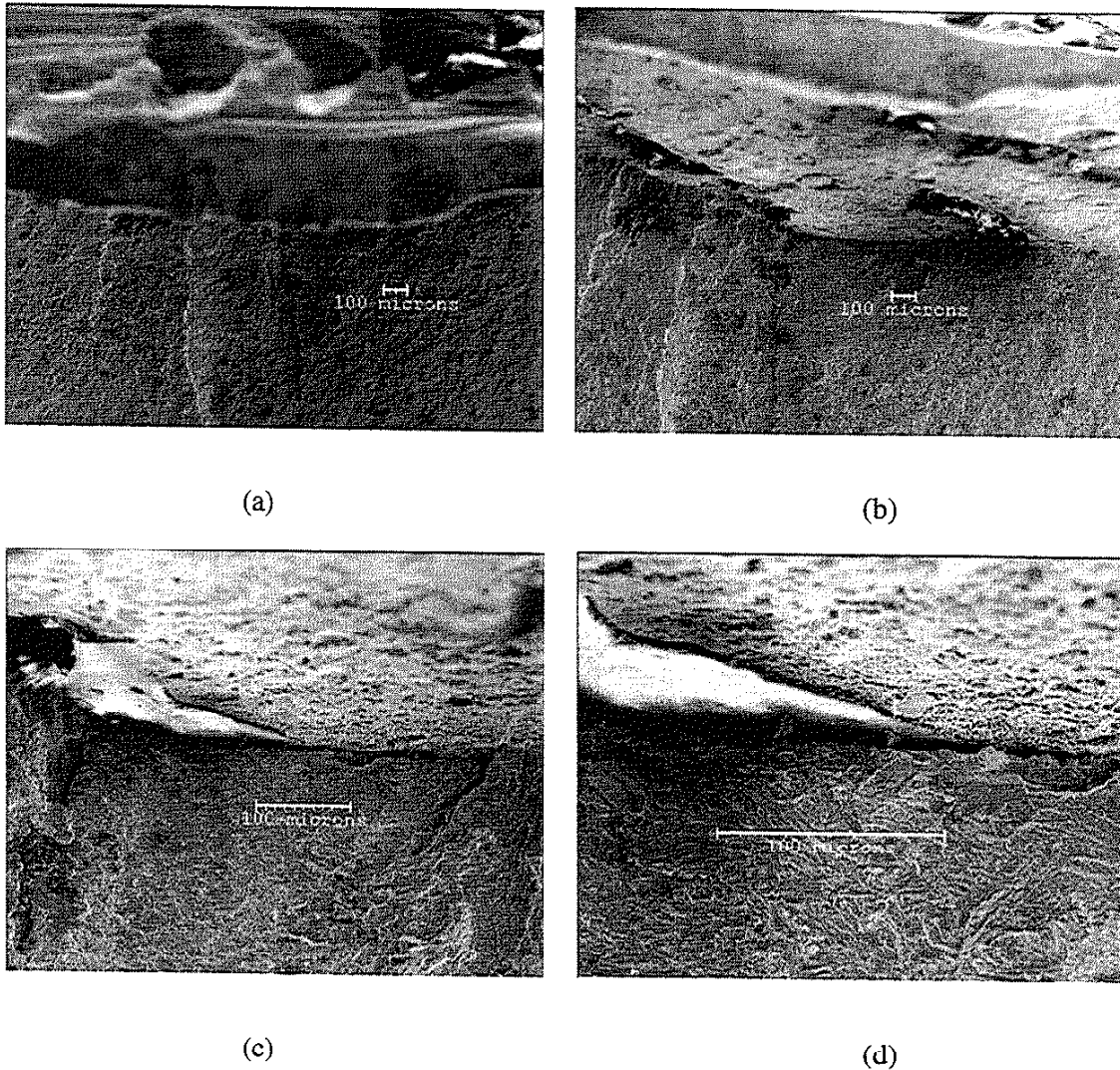


Fig. 2.10 Scanning electron microscope images of the fracture surface showing a cold-lap defect: (a) looking straight down (0°) on the cold-lap defect (30X), (b) specimen tilted 28° to show the depth of the cold-lap defect (30X), (c) specimen tilted 28° at a magnification of 130X, (d) specimen tilted 28° at a magnification of 300X. An impurity from the weld process (probably slag) appears at higher magnification in (c) and (d).

CHAPTER 3

FINITE ELEMENT ANALYSIS OF LONGITUDINAL ATTACHMENTS

3.1 INTRODUCTION

In this chapter, the longitudinal attachment will be examined using finite element methods (FEM). First, the accuracy of the superposition method in determining the weld geometry correction factor (M_K) will be investigated using two-dimensional (2-D) FEM modeling of the longitudinal attachment. Then, the three-dimensional (3-D) nature of the longitudinal attachment will be studied, and the effects of variations in weldment geometry on M_K will be examined. Finally, the effects of bending loads and one-sided longitudinal attachments will be explored.

3.2 PROCEDURES

3.2.1 Finite Element Analysis Software

The longitudinal attachment was studied using primarily¹ the Pro/MECHANICA STRUCTURE² FEM software. The Pro/MECHANICA STRUCTURE FEM software was selected for this study because of its (1) automatic mesh generation feature called "AUTOGEM³" and (2) method of convergence called "Adaptive p Technology⁴." These features allow the use of coarse meshes and assure accuracy without the need to regenerate meshes and therefore make it much simpler to perform analyses [30].

3.2.2 Superposition Method

A weld geometry correction factor, M_K , was developed to modify the stress intensity factor for a plain plate (K_{pp}) and account for the presence of the weld geometry as follows:

¹ An independent check was performed using Patran to generate the mesh and Abaqus to analyze the mesh, and the results were found to be consistent with the results obtained using Pro/MECHANICA STRUCTURE.

² Pro/MECHANICA STRUCTURE uses high-order finite elements called geometric elements which are based on the p-version of the finite element method, p-method. The p-method represents the static, elastic displacements within each element using high-order polynomials [30].

³ AUTOGEM automatically creates and optimizes elements.

⁴ Adaptive p Technology raises the polynomial order for selected elements throughout the model until a specified convergence criteria (percent change between the results of the last two calculations) is satisfied [30].

$$K_{\text{weld}} = M_K Y S \sqrt{\pi a}. \quad (1.1)$$

In this study, the superposition method was used to calculate the weld geometry correction factor, M_{Ks} , using the following equation from the studies of Albrecht et al. [25] and later Hobbacher [26]:

$$M_{Ks} = \frac{2}{\pi} \int_0^a \frac{K_t(y)}{\sqrt{(a^2 - y^2)}} dy \quad (3.1)$$

The stress intensity for the plain plate (K_{pp}) was calculated using the results of Newman and Raju [31] for semi-elliptical surface cracks.

M_K has usually been evaluated along a crack path perpendicular to the applied load and inward from the weld toe (vertical path from the weld toe in this study), and the calculation of K_{weld} ($M_{Ks} \cdot K_{pp}$) has been based on the readily available solutions for stress intensity factor for surface cracks in plain plate (K_{pp}) determined for straight cracks which are perpendicular (vertical) to the applied load: see Appendix 2. However, the crack path for the specimens tested in Chapter 2 was observed to be curved and not straight; therefore, M_K should be evaluated along this curved path. However, the accuracy of determining M_K along such curved crack paths using the superposition method and using the model for K_{pp} based on cracks perpendicular to the applied load should be questioned.

A pilot study was undertaken in which the longitudinal attachment was modeled in 2 dimensions (2-D) (1) to determine the crack path emanating from the weld toe and (2) to determine the best method of estimating M_K with the superposition method for this crack path. The general findings of the pilot study will be presented below, and the details of the pilot study can be found in Appendix 3.

A weld toe radius of 1 mm was assumed in the 2-D FEM analyses. The crack path emanating from the weld toe was determined by propagating a crack in small increments from the weld toe following the trajectory suggested by the maximum circumferential stress criterion [32]. The determined crack path was not straight but curved in the manner experimentally observed: see Fig. 3.1. It can be seen that the modeled crack path and the experimentally observed crack path (Fig. 2.7) are in good agreement despite the difference in weld toe radius modeled (1 mm) and observed experimentally (average of 0.08 mm).

The stress intensity factor for the weld ($K_{\text{weld CG}}$) determined from the cracked geometry along the curved path was normalized by K_{pp} to yield the weld geometry correction factor (M_{KCG}) which is plotted in Fig. 3.2. Similarly, M_{KCG} was determined along the vertical path inward from the weld toe and plotted in Fig. 3.2. M_{KCG} was found to be slightly greater

along the curved path than the traditionally used vertical path. If the solution for M_K derived for the vertical path was used in fatigue crack propagation life estimates, N_p would be slightly overestimated; see Fig 3.2.

The use of either the perpendicular stresses along the vertical path, or the maximum principal stresses along the vertical path, or the projected maximum principal stresses onto the vertical path from the curved path in the calculation of M_{Ks} was found to estimate M_{KCG} determined along the curved path equally well. It was decided to use the maximum principal stresses along the vertical path inward from the weld toe in the calculation of M_{Ks} , because it is believed to provide the most convenient yet accurate solution. Any differences in N_p calculated using M_{Ks} and M_{KCG} were found to be insignificant. Therefore, all further calculations of M_K from the weld toe location in this study will be performed using the maximum principal stresses along the vertical path inward from the weld toe.

Other investigators [33, 34] have considered cracks which emanate from the location of “peak” stress in the weld toe area. A similar pilot study was also undertaken to determine the crack path from the location of “peak” stress in the weld toe area, and to determine the best method of estimating M_{KCG} with the superposition method for the crack path emanating from the location of “peak” stress. The results of this pilot study can be found in Appendix 3.2. Cracks emanating from the location of “peak” stress were not considered in rest of the study for reasons which will be discussed later.

3.2.3 Modeling of the Longitudinal Attachment in 3-D

The longitudinal attachments were modeled using 3-D FEM analyses. The weld toe of the longitudinal attachments was modeled with a weld toe radius. The only previous 3-D study of the longitudinal attachment which considered the finite radius of the weld toe was that of Dahle et al. [27]. The longitudinal attachment was loaded with a uniaxial load applied to main plate; therefore, all the stress results will be stress concentration factors. The longitudinal attachment modeled in 3-D with Pro/MECHANICA is shown in Fig. 3.3. Enlarged views of the weld toe from different angles showing the high stress concentrations at the weld toe and the detail of the weld toe modeling is shown in Fig. 3.4.

The results for the 2-D and 3-D FEM analyses are compared in Fig. 3.5. As discussed in Chapter 1, a 2-D FEM analysis underestimates the state of stress in a longitudinal attachment and therefore M_K ; see Fig. 3.5a. Use of M_K determined with the 2-D FEM analysis will lead to propagation lives which are too long; see Fig. 3.5b.

In all prior studies of the longitudinal attachment [23, 26, 27], the lack of penetration (LOP) between the attachment plate and the main plate was not modeled in the FEM

analyses. The effect of the LOP on the weld geometry correction factor was examined in this study, and the FEM results showed a very small difference in M_K if the LOP was not modeled. However, in this study, the LOP was modeled in all analyses for consistency in comparisons with models developed to decrease the stress concentration of the longitudinal attachment in Chapter 4.

The 3-D FEM results for the longitudinal attachment with dimensions as shown in Fig. 2.2 with a weld leg length of 12.7 mm are compared with the results of Hobbacher [26] in Fig. 3.6. The M_K calculation based on the stresses perpendicular to the vertical path were included in Fig. 3.6, since Hobbacher calculated M_K with these stresses. The results at short crack lengths differ presumably because Hobbacher modeled the weld toe as a sharp corner. At long crack lengths, the results of Hobbacher are slightly larger than the result of this study based on the perpendicular stresses on the vertical path. One reason for this difference may be that the results of Hobbacher presented here were calculated using an equation derived from a regression analysis of many data points. The results of this study are in agreement with the results of Hobbacher.

In Fig. 3.7, the results of Dahle et al. [27] are presented with the FEM results for the longitudinal attachment with dimensions as shown in Fig. 2.2 with a weld leg length of 9.52 mm which is approximately what Dahle et al. modeled. The M_K calculation based on the stresses perpendicular to the vertical path was included in Fig. 3.7, since Dahle et al. calculated M_K with these stresses. Dahle's results are slightly lower than this study at long crack lengths and slightly higher than the current study at short crack lengths. The results of this study are in good agreement with that of Dahle et al. It is believed that the FEM results of the current study are accurate since they are in general agreement with the FEM results of Hobbacher and Dahle et al.

3.3 RESULTS

3.3.1 The Effect of Geometry on the Fatigue Life of Longitudinal Attachments

3-D FEM analyses were carried out to determine the effects of weldment geometry on the fatigue life of longitudinal attachments. The effects of many geometric variables can be seen in Fig. 3.8.

Effect of Plate Thickness: The effect of plate thickness, the ratio of attachment to main plate thickness (t/T), on M_K and N_p can be seen in Fig. 3.8a. For long cracks, it can be seen that an increase in main plate thickness and/or a decrease in attachment height leads to a decrease in

M_K and therefore an increase in N_p ; but for short cracks, an increase in main plate thickness and/or a decrease in attachment height leads to a increase in M_K and therefore a decrease in N_p .

Effect of Main Plate Width: The effect of main plate width normalized by the main plate thickness (B/T) on M_K and N_p can be seen in Fig. 3.8b. As the main plate width increases, there is an increase in M_K and therefore a decrease in N_p . The effect is significant, but there appears to be little further effect when B/T reaches 20.

Effect of Attachment Length: The effect of attachment length normalized by the main plate thickness (L/T) on M_K and N_p can be seen in Fig. 3.8c. An increase in the attachment length leads to an increase in M_K and therefore a decrease in N_p . As L/T reaches a value of 10, an asymptotic effect is seen as no further increases in M_K or decreases in N_p are seen.

Effect of Weld Toe Radius: The effect of weld toe radius (r) on M_K and N_p can be seen in Fig. 3.8d. A decrease in weld toe radius leads to an increase in M_K and therefore to a decrease in N_p for short cracks. For long cracks, the effect of weld toe radius is insignificant.

Effect of Weld Toe Angle: The effect of weld toe angle (θ) on M_K and N_p can be seen in Fig. 3.8e. An increase in weld toe angle leads to an increase in M_K and therefore to a decrease in N_p .

Effect of Weld Leg Length: The effect of weld leg length on M_K and N_p can be seen in Fig. 3.8f. A decrease in weld leg length leads to an increase in M_K and therefore a decrease in N_p .

Effect of Attachment Height and Bevel Angle: Varying the attachment height (V) and bevel angle were found to have no effect on M_K and N_p .

In summary, the fatigue life of longitudinal attachments can generally be increased by:

- Increasing main plate thickness and/or decreasing attachment plate thickness.
- Decreasing main plate width.
- Decreasing attachment length.
- Increasing weld toe radius.
- Decreasing weld toe angle.

3.3.2 Effects of Bending Load

The longitudinal attachment was modeled with a bending load applied by a moment at the end of the main plate. The weld geometry correction factor, M_K , is smaller under bending load than axial load: see Fig. 3.9. At short crack lengths, the M_K determined for axial loading is approximately 10% larger than the M_K developed for bending load. Significant differences in the resulting fatigue crack propagation lives calculated for axial and bending load are observed: see Fig. 3.9. As the initial crack length increases, the difference in N_p is greater. The estimated N_p is seen to be from approximately 2 to 4 times longer under bending load than axial load depending on the initial crack length used.

3.3.3 Effects of One-Sided Longitudinal Attachments

The longitudinal attachment was modeled with an attachment plate on only one side of the main plate. The weld geometry correction factor, M_K , decreases significantly when an attachment is welded on only one side of the main plate: see Fig. 3.10. Significant increases in N_p are predicted to be obtained if one-sided attachments are used. Unfortunately, these significant increases are rarely observed because of the very large distortions due to welding associated with a one-sided attachment.

3.4 SUMMARY

2-D FEM studies of the longitudinal attachment confirm that the superposition method estimates the stress intensity factor determined using crack tip elements for cracks along the curved crack path. The three-dimensional (3-D) nature of the longitudinal attachment was studied. Variations in the weld toe radius, plate thicknesses, main plate width, attachment length, weld toe angle, and weld leg length were shown to influence the weld geometry correction factor (M_K). Longitudinal attachments loaded under bending and one-sided longitudinal attachments were found to have significantly less severe weld geometry correction factors (M_K).

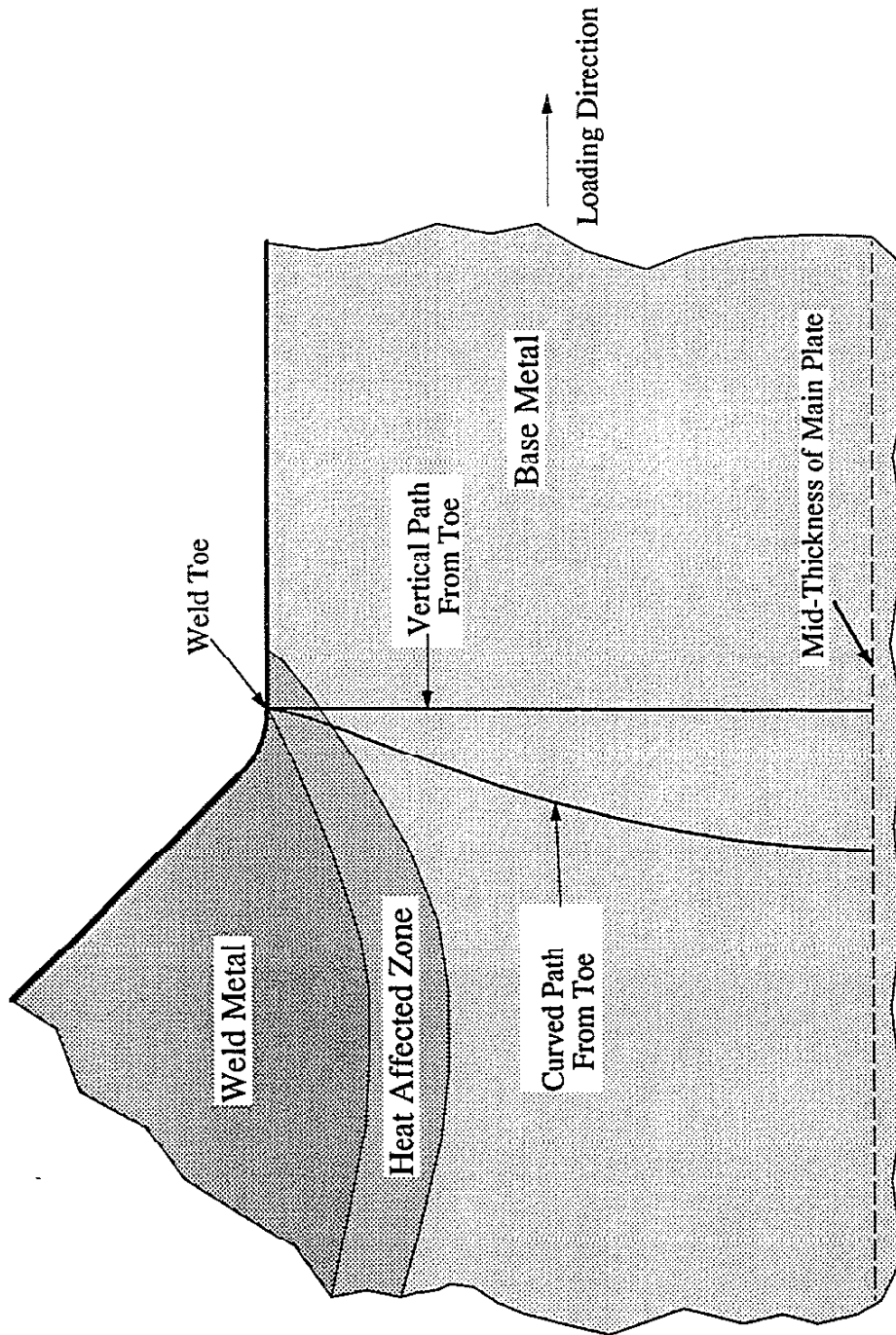
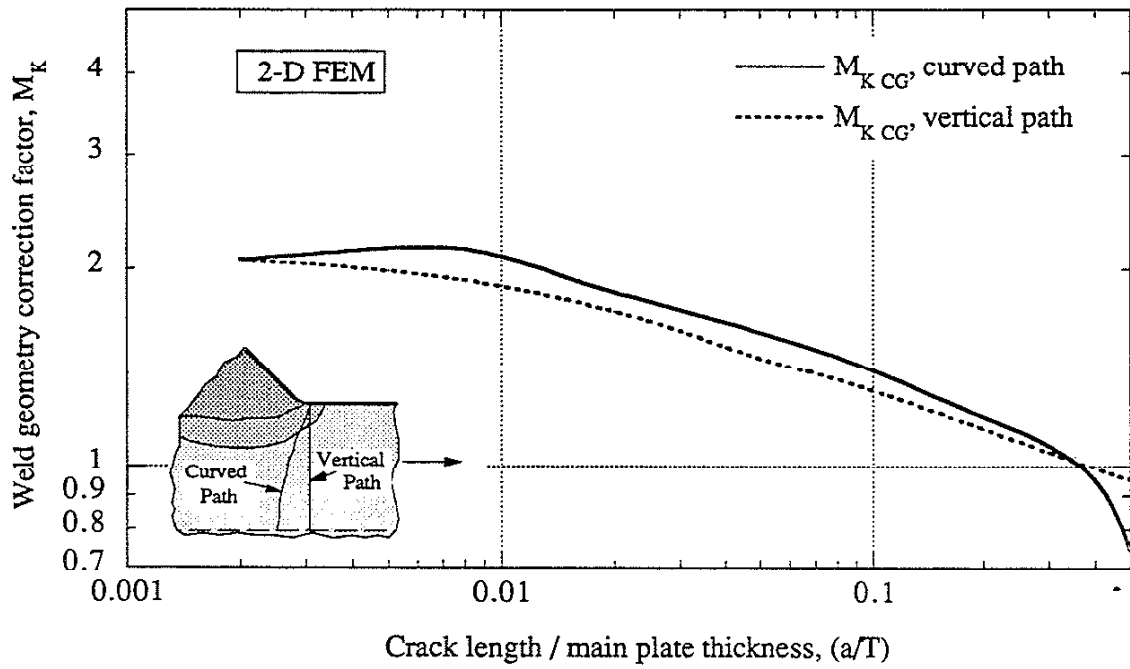
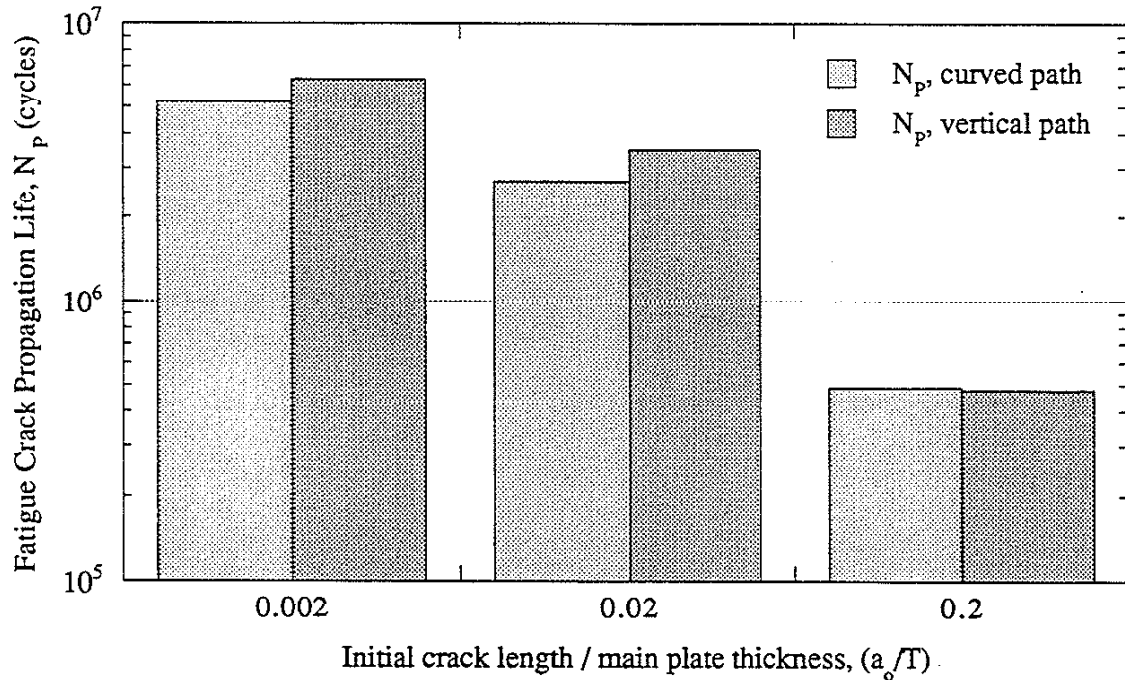


Fig. 3.1 The fatigue crack growth paths determined for a longitudinal attachment with 2-D FEM analyses.



(a)



(b)

Fig. 3.2 Comparison of the (a) the weld geometry correction factors and (b) the fatigue crack propagation lives determined for the vertical and curved crack paths. ($\Delta S = 100$ MPa)

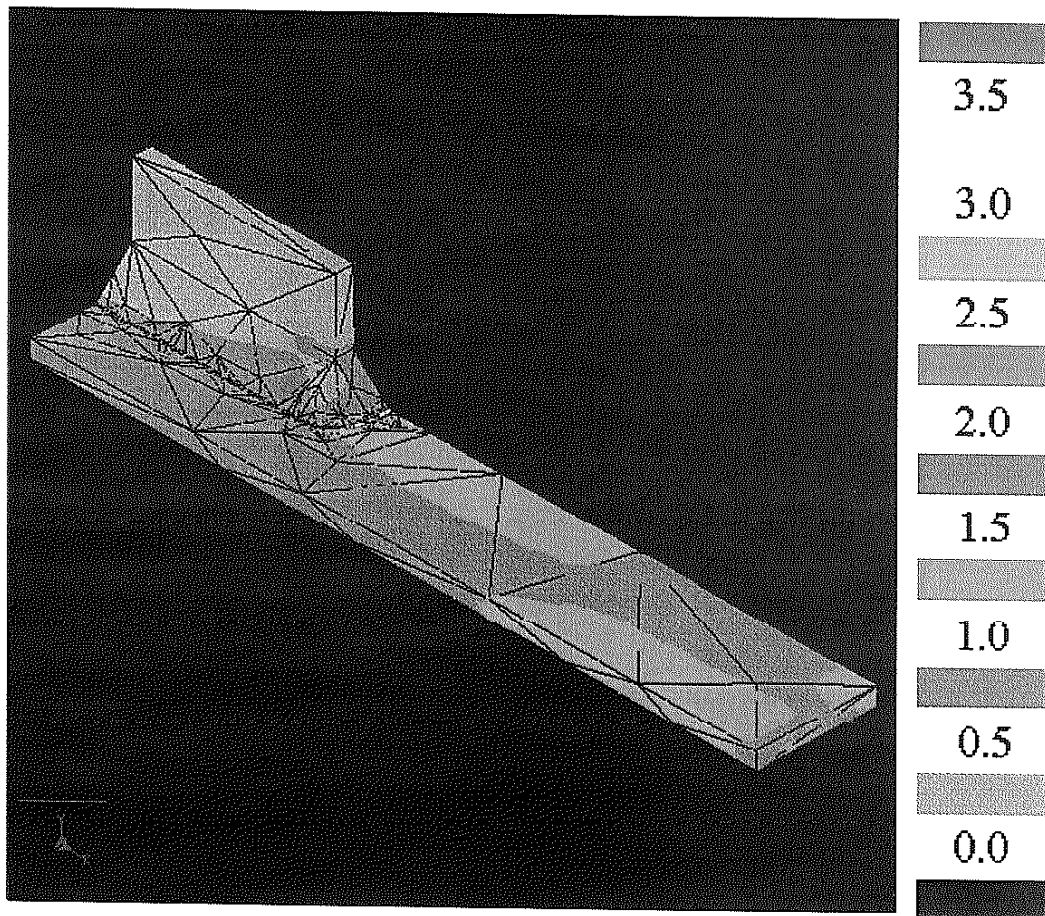


Fig. 3.3 The 3-D FEM modeling of the longitudinal attachment in Pro/MECHANICA presented as a fringe plot of maximum principal stress. One octant of the geometry is modeled due to planes of symmetry.

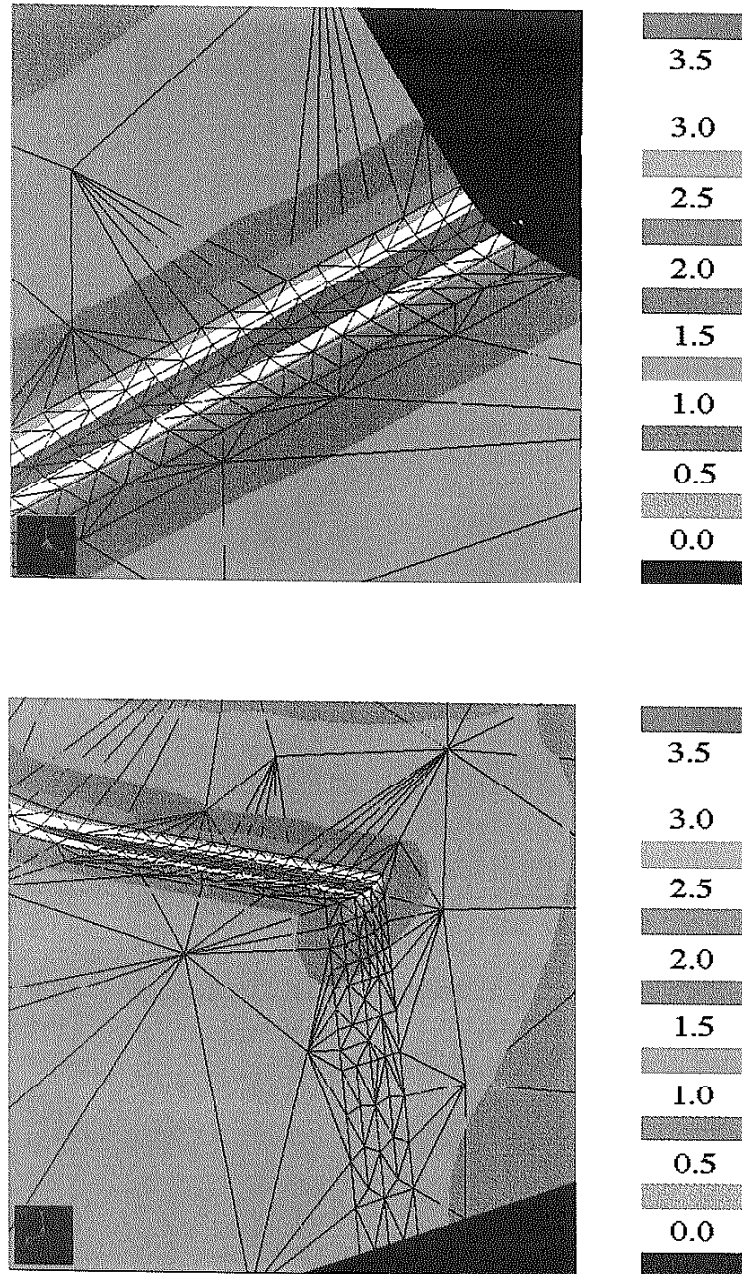
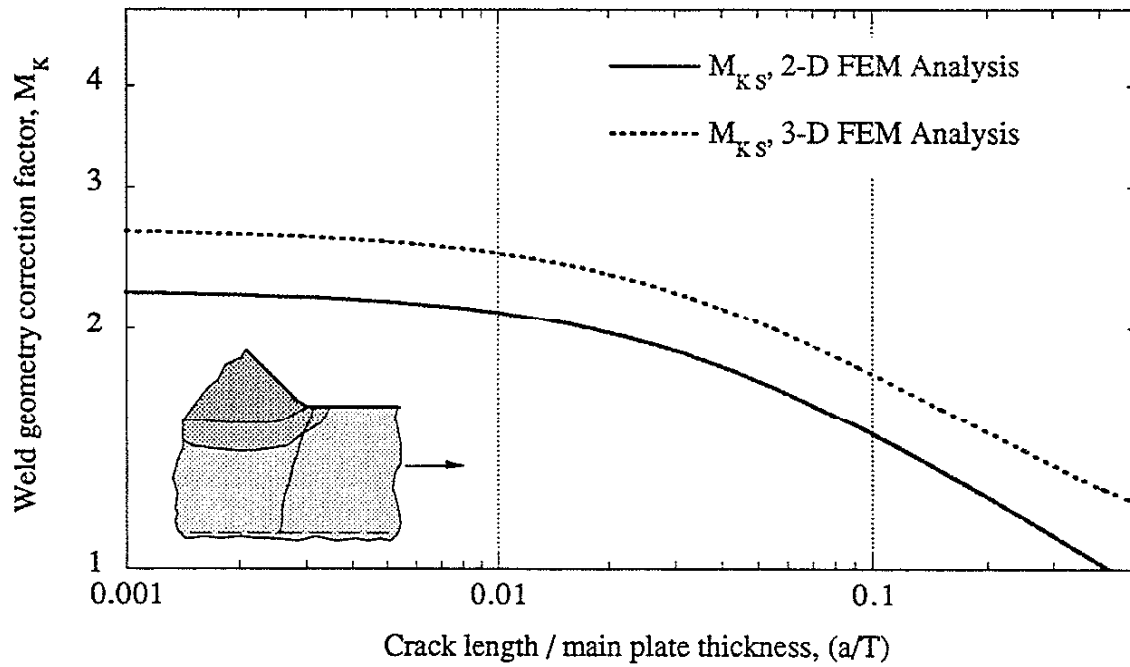
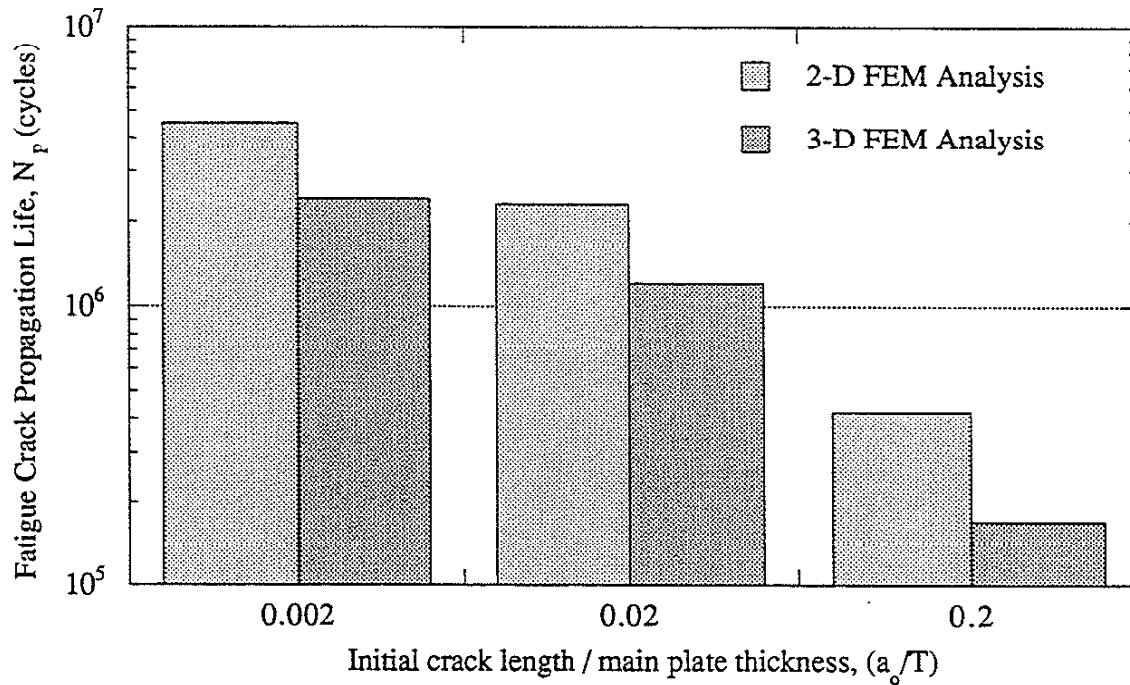


Fig. 3.4 Enlarged views of the weld toe region of the longitudinal attachment modeled in 3-D showing the large stress concentrations and the details of the FEM modeling from two different views.



(a)



(b)

Fig. 3.5 Comparison of the (a) the weld geometry correction factors and (b) the fatigue crack propagation lives determined from 2-D and 3-D FEM analyses. ($\Delta S = 100$ MPa)

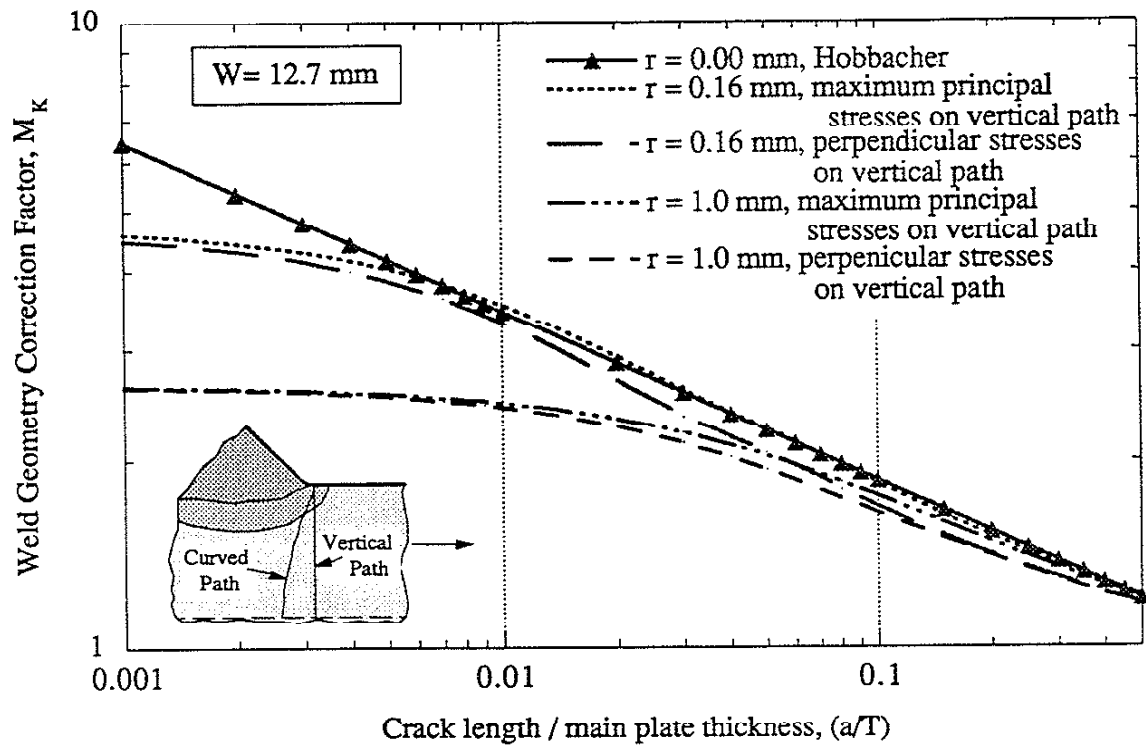


Fig. 3.6 The FEM results of this study compared to the results of Hobbacher.

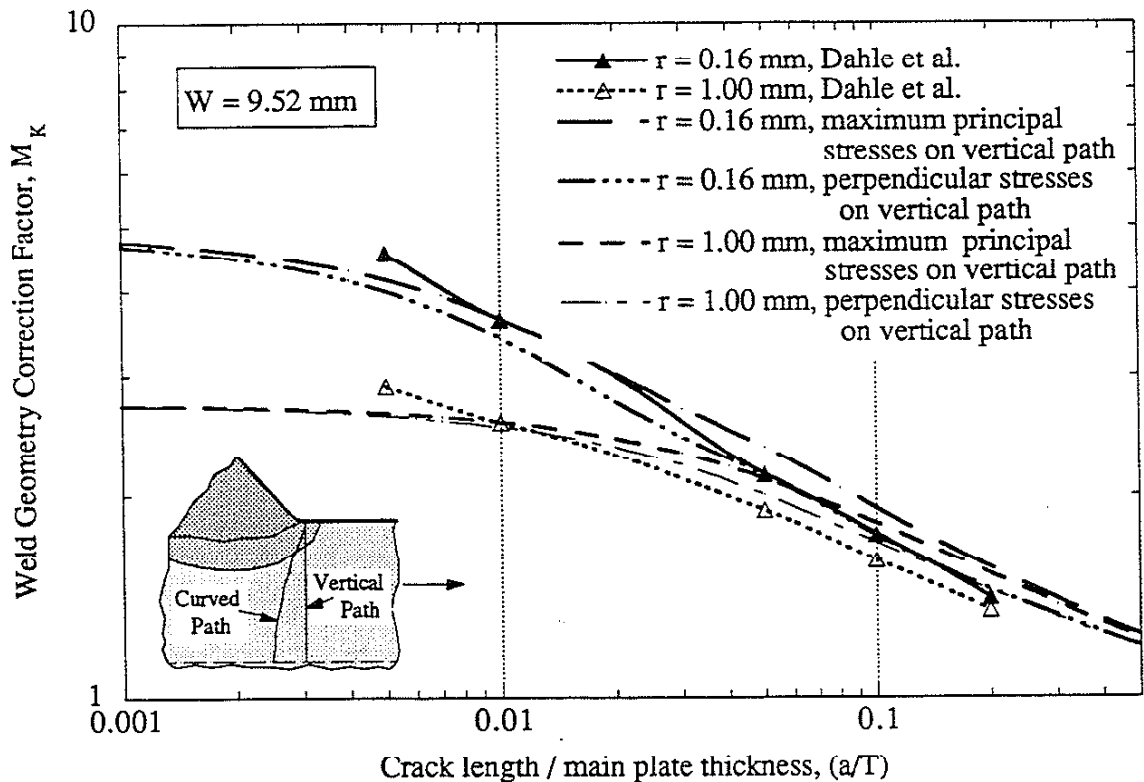
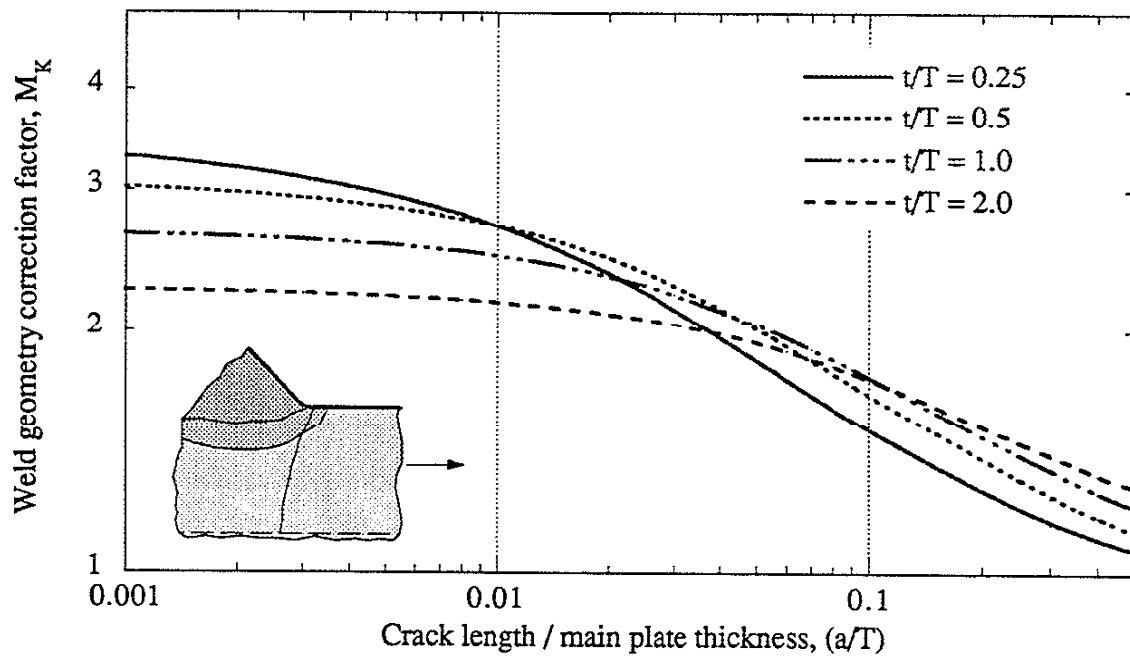
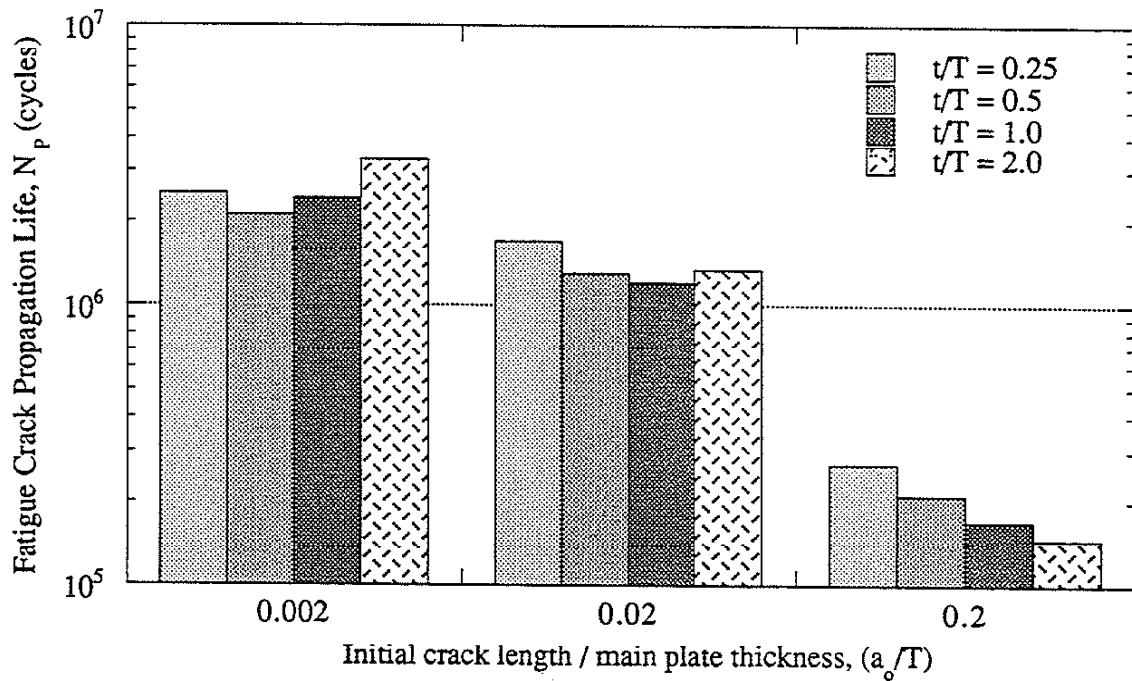


Fig. 3.7 The FEM results of this study compared to the results of Dahle.

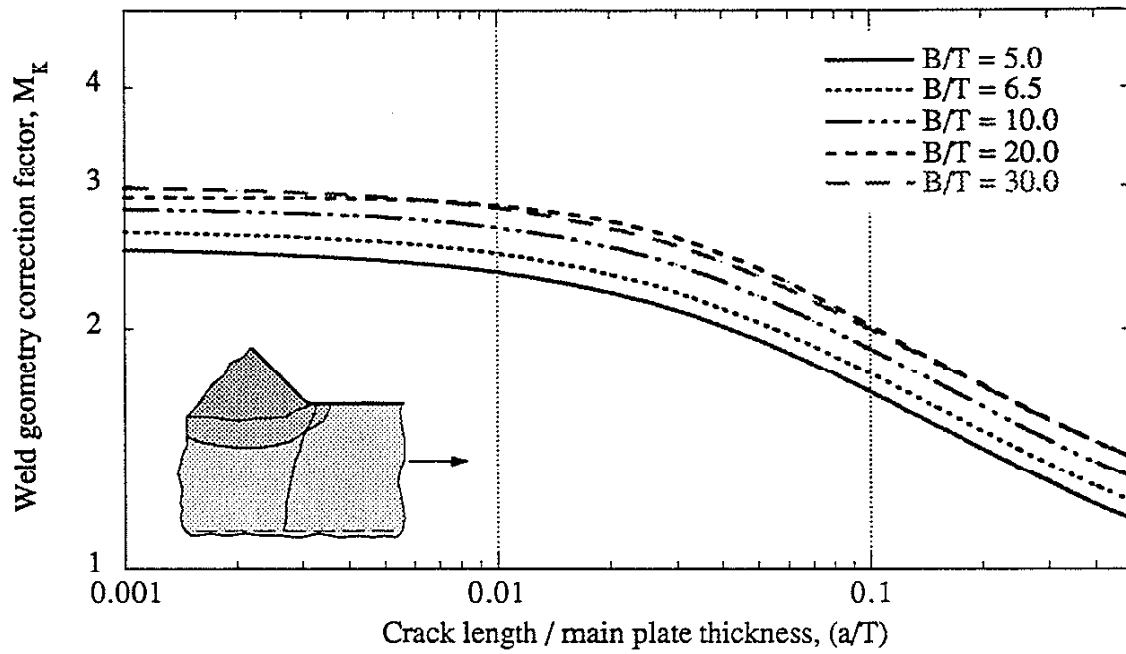


(a)

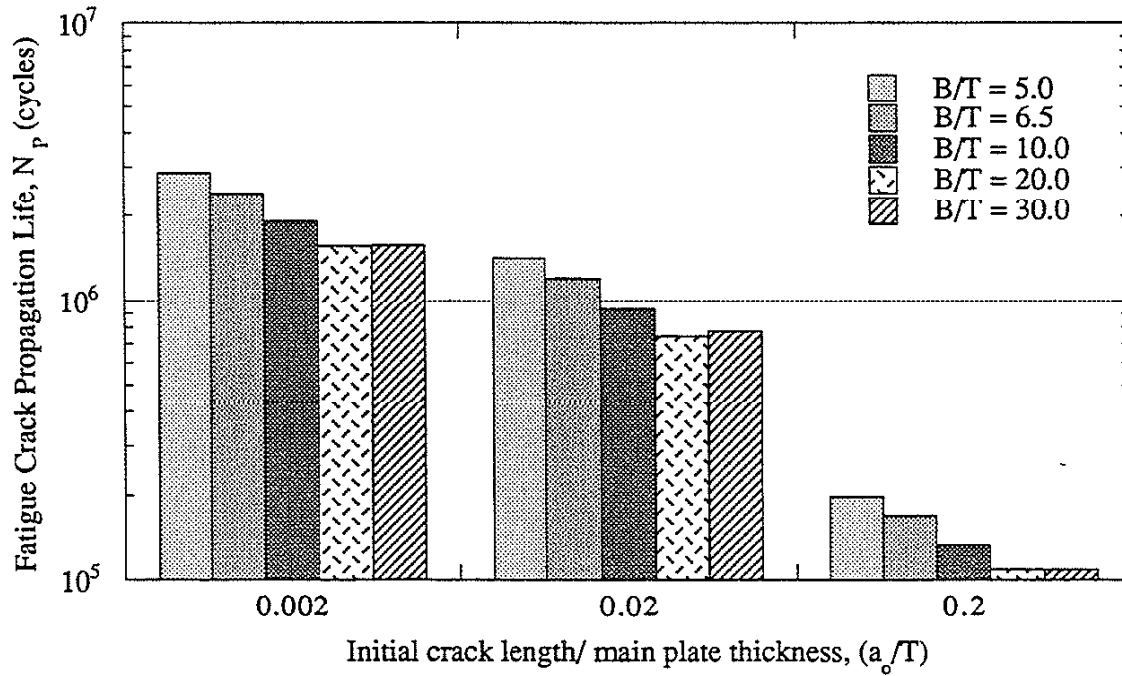


(b)

Fig. 3.8a The predicted effect of plate thickness on (a) the weld geometry correction factor and (b) the fatigue crack propagation lives of longitudinal attachments. ($\Delta S = 100$ MPa)

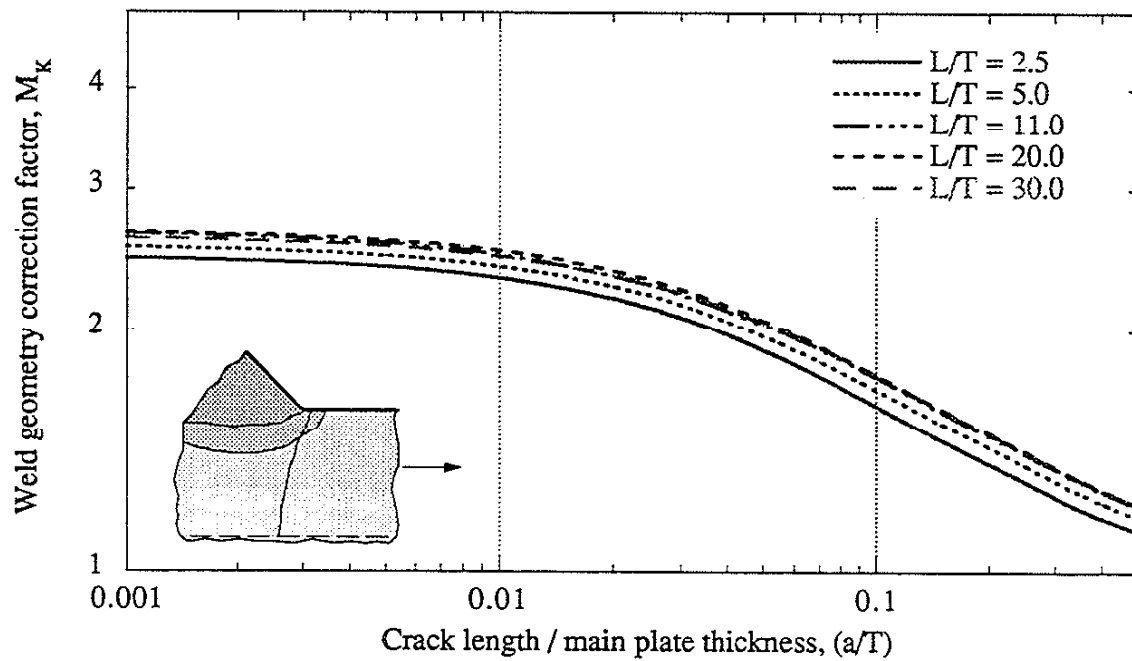


(a)

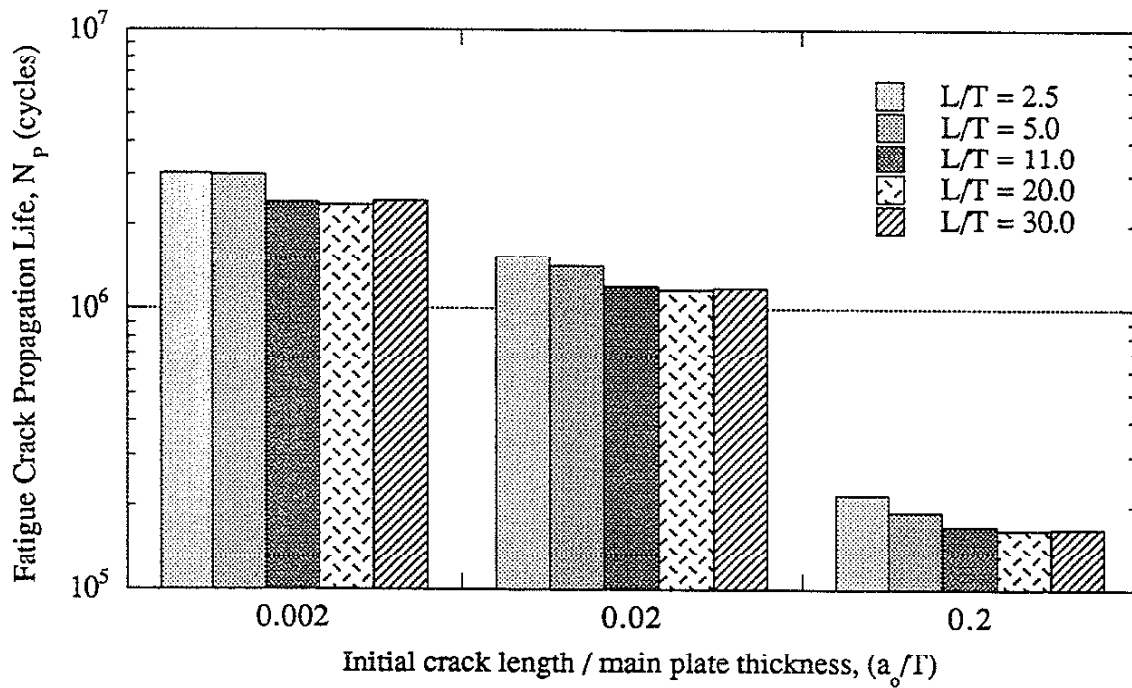


(b)

Fig. 3.8b The predicted effect of main plate width on (a) the weld geometry correction factor and (b) the fatigue crack propagation lives of longitudinal attachments. ($\Delta S = 100$ MPa)

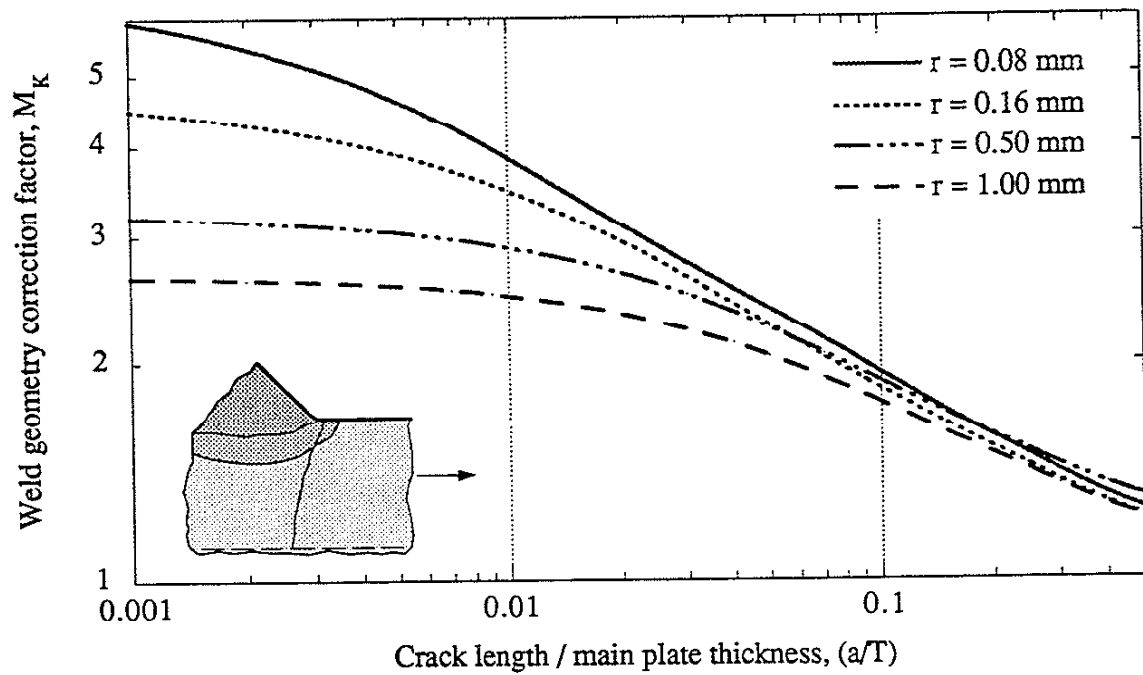


(a)

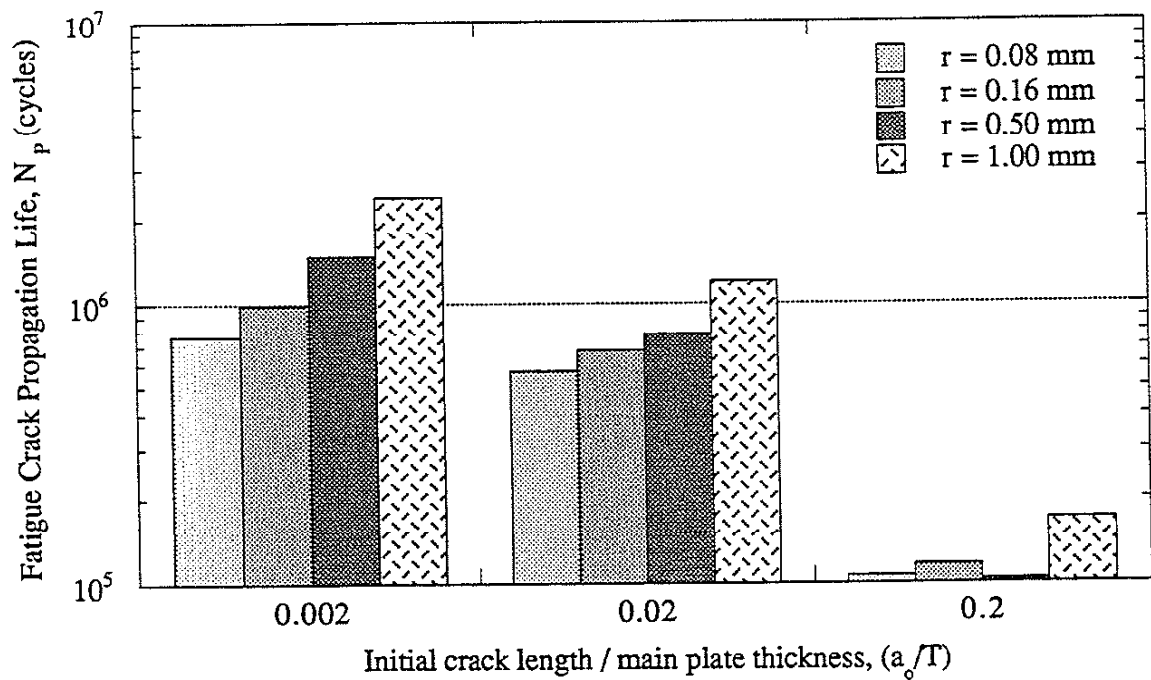


(b)

Fig. 3.8c The predicted effect of attachment length on (a) the weld geometry correction factor and (b) the fatigue crack propagation lives of longitudinal attachments. ($\Delta S = 100$ MPa)

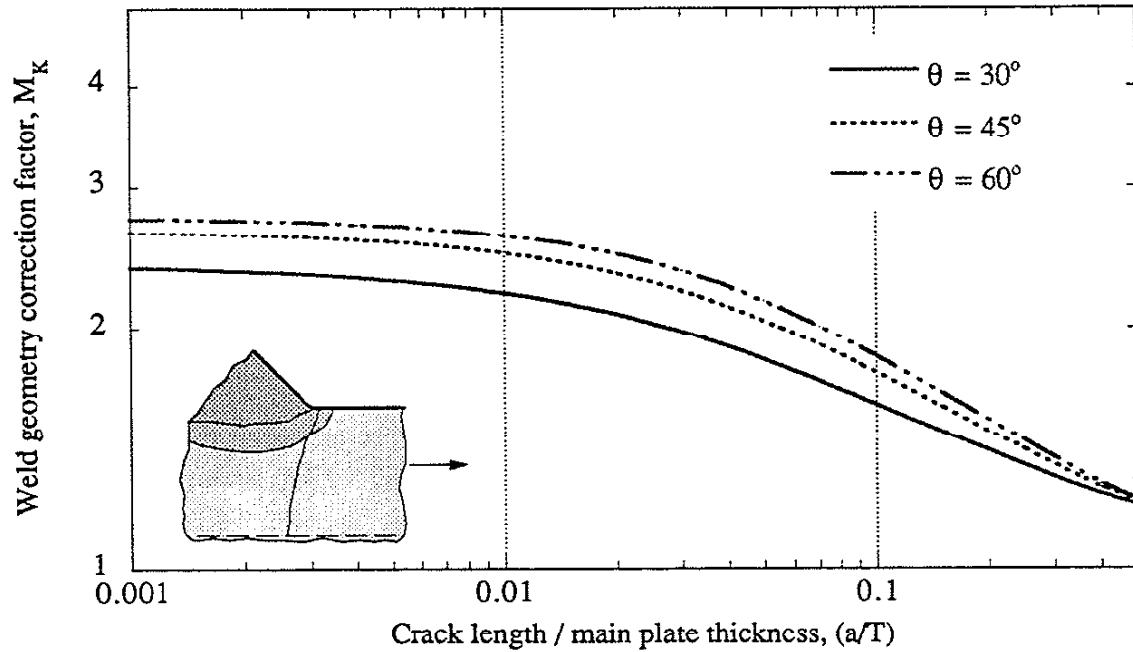


(a)

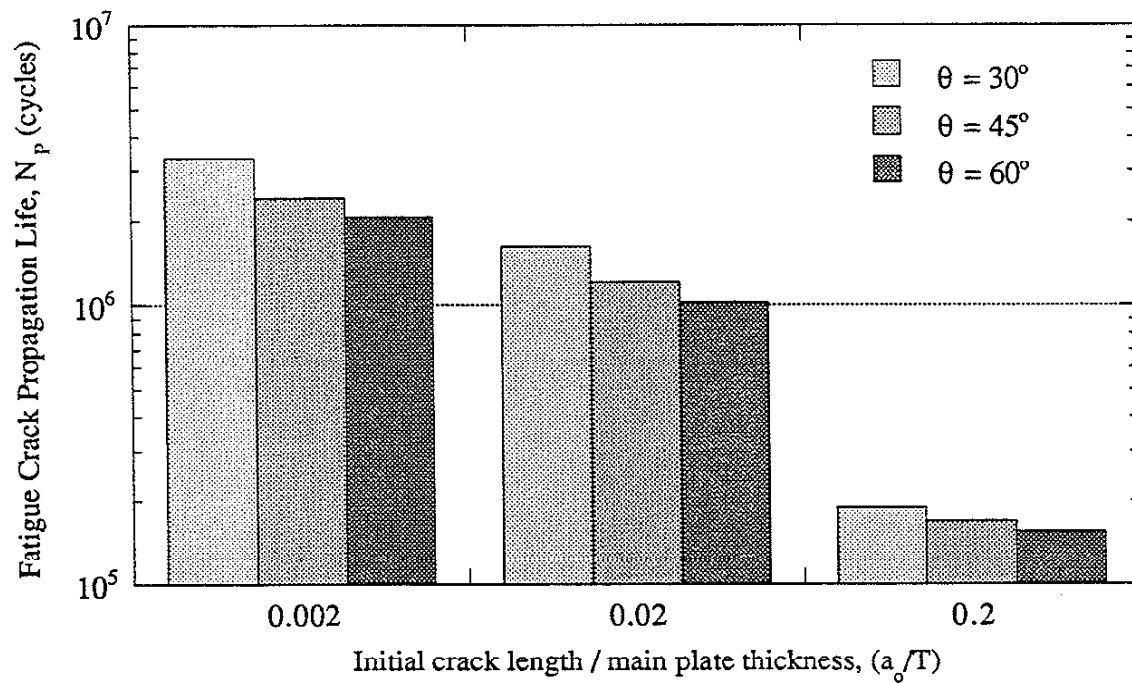


(b)

Fig. 3.8d The predicted effect of weld toe radius on (a) the weld geometry correction factor and (b) the fatigue crack propagation lives of longitudinal attachments. ($\Delta S = 100$ MPa)

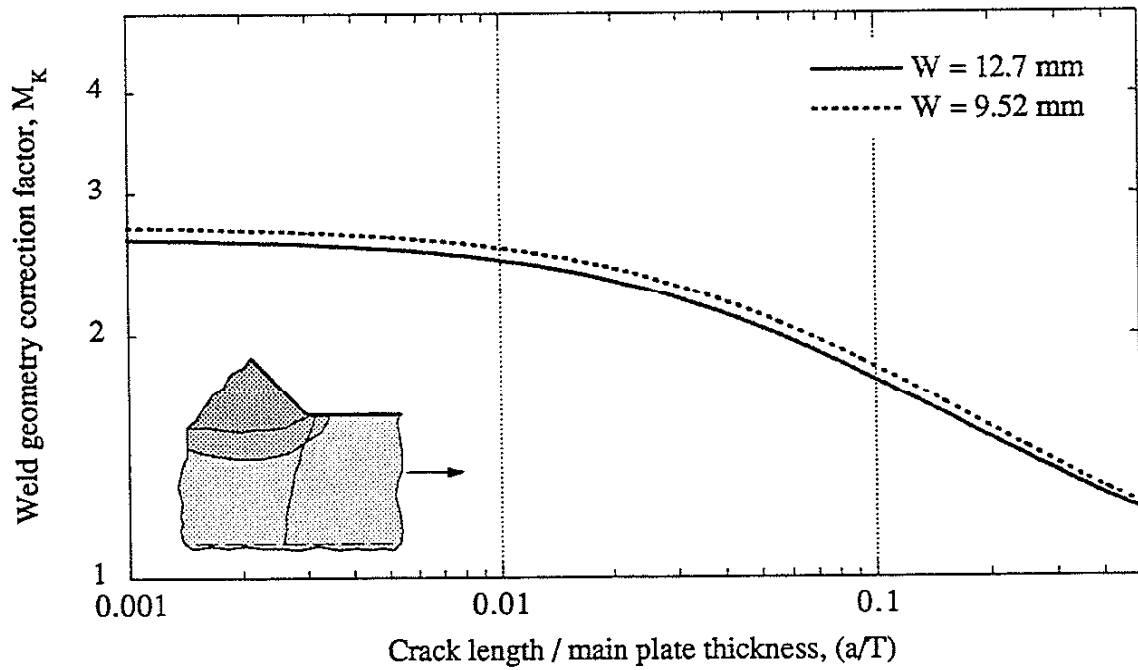


(a)

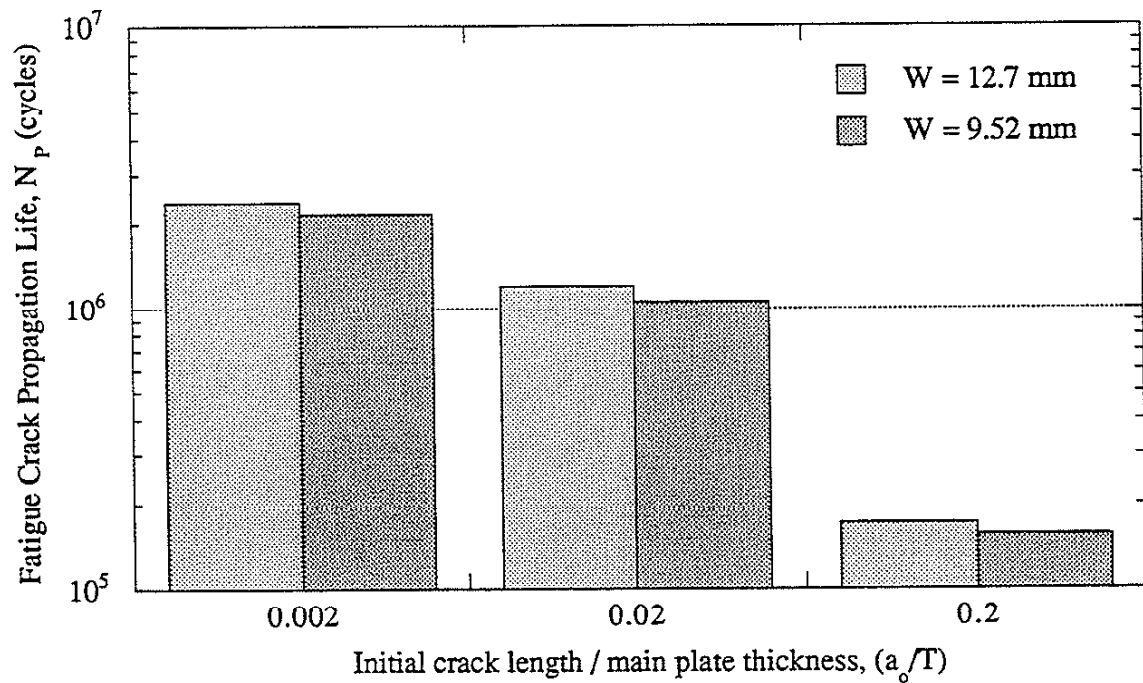


(b)

Fig. 3.8e The predicted effect of weld toe angle on (a) the weld geometry correction factor and (b) the fatigue crack propagation lives of longitudinal attachments. ($\Delta S = 100$ MPa)

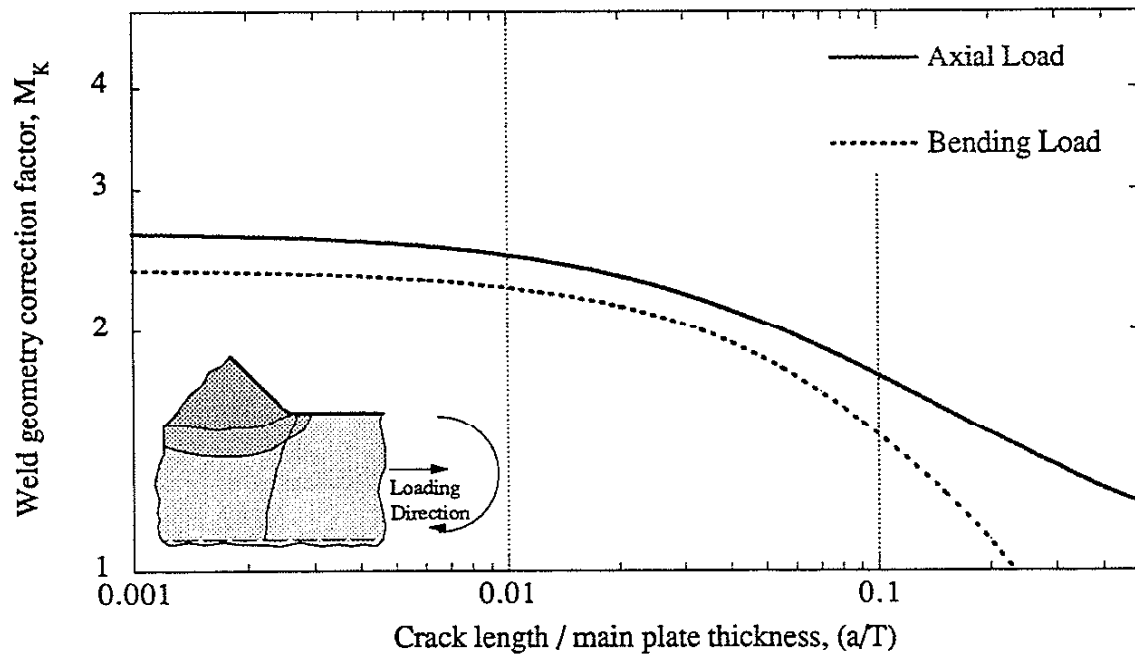


(a)

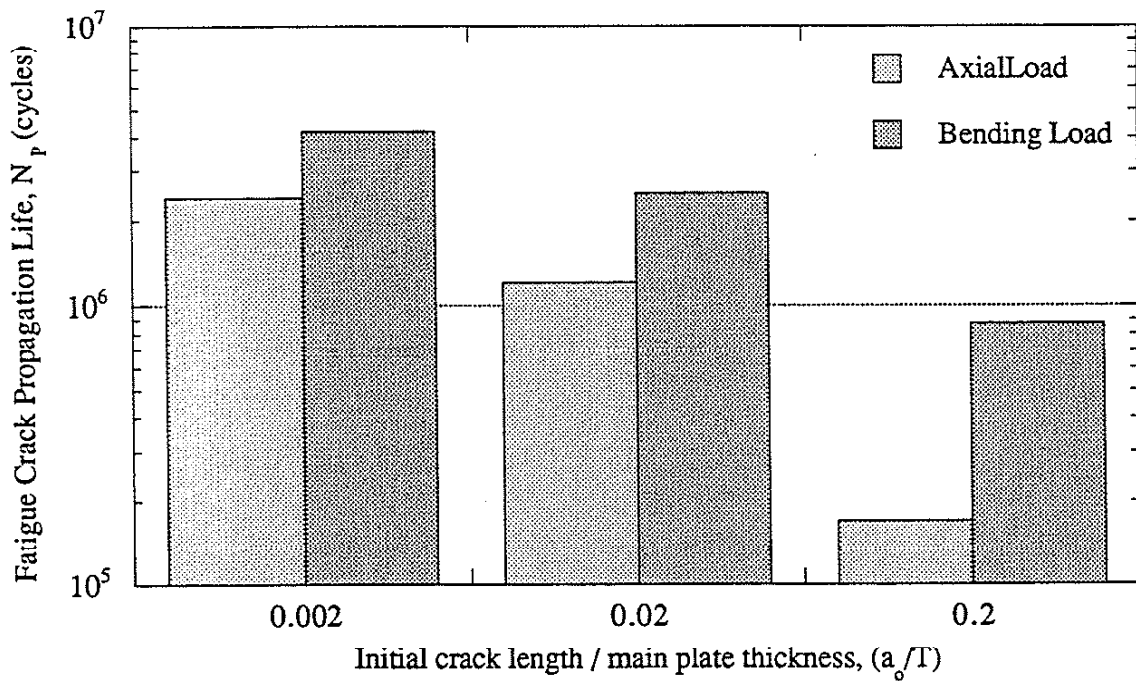


(b)

Fig. 3.8f The predicted effect of weld leg length on (a) the weld geometry correction factor and (b) the fatigue crack propagation lives of longitudinal attachments. ($\Delta S = 100 \text{ MPa}$)

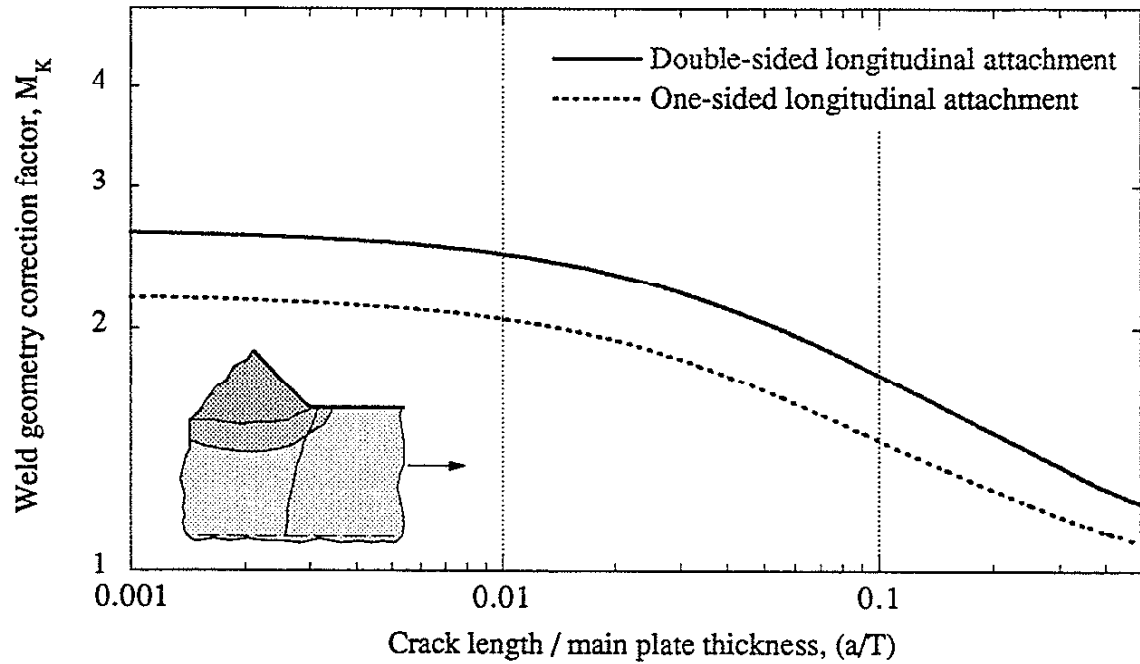


(a)

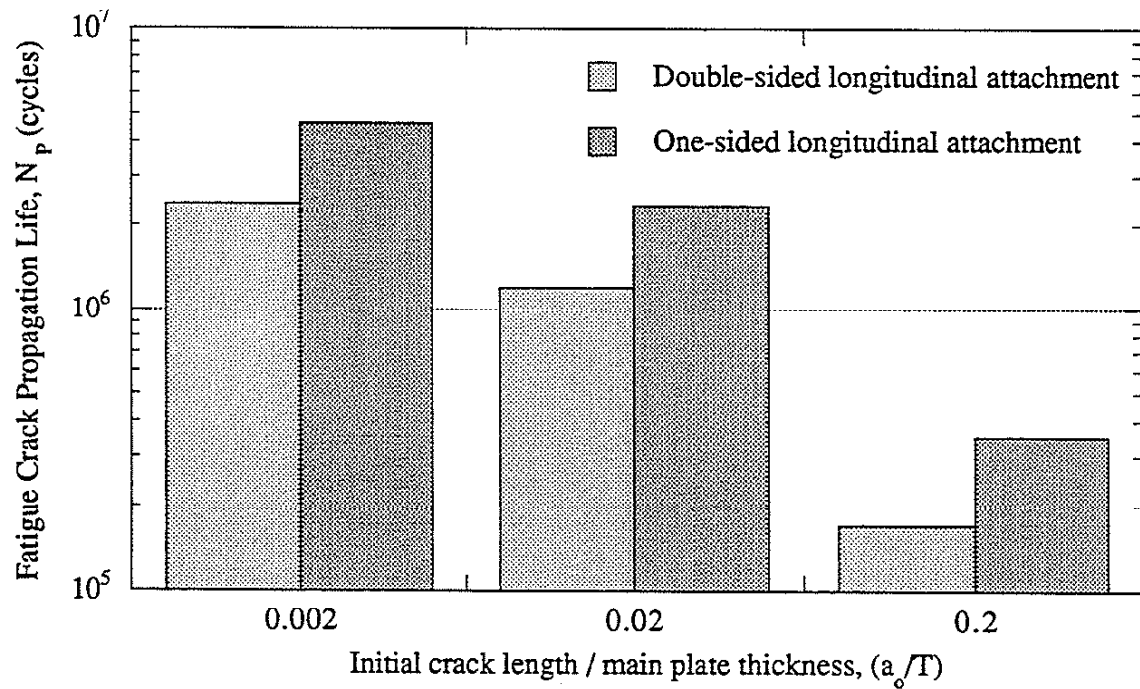


(b)

Fig. 3.9 The effect of bending load as opposed to axial load on (a) the weld geometry correction factor and (b) the fatigue crack propagation lives of longitudinal attachments. ($\Delta S = 100$ MPa)



(a)



(b)

Fig. 3.10 The effect of one-sided longitudinal attachment on (a) the weld geometry correction factor and (b) the fatigue crack propagation lives of longitudinal attachments. ($\Delta S = 100$ MPa)

CHAPTER 4

IMPROVING THE FATIGUE LIFE OF LONGITUDINAL ATTACHMENTS
WITH THE USE OF STRESS DIFFUSERS

4.1 INTRODUCTION

The previous chapters have documented the poor fatigue performance of longitudinal attachments. The poor fatigue performance was found to be primarily due to the combination of the high stress concentration, the very high tensile residual stresses, and the poor weld quality associated with the welds at the ends of the attachments. Currently, post-weld improvement techniques are the only method available to improve the fatigue life of longitudinal attachments. Unfortunately, post-weld improvement techniques are often quite expensive and sometimes unreliable [18] and are therefore rarely used.

In this chapter, improving the fatigue life of longitudinal attachments by modifying the geometry of their welds geometry will be explored. Specially designed parts termed “stress diffusers” were incorporated in the wrap-around welds at the ends of the longitudinal attachments. These added parts reduced the stress concentrations at these locations and improved the predicted fatigue resistance to equal that of weldments with transverse attachments.

4.2 IMPROVING THE FATIGUE LIFE OF LONGITUDINAL ATTACHMENTS

Longitudinal attachments exhibit very short fatigue lives because of the combination of the high stress concentration, very high tensile residual stresses, and poor weld quality associated with the welds at the end of the attachments. Therefore, in order to obtain any increases in the fatigue lives of longitudinal attachments, the stress concentration and/or the tensile residual stresses of the longitudinal attachment would have to be reduced and/or the weld quality would have to be improved. Very high tensile residual stresses and poor weld quality are inherently associated with the welds of the longitudinal attachments, therefore, attempts were made to reduce the high stress concentration.

4.2.1 Simple Modifications of Weld Detail Geometry

The 3-D FEM results in Chapter 3 revealed a high stress concentration at the toe of the wrap-around weld at the end of the attachment: see Fig. 3.4. In order to reduce the stress

concentration at this location, one can modify the existing geometry (plates and/or weld) of the longitudinal attachment to reduce the stiffness at the end of the attachment. First, simple modifications commonly used to reduce the high stress concentration of transverse attachments were considered to determine if these simple modifications would reduce the stress concentration of longitudinal attachments. Variations in the attachment height and the bevel angle were found to have an insignificant effect on the high stress concentration. The introduction of holes into the attachment plate near the end of the attachment was also investigated, but these holes had no significant effect on the high stress concentration of longitudinal attachments. Eliminating wrap-around welds and stopping the weld even with the ends of the attachment¹ was found to increase the stress concentration and the weld geometry correction factor and worsen the situation.

4.2.2 Development of "Stress Diffusers"

Since simple modifications of the longitudinal attachment did not effectively reduce the high stress concentration, significant changes in the geometry of the longitudinal attachment were considered. It would be ideal to eliminate the 3-D stress-concentrating effects and alter the stress distribution in the longitudinal attachment to be the same as the stress distribution in a transverse attachment, and hence obtain the same fatigue life. It is highly unlikely that the 3-D stress-concentrating effects can be completely eliminated, but it is realistic to imagine that the 3-D stress-concentrating effects can be minimized so that the stress distribution in the longitudinal attachment is similar to that of a transverse attachment. The goal of these modifications would be to increase the fatigue life of the longitudinal attachment to that of a transverse attachment. Therefore, comparisons with the stress concentration and fatigue life in a transverse attachment will be considered throughout this analysis as a benchmark.

Specially designed parts termed "stress diffusers" were incorporated in the wrap-around weld at the ends of the longitudinal attachments. These added parts reduced the stress concentrations at these locations by diffusing stress along a greater portion of the weld toe. The shapes of the stress diffusers in Fig. 4.1 have been optimized by trial and error with the use of 3-D FEM analyses. Many different types and shapes of stress diffusers were evaluated: see Fig. 4.1.

The most effective and final stress diffuser shape is shown at the bottom of Fig. 4.1, and an isometric view of the shape is shown in Fig. 4.2. The addition of stress diffusers in

¹ The stress concentration is highly dependent on the radius modeled.

the longitudinal attachment is shown in Fig. 4.2. The dimensions of the stress diffuser are shown in Fig. 4.3. The dimensions of the longitudinal attachment with stress diffusers are shown in Fig. 4.4.

4.3 FEM RESULTS OF STRESS DIFFUSERS

The longitudinal attachment with stress diffusers modeled in Pro/MECHANICA is shown in Fig. 4.5 as a fringe plot of the maximum principal stresses. A weld toe radius of 1.00 mm was assumed for the FEM results presented in this section. The stress concentrations are seen to be fairly uniform along the entire weld toe. In Fig. 4.5, fringe plots of the maximum principal stresses for the longitudinal attachment and the longitudinal attachment with stress diffusers with weld leg lengths of 12.7 mm are compared.

It can be seen that the stress diffuser effectively reduces the high stress concentration at the end of the attachment by diffusing stress along a greater portion of the weld toe. The maximum weld toe stress concentration factor (K_t) for the longitudinal attachment was found to be 2.64. The introduction of stress diffusers decreased the maximum K_t to 2.03 (23%). For the details modeled with 9.52 mm weld leg lengths, the use of stress diffusers reduced the maximum weld toe stress concentration factors from 2.73 to 1.96 (28%).

The weld geometry correction factor (M_k) was then calculated using the superposition method for both weld details and compared in Fig. 4.7a. The use of stress diffusers leads to significant decreases in M_k . Significant increases in the fatigue crack propagation life are predicted with the use of stress diffusers: see Fig. 4.7b. The predicted increases in propagation life are 1.9 to 2.7 times longer depending on the initial crack length assumed in the LEFM predictions.

The M_k determined for both weld details was plotted in Fig. 4.8a along with the M_k determined from a 2-D FEM analysis of the longitudinal attachment (i.e. transverse attachment). As can be seen from Fig. 4.8a, the use of stress diffusers decreases M_k of the longitudinal attachment to values less than those determined from a 2-D FEM analysis (i. e. transverse attachment). The 3-D stress-concentrating effects have been eliminated. With the use of stress diffusers, the fatigue crack propagation life of a longitudinal attachment is predicted to be the same or even longer than that of a transverse attachment depending on the initial crack length assumed: see Fig. 4.8b.

4.4 SUMMARY

Specially designed parts termed “stress diffusers” were incorporated in the wrap-around welds at the ends of the longitudinal attachments. These added parts reduced the stress concentrations at these locations and improved the predicted fatigue resistance of such weldments to equal that of weldments with transverse attachments.

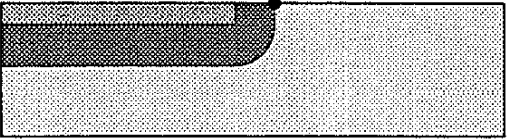
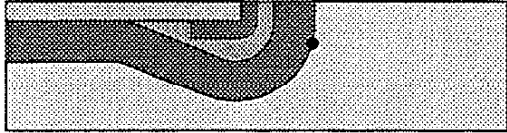
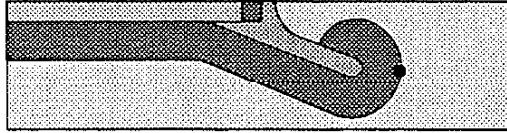
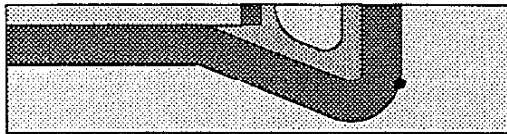
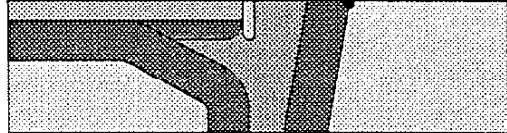

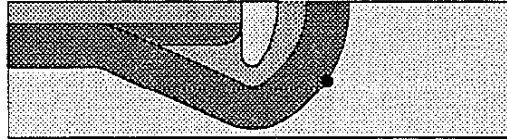
Shape	K_t	Remarks
	2.64	Weldment with longitudinal attachment
	2.52	Early attempt with stress diffuser. Stress concentrations at hot spot not much affected
	2.43	Idea of grabbing stress out in the plate away from the attachment. Somewhat better.
	2.32	Idea of reducing stress at the centerline by reducing the stiffness of the stress diffuser at the center by introducing a hole in it.
	2.17	Idea of widening the stress diffuser and inclining its shoulders.
	2.12	Extremely wide stress diffuser becomes a virtual transverse attachment. Low K_t achieved.
	2.03	Highly evolved and current final design. Stress concentration reduced to approximately that of a transverse attachment.

Fig. 4.1 Plan view of one octant of the stress diffuser concepts. The final and most effective shape is at the bottom and reduced the K_t of the weldment with longitudinal attachments from 2.64 to 2.03, a reduction of about 23%.

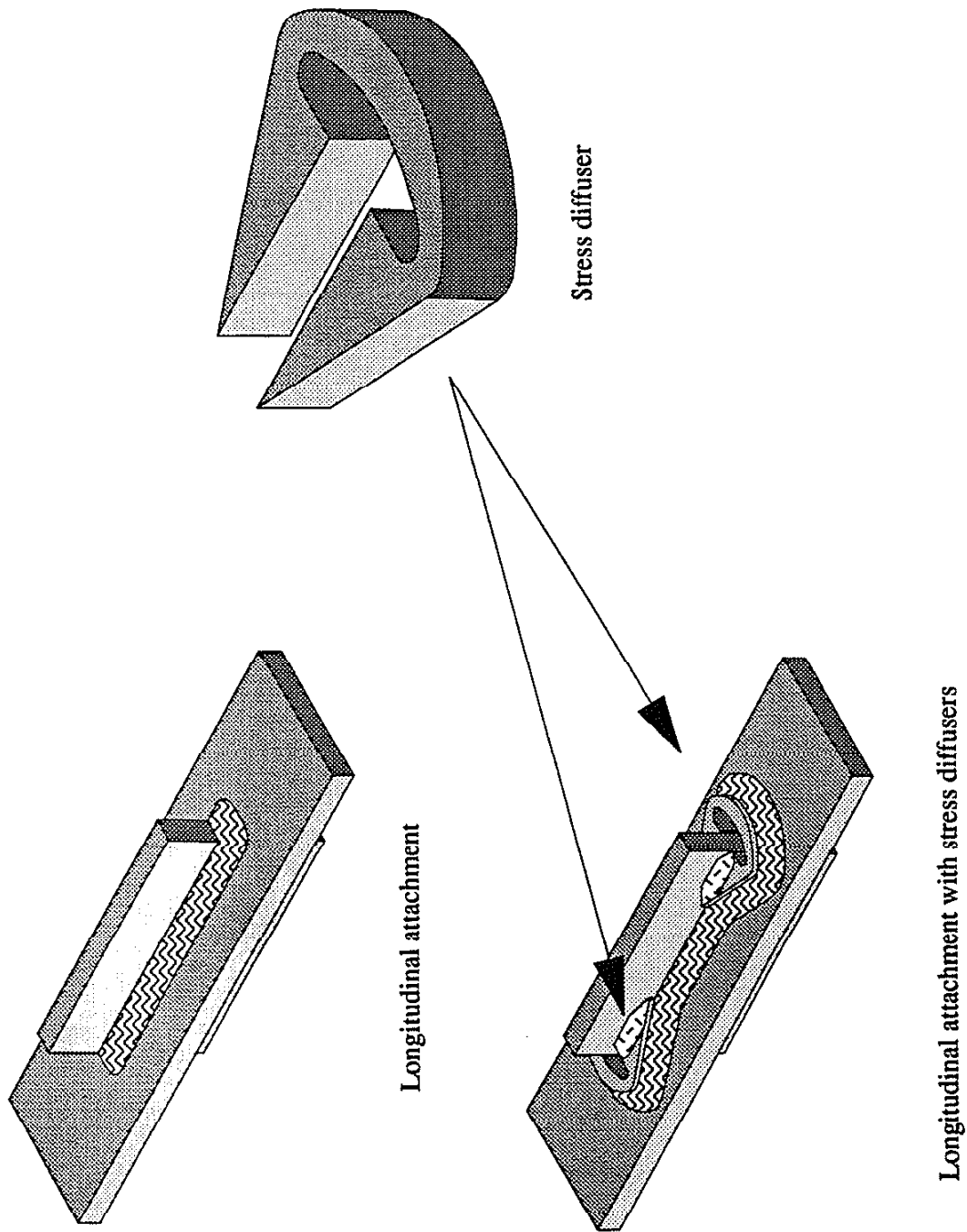


Fig. 4.2 (Above) Longitudinal attachment. (Below) Added stress diffuser at right incorporated in longitudinal attachment.

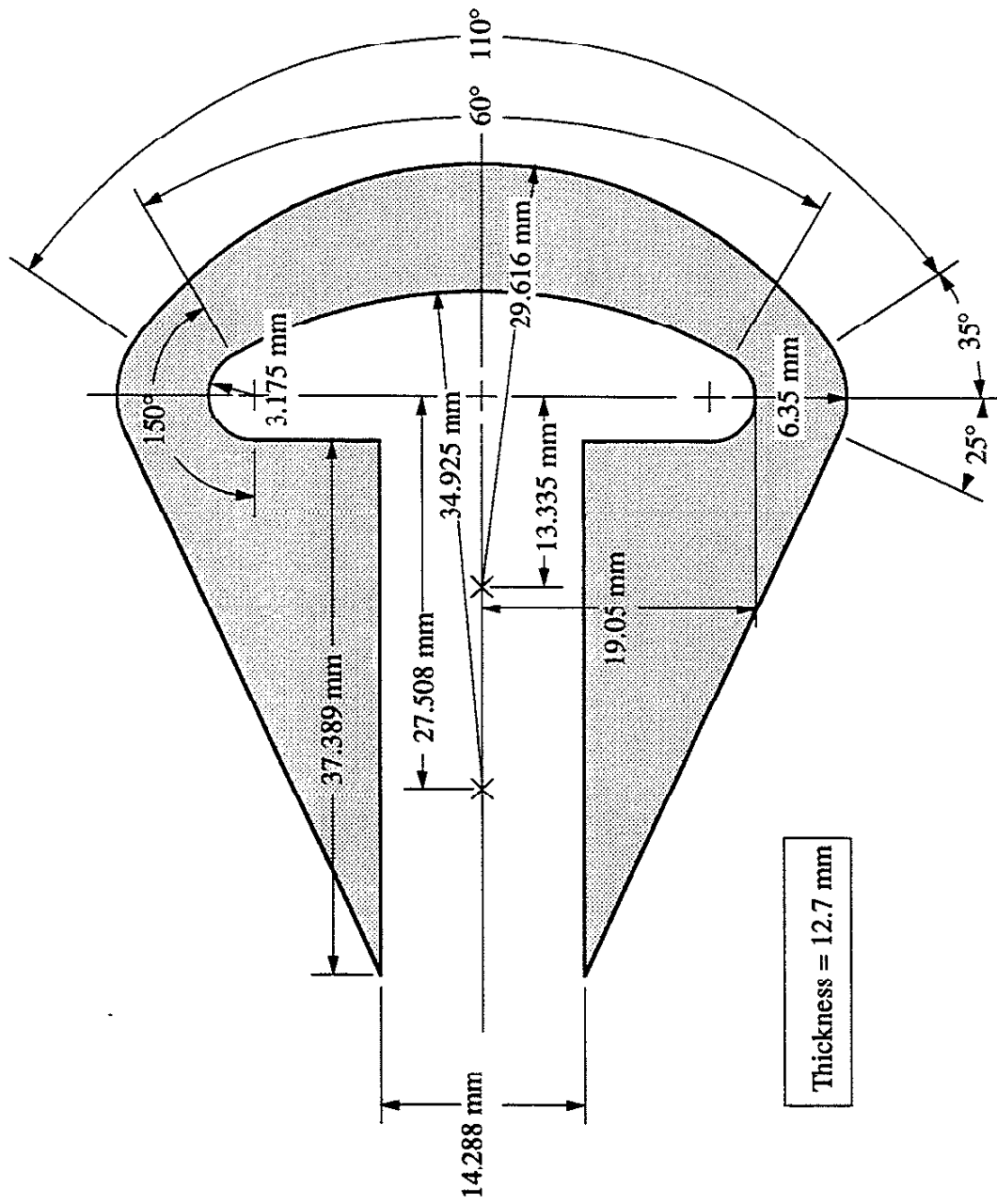


Fig. 4.3 The dimensions of the stress diffuser modeled and used in the testing program.

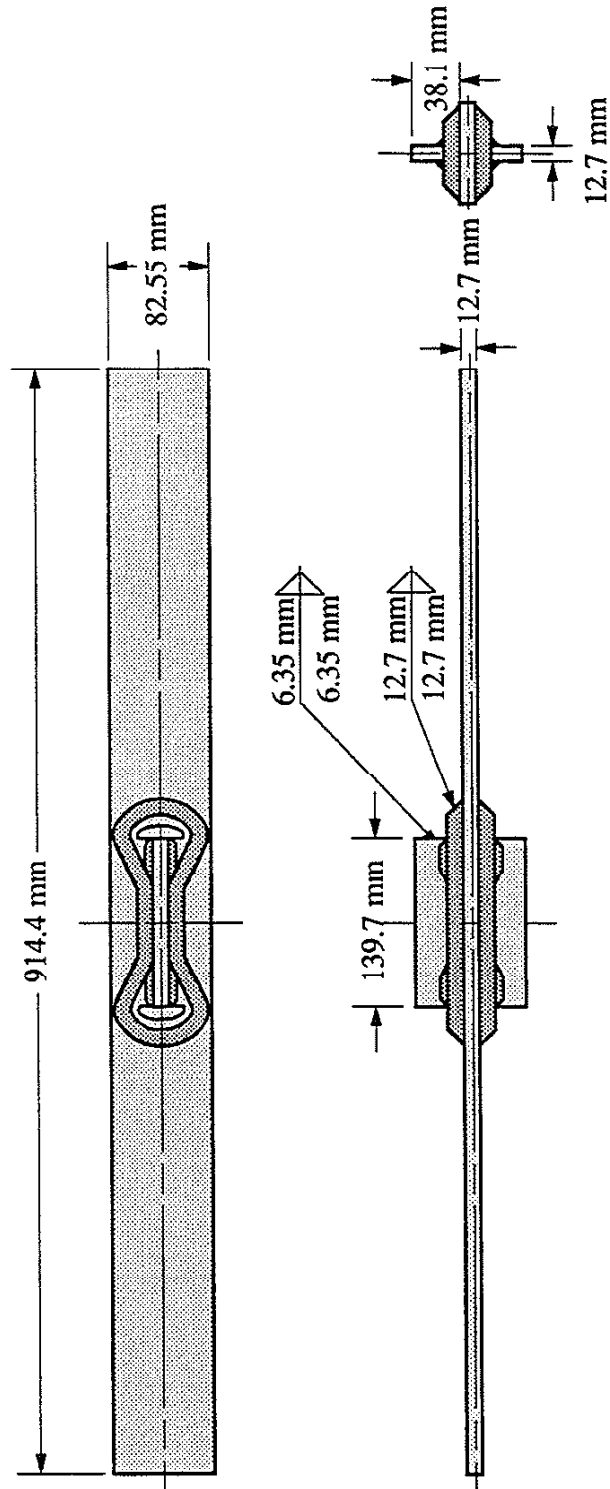


Fig. 4.4 The dimensions of the longitudinal attachment with stress diffusers modeled and used in the testing program. The drawing shows welds with 12.7 mm weld leg lengths for the lower weld and 6.35 mm. leg lengths for the upper weld.

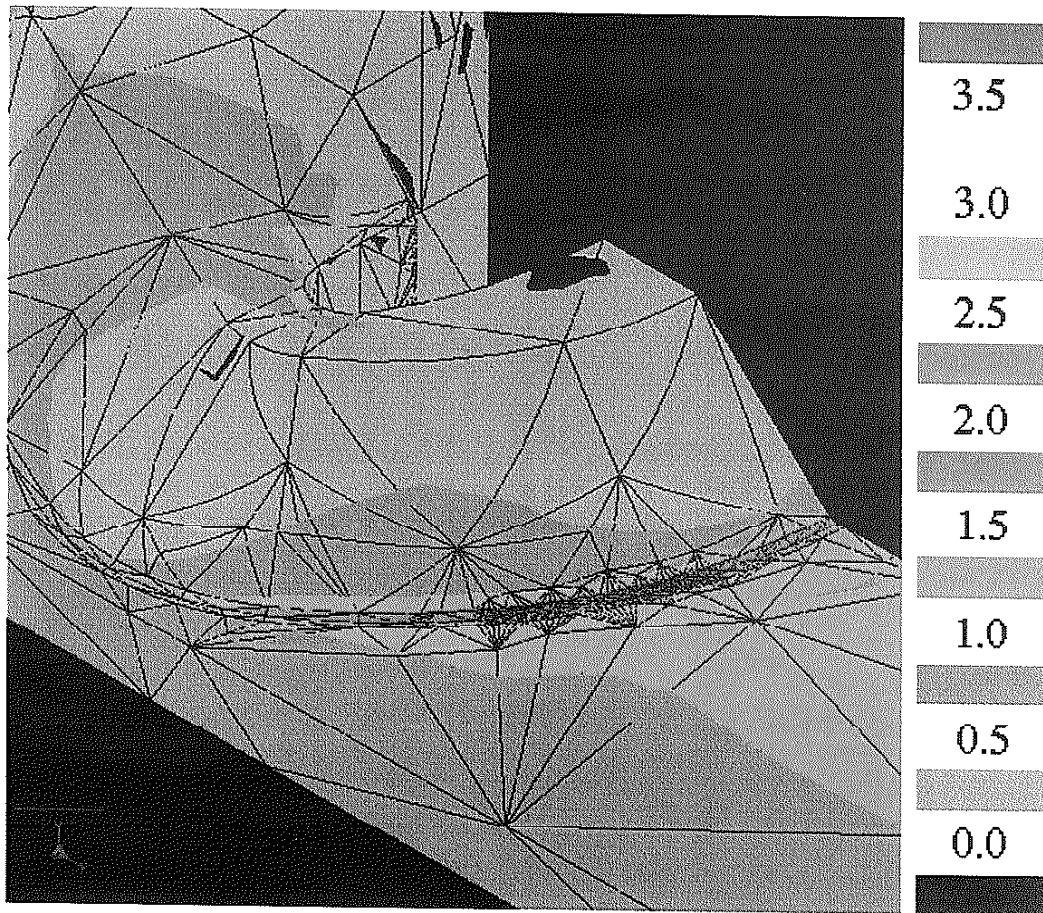
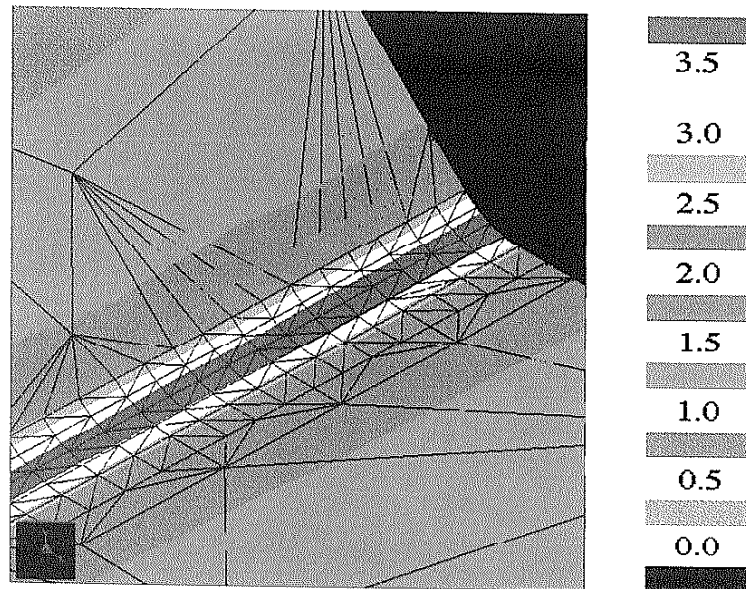
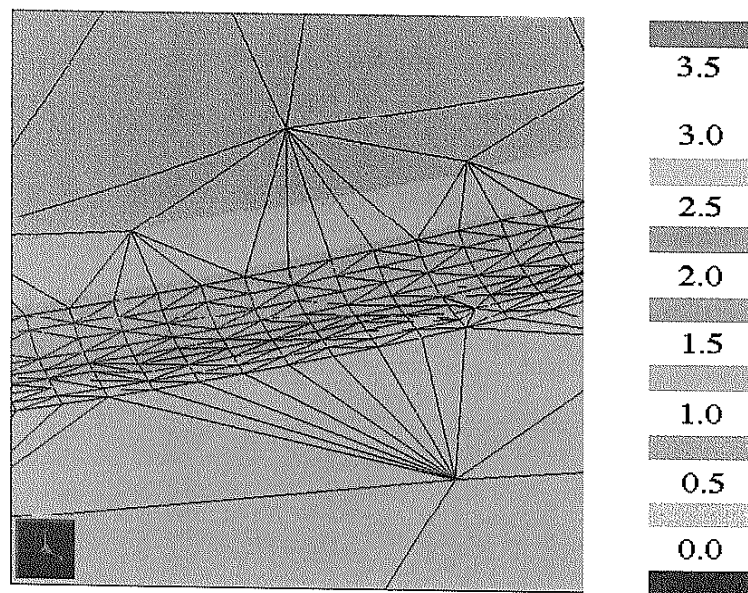


Fig. 4.5 The modeling of a stress diffuser in a longitudinal attachment presented as a fringe plot of maximum principal stress. One octant of the geometry is modeled due to planes of symmetry.

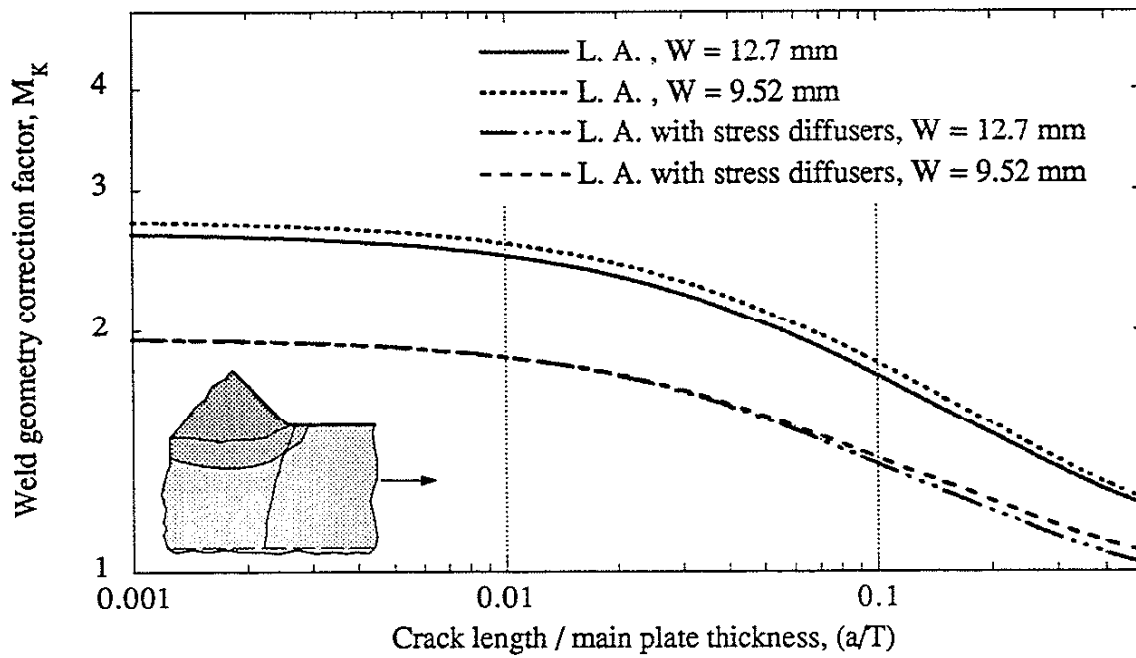


Longitudinal attachment

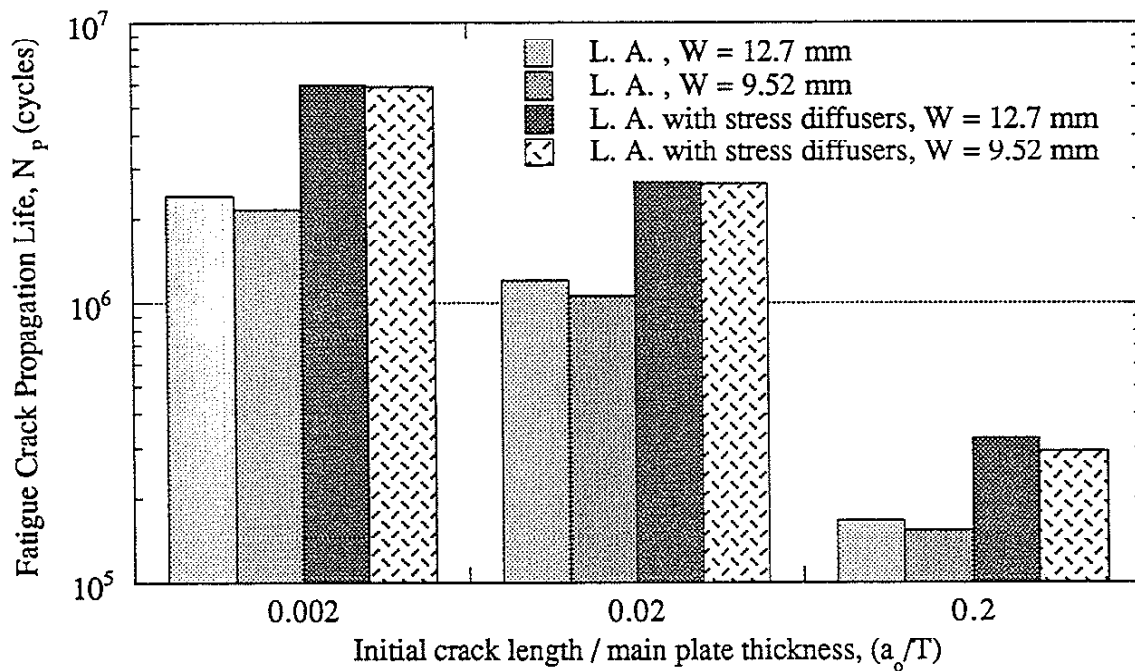


Longitudinal attachment with stress diffuser

Fig. 4.6 The effectiveness of using a stress diffuser to reduce the maximum principal stresses at the weld toe region. Fringe plots of the maximum principal stress at the critical weld toe regions for the longitudinal attachment (Above) and the longitudinal attachment with a stress diffuser (Below).

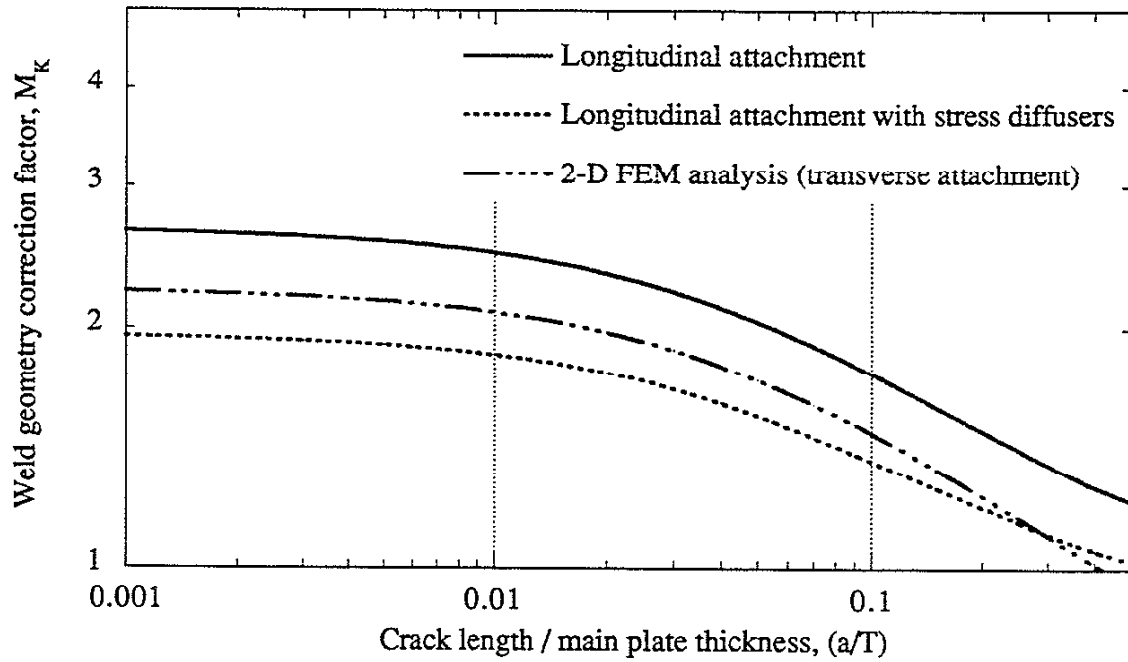


(a)

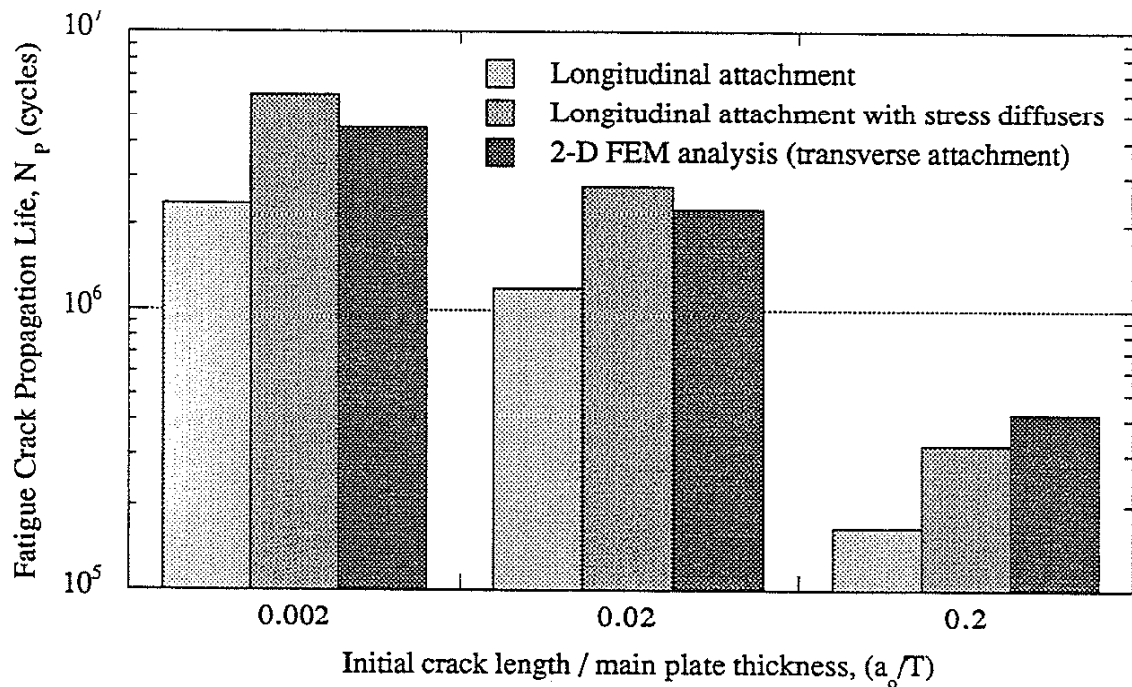


(b)

Fig. 4.7 The predicted effectiveness of the use of stress diffusers on (a) the weld geometry correction factor and (b) the fatigue crack propagation lives of longitudinal attachments. ($\Delta S = 100$ MPa)



(a)



(b)

Fig. 4.8 Comparison of (a) the weld geometry correction factor and (b) the fatigue crack propagation lives of longitudinal attachments with stress diffusers and transverse attachments. ($\Delta S = 100$ MPa)

CHAPTER 5

EXPERIMENTAL STUDY OF LONGITUDINAL ATTACHMENTS WITH STRESS DIFFUSERS

5.1 INTRODUCTION

In this chapter, the results of experiments conducted to verify the predicted increases in fatigue life obtained by using stress diffusers with longitudinal attachments will be presented.

5.2 PROCEDURES

5.2.1 Specimen Fabrication

Specimens were fabricated from a SAE/AISI 1020 mild steel to the dimensions shown in Fig 4.3 and 4.4. Two series of specimens (Series 1 and 3) were fabricated for the longitudinal attachments with stress diffusers. These specimens used the same fabrication procedures and welding process as the longitudinal attachments presented in section 2.2.1 and were therefore given the same series number for consistency. Specimens were not made for Series 2 because it was realized that the welding procedure would give rise to cold-lap defects.

The weld sequence employed is shown in Fig. 5.1 and was devised to limit the weld distortions. All of the welds around the stress diffuser were made first, and then the longitudinal fillet welds were made. Starts and stops were not permitted in front of the stress diffusers in order to avoid the effect of serious weld defects usually associated with them.

5.2.2 Testing Procedure

To determine the magnitude of the bending stresses induced during testing, four strain gauges were mounted on each specimen as shown in Fig. 5.1. The strain gages were placed at a distance of $2T$ from the weld toe so that the stress concentrating effects of the weld itself would not be measured. These specimens were tested with the same testing procedures of the longitudinal attachments presented in section 2.2.2.

5.3 EXAMINATION OF SPECIMENS

5.3.1 Weld Toe Geometry

The weld toe geometry of untested specimens from Series 1 and Series 3 were examined by sectioning the specimens along the weld toe region in front of the stress diffuser. All sections of the specimens from Series 1 revealed the presence of cold-lap defects; therefore, the weld toe radius and angle were not measured for these specimens. A typical cold-lap defect observed for the specimens of Series 1 can be seen in Fig. 5.2. The results of the measurements for the sections of specimens for Series 3 are listed in Table 5.1. A typical weld toe for the specimens of Series 3 showing the weld toe radius and local weld toe angle can be seen in Fig. 5.2. The average weld toe radius (r) was found to be 0.27 mm. The mean was found to 0.27 mm with a standard deviation of the log r of 0.33. The average overall and local weld toe angles were both found to be 40° with standard deviations of 5.0° and 9.1° , respectively.

5.3.2 Residual Stresses

A longitudinal attachment with stress diffusers from Series 3 was sent to Lambda Research for the determination of residual stresses. The measurements were made adjacent to the weld toe at the surface and at 0.46 mm below the surface. The measurements were made using the X-ray diffraction technique in accordance with SAE J784a. The residual stress measurement at the surface and 0.46 mm below the surface were found to be 252 and 124 MPa, respectively: see Table 5.2. The residual stress measurement at the surface approaches the yield strength of the base metal.

The surface residual stress measurement of 252 MPa shows a significant decrease when compared to the surface residual stress measurement of 595 MPa found for the longitudinal attachment. A reduction in surface residual stress of approximately 58% is obtained with the use of stress diffusers. This observation confirms the hypothesis made in the previous chapter that residual stresses would be reduced since the weld will change from being longitudinal to being nearly transverse in the critical region at the front of the stress diffuser. It should be noted that these stresses are higher than the values reported elsewhere, but this may be due to the higher heat input of the welding process used in the fabrication process of Series 3.

5.4 THE FATIGUE STRENGTH OF LONGITUDINAL ATTACHMENTS WITH STRESS DIFFUSERS

The fatigue test results for Series 1 and 3 are listed in Table 5.2 and plotted in Fig. 5.3. Large bending stresses were encountered in the testing, but these were measured and accounted for in the results. The bending stresses measured near the failure location are listed in the final column of Table 5.2. At long lives (low stresses), the specimens of Series 3 exhibit much longer fatigue lives than the specimens of Series 1. For longitudinal attachments with a fatigue life of $2E+06$ cycles, increases of 360% in fatigue life and 32% in fatigue strength were obtained with the use of stress diffusers. The increase in fatigue life for the specimens of Series 3 could result from the elimination of cold-lap defects.

The fatigue test results for the longitudinal attachments with stress diffusers are plotted along with the fatigue test results for the longitudinal attachments in Fig. 5.4. Significant increases in fatigue life can be seen with the use of stress diffusers at long lives (low stresses) for specimens of Series 3. At short lives (high stresses), the use of stress diffusers was not as effective.

5.5 POST-TEST EXAMINATION OF SPECIMENS: COLD-LAP DEFECTS

As mentioned previously, the evaluation of the weld toe geometry of specimens from Series 1 revealed the existence of cold lap defects. Examination of the fracture surfaces revealed that the fatigue cracks in Series 1 initiated from these cold-lap defects. The cold-lap defects were measured, and the depth(s) of the cold-lap defect(s) at the failure location for each specimen are listed in Table 5.2. The average size of the largest cold-lap defect found in each specimen for Series 1 was approximately 1.4 mm.

These results are consistent with the results in the experimental study of the longitudinal attachment in Chapter 2 where specimens of Series 1 had cold-lap defects and specimens of Series 3 had no defects. However, the average cold-lap defect depth of specimens of Series 1 reduced from 2.1 mm. to 1.4 mm with the use of stress diffusers. The use of stress diffusers eliminates need for wrap-around welds (welding around the attachment plate), thus the stress diffuser allows greater control of the welding process and thus a lesser number of smaller welding defects are formed.

5.6 SUMMARY

The predicted increase in the fatigue life of longitudinal attachments with the use of stress diffusers was verified experimentally. For longitudinal attachments with a fatigue life of $2\text{E}+06$ cycles, increases of 360% in fatigue life and 32% in fatigue strength were obtained with the use of stress diffusers. The residual stresses were shown to decrease from 595 MPa to 252 MPa (58 % reduction) with the use of stress diffusers. In addition, the weld quality was shown to improve with the use of the stress diffusers: the average cold-lap defect depth was reduced (2.1 to 1.4 mm), and the average weld toe radius increased (0.08 to 0.27 mm).

Table 5.1 The weld toe geometry of the longitudinal attachments with stress diffusers of Series 3.

Measurements	8
Average Radius, r (mm)	0.27
Average Overall Weld Toe Angle (°)	40
Average Local Weld Toe Angle (°)	40

Table 5.2 Residual stress measurements made on the longitudinal attachments with stress diffusers of Series 3.

Depth (mm)	a/T	Residual Stress (MPa)	Error (MPa)	Peak Width (°)
0.00	0.000	+252	± 12	2.20
0.46	0.036	+124	± 24	1.81

Table 5.3 The fatigue test results for Series 1 and Series 3.

Series 1:

Specimen	Corrected Stress Range (MPa)	Fatigue Life (cycles)	% Bending Stress at Failure Location	Cold-Lap Defect Depth(s) (mm)
SD-1-1	107.0	4.146E+06	21.0	1.2, 1.3, 1.2
SD-1-2	105.8	3.514E+06	40.3	1.3, 0.75
SD-1-3	239.1	1.428E+05	12.7	1.2, 1.0, 0.75
SD-1-4	158.0	6.128E+05	14.6	1.25, 1.0, 1.0, 1.25
SD-1-5	67.1	6.321E+06	-11.0	2.0, 1.5, 0.75, 1.0

Series 3:

Specimen	Corrected Stress Range (MPa)	Fatigue Life (cycles)	% Bending Stress at Failure Location	Cold-Lap Defect Depth(s) (mm)
SD-3-1	98.7	3.770E+06	5.5	-
SD-3-2	99.8	1.331E+07*	6.7	-
SD-3-3	191.1	3.172E+05	5.9	-
SD-3-4	130.2	1.047E+06	8.2	-
SD-3-5	159.0	6.455E+05	9.1	-
SD-3-6	124.5	2.263E+06	16.5	-
SD-3-7	93.1	1.030E+07*	1.9	-

* Runout

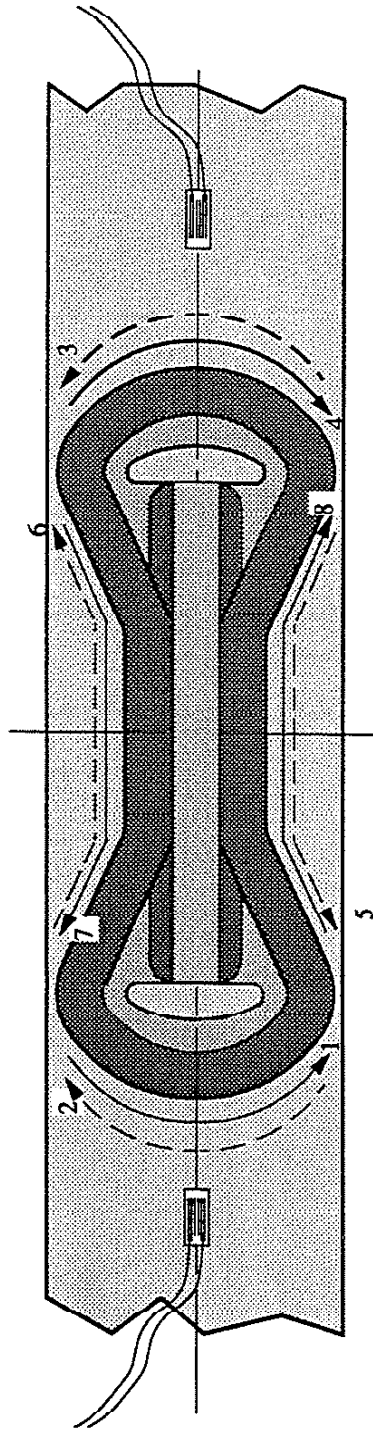
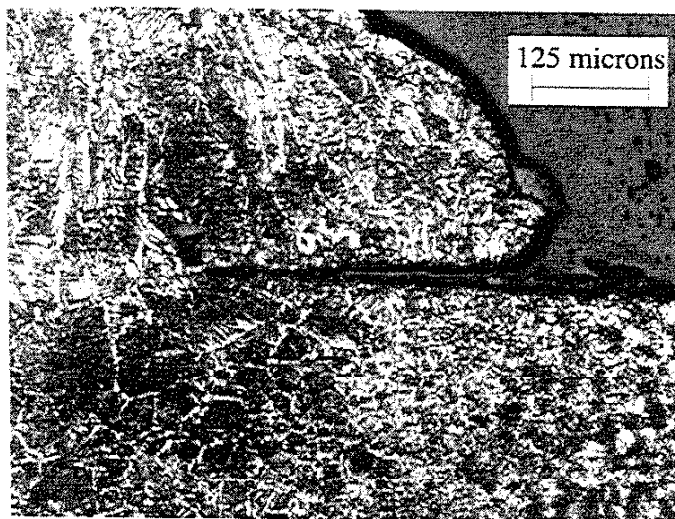
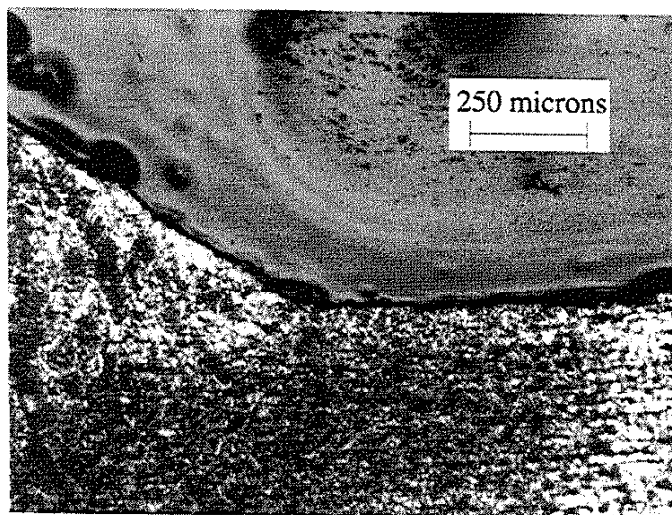


Fig. 5.1 Weld sequencing and strain gauging for the longitudinal attachments with stress diffusers . The solid arrows indicate the welds on top of the specimen and the dashed arrows indicate the welds below the specimen. The strain gages were placed at a distance 2T from the weld toe.



Series 1



Series 3

Fig. 5.2 (Above) A typical cold-lap defect observed for the longitudinal attachments with stress diffusers of Series 1 (125X). (Below) A typical weld toe for the longitudinal attachments with stress diffusers of Series 3.

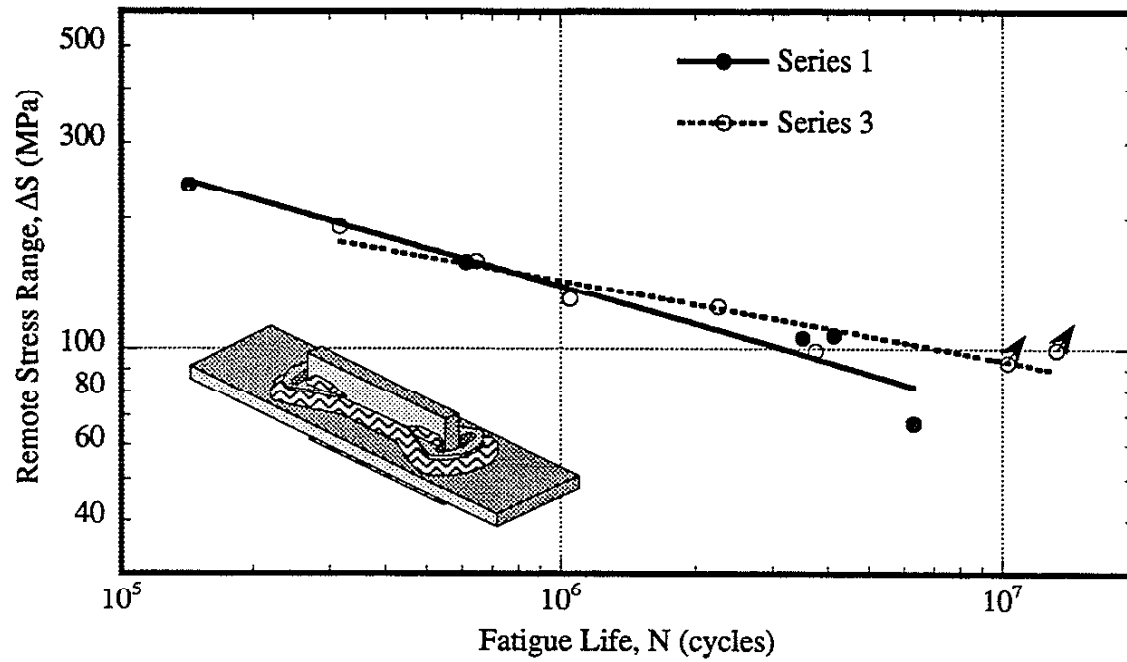


Fig. 5.3 The fatigue test results of longitudinal attachments with stress diffusers. The data has been corrected for bending stresses.

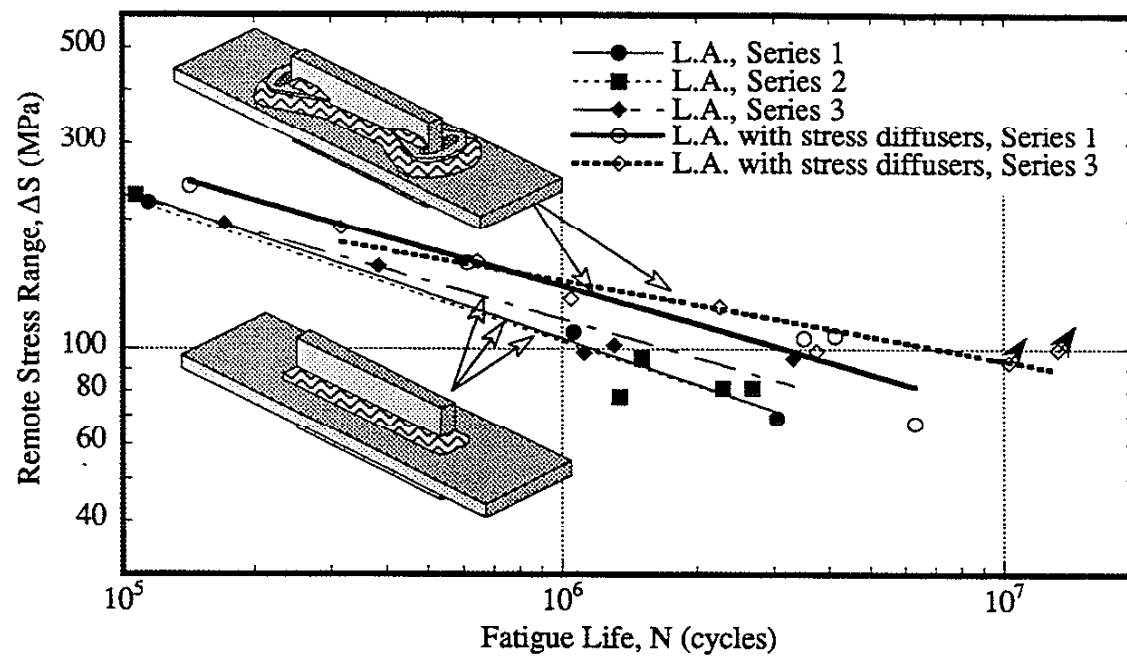


Fig. 5.4 The effect of using stress diffusers on the fatigue life of longitudinal attachments. The data has been corrected for bending stresses.

CHAPTER 6

APPLICATION OF STRESS DIFFUSERS TO A BEAM-TO-COLUMN CONNECTION

6.1 INTRODUCTION

6.1.1 Northridge Beam-to Column Connections

Fracture occurred in the welded steel moment-frames of many large buildings during the Northridge earthquake. Extensive cracking was found particularly in the welded beam-to-column connections. A typical pre-Northridge welded beam-to-column connection is shown in Fig. 6.1. Cracking occurred in a region of high stress concentration at the intersection of the bottom beam flange and column flange. The cracks started from the backing bar which acts as a stress raiser [35]: see Fig. 6.1.

Since the Northridge earthquake, many researchers [35,36] have investigated the beam-to-column connection. Improvements in the connection were made by modifying or even eliminating the backing bar and by overmatching the weld metal to beam flange yield strength. Even with these modifications, researchers still observed cracks at the intersection of the bottom beam flange and column flange. In addition, cracks have also been observed to start from the weld access hole which acts as a stress raiser.

The very high stresses in the regions of high stress concentration in the beam-to-column connection were analyzed, and the feasibility of using a stress diffuser to reduce these high stress concentrations is demonstrated.

6.2 PROCEDURES

6.2.1 Beam-to-Column Connection Modeling

The dimensions and loading conditions of the beam-to-column connection modeled are shown in Fig. 6.2. These dimensions and loading conditions were selected to model full-scale tests that will be carried out in the future at Texas A&M University¹. The dimensions of the weld access hole (Fig. 6.2) were chosen to satisfy the requirements in the Structural Steel Welding Code (ANSI/AWS D1.1-98)[37].

¹ The modeling of the beam-to-column connection was carried out to supplement the studies of Gary T. Fry at Texas A&M University which consists of both theoretical and experimental work.

All modeling was carried out in three dimensions (3-D), and all analyses were elastic. Since a plane of symmetry exists in the y direction, only half of the connection was modeled thereby reducing the size of the required mesh.

6.3 FEM RESULTS

6.3.1 Beam-to-Column Connection

The stress concentrations associated with two different regions were studied. The first region of interest was the weld access hole, and the second region of interest was the intersection of the bottom beam flange and column flange. In order to obtain accurate stresses for both regions from one analysis, both regions would have to be finely meshed. This course of action would lead to a very large and inefficient analysis; therefore, separate analyses were made in which mesh refinement was fine in only one region of interest.

A view of the entire beam-to-column connection modeled with Pro/MECHANICA STRUCTURE can be seen in Fig. 6.3. A close-up view of the beam-to-column connection showing the detail of the weld access hole can be seen in Fig. 6.4.

In all of the FEM analyses presented in this study, a displacement of a 1/2" was applied to the beam-to-column connection as shown in Fig. 6.2. First, the weld access hole was modeled, and the resulting maximum principal stresses are presented as fringe plots of maximum principal stress in Fig. 6.4. As can be seen from Fig. 6.4, many elements were used at the intersection of the beam flange and the weld access hole in order to obtain an accurate estimate of the peak stresses in the region. The peak maximum principal stress was found to be 53.4 ksi. As seen in Fig. 6.4b, the loads in the structure are transferred through the weld access hole region to the intersection of the bottom beam flange and the column flange. Thus, there is an extensive and continuous high stress region which extends from the weld access hole to the intersection of two mentioned flanges.

Next, the intersection of the bottom beam flange and column flange was modeled as shown in Fig. 6.5. Many elements were used in order to obtain an accurate estimate of the stresses in this region. Since the stresses at the intersection of the bottom beam flange and column flange approach infinity, the maximum principal stress at a location of 0.1-in. from the column face along the bottom beam flange has been selected as the location to evaluate the stresses in this region. The maximum principal stress at 0.1-in. from the column face was found to be 61.8 ksi. Local bending in the beam flange can be seen from Figs. 6.4 and 6.5.

Comparison of the fringe plots for the two locations reveals that the modeled stresses at the intersection of the bottom beam flange and column flange are higher than the modeled

stresses at the weld access hole. However, it should be noted that the weld access hole was modeled with a radius of 0.935-in. which exceeds the radius of 0.375-in. which is required in the ANSI/AWS D1.1-98 Code. In addition, the radius of the weld access hole was modeled tangent to the beam flange to provide a very smooth transition at the weld access hole which is not required in the ANSI/AWS D1.1-98 Code. Thus, if a smaller radius was modeled and/or the transition of the radius to the beam flange was not as smooth, the stresses near the weld access hole could possibly be larger than those at the intersection of the bottom beam flange and column flange.

6.3.2 Modeling of the Stress Diffuser

A stress diffuser shape slightly different than that used in Chapter 4 was developed. The stress diffuser shown in Fig. 6.6 was developed with regard to minimizing increased fabrication costs. An optimal shape of the stress diffuser for the beam-to-column connection was not developed. The stress diffuser was incorporated into the geometry of the beam-to-column connection as shown in Fig. 6.7. The FEM results for the two regions of interest are shown as fringe plots of maximum principal stress in Fig. 6.8.

With the inclusion of the stress diffuser, the peak maximum principal stress in the region of the weld access hole was reduced from 53.4 to 47.6 ksi. (10.9%). The maximum principal stress at 0.1-in. from the column face was reduced from 61.8 to 58.8 ksi. (4.9%) with the use of a stress diffuser. Unfortunately, these reductions in maximum principal stress are small.

The stress diffuser was unable to diffuse load away from the center of the connection (critical locations) and towards the edges of the connection. It is apparent from Fig. 6.8 that a significant amount of load still flowed from the beam web and into the beam flange at the weld access hole. Earlier, the stress diffuser was shown to be effective in reducing the peak stresses in the longitudinal attachment (non-load-carrying fillet welded attachment). One of the primary reasons for the effectiveness of the stress diffuser in reducing the peak stresses of the longitudinal attachment was that the longitudinal attachment consists of separate plates connected only by fillet welds. No loads could be transferred through the plates. Since loads could only be transferred through the fillet welds whose path was determined by the shape of the stress diffuser, the shape of the stress diffuser controlled how load was transferred to the attachment. Therefore, the shape of the stress diffuser effectively reduced the high stress concentration at the end of the attachment.

The beam-to-column connection differs from the longitudinal attachment in several ways. Unlike the longitudinal attachment which consists of separate plates fillet welded

together, the beam of the beam-to-column connection modeled in this study is a rolled shape in which the beam web and flanges are connected. Since the beam web and flanges are connected, load can be transferred from the beam web and flanges directly; thus, in this case the stress diffuser is less effective. In addition, the loading in the beam-to-column connection is different than the loading in a longitudinal attachment. In the longitudinal attachment, only the main plate is loaded and small amounts of load are transferred to the attachment plate. In the beam-to-column connection, significant amounts of load are transferred through the beam web and flange, especially near the weld access hole.

Thus, the beam web and flange were separated near the weld access hole so that load could not be transferred to the beam flange from the beam web near the access hole. The details of the modifications made to the beam-to-column connection can be seen in Fig. 6.9. The FEM results are presented as fringe plots of the maximum principal stress in Fig. 6.10. The separation of the beam web and flange can be seen in Fig. 6.10a. As can be seen from Fig. 6.10a, separating the beam web and flange eliminated the weld access hole as a region of high stress concentration. The maximum principal stresses at the intersection of the bottom beam flange and column flange were significantly reduced: see Fig. 6.10b. Separating the beam and web flange near the weld access hole combined with using the stress diffuser reduced the maximum principal stress at 0.1-in. from the column face from 61.8 to 42.7 ksi. or 31%: this is a significant reduction.

6.4 SUMMARY

The regions of high stress concentration in the beam-to-column connection were shown to occur at the weld access hole and the intersection of the bottom beam flange and column flange. The high stress concentrations in the beam-to-column connection were reduced by only a small amount with the use of a stress diffuser without any alteration to the existing geometry. The use of a stress diffuser with a beam-to-column connection in which the beam web and bottom flange are separated near the weld access hole was found to eliminate the high stress concentration at the weld access hole and reduces the maximum principal stresses in the region of the intersection of the bottom beam flange and column flange by 31%.

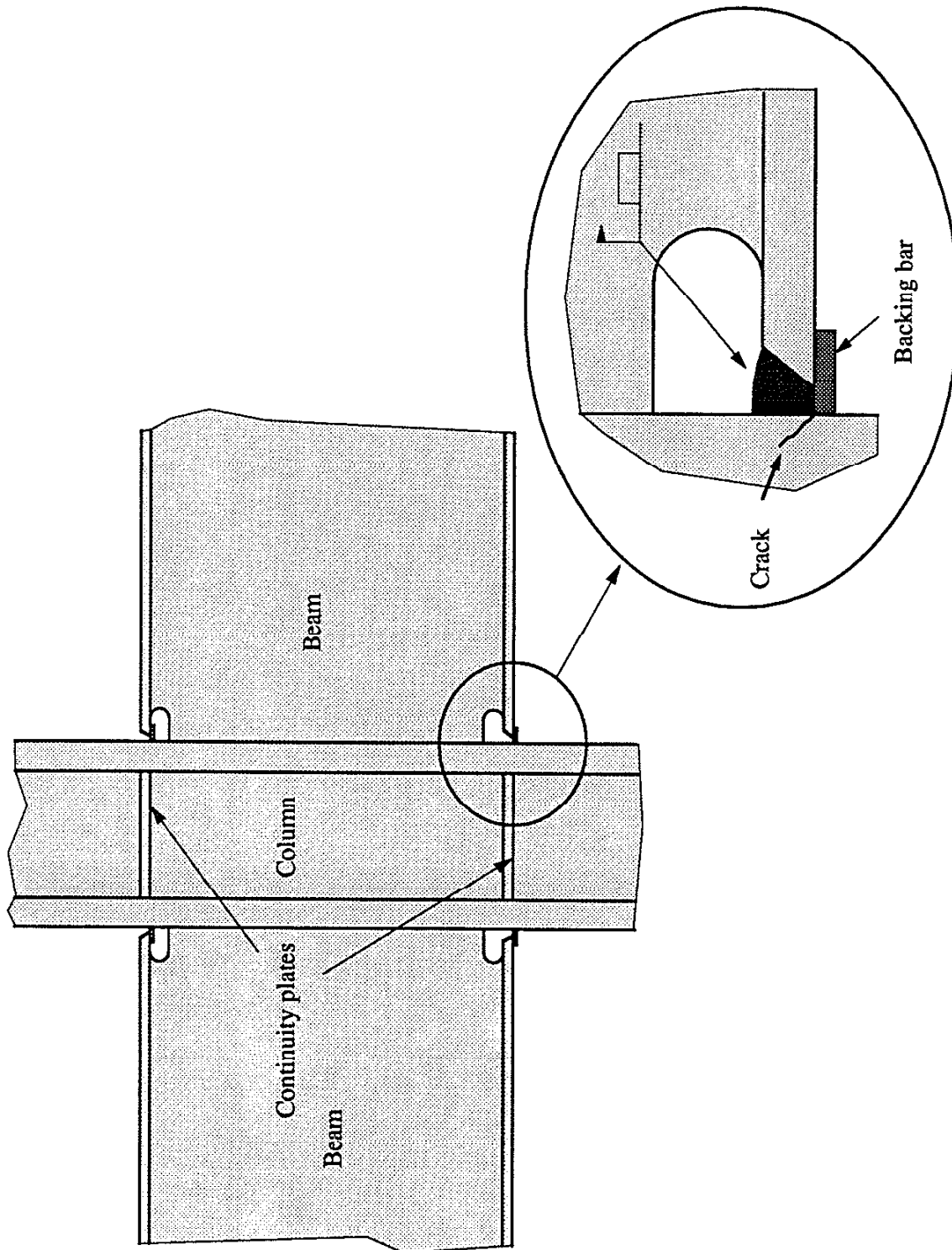


Fig. 6.1 A typical pre-Northridge beam-to-column connection. The crack starts from the backing bar.

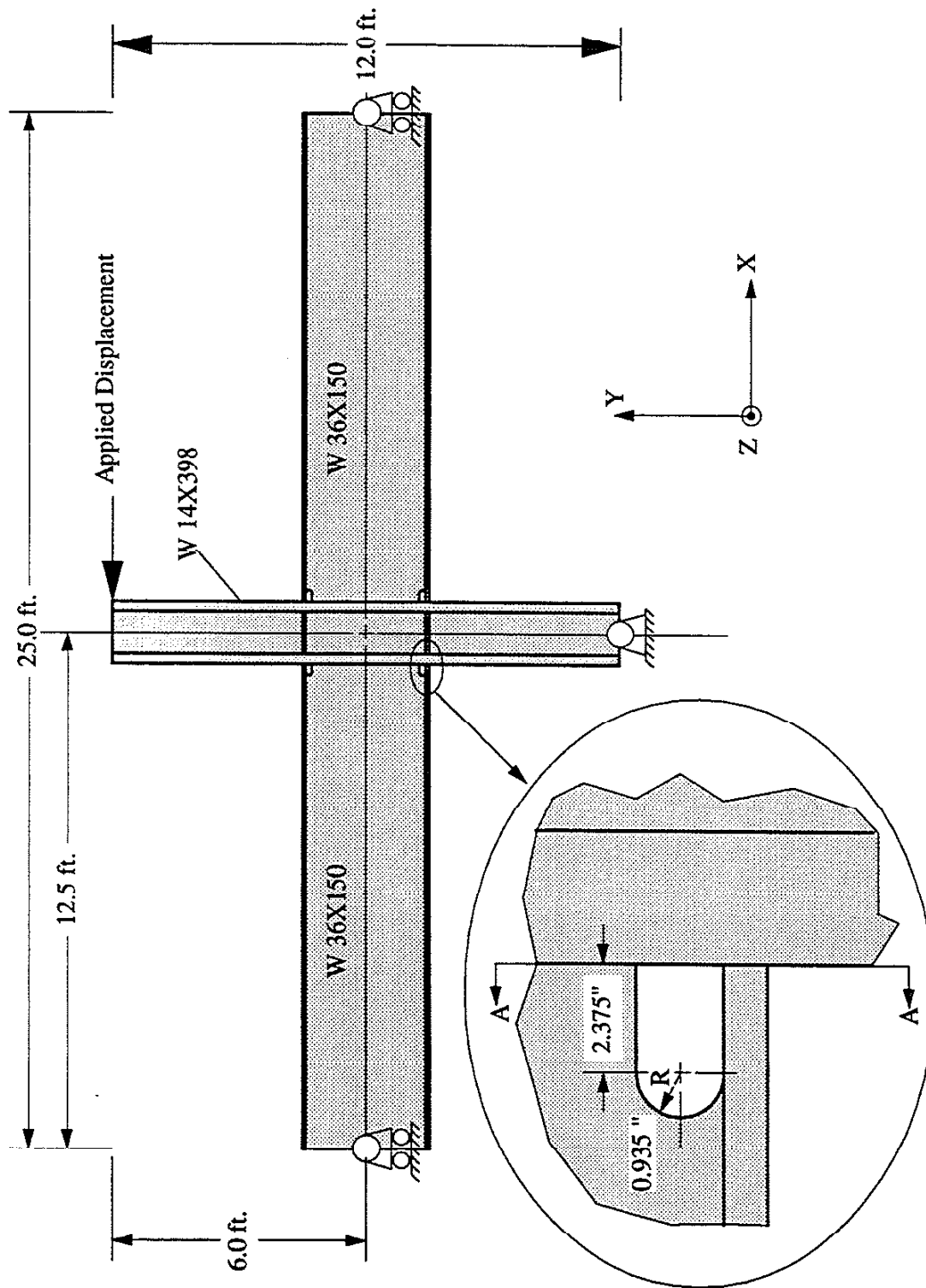


Fig. 6.2 The dimensions and loading conditions of the beam-to-column connection modeled in this study. The displacement was applied to the column as shown.

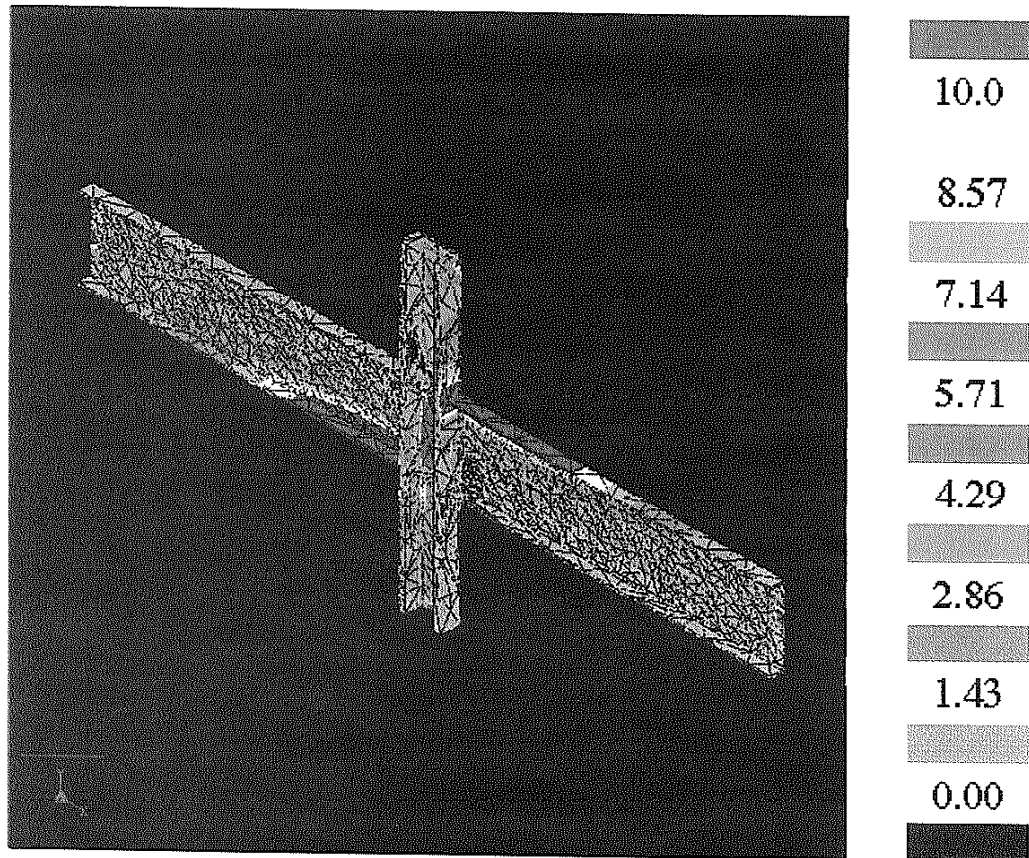


Fig. 6.3 The beam-to-column connection modeled in Pro/MECHANICA STRUCTURE. The results are presented as fringe plots of maximum principal stress in units of ksi.

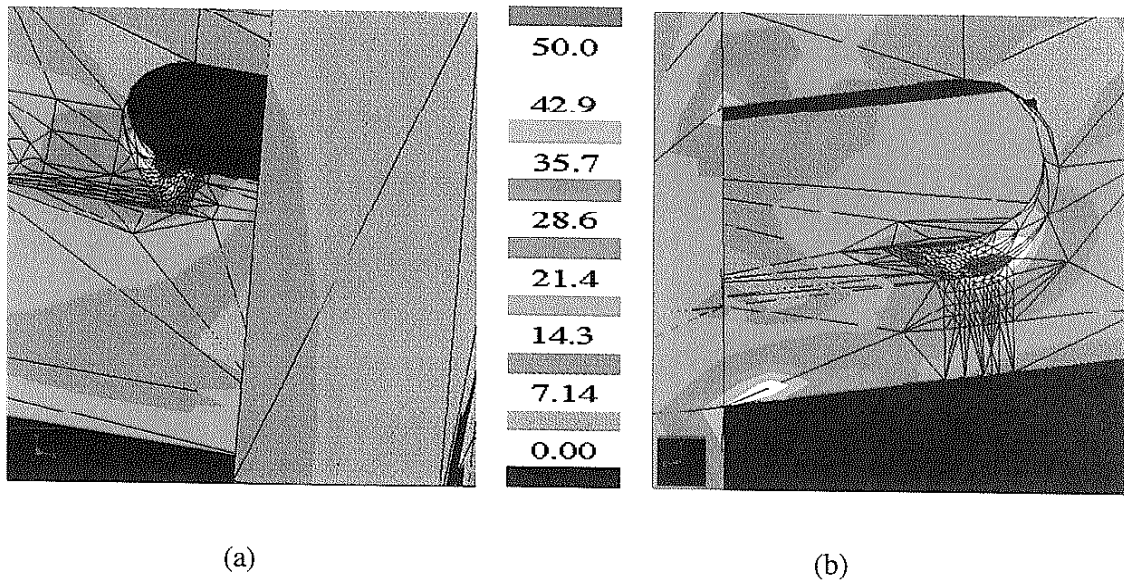


Fig. 6.4 Fringe plots of maximum principal stress (ksi) in the region of the weld access hole showing the details from two different angles.

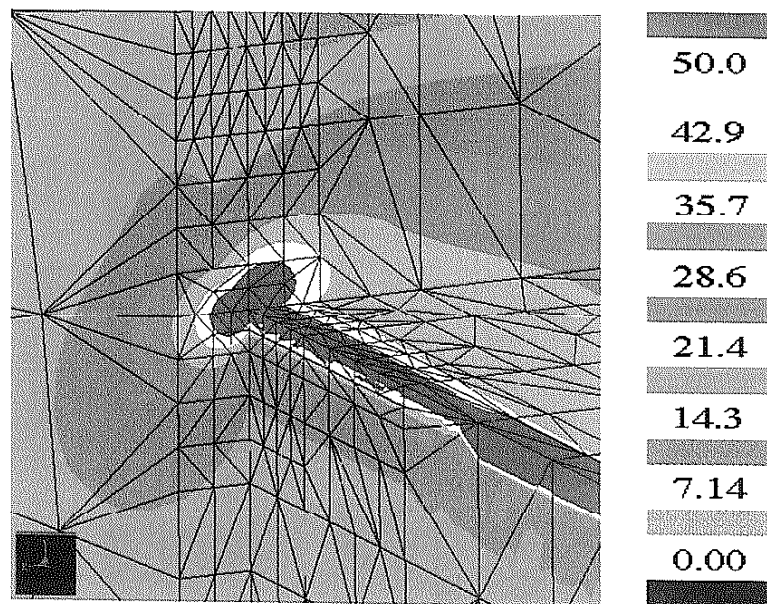


Fig. 6.5 Fringe plot of maximum principal stress (ksi) in the region of the intersection of the bottom beam flange and column flange.

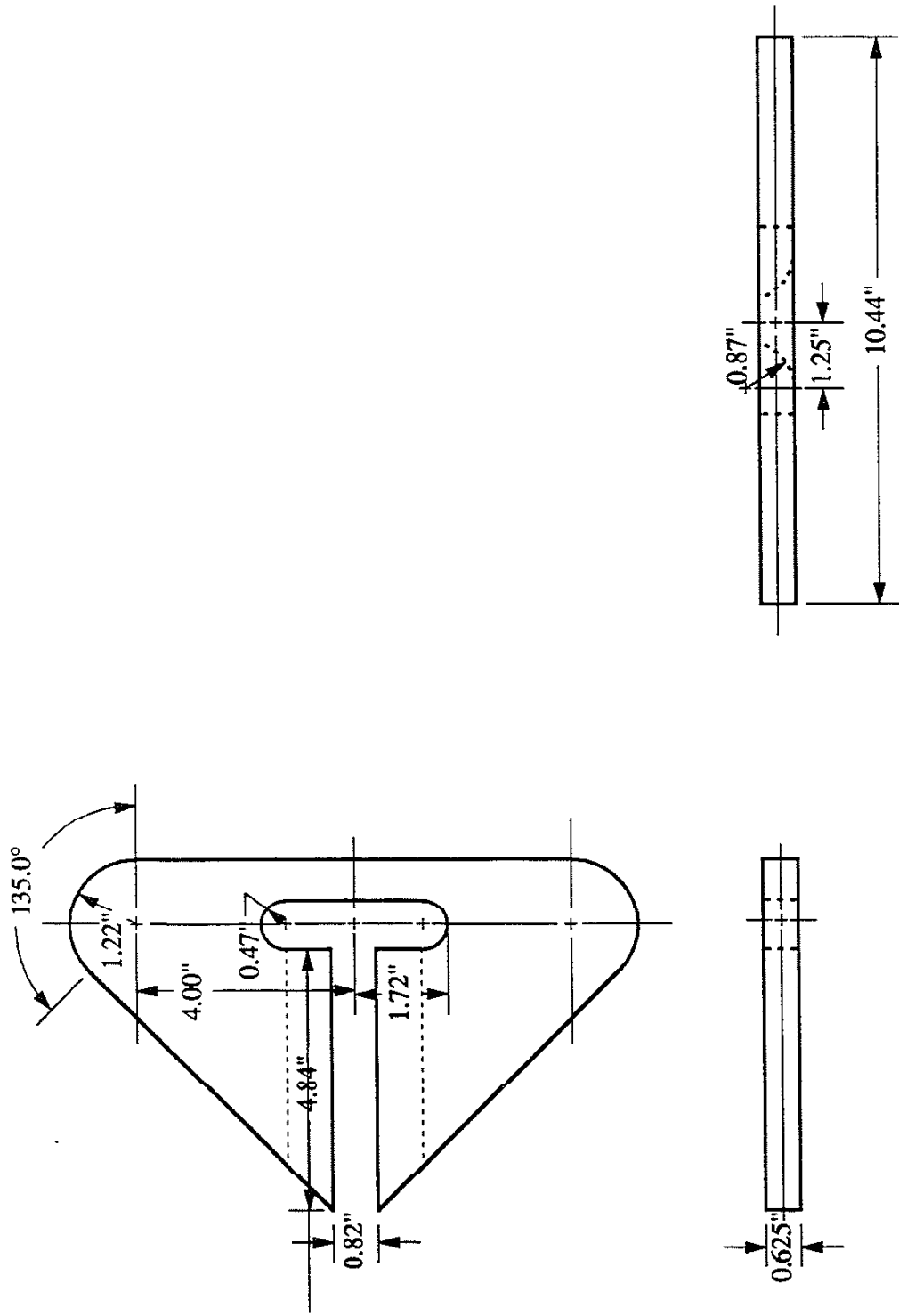


Fig. 6.6 The dimensions of the stress diffuser modeled in the beam-to-column connection.

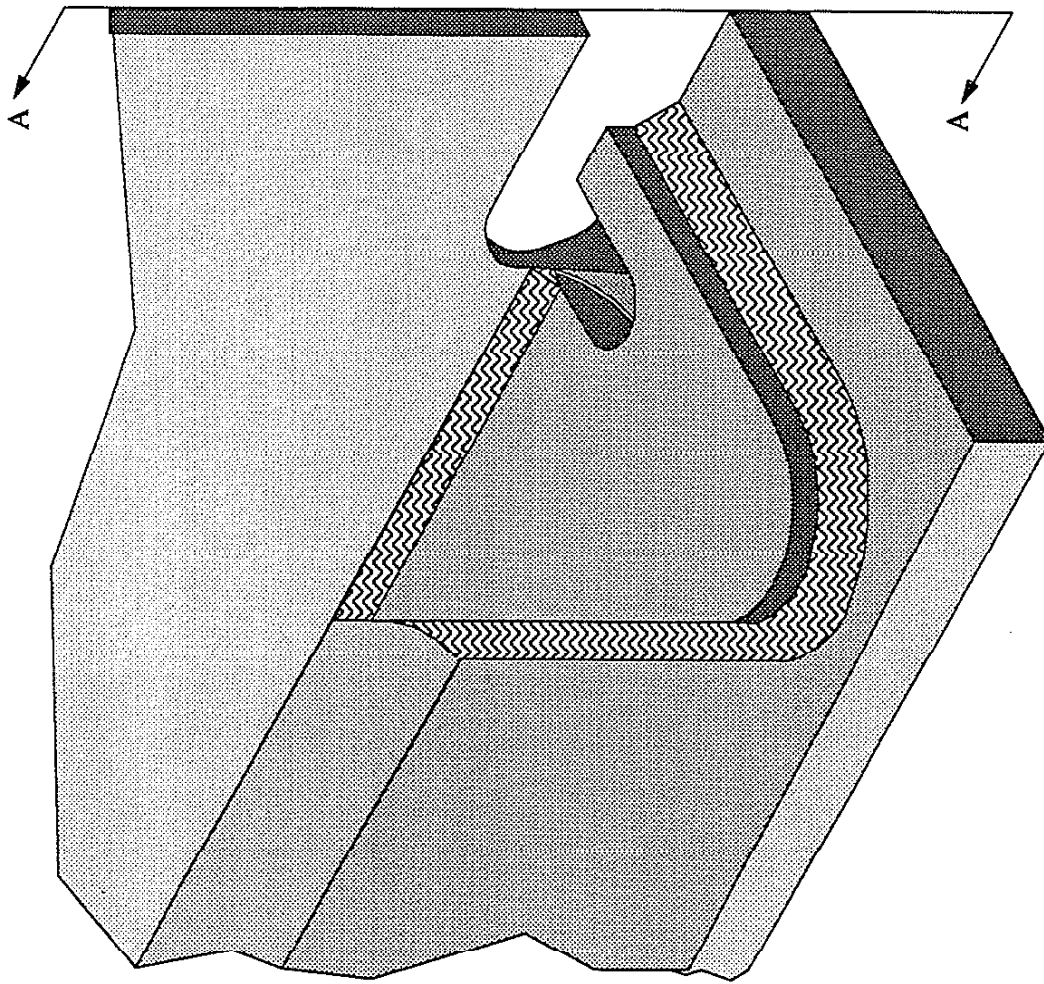
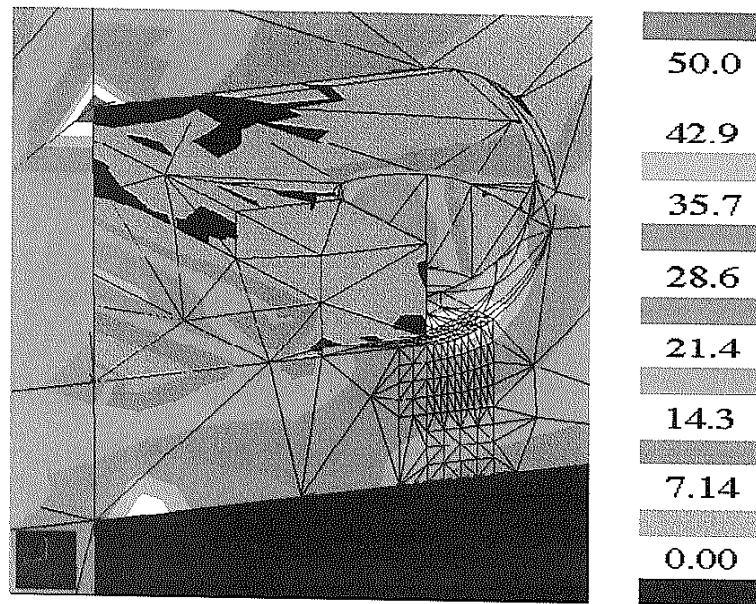
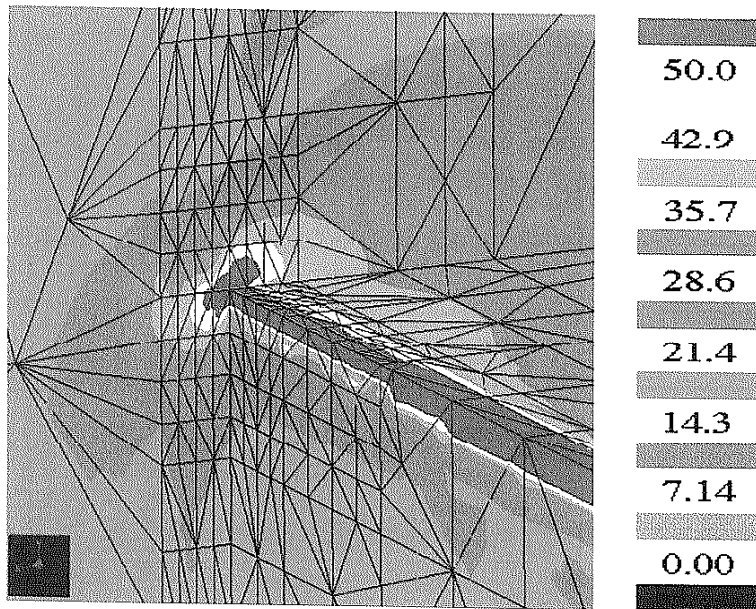


Fig. 6.7 Modeling of the stress diffuser in the beam-to-column connection (section A-A from Fig. 6.2). The fillet weld on top of the beam flange has a leg length of 0.375 in., and the fillet weld on top of the stress diffuser has a leg length of 0.25 in. Note the fit of radius of the stress diffuser to the beam fillet.



(a)



(b)

Fig. 6.8 Fringe plots of maximum principal stress (ksi) in (a) the region of the weld access hole and (b) the region of the intersection of the bottom beam flange and column flange for the beam-to-column connection modeled with a stress diffuser.

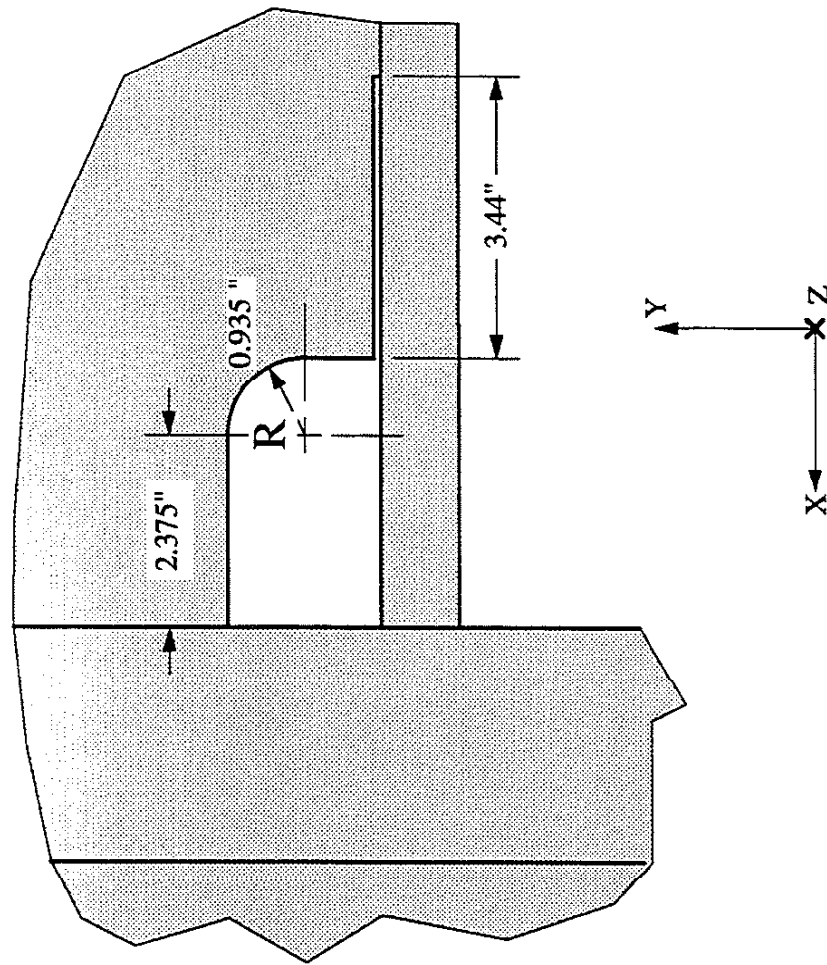


Fig. 6.9 The details of the beam-to-column connection in which the beam flange and web were separated.

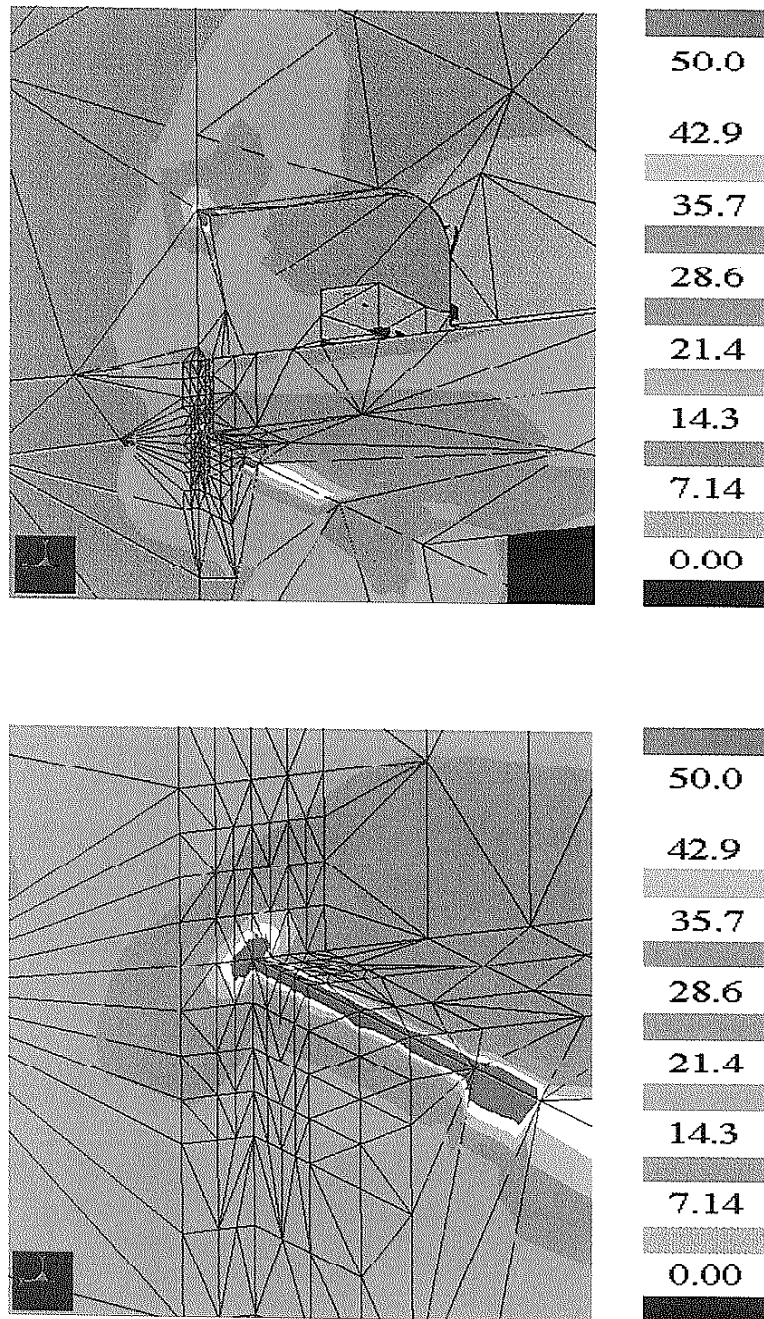


Fig. 6.10 Fringe plots of maximum principal stress (ksi) in the region of the intersection of the bottom beam flange and column flange for the beam-to-column connection in which the beam web and bottom flange are separated for a distance in addition to modeling a stress diffuser.

CHAPTER 7

INFLUENCE OF "COLD-LAP" DEFECTS

7.1 INTRODUCTION

"Cold-lap" defects were modeled using FEM analyses to examine their influence on the stress concentration factor (K_t) and the weld geometry correction factor (M_k). Cold-lap defects were found in the experimental phases (Chapter 2 and 5) of this study. Photographs of typical cold lap defects observed can be seen in Figs. 2.3 and 5.2. A drawing of a 2-D section of the weld toe area showing a cold lap defect is shown in Fig. 7.1. Cold lap defects lie on a plane parallel to the loading direction and present a modeling problem as the very short crack emanating from a cold-lap defect grows under mixed-mode (Mode I and II) loading. When the crack turns to almost perpendicular to the loading direction, the crack grows under predominantly Mode I loading.

7.2 PROCEDURES

7.2.1 Superposition Method

The superposition method was used to determine the weld geometry correction factor, M_k , for cracks emanating from the root of a cold-lap defect. M_k has usually been evaluated along a crack path perpendicular to the applied load and inward from the weld toe (vertical path from the weld toe in this study), and the calculation of K_{weld} ($M_{k_s} \cdot K_{pp}$) has been based on the readily available solutions for stress intensity factor for surface cracks in plain plate (K_{pp}) determined for straight cracks which are perpendicular (vertical) to the applied load. However, the crack path for the specimens with cold laps tested in Chapter 2 was observed to be curved and not straight; therefore, M_k should be evaluated along this curved path. However, the accuracy of determining M_k along such curved crack paths using the superposition method and using the model for K_{pp} based on cracks perpendicular to the applied load should be questioned.

A pilot study was undertaken in which the longitudinal attachment was modeled in 2 dimensions (2-D) (1) to determine the crack path emanating from the root of the cold lap and (2) to determine the best method of estimating $M_{k_{CG}}$ with the superposition method for this

crack path. The general findings of the pilot study will be presented below, and the details of the pilot study can be found in Appendix 4.

A weld root radius of 0.025 mm was assumed in the 2-D FEM analyses of the pilot study. The crack path emanating from the weld toe was determined by propagating a crack in small increments from the weld toe following the trajectory suggested by the maximum circumferential stress criterion [32]. The determined crack path was not straight but curved in the manner experimentally observed: see Fig. 7.2. It can be seen from Fig. 2.8 that the modeled and experimentally observed crack paths are in good agreement¹.

The use of the maximum principal stresses along the vertical path, or the projected maximum principal stresses onto the vertical path from the curved path in the calculation of M_{Ks} was found to estimate M_{KCG} determined along the curved crack path equally well. The author has decided to use the maximum principal stresses along the vertical path down from the cold-lap defect in the calculation of M_{Ks} , because it is believed to provide the most convenient yet accurate solution. Any differences in N_p calculated using M_{Ks} and M_{KCG} were found to be insignificant. Therefore, all further calculations of M_{Ks} from a cold-lap defect in this study will be performed using the maximum principal stresses along the vertical path down from the cold-lap defect.

7.3 INFLUENCE OF "COLD-LAP" DEFECTS ON LONGITUDINAL ATTACHMENTS

The cold-lap defects were first modeled using 2-D FEM analyses to examine the effects that changing cold-lap defect depth, weld root radius, and weld toe angle have on K_t and M_K . The goal of the simpler 2-D FEM analyses was to obtain trends of how the geometric variables affect K_t and M_K for weld details in general. Then the cold-lap defects were modeled using the more complex 3-D FEM analyses which are necessary to accurately determine the stresses in the longitudinal attachment (Fig. 3.5) to verify the applicability of the trends found in 2-D.

7.3.1 2-D FEM Analyses of Cold-Lap Defects

The cold-lap defects were modeled using 2-D FEM analyses of the geometry shown in Fig. 7.3a. A typical mesh is shown in Fig. 7.3b. The weld root of the cold-lap defect was modeled with a radius, r_{cl} . Since the cold-lap defects found in the experimental study were as deep as 2.0 mm (Table 2.2), cold-lap defect depths (D) of 1.0 and 2.0 mm were modeled in

¹ The small differences may be due to the increment length or the inability of the 2-D FEM analysis to properly estimate the 3-D nature of the longitudinal attachment.

the 2-D FEM analyses. Weld root radii (r_w) of 0.025 and 0.146 mm were modeled. The weld root radii observed in the experimental study were very small and could even be considered cracks. However, a notch root radius of 0.025 mm was modeled because it was considered a severe notch and modeling radii much smaller was considered unnecessary. The larger radius of 0.146 mm was modeled to allow for the extrapolation of K_t to other root radii as will be seen below. The weld toe radius (r) was modeled as 1.0 mm because this radius would not have any significant influence on the stresses at the maximum depth of the cold-lap defect.

The fatigue crack was assumed to nucleate at the location of peak maximum principal stress at the weld root. The azimuth angle (ϕ) to the location of peak maximum principal stress at the weld root is listed in Table 7.1 along with the associated K_t for the cases studied. The location of the peak maximum principal stress was found to be at an azimuth angle of about 33.75° for all of the cases investigated². An increase in defect depth results in an increase in K_t (Table 7.1) because the weld root lies in a region of higher stress.

The stress concentration factor (K_t) for a notch can be expressed as [38]:

$$K_t = 1 + \alpha \left(\frac{t}{r} \right)^\lambda \quad (7.1)$$

where K_t is the ratio of the local stress to the remote stress, t is the plate thickness, r is the notch root radius, α is the macrogeometry coefficient, and λ is the exponent. Thus, K_t can be estimated for any notch root radius once α and λ are determined. The macrogeometry coefficients and exponents for the data are listed in Table 7.1. Exponents of 0.49 and 0.50 were obtained which are similar to values of approximately 0.50 found in past studies [38, 39]. These results and the use of equation 7.1 will facilitate N_f calculations for any root radii desired.

The weld geometry correction factor for the cracked geometry ($M_{k\ CG}$) was determined along the curved crack path by normalizing $K_{weld\ CG}$ by K_{pp} ; see Fig. 7.4. In addition, $M_{k\ CG}$ was determined along the vertical path and plotted in Fig. 7.4. It can be seen that $M_{k\ CG}$ is similar whether it is determined along the curved or vertical crack path. $M_{k\ CG}$ determined from the weld toe location for the geometry without a cold-lap defect and with a weld toe radius of 1.0 mm are plotted with $M_{k\ CG}$ determined for the vertical and curved crack paths for the geometry with a cold-lap defect in Fig. 7.4. It can be seen that $M_{k\ CG}$ is similar for long crack lengths but for short crack lengths $M_{k\ CG}$ is greater for the geometry with a cold-lap defect. If a smaller weld toe radius was used in the analysis, the difference in M_k would be smaller.

² It should be noted that the azimuth angle is a function of the weld root radius and could change if different radii were modeled. The stresses were evaluated at 11.25° increments around the weld root radius.

The weld geometry correction factor (M_K) determined with the superposition method for cold lap defect depths (D) of 1.0 and 2.0 mm can be seen in Fig. 7.5 along with the M_K for the geometry without a cold lap ($D = 0.0$ mm). It can be seen from Fig. 7.5 that the presence of a cold-lap defect considerably increases M_K at short crack lengths. At long crack lengths, the presence of a cold-lap defect does not significantly increase M_K . At short crack lengths, an increase in defect depth results in a small increase in M_K as the crack path lies in a region of slightly higher stress.

The weld toe angle was varied to determine its effect on the weld geometry correction factor for a crack growing from a cold-lap defect. Weld toe angles of 30° and 60° were considered in addition to the 45° angle that has been investigated thus far in the study. The stress concentration factors determined at the weld root are listed in Table 7.2 and the weld geometry correction factors are plotted in Fig. 7.6a. It can be seen that as the weld toe angle increases, both K_t and M_K increase as well. Decreases in the weld toe angle result in increases in N_p : see Fig. 7.6b.

7.3.2 3-D FEM Analysis of Cold-Lap Defects

The cold-lap defects were then modeled with a 3-D FEM analysis of the uncracked geometry. The geometry modeled with Pro/MECHANICA can be seen in Fig. 7.7. A cold-lap defect depth of 2.0 mm and weld root radii (r_w) of 0.025 and 0.146 mm were used in the 3-D FEM analyses. The resulting stress concentrations at the weld root are listed in Table 7.3. An exponent of 0.53 is obtained from these values which is consistent with the values of 0.50 discussed previously.

The superposition method was used to calculate M_K , and the weld geometry correction factor determined from the 2-D and 3-D FEM analyses are plotted in Fig. 7.8. At long crack lengths, the 2-D and 3-D solutions are similar. At short crack lengths, M_K determined from the 2-D FEM analysis is greater than the M_K determined from the 3-D FEM analysis, unlike what was observed for the geometry without a cold-lap defect. In the 2-D geometry, the cold lap is modeled along the entire weld path much like an edge crack in a plain plate. In the 3-D geometry, weld material exists on both sides of the cold lap which provides additional constraint to cracks opening which leads to the smaller M_K . The reduction in M_K due to the presence of additional material is greater than the increase in M_K due to the 3-D stress-concentrating effects of the weldment.

The weld geometry correction factors (M_K) determined from 3-D FEM analyses for root radii of 0.025 and 0.146 mm are compared with the results for a 3-D FEM analysis without a

cold-lap defect in Fig. 7.9. At short crack lengths, the presence of a cold-lap defect increases M_K considerably; see Fig. 7.9. It can be seen from Fig. 7.9 that the weld root radius has an effect on M_K at short crack lengths. The effect of the cold-lap defect on the fatigue crack propagation life for different initial crack lengths can be seen in Fig. 7.9. The results suggest that the N_p would be reduced if the initial crack length was small, but the results also suggest that N_p would not be much affected by the presence of a cold lap if the initial crack length is large.

7.4 INFLUENCE OF "COLD-LAP" DEFECTS ON LONGITUDINAL ATTACHMENTS WITH STRESS DIFFUSERS

Cold-lap defects were modeled using 3-D FEM analyses to determine the influence of cold-lap defects on the fatigue life of longitudinal attachments with stress diffusers. A cold-lap defect with a depth of 1.0 mm was modeled at the location of maximum stress for the longitudinal attachment with stress diffusers as shown in Fig. 7.10. The location of maximum stress does not occur at the center of the specimen; therefore, a plane of symmetry does not exist for the cold-lap defect and the entire cold-lap defect must be modeled. A cold-lap defect was also modeled at the center of the specimen as shown in Fig. 7.11 to determine the influence of a cold lap defect there. The stress concentration factors (K_t) for the two locations at the weld root were found to be 9.78 and 7.92 for the maximum and center locations, respectively. The location of peak maximum principal stress was found to be at an azimuth angle of about 33.75°.

The weld geometry correction factors (M_K) determined for the peak stress path with the superposition method are plotted along with the M_K for a specimen without a cold-lap defect in Fig. 7.12a. At short crack lengths, the presence of a cold lap increases M_K considerably. The effect of a cold-lap defect on the fatigue crack propagation life for different initial crack lengths can be seen in Fig. 7.12b. The results suggest that the N_p would be reduced significantly if the initial crack length was small, but the results also suggest that N_p would not be much affected by the presence of a cold-lap defect if the initial crack length is large.

The weld geometry correction factor (M_K) was also calculated for a cold-lap defect located at the center of the specimen which is not the location of peak stress and plotted in Fig. 7.13a. For short crack lengths, M_K is larger for the specimen with a cold-lap defect. However, at long crack lengths, M_K is smaller for the specimen with a cold-lap defect. Therefore, N_p of a crack growing from the weld toe may be shorter than the N_p of a crack growing from a cold-lap defect: see Fig. 7.12b.

The weld geometry correction factor (M_k) for the crack growing from a cold-lap defect in a longitudinal attachment is plotted in Fig. 7.12a. The M_k is greater for the crack growing from a cold-lap defect in a longitudinal attachment than the M_k for the crack growing from a cold-lap defect in a longitudinal attachment with stress diffusers; therefore, the N_p is greater for the longitudinal attachment with stress diffusers: see Fig. 7.12b.

7.5 SUMMARY

Cold-lap defects were modeled using both 2-D and 3-D FEM analyses to examine their influence on the stress concentration factor (K_t) and the weld geometry correction factor (M_k). The superposition method was found to estimate properly $M_{k\ CG}$ determined for the curved crack path using crack tip elements. The presence of cold-lap defects was found to increase K_t at the notch root and M_k for short crack lengths. An increase in cold-lap defect depth and weld toe angle were found to increase K_t and M_k also. The M_k was found to be greater for a crack growing from a cold-lap defect in a longitudinal attachment than the M_k for a crack growing from a cold-lap defect in a longitudinal attachment with a stress diffuser.

Table 7.1 2-D FEM results for the longitudinal attachments with a cold-lap defect.

Defect Depth D (mm)	Weld Root Radius r_{cl} (mm)	Azimuth Angle ϕ (°)	Stress Concentration Factor K_t	Weld Toe Angle θ (°)	Macrogeometry Coefficient α	Exponent λ
1.0	0.025	33.75	15.90	45	0.689	0.49
1.0	0.146	33.75	7.24	45	0.689	0.49
2.0	0.025	33.75	18.40	45	0.787	0.50
2.0	0.146	33.75	8.24	45	0.787	0.50

Table 7.2 The effect of weld toe angle on 2-D FEM results for the longitudinal attachments with a cold-lap defect.

Defect Depth D (mm)	Weld Root Radius r_{cl} (mm)	Azimuth Angle ϕ (°)	Stress Concentration Factor K_t	Weld Toe Angle θ (°)
1.0	0.025	33.75	11.6	30
1.0	0.025	33.75	15.9	45
1.0	0.025	33.75	18.3	60

Table 7.3 3-D FEM results for the longitudinal attachments with a cold-lap defect.

Defect Depth D (mm)	Weld Root Radius r_{cl} (mm)	Azimuth Angle ϕ (°)	Stress Concentration Factor K_t	Weld Toe Angle θ (°)	Macrogeometry Coefficient α	Exponent λ
2.0	0.025	22.5	15.6	45	0.537	0.53
2.0	0.146	22.5	6.7	45	0.537	0.53

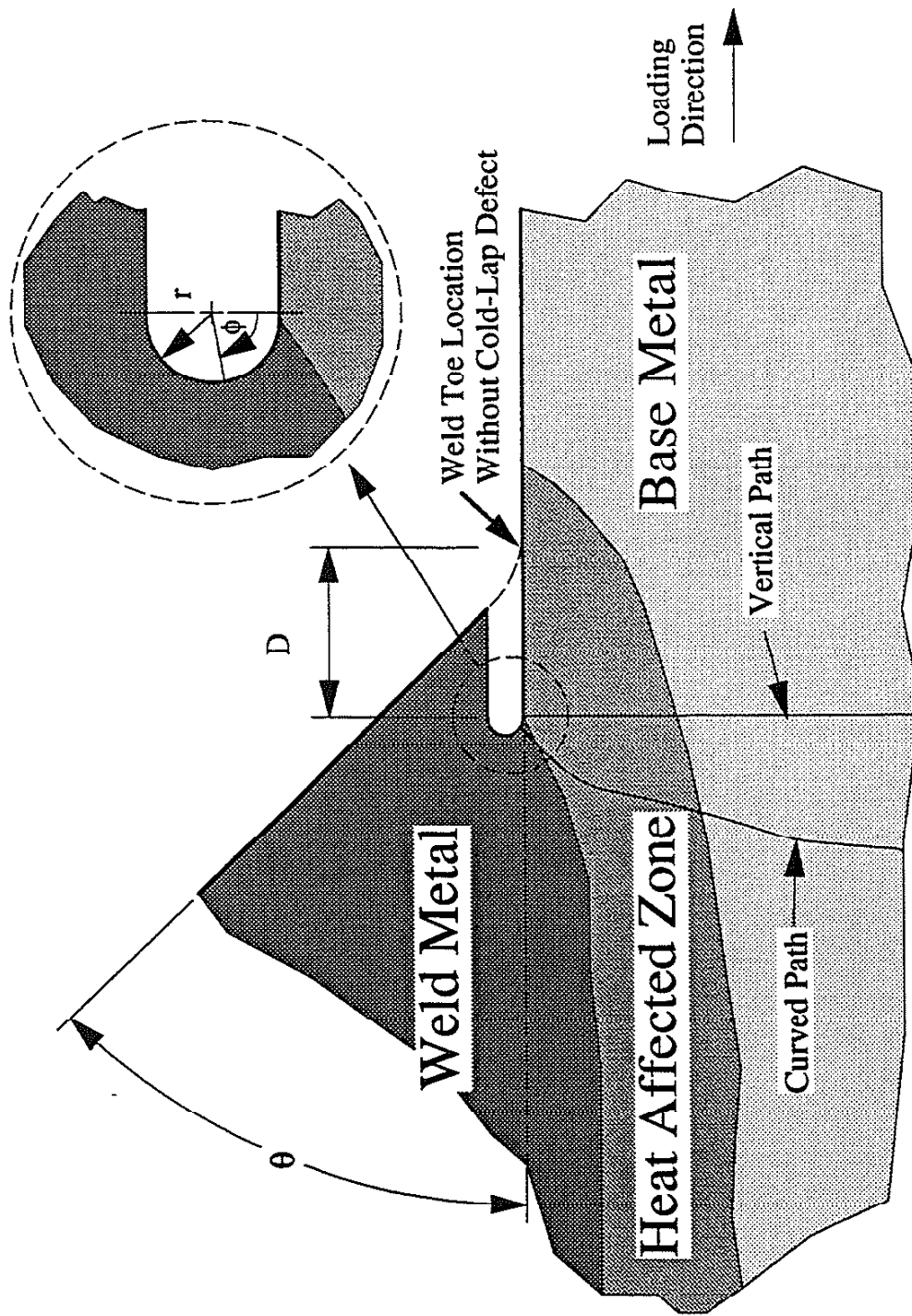


Fig. 7.1 A 2-D section of the weld toe area showing a cold-lap defect.

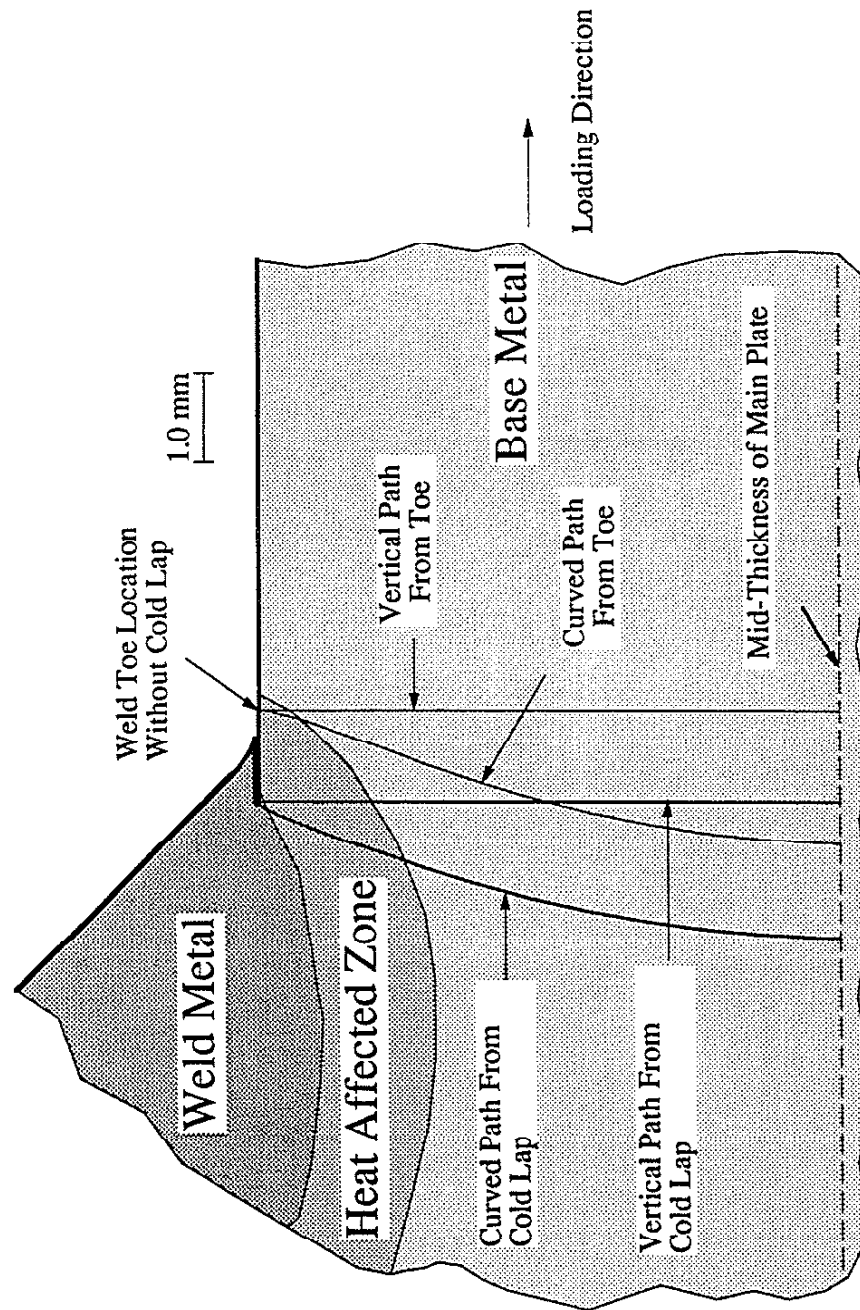


Fig. 7.2 The models crack paths from the weld root of the cold lap. The paths modeled from the weld toe have been included for comparison. The drawing has been drawn to scale.

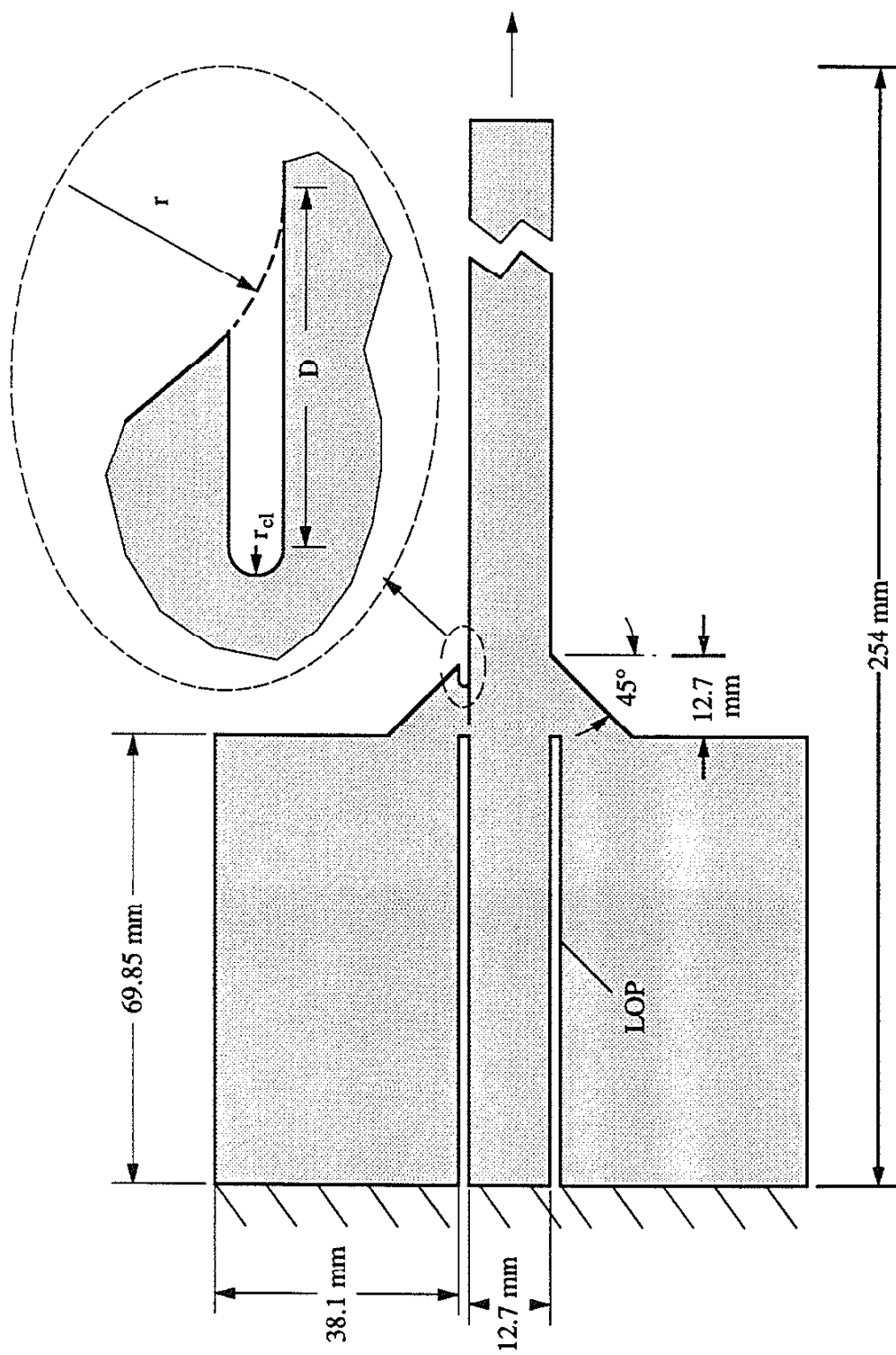


Fig. 7.3a The geometry and loading conditions used in the 2-D FEM analyses of longitudinal attachments with cold lap defects.

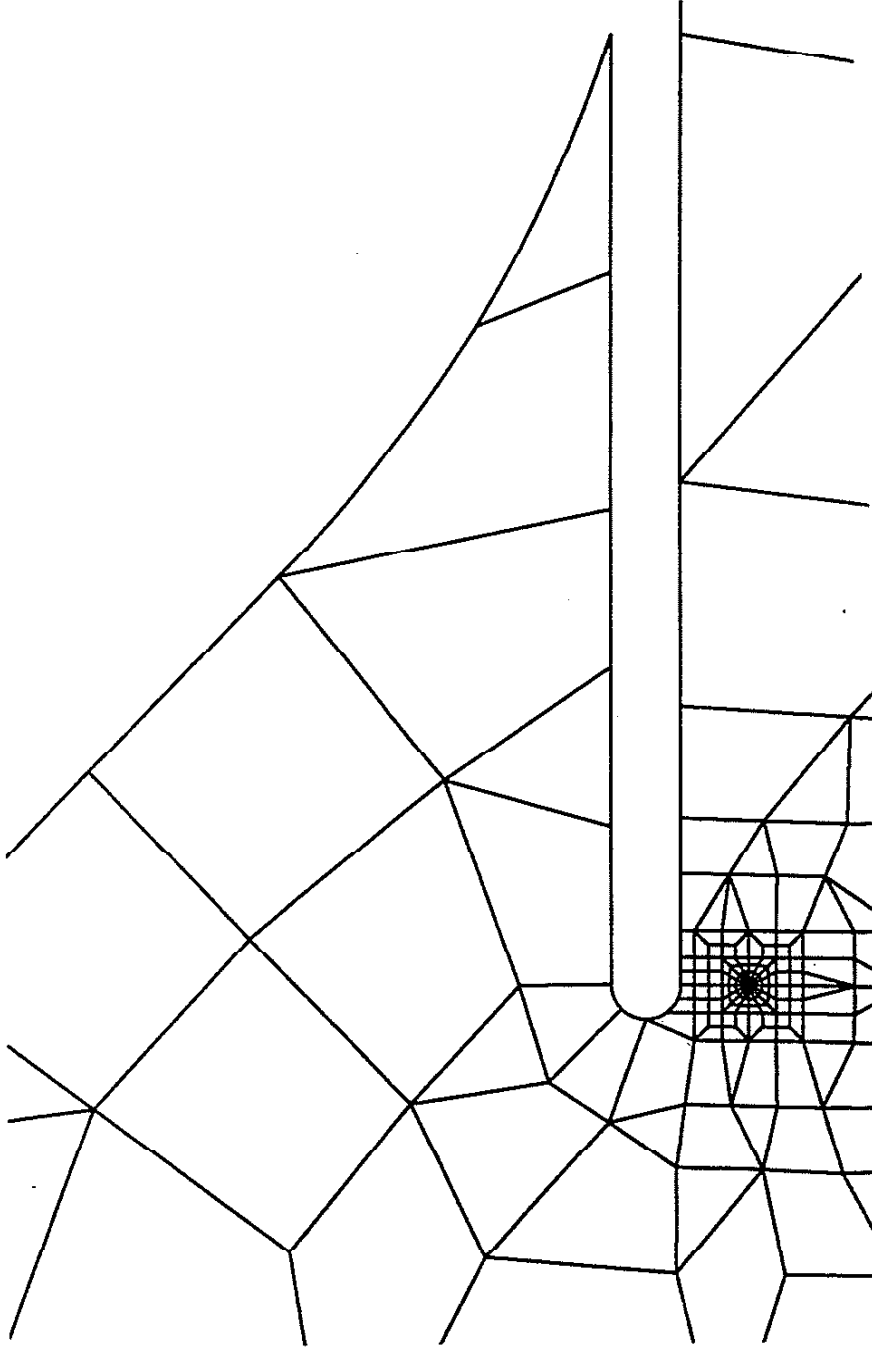
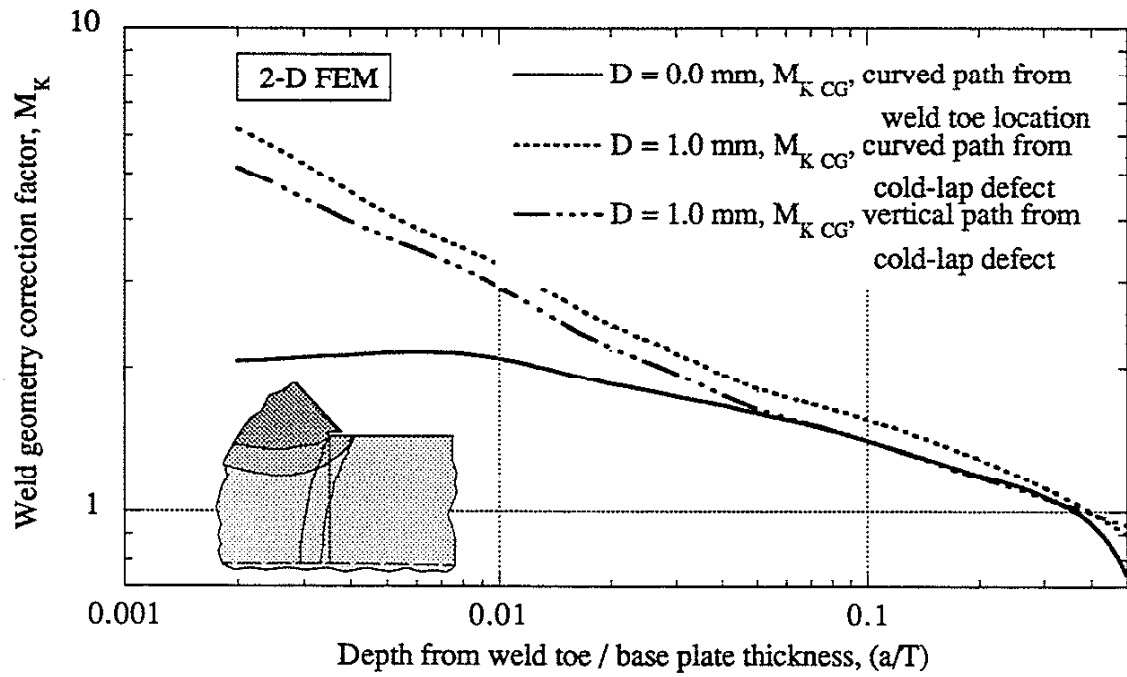
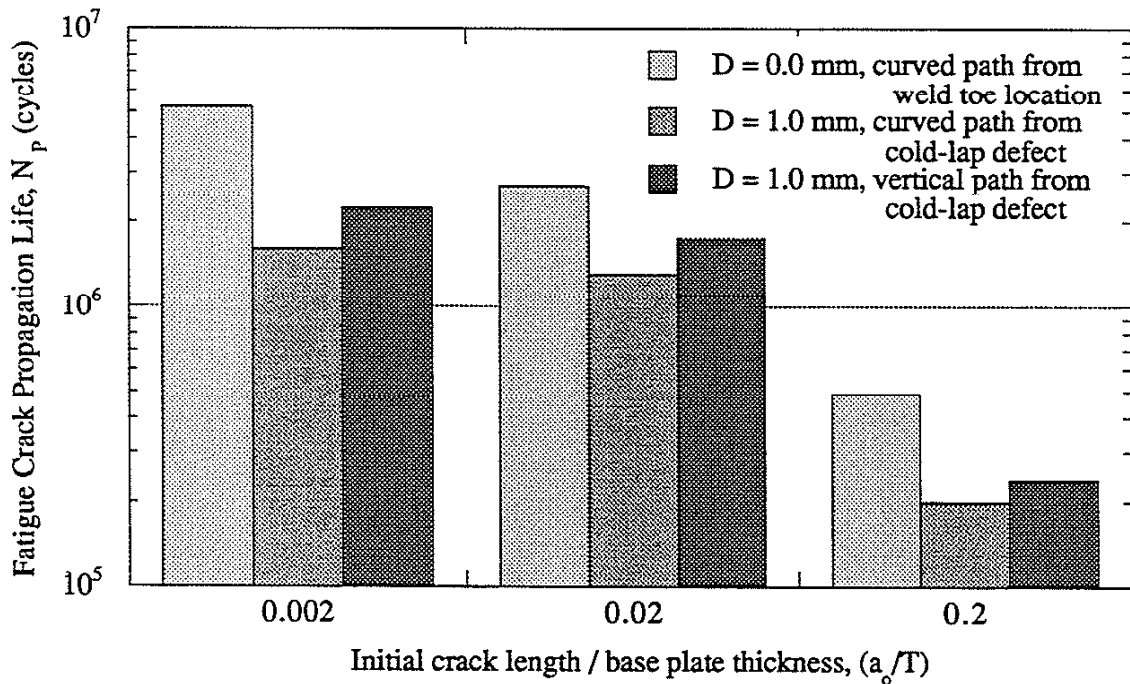


Fig. 7.3b 2-D FEM mesh of a cold-lap defect with a depth of 1 mm.

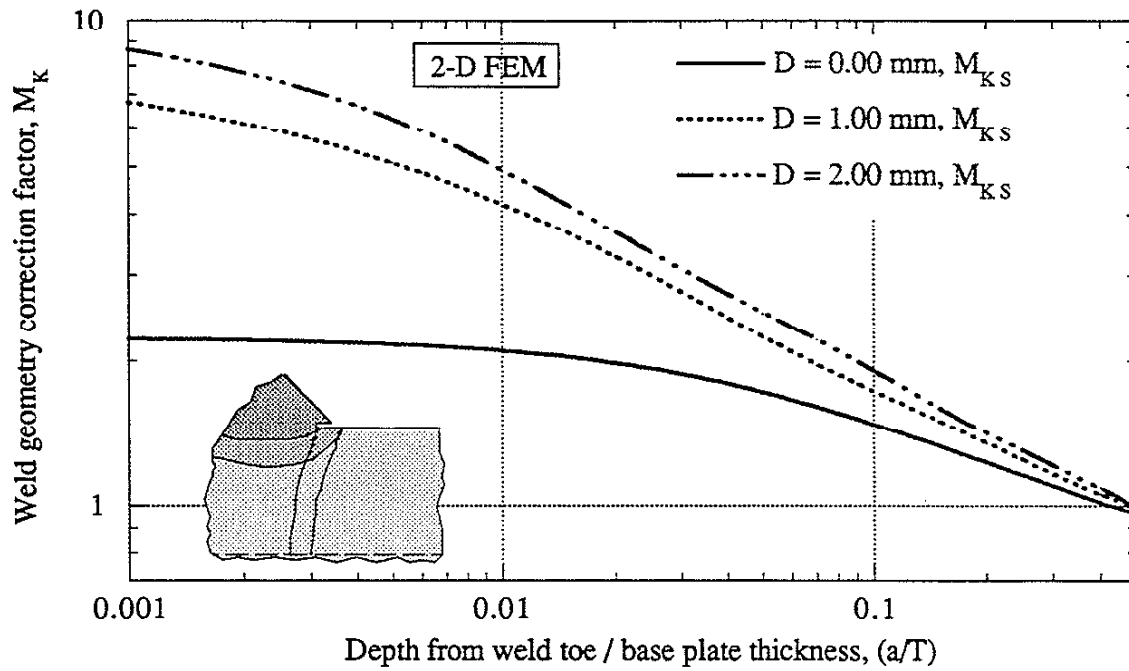


(a)

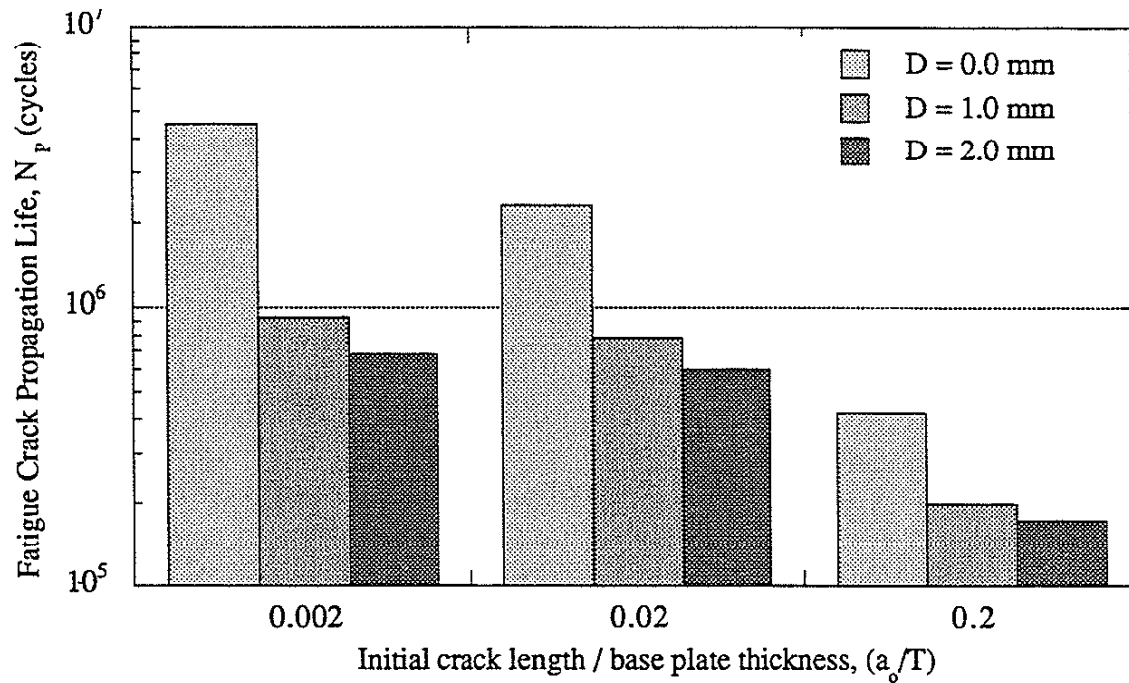


(b)

Fig. 7.4 The predicted effect of a cold lap of 1.0 mm on (a) the weld geometry correction factor and (b) the fatigue crack propagation lives of longitudinal attachments. ($\Delta S = 100 \text{ MPa}$)

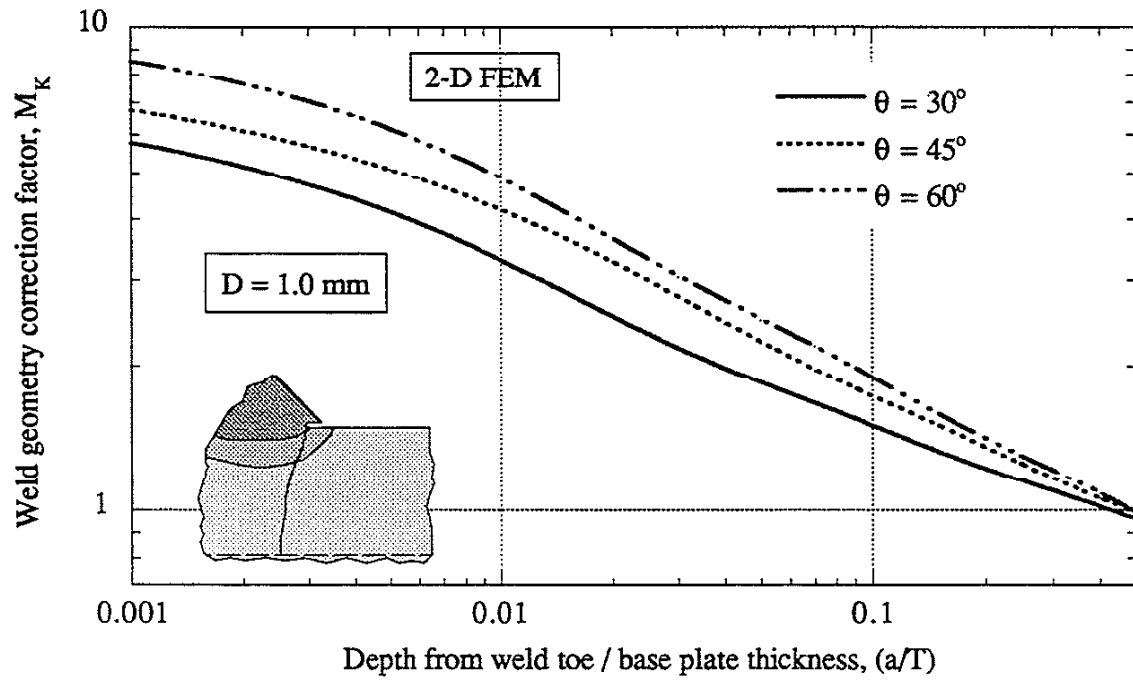


(a)

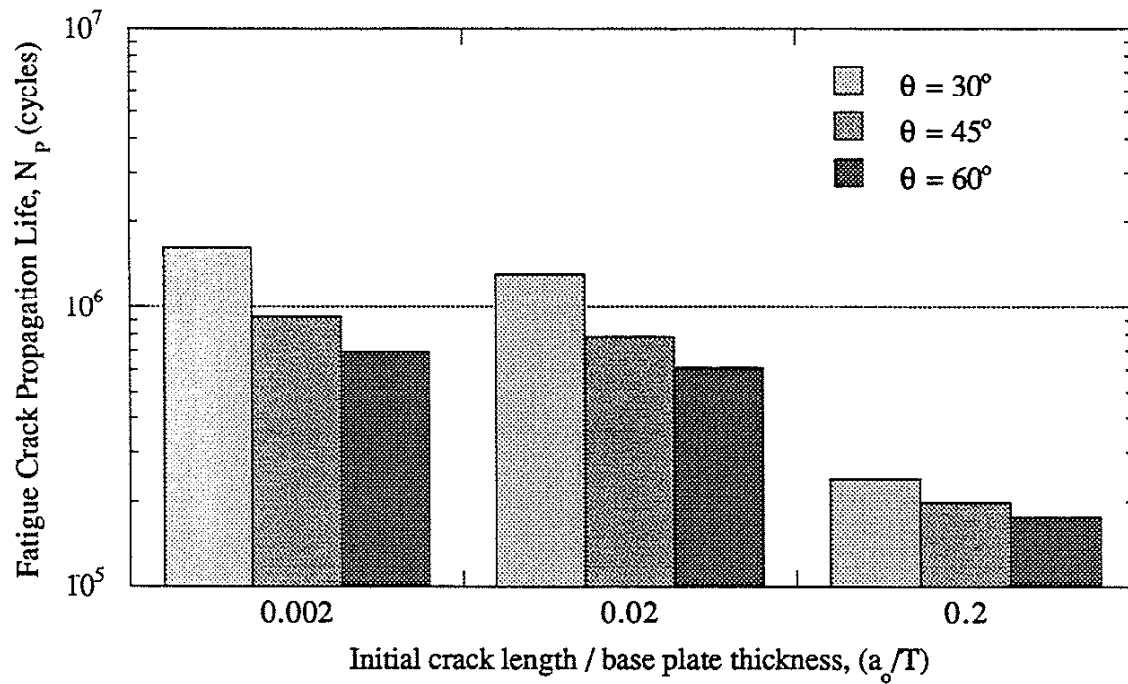


(b)

Fig. 7.5 The predicted effect of cold-lap defect depth (D) on (a) the weld geometry correction factor and (b) the fatigue crack propagation lives of longitudinal attachments. ($\Delta S = 100 \text{ MPa}$)



(a)



(b)

Fig. 7.6 The predicted effect of weld toe angle on (a) the weld geometry correction factor and (b) the fatigue crack propagation lives of longitudinal attachments. ($\Delta S = 100 \text{ MPa}$)

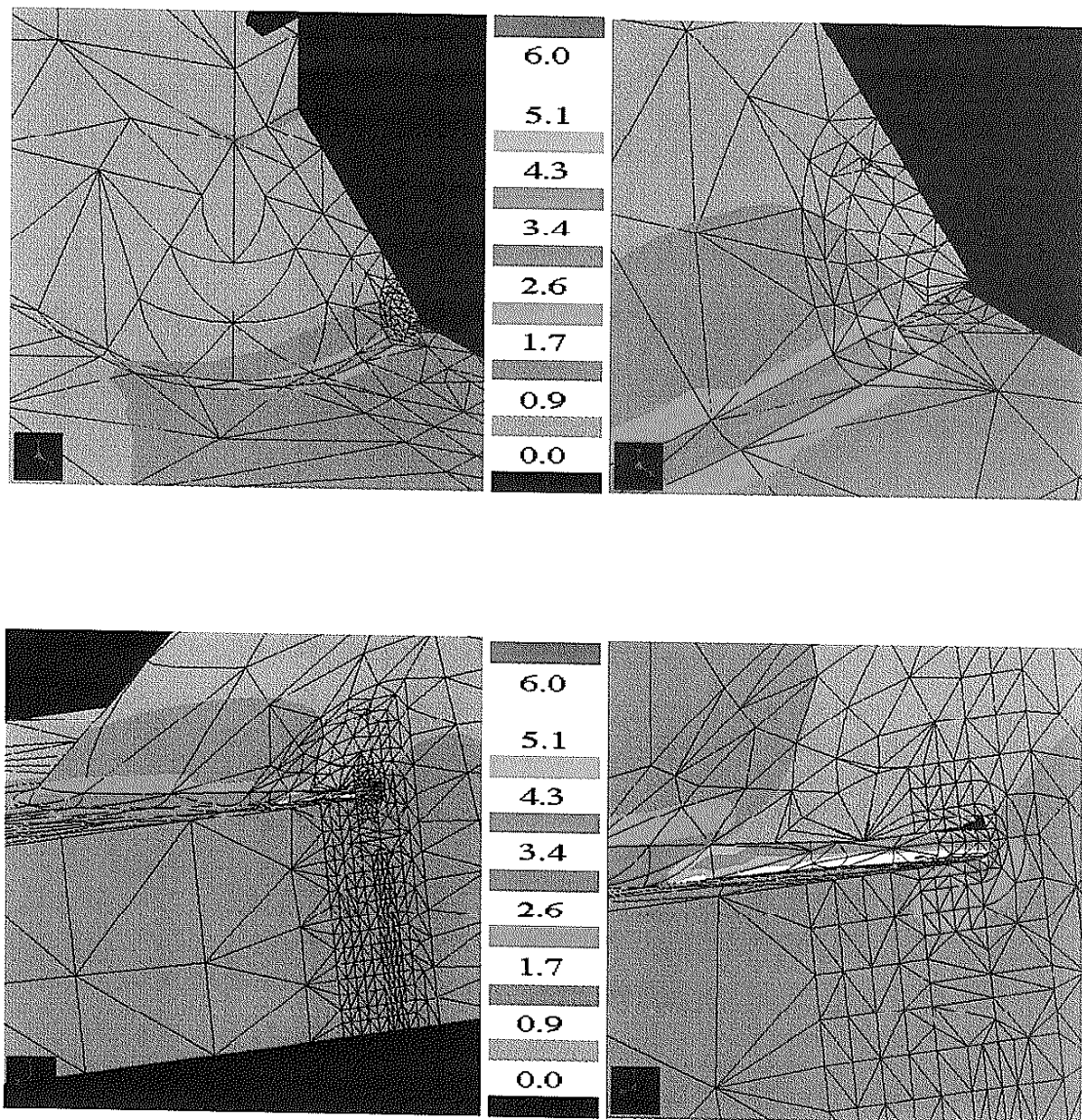
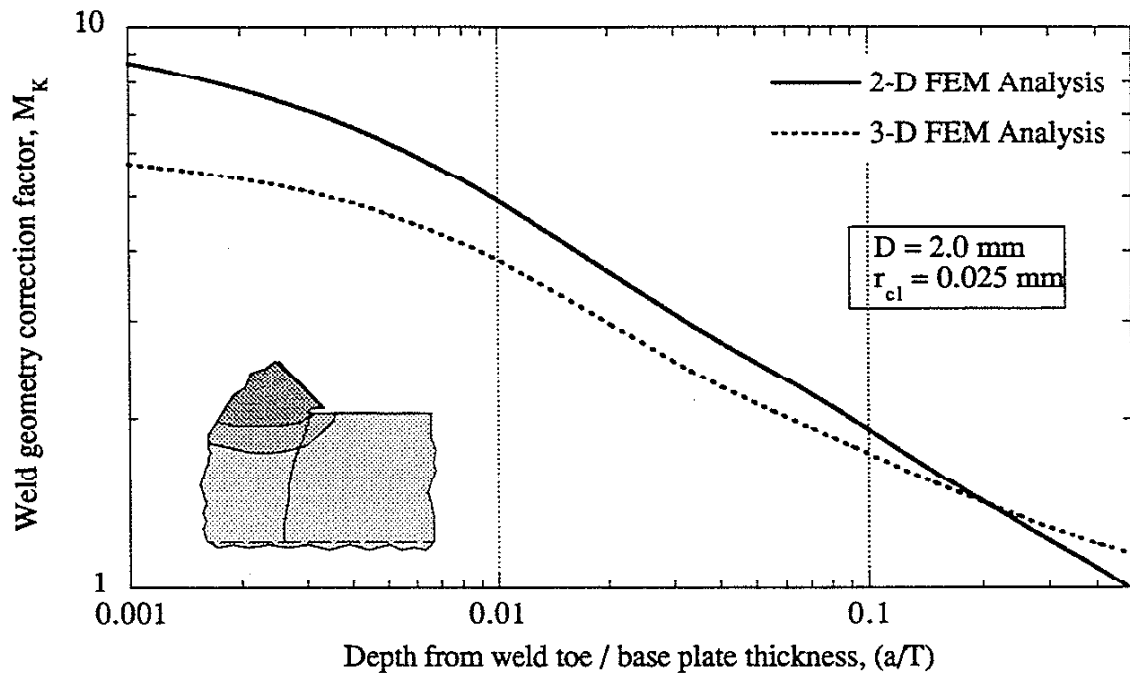
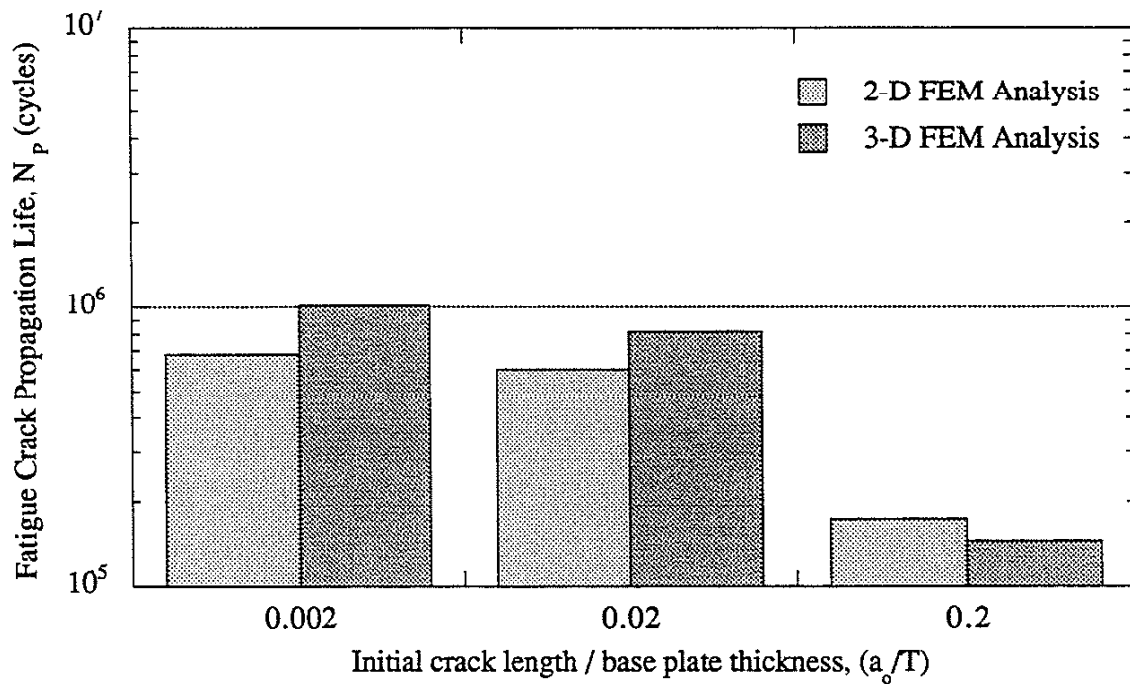


Fig. 7.7 Fringe plots of the maximum principal stress (ksi) in a longitudinal attachment modeled with a cold-lap defect having a weld root radius of 0.146 mm. The details of the modeling and results are shown for two different angles.

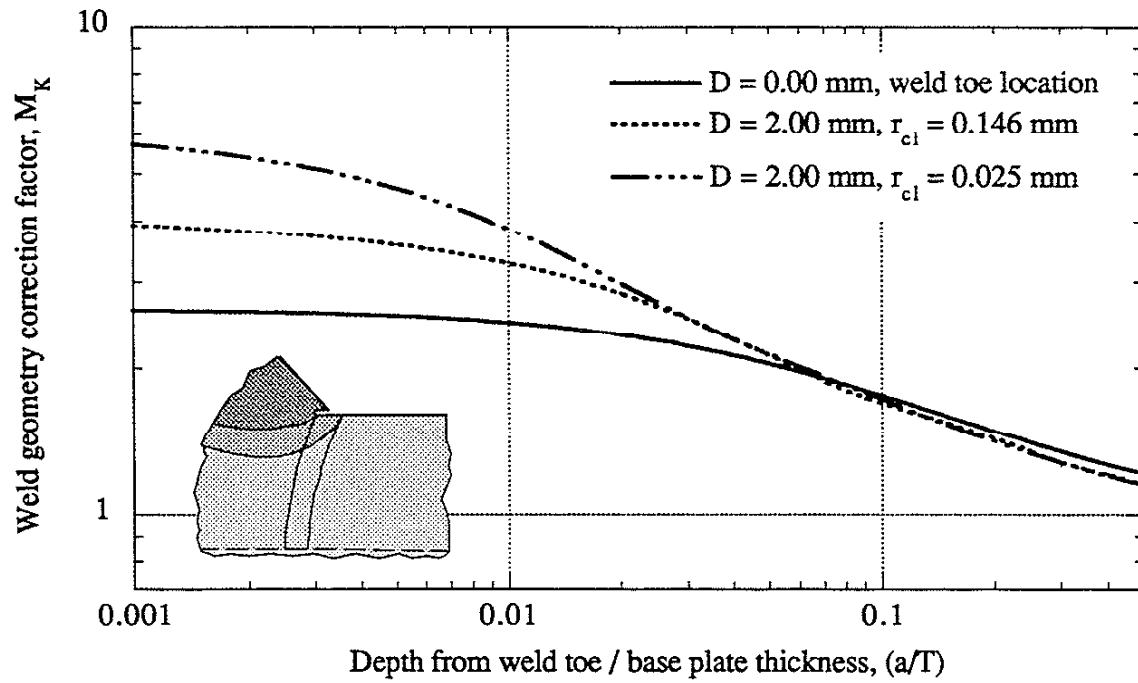


(a)

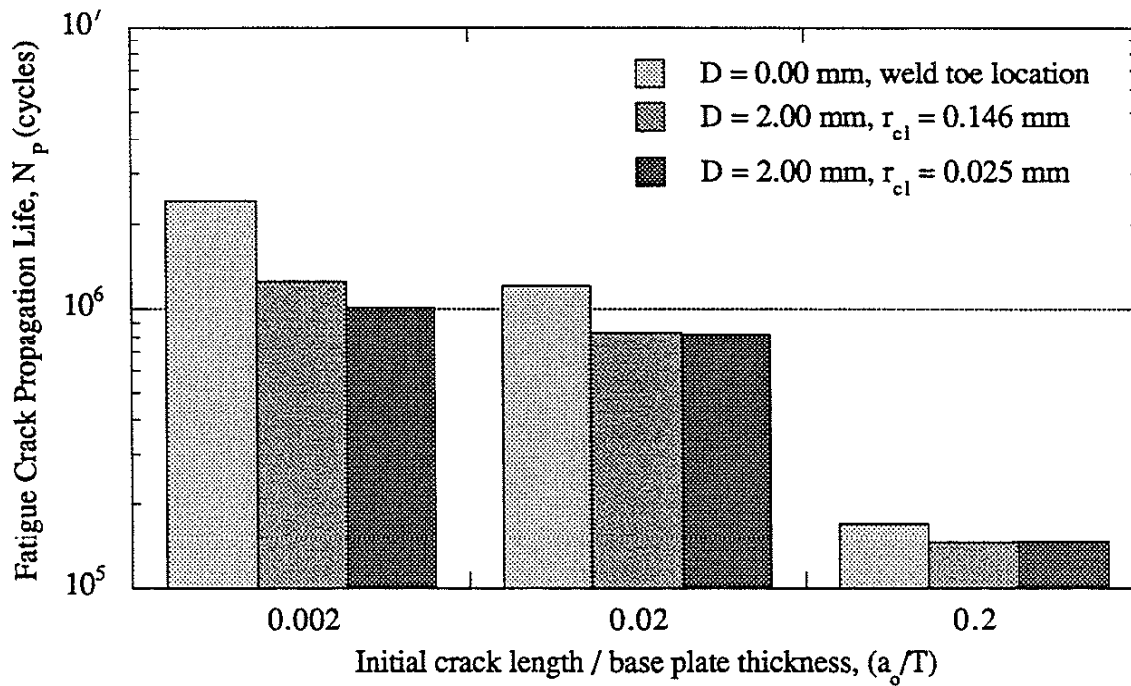


(b)

Fig. 7.8 The effect of 2-D vs. 3-D FEM analysis on (a) the weld geometry correction factor and (b) the fatigue crack propagation lives of longitudinal attachments. ($\Delta S = 100 \text{ MPa}$)



(a)



(b)

Fig. 7.9 The effect of weld root radius on (a) the weld geometry correction factor and (b) the fatigue crack propagation lives of longitudinal attachments. ($\Delta S = 100$ MPa)

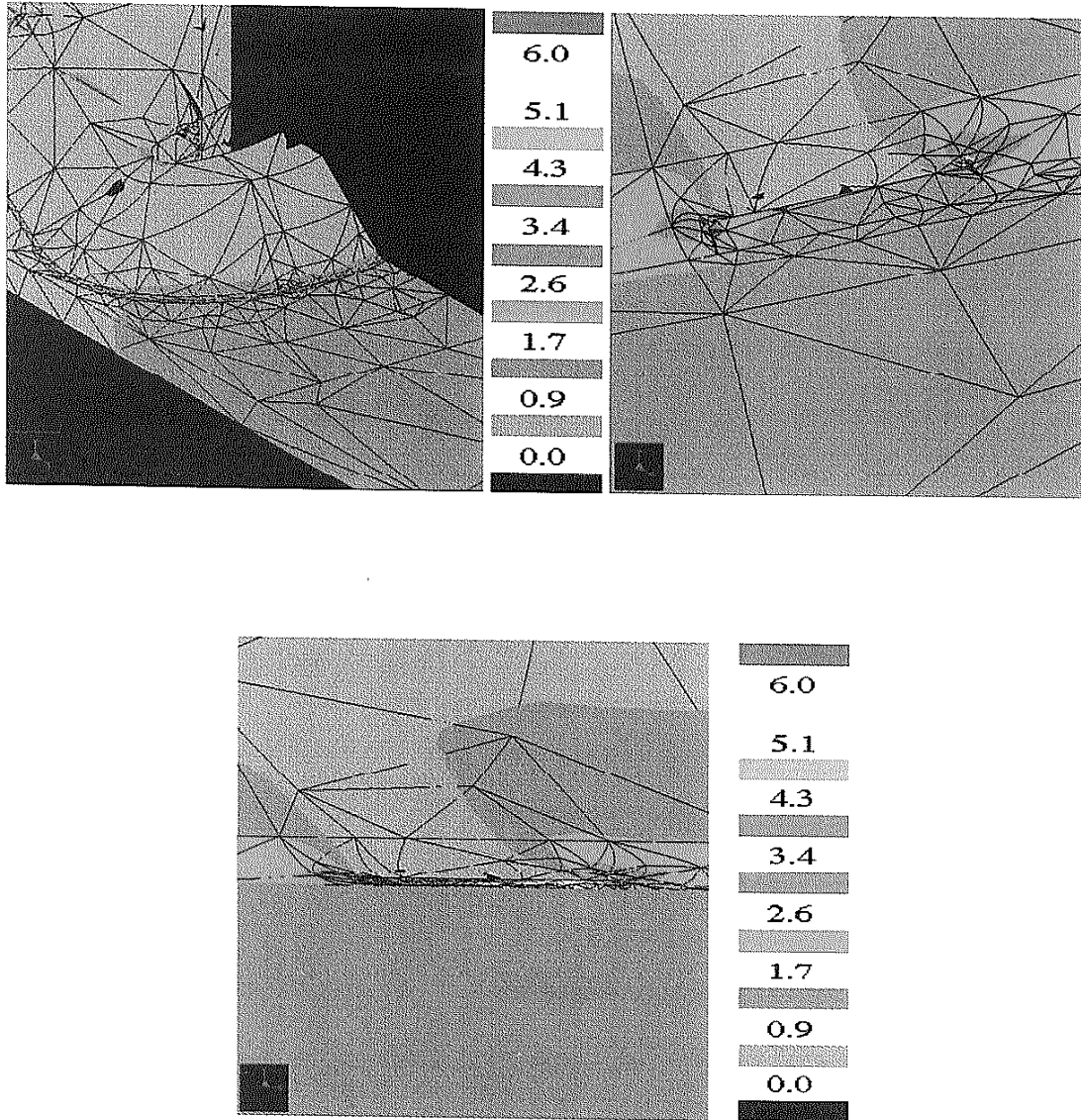


Fig. 7.10 Fringe plots of the maximum principal stress (ksi) in a longitudinal attachment with a stress diffuser modeled with a cold-lap defect having a weld root radius of 0.025 mm. The details of the modeling and results are shown for two different angles.

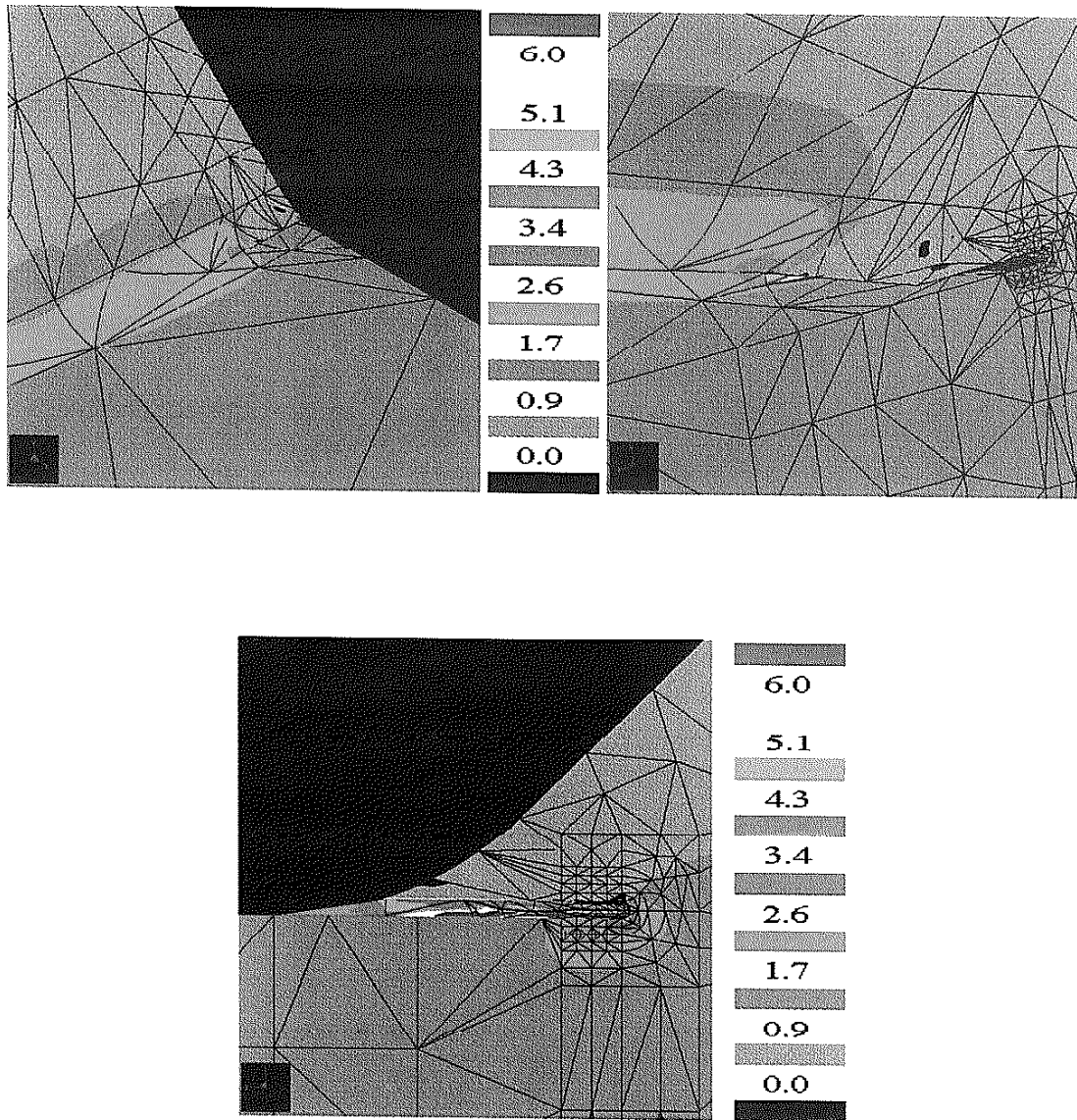


Fig. 7.11 Fringe plots of the maximum principal stress (ksi) in a longitudinal attachment with a stress diffuser modeled with a cold-lap defect having a weld root radius of 0.025 mm. The details of the modeling and results are shown for different angles.

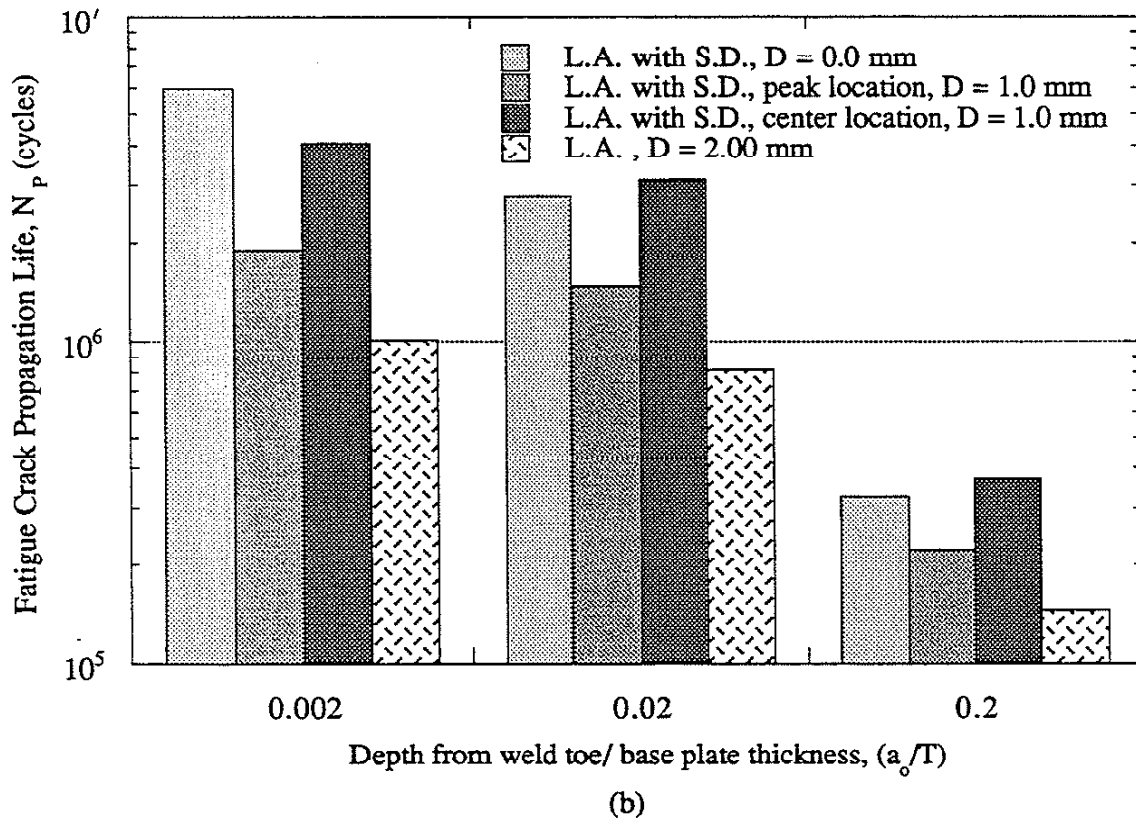
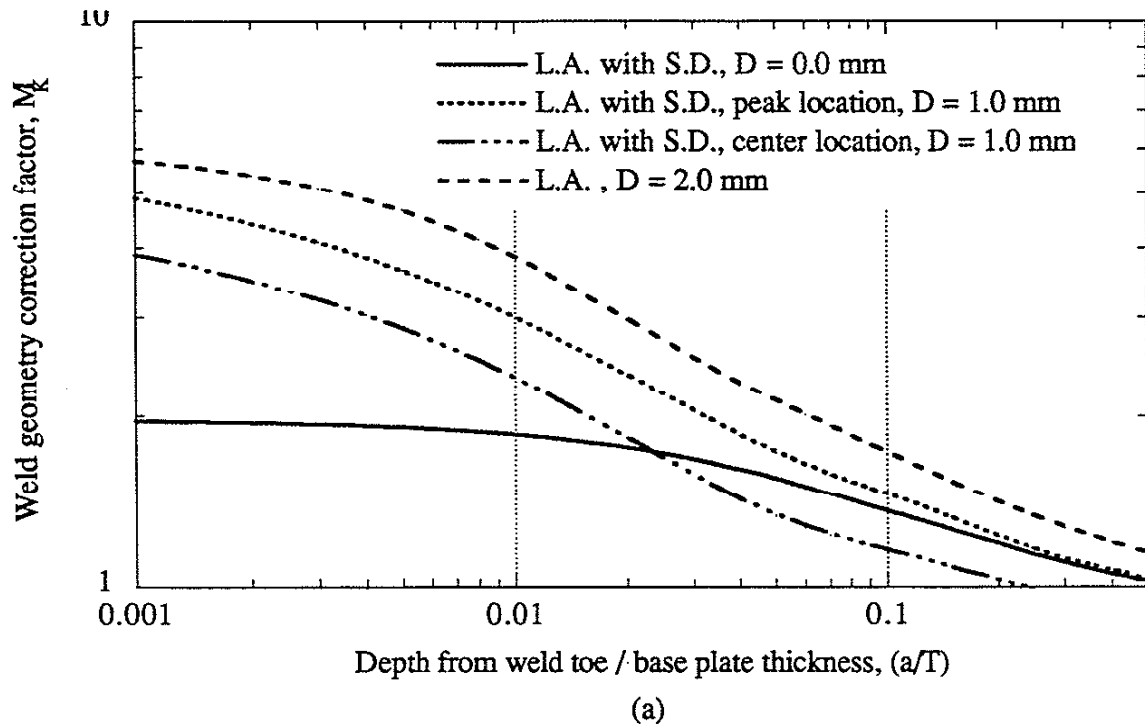


Fig. 7.12 The effect of cold-lap defects on (a) the weld geometry correction factor and (b) the fatigue crack propagation lives of longitudinal attachments with and without stress diffusers. ($\Delta S = 100$ MPa)

CHAPTER 8

FATIGUE LIFE PREDICTIONS

8.1 INTRODUCTION

In this chapter, fatigue life predictions will be made in order to see how well the FEM results of this study can predict the fatigue behavior of the experimental results of this study. The fatigue life predictions will first be made for the longitudinal attachments and the longitudinal attachments with stress diffusers without the presence of cold-lap defects. Finally, the fatigue life predictions will be made for both the longitudinal attachments and the longitudinal attachments with stress diffusers with the presence of cold-lap defects.

8.2 PROCEDURES

The values appropriate for the mild steel weldments of this study were used in all fatigue life predictions unless otherwise noted (Table 8.1). Strain-life predictions of the fatigue crack initiation life (nucleation and short crack growth) were made using the elastic stress concentration factor (K_t). Since the weldments were found to contain high tensile residual stresses, it was assumed that the fatigue cracks were fully open [40, 41]; thus, no crack closure was presumed in the calculation of the fatigue crack propagation life (N_p). An initial crack length of 100 μm was used for all fatigue crack propagation life predictions. Since the weld toe radii measured in the experimental study were very small, the differences in M_K determined from the weld toe and peak stress locations for these very small radii would be insignificant; therefore, predictions for cracks emanating from the peak stress location were not made in this study.

8.3 FATIGUE LIFE PREDICTIONS OF SPECIMENS WITHOUT COLD-LAP DEFECTS

8.3.1 Longitudinal Attachments

Predictions of the fatigue crack propagation life (N_p) and the total fatigue life ($N_T = N_i + N_p$) for a longitudinal attachment with a weld toe radius of 0.08 mm (average radius experimentally observed) are plotted in Fig. 8.1 along with the experimental results of this study and those of the database. Since no difference in fatigue life was observed in Chapter 3

for longitudinal attachments with weld leg lengths of 12.7 and 9.52 mm, all predictions in this section were made for longitudinal attachments with a weld leg length of 12.7 mm. The fatigue life predictions predict the experimental results well, especially at long lives.

At short lives (high stresses), the predictions fall slightly short of the experimental results. One possible reason could be the existence of crack closure for these higher stress levels which was not taken into account. Predictions of N_p and N_T using the bilinear Paris power law in the calculation of N_p are plotted in Fig. 8.1 also. Use of the bilinear Paris power law predicts the experimental results of this study well but drastically overpredicts the database results. Further review of the database results [21] revealed the presence of undercuts continuously along the weld toe as opposed to no defects for the specimens of Series 3 of this study; therefore, crack shape development was different. Use of the crack shape development function recommended by Smith et al. [21] gives the fatigue life predictions shown in Fig. 8.2. Use of this crack shape development function better predicts the results of the database at long lives.

8.3.2 Longitudinal Attachments with Stress Diffusers

All of the predictions made in this section are for the longitudinal attachments with stress diffusers of Series 3 (weld leg length = 9.52 mm.) since these were the only specimens without cold lap defects. Predictions of the fatigue crack propagation life (N_p) and the total fatigue life ($N_T = N_i + N_p$) for a longitudinal attachment with stress diffusers with a weld toe radius of 0.27 mm (average experimentally observed) are plotted in Fig. 8.3 along with the experimental results of this study and the transverse attachment results of the database.

The fatigue crack propagation life prediction provides a lower bound to the longitudinal attachments with stress diffusers and the transverse attachments. The total life predictions overpredict the longitudinal attachments with stress diffusers at short lives (high stresses) implying that the contribution of N_i to total fatigue life are overestimated. At long lives, N_T estimates the fatigue life of the experimental results of this study well. Predictions of N_p using the bilinear Paris power law are plotted in Fig. 8.3 also. Use of the bilinear Paris power law predicts the experimental results of this study even better.

8.4 FATIGUE LIFE PREDICTIONS OF SPECIMENS WITH COLD-LAP DEFECTS

8.4.1 Longitudinal Attachments

Predictions of the fatigue crack propagation life (N_p) and the total fatigue life ($N_T = N_i + N_p$) for a longitudinal attachment with a cold-lap defect with a weld root radius (r_d) of 0.025 mm and a defect depth of 2.0 mm (average experimentally observed) are plotted in Fig. 8.4

along with the experimental results of this study and those of the database. The fatigue life predictions for the specimen without a cold-lap defect with a weld toe radius of 0.08 mm (average experimentally observed) is shown in Fig. 8.4 for comparison. The fatigue crack propagation life (N_p) is predicted to be slightly longer for a crack propagating from a cold-lap defect. The fatigue crack initiation life (N_i) is completely eliminated by the presence of a cold-lap defect, and the total fatigue life (N_T) consists of only (N_p). At long lives (high stresses), the presence of an initiation life for the specimen without a cold-lap defect leads to predictions of total lives which are longer for specimen without a cold-lap defect. Use of the bilinear Paris power law predicts the data of this study well: see Fig. 8.5.

8.4.2 Longitudinal Attachments with Stress Diffusers

Predictions of the fatigue crack propagation life (N_p) and the total fatigue life ($N_T = N_i + N_p$) for a longitudinal attachment with stress diffusers with a cold-lap defect with a weld root radius (r_d) of 0.025 mm and a defect depth of 1.0 mm (average experimentally observed) are plotted in Fig. 8.6 along with the experimental results of this study and the database results for the transverse attachments. The fatigue life predictions for the specimen without a cold-lap defect with a weld toe radius of 0.27 mm (average experimentally observed) are shown in Fig. 8.6 for comparison.

In the presence of a cold-lap defect, the fatigue crack propagation life (N_p) is predicted to be slightly shorter. Once again, the presence of a cold-lap defect is predicted to eliminate any contributions to fatigue life from N_i ; thus, the presence of a cold-lap defect significantly decreases the predicted total fatigue life (N_T).

8.5 SUMMARY

The fatigue life predictions made using the FEM results of this study were in good agreement with the experimental results of this study. The long-life longitudinal attachment results from the database were explained with the use of crack shape development reported by other researchers for those weld details. The presence of cold-lap defects were predicted to eliminate the fatigue crack initiation life and not much affect the fatigue crack propagation life since the effect of cold-lap defects is mostly local. The experimentally observed decreases in the total fatigue life of longitudinal attachments with stress diffusers in the presence of cold-lap defects were predicted.

Table 8.1 The material properties used for the fatigue life predictions.

Yield Strength, S_y (MPa)	333
Ultimate Strength, S_u (MPa)	510
C' (mm/cycle)	2.2×10^{-9} [40]
	$6.1 \times 10^{-12} *$ [40]
m	3.3 [40]
	$6.3 *$ [40]

* Constants for Stage I crack propagation

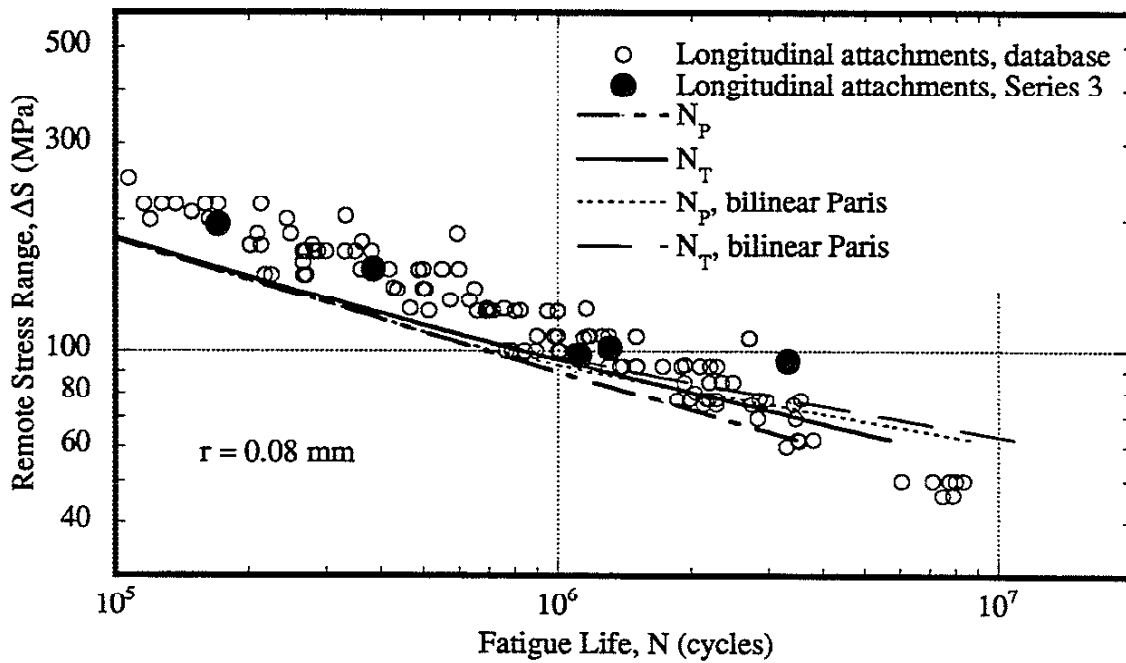


Fig. 8.1 The fatigue life predictions of the longitudinal attachments without cold-lap defects. A weld toe radius of 0.08 mm was modeled which was the average value experimentally observed.

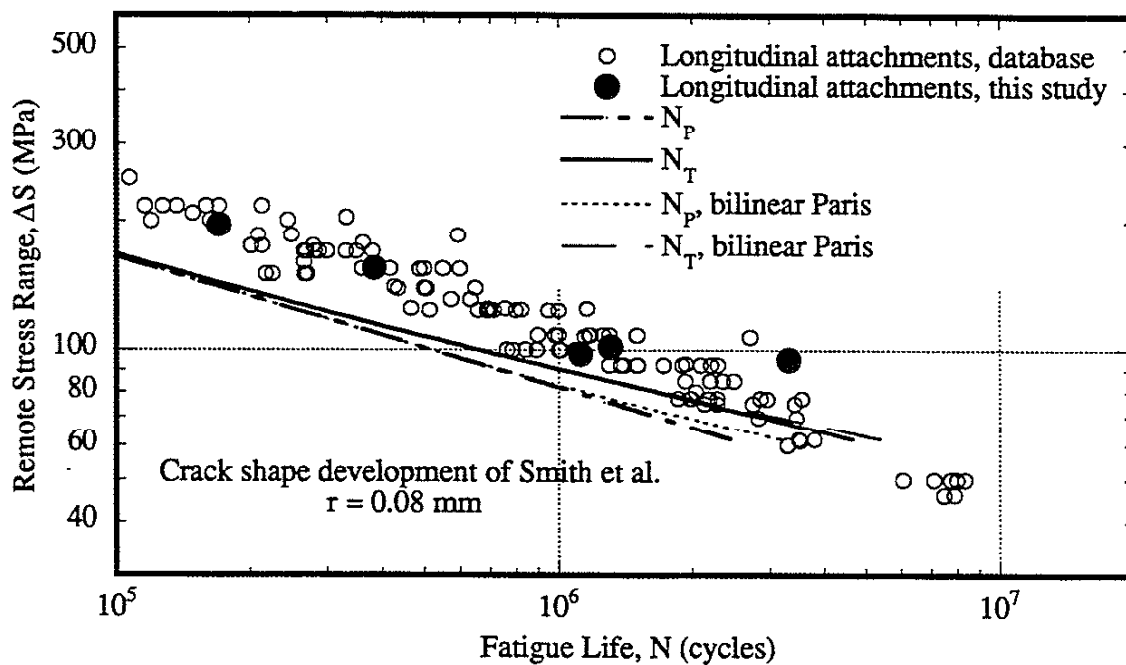


Fig. 8.2 The fatigue life predictions of the longitudinal attachments without cold-lap defects using the crack shape development of Smith et al.

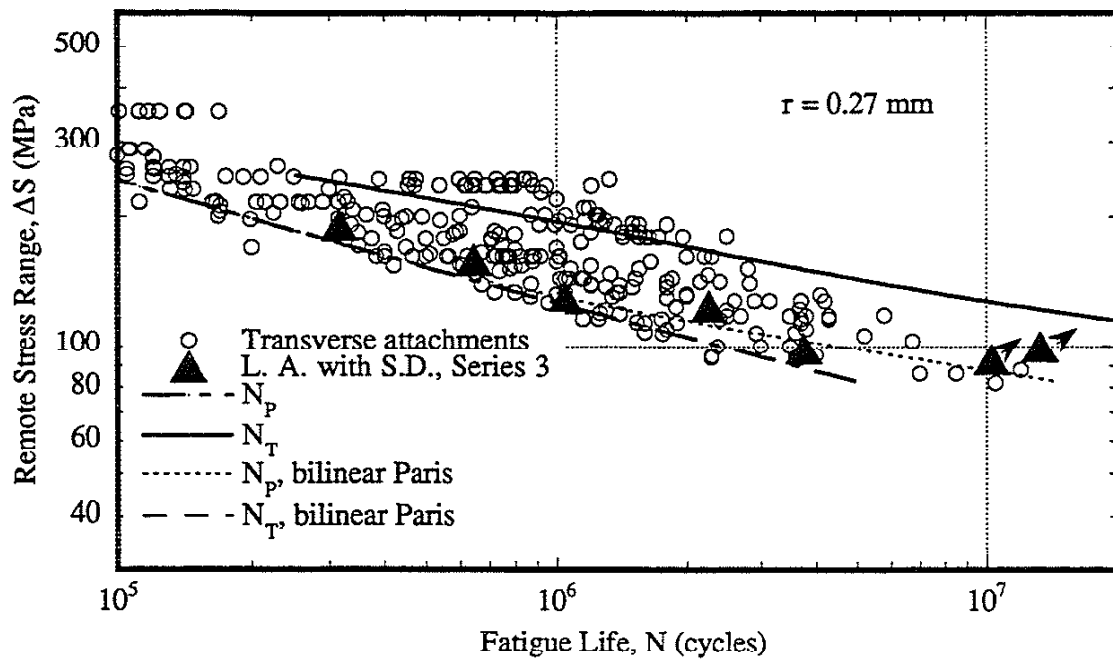


Fig. 8.3 The fatigue life predictions of the longitudinal attachments with stress diffusers without cold-lap defects. The weld toe was modeled with a radius of 0.27 mm (average value experimentally observed).

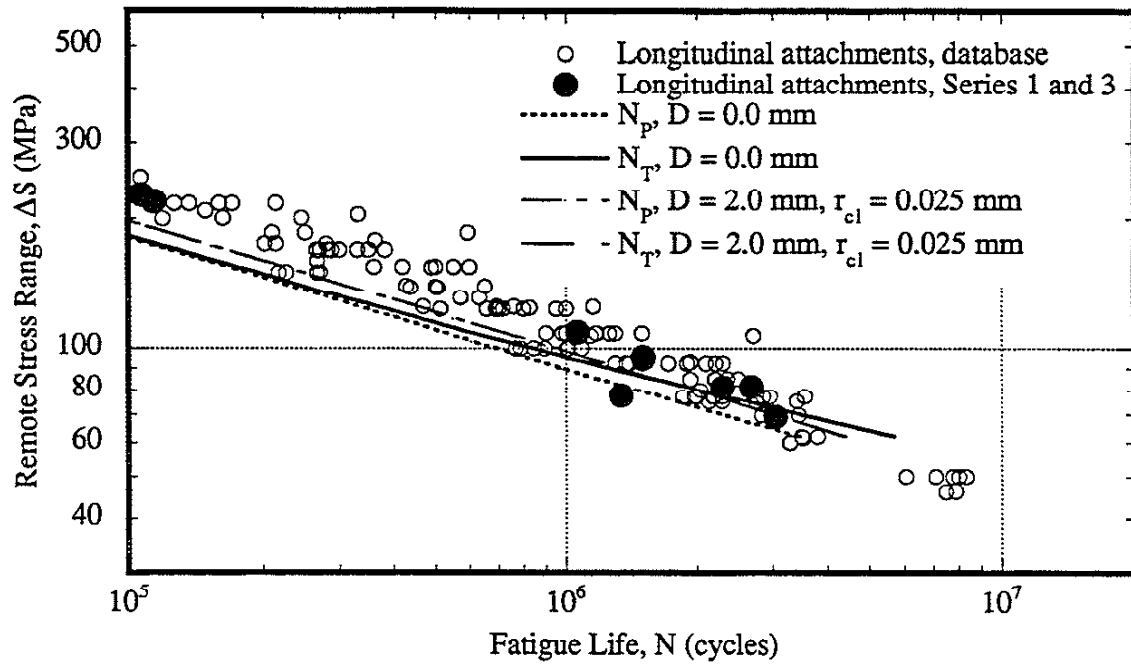


Fig. 8.4 The fatigue life predictions of the longitudinal attachments with stress diffusers with the presence of cold-lap defects.

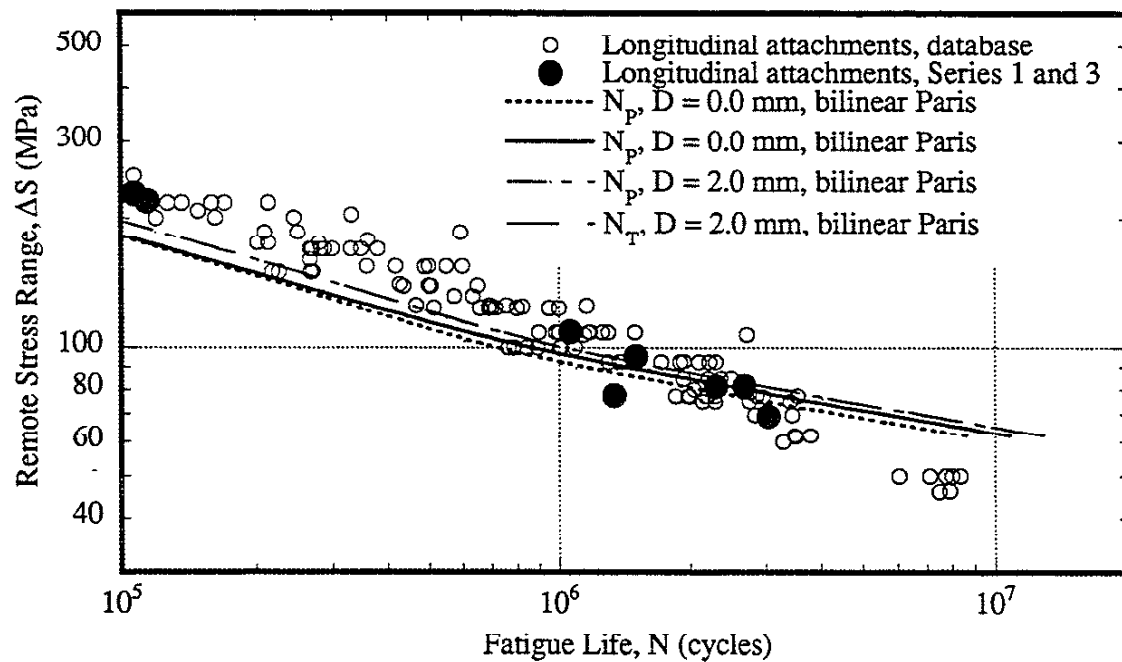


Fig. 8.5 The fatigue life predictions of the longitudinal attachments with stress diffusers with the presence of cold-lap defects.

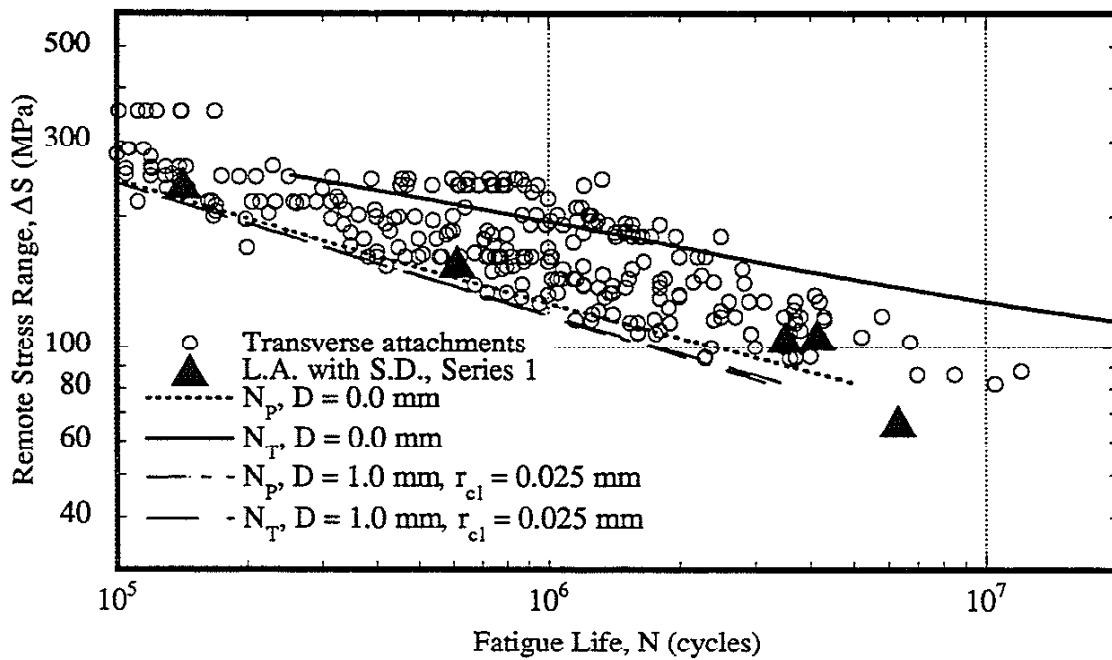


Fig. 8.6 The fatigue life predictions of the longitudinal attachments with stress diffusers with the presence of cold-lap defects.

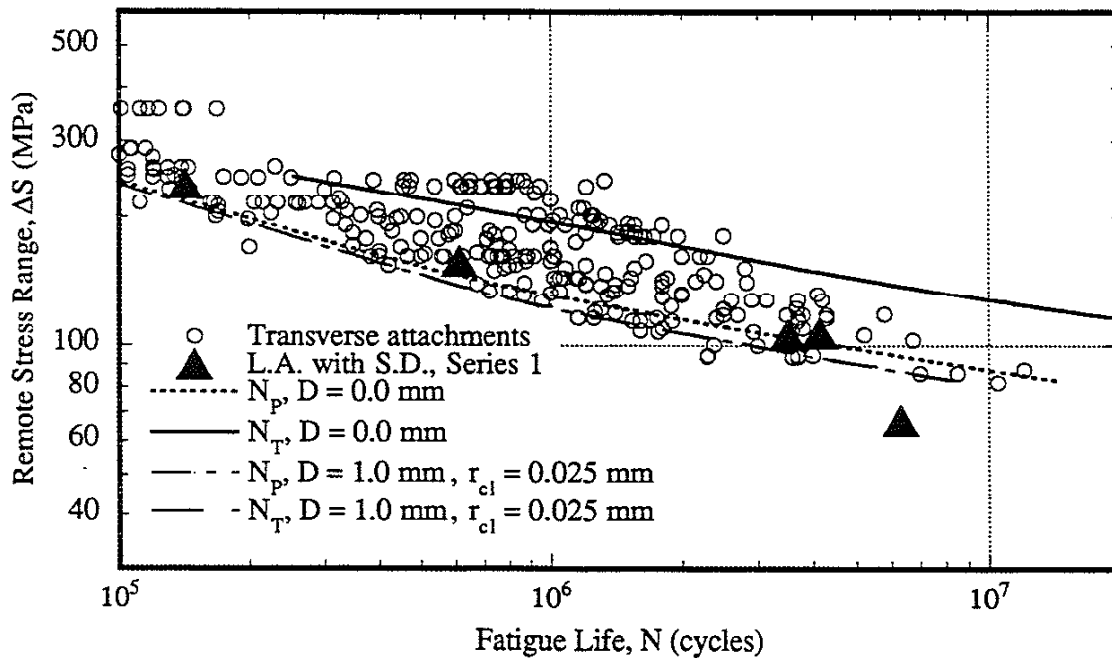


Fig. 8.7 The fatigue life predictions of the longitudinal attachments with stress diffusers with the presence of cold-lap defects. All N_p predictions used the bilinear Paris power law.

CHAPTER 9

DISCUSSION

9.1 WELD CLASSIFICATION BY CRACK INITIATION SITE

Five common scenarios for fatigue crack initiation in weldments were proposed:

- Initiation at Weld RIPPLE of longitudinally loaded groove or fillet welds
- Initiation at the weld toes of transversely loaded GROOVE welds
- Initiation at the weld toes of transversely loaded NON-LOAD-CARRYING FILLET welds
- Initiation at the weld toes of transversely loaded LOAD-CARRYING FILLET welds
- Initiation at the weld toes of longitudinally loaded welds (TERMINATIONS)

The S-N curves for the ripple, groove, non-load-carrying fillet, and load-carrying fillet scenarios are similar, but the S-N curves for the fillet weld terminations scenarios are lower than all others (see Fig. 1.3) suggesting that there are essentially:

- “Good” weldments with high fatigue resistance (ripple, groove, non-load-carrying fillet scenarios),
- “Maverick!” weldments having a variable fatigue resistance due to uncertainty in some critical variable like the size of the incomplete joint penetration (load-carrying fillet scenario),
- “Bad” weldments with low fatigue resistance (termination scenarios).

Figure 9.1 shows the S-N mean curves of “good”, “maverick”, and “bad” weldments. The example of a maverick included in Figs. 1.3 and 9.1 (the load-carrying fillet weld) has been found to have fatigue lives as long as the “good” weldments or almost as short as the “bad” weldments depending on the amount of incomplete joint penetration.

It can be seen from Fig. 1.3, that the mean S-N curve of the fillet weld termination (and thus the longitudinal attachment) has a lower slope than the mean curve-fit lines of the other S-N curves indicating the virtual elimination of a fatigue crack initiation life (N_i) (nucleation and short crack growth). The high stress concentrations (3-D stress effects and

¹ “Maverick” weldments which do not fit in either category because some aspect of their geometry is undefined (partial penetration, undercut) or the definition of nominal stress is unclear and varies from investigator to investigator. This large group of weldments have been termed “mavcricks” by Lawrence [42]

small weld toe radius often due to poor weld quality) and high tensile residual stresses associated with weld terminations virtually eliminate N_i . Further, the high stress concentrations² of weld terminations initiate many cracks along the weld toe which coalesce rapidly and lead to low-aspect-ratio initiated cracks. Thus, the fatigue crack propagation life (N_p) for weld terminations (longitudinal attachments) is also diminished by the lesser contribution from crack shape development to N_p .

9.2 THE FATIGUE BEHAVIOR OF LONGITUDINAL ATTACHMENTS

9.2.1 Significance of Welding Process on Defect Distribution

Almost all of the longitudinal attachments included in the database have been fabricated with the shielded metal arc welding (SMAW) process. Smith et al. [21] inspected longitudinal attachments fabricated with the SMAW process and found undercuts at every location inspected. Smith et al. suggested there was virtually a single continuous defect along the weld toe of the wrap-around weld.

The Series 1 and 2 longitudinal attachments of this study and those of the Nordic Project [22] were fabricated using the Gas Metal Arc Welding (GMAW) process using gravitational and/or short-circuit transfer. In both studies, the inspection of the weld toes of these specimens revealed the presence of cold-lap defects. In his study, some specimens were welded using GMAW spray transfer (Series 3). The use of spray transfer improved the weld quality and eliminated the presence of the cold-lap defects.

Thus, the nature of the initial defects in the weld toe region is completely dependent on the weld process used. Furthermore, weld toe defects can be completely eliminated using proper welding parameters.

9.2.2 The Poor Fatigue Behavior of Longitudinal Attachments

This study has shown that the poor fatigue behavior of longitudinal attachments results from a combination of three factors associated with the weld terminations or wrap-around-welds at the ends of the attachments:

- Very high 3-D stress concentrations,
- Very high tensile residual stresses,

² Crack shape development has been found to be a function of K_t [43].

- Poor weld quality.

Using 3-D FEM analyses, it was found that the longitudinal attachment has very high 3-D stress concentrations at the end of the attachments. The stress concentration factor (K_t) at the weld toe and the weld geometry correction factor (M_K) have been found to be considerably larger than those of a weldment with transverse attachments (transverse attachment). These higher values of K_t and M_K lead to significant decreases in the fatigue crack initiation (N_i) and propagation (N_p) lives of longitudinal attachments.

Very high tensile residual stresses were measured in the longitudinal direction of the weld at the end of the longitudinal attachments with wrap-around welds. This observation is consistent with that of Gurney [2] who found the longitudinal residual stresses to be considerably larger than the transverse residual stresses. In other studies of the longitudinal attachment [12, 17, 19], the residual stresses have been found to approach the yield strength of the base metal. However, this study has shown the tensile residual stresses (595 MPa) far exceed the yield strength (333 MPa) of the base metal probably as a result of the high yield strength of the weld metal. Since the axial load is applied in the same direction as the high tensile residual stresses in the longitudinal attachment (longitudinal direction of the weld), the residual stresses much affect the fatigue life of the longitudinal attachment. The presence of these very high tensile residual stresses along with the 3-D stress concentration mentioned above eliminate any contribution to fatigue life obtained from the fatigue crack initiation life (nucleation and short crack growth). In addition, the presence of very high tensile residual stresses assure that no crack closure takes place thereby minimizing the fatigue crack propagation life (N_p), as well.

Creating the wrap-around welds at the end of the attachment is very difficult, and the welder has little control of the welding process. These difficulties contribute to poor weld quality. Severe cold-lap defects were found at the toes of wrap-around welds for the Series 1 longitudinal attachments which used gravitational and short-circuit transfer in the GMAW process. The most severe cold-lap defects were found to have a depth of around 2 mm. The presence of even small cold-lap defects eliminates any contribution to the fatigue life from fatigue crack initiation, and deeper cold-lap defects also reduces the fatigue crack propagation life: see Fig. 7.6.

The welding procedures for the Series 3 specimens employed spray transfer and were found to have no cold-lap defects. The average weld toe radius for the Series 3 longitudinal attachments was found to be 0.08 mm. The very small radius of the longitudinal attachments results in a very high K_t and M_K and therefore short N_i and N_p .

9.3 THE USE OF STRESS DIFFUSERS

9.3.1 Stress Diffusers

Specially designed parts termed “stress diffusers” were incorporated in the wrap-around welds at the ends of the attachments to improve the fatigue resistance of longitudinal attachments. The introduction of stress diffusers into the weld detail geometry increased the fatigue life of longitudinal attachments by:

- Reducing stress concentrations,
- Reducing residual stresses,
- Improving weld quality.

The stress diffusers effectively reduce the high stress concentration at the end of the attachments by diffusing stress along a greater portion of the weld toe. The weld toe stress concentration factor was shown to be reduced by 23% and the weld geometry correction factor was shown to be significantly reduced: see Fig. 4.7.

The residual stresses in a longitudinal attachment are reduced with the use of stress diffusers. Measurements showed that the stress diffusers reduce the residual stresses adjacent to the weld toe from 595 to 252 MPa (58%). This reduction in residual stress is expected as the weld will change from being longitudinal to the load to being nearly transverse to the load at the critical area in front of the stress diffuser. Residual stresses transverse to a weld are considerably lower than longitudinal residual stresses in a weld [2].

The use of stress diffusers in a longitudinal attachment improves the weld quality. The use of stress diffusers eliminates the wrap-around welds. Consequently, the welder has better control of the welding process; and the formation of severe cold-lap defects is avoided. For example, the cold-lap defects of the longitudinal attachments with stress diffusers were reduced in size from 2.1 mm to 1.4 mm.

In the absence of cold-lap defects (Series 3), the average weld toe radius for longitudinal attachments was found to be 0.08 mm. The use of stress diffusers in the longitudinal attachment leads to improved weld quality: the average weld toe radius increases from 0.08 mm without the stress diffuser to 0.27 mm with a stress diffuser.

9.3.2 Comparison with Transverse Attachments

A database of both longitudinal and transverse attachment fatigue results was created, and all its data are plotted in Fig. 9.2. At short lives (high stresses), transverse attachments show slightly longer fatigue lives than longitudinal attachments. It should be noted that the scatter for transverse attachments is much larger. At long lives (low stresses), there is a considerable difference between the two since transverse attachments have fatigue lives much longer than longitudinal attachments.

Longitudinal attachments with stress diffusers should exhibit similar fatigue behavior to transverse attachments, and similar fatigue lives because longitudinal attachments with stress diffusers and transverse attachments have similar hot spot stresses or M_x (Fig. 4.8), residual stresses, and weld quality. The fatigue results from this study are plotted with the fatigue results from the database in Fig. 9.2. The data for longitudinal attachments of this study are consistent with the fatigue database results. At short lives (high stresses), there is very little effect of the stress diffuser; likewise, there is really no difference in fatigue lives for transverse and longitudinal attachments. At long lives (low stresses), significant increases in the fatigue life are obtained with the use of stress diffusers for specimens of Series 3 (no cold-lap defects). For longitudinal attachments with a fatigue life of $2E+06$ cycles, increases of 360% in fatigue life and 32% in fatigue strength were obtained with the use of stress diffusers. Even when cold-lap defects are present (Series 1 and 2), stress diffusers still increase the fatigue life. In general, it can be said that the fatigue life of longitudinal attachments with stress diffusers are similar to transverse attachments and that stress diffusers are very effective.

9.3.3 Applicability and Limitations of Stress Diffusers

Stress diffusers can probably be used in many different applications. One possible application was investigated thoroughly in Chapter 6 where stress diffusers were included in the beam-to-column connection. There are certainly other applications for stress diffusers to improve the fatigue life of common weld details. Stress diffusers can be used in any weld details (simple or complex) which have longitudinally welded attachments (load-carrying or non-load-carrying) which permit the inclusion of a stress diffuser(s). The stress diffuser can vary in dimensions and shape depending on the particular weld detail. The most common weld details [1] are shown in Fig. A1.1. Stress diffusers could be used to improve the fatigue life of longitudinally welded attachments such as details 25B, 30, 30A, 36, 37, 39A, 39B, 49, 50, 51, and 52.

Stress diffusers used in this study were expensive to make because they were machined from plate material. An alternative method of construction could be to punch out stress diffusers from thinner plates and then stack them to achieve the desired height. This alternate method of construction would create unbonded interfaces between the stacked stress diffusers which might alter the stress distribution in the joint. Further FEM analysis is necessary to determine the effect of these interfaces.

9.4 MODELING ISSUES

9.4.1 Cold-lap defects

FEM analyses of cold-lap defects have shown that their presence virtually eliminates the fatigue crack initiation life (N_i), because their notch-root stress concentration factors (K_t) are very large (≈ 16). Longitudinal attachments without cold-lap defects have been shown to have a very short N_i as high stress concentrations (3-D effect and small weld toe radius ($r = 0.08$ mm)) and tensile residual stresses (595 MPa) exist at the weld toe: see Fig. 8.1. Therefore, the presence of cold-lap defects does not significantly reduce the total fatigue life ($N_T = N_i + N_p$) of longitudinal attachments because N_i was already eliminated by the combination of the high weld toe K_t and tensile residual stresses. The presence of a cold-lap defect was shown to reduce the fatigue crack propagation life (N_p) very little because its effect is rather local.

Longitudinal attachments with stress diffusers without cold lap defects have been shown to have a significant N_i because lower stress concentrations (3-D stress effects minimized and $r = 0.27$ mm) and tensile residual stresses (252 MPa) exist at the weld toe: see Fig. 8.3. Therefore, the presence of cold-lap defects which eliminate N_i significantly reduce the total fatigue life ($N_T = N_i + N_p$) of longitudinal attachments with stress diffusers. The presence of a cold-lap defect was shown to affect the fatigue crack propagation life (N_p) very little because its effect is local.

Even though the presence of cold-lap defects have been shown to have a greater effect on the fatigue life of longitudinal attachments with stress diffusers than the fatigue life of longitudinal attachments, the fatigue lives of longitudinal attachments with stress diffusers having cold-lap defects are longer than the fatigue lives of longitudinal attachments with cold-lap defects: see Figs 7.13 and 9.3.

9.4.2 Crack Shape Development

Crack shape development influences the fatigue crack propagation life (N_p). The nature of the initial defect(s) is critical and will control the crack shape development for very

short cracks, a large portion of N_p . The effect of welding process on the initial defect distribution was shown in section 9.2.2 and the type and size of the initial defects in the weld toe region were found to depend on the weld process used. The crack shape development pattern found in this study (see Figs. 2.9) was plotted with that reported by Smith et al. [21] for cracks growing in a longitudinal attachment welded with the SMAW process in Fig. 9.3. It can be seen from Fig. 9.3, that the crack shape development patterns observed in the two studies are different for cracks less than 1 mm. This difference in crack shape development is due to differences in initial defects resulting from the different weld processes of the two studies. The very small values of Smith et al. reflect the continuous undercut defect found at the weld toe.

The crack shape development results of Bell et al. [43] and Otegui et al. [44] found for T-plate specimens are plotted in Fig. 9.3 along with the crack shape development results of this study and Smith et al. It can be seen that each study suggested different crack shape development patterns. For the very short crack lengths examined, the results of this study are in best agreement with the results of Otegui et al. The crack aspect ratio of cracks for this study and that of Otegui et al. were observed to increase for very short cracks. The crack shape development pattern of Bell et al. suggests the presence of a semi-circular crack ($a = c$) at the onset of fatigue crack propagation. At long crack lengths, the crack shape development functions are not as important to fatigue crack propagation life, and the small differences between all the functions are not as important.

The results of this study for crack shape development up to 1 mm were used, and then crack shape development function of Bell et al. was adopted for crack lengths greater than 1 mm. The use of this combined crack shape function did not predict the results of the database at very long fatigue lives: see Fig. 8.1 which shows results for SMAW fabricated specimens. The use of the crack-shape development function of Smith et al. leads to slightly better predictions of the fatigue crack propagation life: compare Figs. 8.1 and 8.2.

9.5 FUTURE WORK

The shapes of the alternative stress diffusers shown in Fig. 4.1 should be optimized, and then their effect determined through an experimental study. Some of these alternative shapes may be less expensive to fabricate and use. For example, the stress diffuser which spans the entire width of the main plate would require less machining and would provide a straight, transverse weld which may improve weld quality. For certain applications in which the main plate width is small, this shape of stress diffuser may be the best design.

Additional studies of longitudinal attachments fabricated using spray transfer GMAW should be undertaken to see if this less-defect-prone welding process can provide substantial increases in the fatigue life over those fabricated using SMAW .

Inelastic analyses should be performed to understand the performance of the stress-diffuser-enhanced connection in the plastic regime. The use of the stress diffuser in the Northridge beam-to-column connection may be further improved by reducing the stiffness of the current design through reductions in the diffuser plate thickness and its weld sizes.

A study of residual stresses should be undertaken to determine the influence of many variables such as weld process, weld metal strength, and base metal strength on residual stresses. Measurements should be made for both longitudinal attachments and transverse attachments.

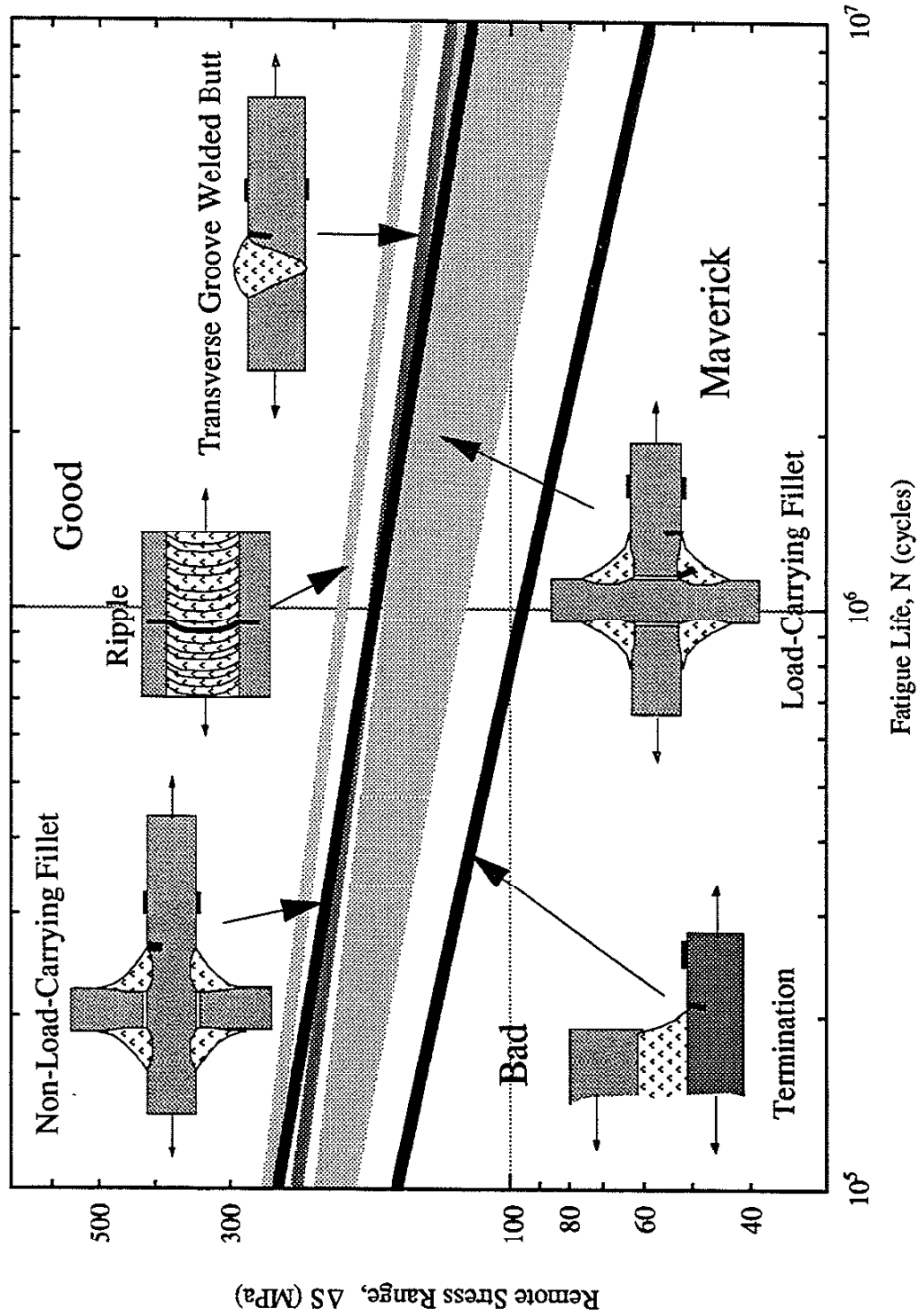


Fig. 9.1 Comparison of the mean S-N curves for weldments with different fatigue crack initiation sites. There are "good" weldments having a high fatigue resistance, "bad" weldments having a low fatigue resistance, and "maverick" weldments having a variable fatigue resistance due to uncertainty in some critical variable. The longitudinal attachment is one of the several weldment geometries referred to as terminations.

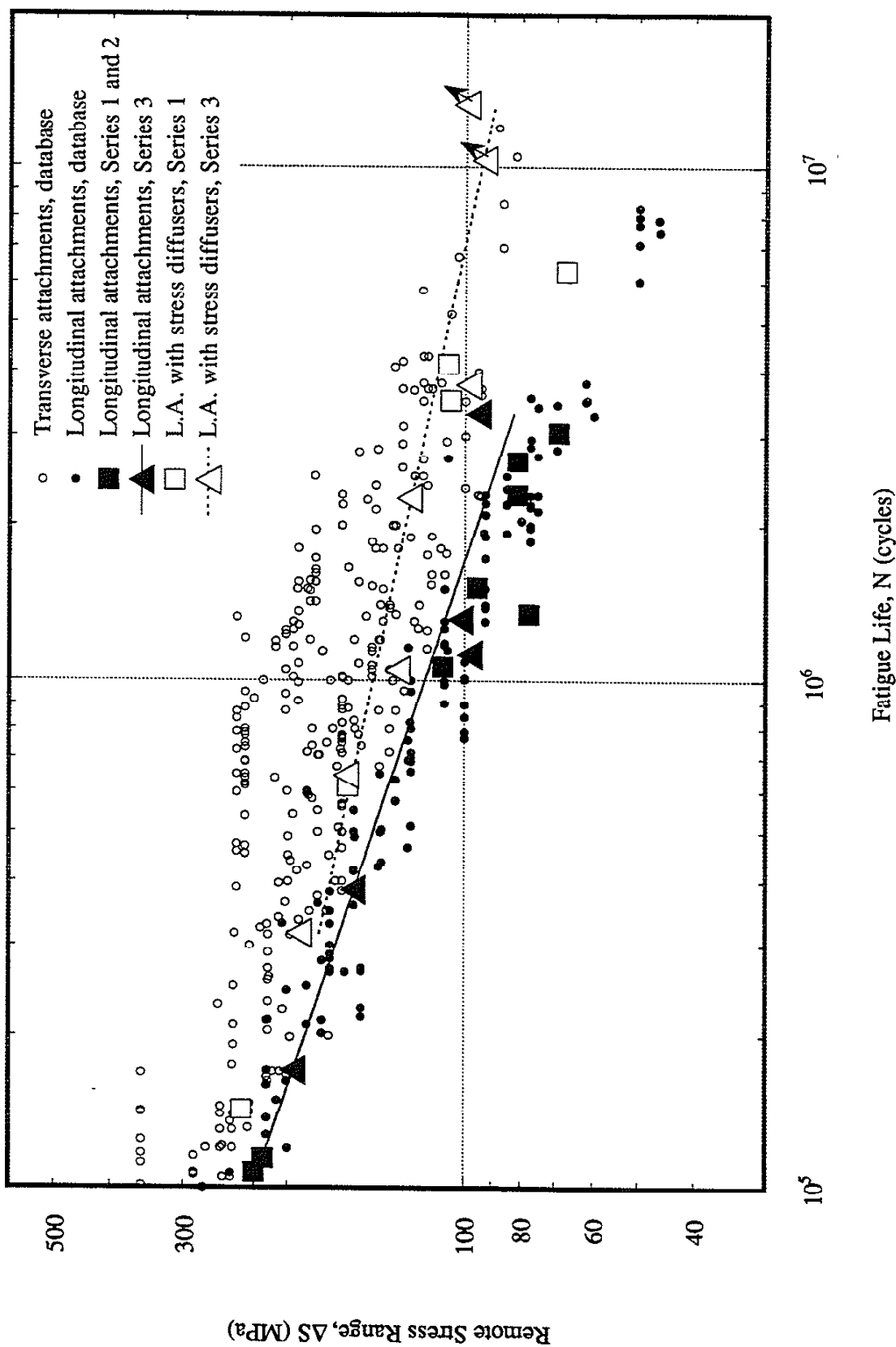


Fig. 9.2 Comparison of the fatigue database results for transverse and longitudinal attachments with the results of this study. An increase in the fatigue life of longitudinal attachments with stress diffusers is observed at long lives (low stresses) for the Series 3 specimens (no cold-lap defects).

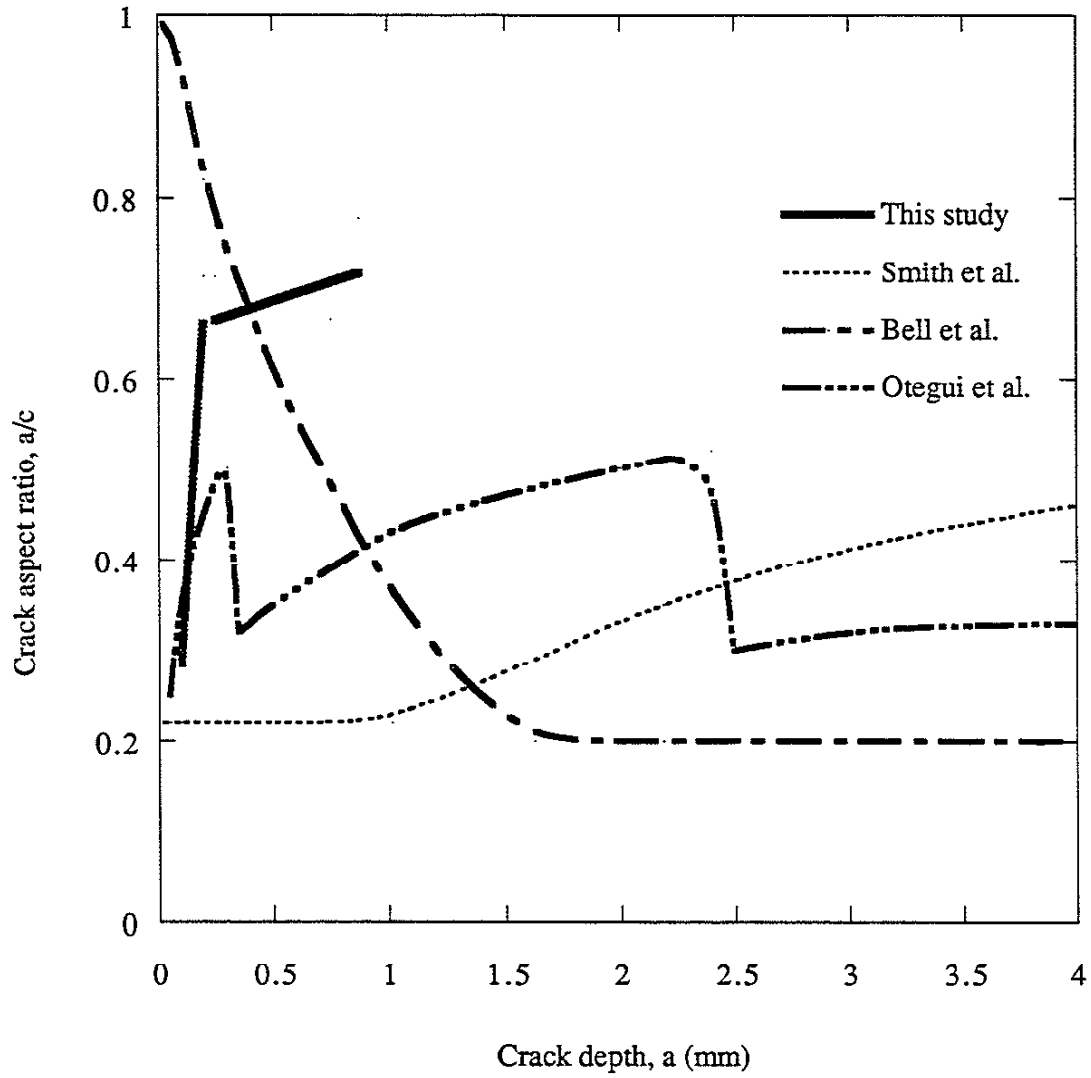


Fig. 9.3 Comparison of crack shape development patterns for weldments.

CHAPTER 10

CONCLUSIONS

1. Weldments with fillet weld terminations exhibit the shortest fatigue lives of all weldments, especially at long lives. The poor fatigue strength of longitudinal attachments is due to the combination of a very high 3-D stress concentration, very high tensile residual stresses, and poor weld quality. The poor weld quality associated with the ends of the attachments is manifest as cold-lap defects or small weld toe radii depending on the weld process used.
2. Cold-lap defects were the fatigue-crack-initiating defect for longitudinal attachment weldments fabricated using gravitational and/or short circuit transfer gas-metal-arc-welding (GMAW). The use of a higher heat input (spray transfer) in GMAW was found to eliminate the cold-lap defects.
3. Specially designed stress-concentration-reducing parts termed "stress diffusers" were incorporated in the wrap-around welds at the ends of the longitudinal attachments. For longitudinal attachments with a fatigue life of $2E+06$ cycles, increases of 360% in fatigue life and 32% in fatigue strength were obtained with the use of stress diffusers. Stress diffusers increased the fatigue strength of longitudinal attachments to equal that of transverse attachments.
4. The use of a stress diffuser in a beam-to-column connection was found to eliminate the high stress concentration at the weld access hole and to reduce the maximum principal stresses in the region of the intersection of the bottom beam flange and column flange by 31%.
5. Fatigue life predictions made using the FEM results of this study were in good agreement with experimental results. The presence of cold-lap defects was predicted to eliminate the fatigue crack initiation life and to affect the fatigue crack propagation life very little since the influence of cold-lap defects is localized.

APPENDIX 1: EXPERIMENTAL INDICATION OF THE POOR FATIGUE BEHAVIOR OF FILLET WELD TERMINATIONS

A1.1 DATABASE INFORMATION

The 53 structural details of SSC-318 [1] shown in Fig. A1.1 were re-evaluated. First the number of details considered were reduced by eliminating everything which was not a welded joint except for plain plate (Details 1 and 2) which were used as a reference. The data was then screened¹ to create a data set representative of as-welded details. Any data with a thickness greater than 7/8" was corrected for the effect of weldment size with an weldment size effect exponent of 0.25 as recommended by Gurney [2]. The mean fatigue strength of each structural detail at 1E+06 cycles for various load ratios and material strengths is listed in Table A1.1.

A1.2 THE EFFECT OF LOAD RATIO AND MATERIAL STRENGTH

The importance of load ratio, R , is evident as most of the details tested under reversed loading ($R = -1$) exhibit higher fatigue strengths: see Table A1.1. The effect of load ratio becomes less important for weldments with high tensile residual stresses such as Detail 30 which has a fillet weld termination. The effect of material strength can also be important: see Table 1.1. For most weld details, such as Detail 10, there is a direct correlation between material strength and fatigue strength. If a weld detail exhibits only a fatigue crack propagation life, an increase in material strength could lead to a decrease in fatigue strength. This decrease can be explained by fatigue crack closure.

A1.3 A WELD CLASSIFICATION SYSTEM BASED ON THE SITE OF CRACK INITIATION

In order to eliminate the effects of material strength and load ratio, only mild steel ($S_y < 310$ MPa) data tested at $R = 0$ loading was considered. Thus, all entries in Table A1.1 for which there was no data for the case " $R = 0, S_y < 310$ MPa" were eliminated. This process resulted in the entries of Table A1.2. The structural details were sorted in the order of increasing fatigue notch factor, K_f^2 . The corresponding fatigue crack initiation site for each

¹ All data for specimens altered by post-weld improvement techniques, tested in a corrosive environment, tested with unusual methods, fabricated with unusual procedures, and which were unfailed were eliminated.

² The fatigue notch factor is defined as the ratio of the fatigue life of a smooth specimen to that of a notched specimen at a given fatigue life.

detail is listed in Table A1.2. In general, there are four usual fatigue crack initiation sites (see Fig. 1.1):

- Weld ripple
- Weld toes
- Weld terminations
- Weld roots³

Upon an even further and more detailed inspection of the data, it was recognized that these general categories lead to five common weldment fatigue crack initiation scenarios:

- Initiation at weld RIPPLE of longitudinally loaded groove or fillet welds (R)
- Initiation at the weld toes of transversely loaded GROOVE welds (G)
- Initiation at the weld toes of transversely loaded NON-LOAD-CARRYING FILLET welds (F)
- Initiation at the weld toes of transversely loaded LOAD-CARRYING FILLET welds (F')
- Initiation at the weld toes of longitudinally loaded welds (TERMINATIONS) (T)

Each of these five locations has been termed an initiation site category and given a letter designation. The SSC-318 detail describing each initiation site category in its purest form is shown in Fig. 1.2.

The initiation site of each entry in Table A1.2 was associated with one of the five initiation site categories, R, G, F, F', or T. Upon comparing all the entries in Table A1.2 having a certain initiation site category, it was apparent that all of these details had roughly the same S-N diagram. Some details differed from the rest for one of several apparent reasons: the loading was pure bending as opposed to axial or pseudo-axial⁴ loading; the stress was based on shear loading; weldment geometry (notch severity) was actually undefined because of a variable or unknown depth of weld penetration or the possibility of serious undercuts (resulting from wrap-around welds), and finally for other reasons such as changes in section thickness, transition details, intermittent welds, etc. Those details deemed a little strange for their initiation site category have a comment entered in the final column of Table A1.2. These welds were eliminated to create Table A1.3. The selected details of Table A1.3 were used to validate the concept of categorizing weldments based on initiation site: see Fig A1.2. It can be seen in Fig. A1.2 that all of the data within an initiation site category have similar fatigue strengths.

Mean S-N curves were calculated for each of the initiation site categories based on all the available data for that category: see Fig. A1.3. All of the weld initiation site category data sets and their corresponding mean lines were plotted together on one graph: see Fig. 1.2.

³ Only failures at the welds exterior were considered in this study. Root failures were not considered.

⁴ Bending of deep sections designated as AB in Table A1.2.

Figure 1.2 shows that the S-N curves for ripple, groove, non-load-carrying fillet, and load-carrying fillet scenarios are similar and that the S-N curves for fillet weld terminations scenarios are lower than all others.

Table A1.1 The mean fatigue strength of the SSC-318 weldment details at 1E+06 cycles.

SSC - 318 Weldment Details	Mean Fatigue Strength ΔS at 1E+06 cycles (MPa)			
	All R	R = 0	R = -1	R = 0, $S_y < 310$ MPa R = -1, $S_y < 310$ MPa
1 (All)	242.5	255.6	284.3	-
1M	241.5	239.8	291.0	-
1H	280.0	288.2	351.1	-
1Q	260.5	299.8	353.0	-
2	301.6	287.9	-	-
3	179.1	184.9	-	188.5
4	196.0	203.7	-	219.1
4A	145.1	145.1	-	145.1
5	82.1	79.2	-	81.8
5A	83.9	89.0	-	89.0
5B	61.7	63.1	-	63.1
7(B)	167.0	171.3	-	178.5
10M	142.5	148.6	108.2	-
10H	194.6	188.0	289.2	-
10Q	159.6	165.5	239.4	-
10A	191.6	268.2	102.9	102.9
11	156.6	147.3	152.3	143.4
12	128.2	128.2	-	128.2
13	196.0	191.6	-	202.1
14	144.8	142.5	180.0	138.5
15,32A	94.2	94.2	-	94.2
16	124.9	124.9	-	125.9
17	97.9	97.9	-	97.9
17A	97.3	99.1	108.2	108.2
18	63.1	63.1	95.0	95.0
19	92.0	95.4	-	64.9
20	86.0	115.1	-	114.7
21	123.7	123.7	-	123.7
22	134.1	136.5	141.7	132.7
24	111.8	113.1	-	-

Table A1.1 (cont.) The mean fatigue strength of the SSC-318 weldment details at 1E+06 cycles.

SSC - 318 Weldment Details	All R	Mean Fatigue Strength ΔS at 1E+06 cycles (MPa)			
		R = 0	R = -1	R = 0, Sy < 310 MPa	R = -1, Sy < 310 MPa
25	148.4	148.9	146.4	165.0	205.4
25A	232.5	198.6	285.0	217.5	311.0
25B,36	170.5	170.5	-	170.5	-
26	88.7	121.1	184.9	121.1	184.9
30	110.5	112.3	121.0	112.5	121.0
30A	158.2	158.2	-	158.2	-
30B	111.4	111.4	-	111.4	-
31	100.8	100.8	-	100.8	-
31A	99.5	102.2	-	-	-
31B	106.1	107.4	-	-	-
31C	159.1	-	-	-	-
33	69.0	78.8	62.3	78.8	62.3
36A	147.1	147.1	-	147.1	-
38	104.8	104.8	-	104.8	-

Table A1.2 The mean fatigue strength of the SSC-318 weldment details made of mild steel.

SSC-318 Weldment Details	Loading	Mean Fatigue Strength (ΔS) at 1E+06 cycles (MPa) R = 0, $S_y < 310$ MPa	Kf	Fatigue Crack Initiation Sites	Initiation Site Category	Comments
10A	B	279.2	1.23	Toe	G	pure bending
2	A	243.4	1.41	-	-	plain plate
1	A	239.9	1.43	-	-	plain plate
4,6	AB	219.3	1.57	Ripple	R	
25A	A	217.9	1.58	Toe	F	change in flange width
13	AB	202.0	1.7	Toe	G	
3	A	188.9	1.82	Ripple	R	toe or termination failure
7B	AB	178.6	1.92	Toe and C.T.	F	toe or termination failure
25B,36	AB	170.3	2.01	Toe or Toe and D.T.	T	
25	A	164.8	2.08	Toe	F	
30A	B	158.6	2.17	Toe and D. T.	T	pure bending
10M	A	148.9	2.31	Toe	G	
36A	AB	146.9	2.33	D.T.	R-T	intermittent weld
4A	AB	145.5	2.36	D.T.	R-T	intermittent weld
11	AB	143.4	2.40	Toe	G	
14	A	138.6	2.48	Toe	F'	attachment or cruciform
22	AB	133.1	2.58	Toe	F	change in flange slope
12	AB	128.2	2.67	Toe	G	partial penetration
16	A	126.2	2.72	Toe or Root	G	
21	AB	123.4	2.77	Toe	F'	
26	A	121.4	2.83	Toe	F	
20	A	114.5	2.99	Toe	F'	
30	A	112.4	3.05	Toe at C.T. or D.T.	T	
30B	A	111.7	3.08	D.T.	T	
38	AB	104.8	3.27	Toe	F	high restraint
31	AB	100.7	3.4	D.T.	T	
17A	A	99.3	3.46	D.T.	T	

Table A1.2 (cont.) The mean fatigue strength of the SSC-318 weldment details made of mild steel.

SSC-318 Weldment Details	Loading	Mean Fatigue Strength (ΔS) at 1E+06 cycles (ksi.) R = 0, $S_y < 45$ ksi.	K _f	Fatigue Crack Initiation Sites	Primitive	Comments
17	A	97.9	3.5	D.T.	T	
15.32A	AB	94.5	3.64	D.T.	T	
5A	AB	88.9	3.85	Toe or D.T.	T	toe or termination failure
5	AB	80.7	4.26	Toe or Toe at C.T.	T	toe or termination failure
33	A	78.6	4.35	D.T.	T	
19	A	64.8	5.29	Toe	F'	reduced section
5B	AB	63.4	5.44	D.T.	T	
18	A	62.7	5.48	D.T.	T	

* C.T. - Continuous Termination, ** D.T. - Discontinuous Termination,

A - Axial, B - Bending, AB - Deep section loaded under bending but stress at hot-spot pseudo-axial.

Table A1.3 Welded details from SSC-318 selected for similarity to the primitive weldments.

SSC-318 Weldment Details	Loading	Mean Fatigue Strength (ΔS) at 1E+06 cycles (MPa) R = 0, Sy < 310 MPa	K _f	Fatigue Crack Initiation Sites	Initiation Site Category
4,6	AB	219.3	1.57	Ripple	R
25A	A	217.9	1.58	Toe	F
3	A	188.9	1.82	Ripple	R
25	A	164.8	2.08	Toe	F
10M	A	148.9	2.31	Toe	G
11	AB	143.4	2.4	Toe	G
14	A	138.6	2.48	Toe	F'
21	AB	123.4	2.77	Toe	F'
26	A	121.4	2.83	Toe	F
20	A	114.5	2.99	Toe	F'
30	A	112.4	3.05	Toe	T
30B	A	111.7	3.08	Toe at C.T.* or D.T. D.T.**	T
31	AB	100.7	3.4	D.T.	T
17A	A	99.3	3.46	D.T.	T
17	A	97.9	3.5	D.T.	T
15,32A	AB	94.5	3.64	D.T.	T
33	A	78.6	4.35	D.T.	T
5B	AB	63.4	5.44	D.T.	T
18	A	62.7	5.48	D.T.	T

* C.T. - Continuous Termination, ** D.T. - Discontinuous Termination,

A - Axial, B - Bending, AB - Deep section loaded under bending but stress at hot-spot pseudo-axial.

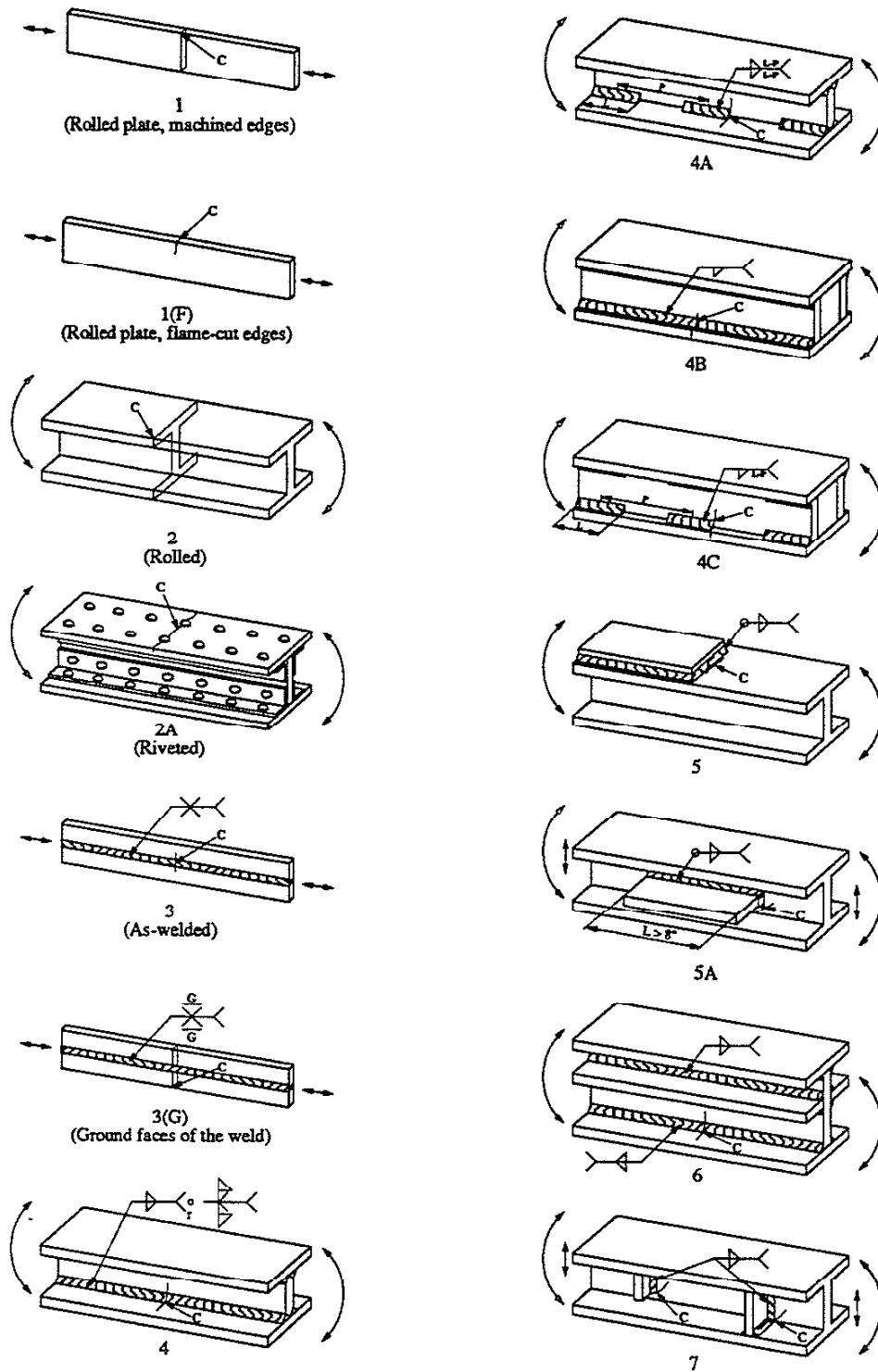


Fig. A1.1 The structural details contained in the UIUC database.

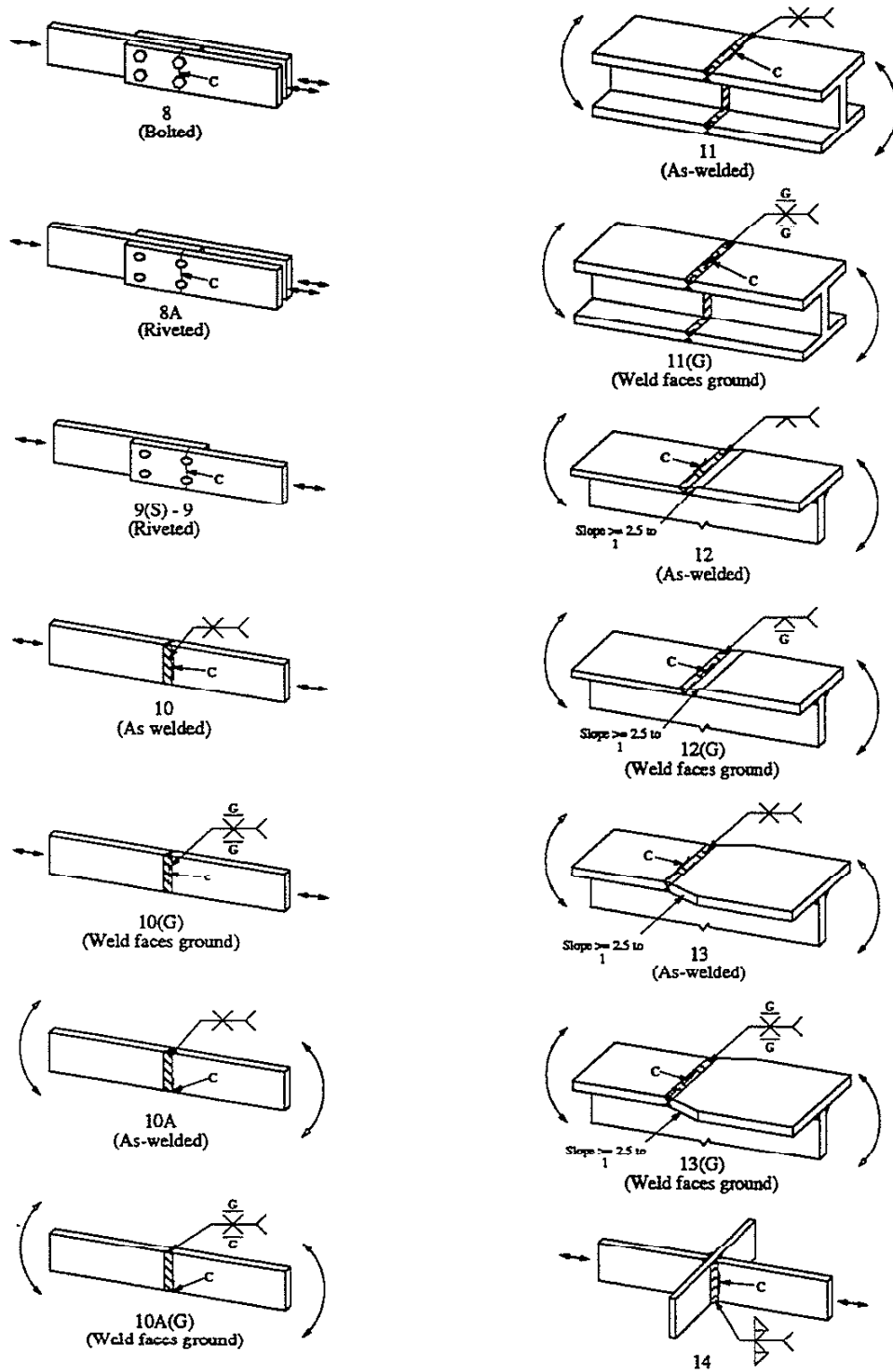


Fig. A1.1 (cont.) The structural details contained in the UIUC database.

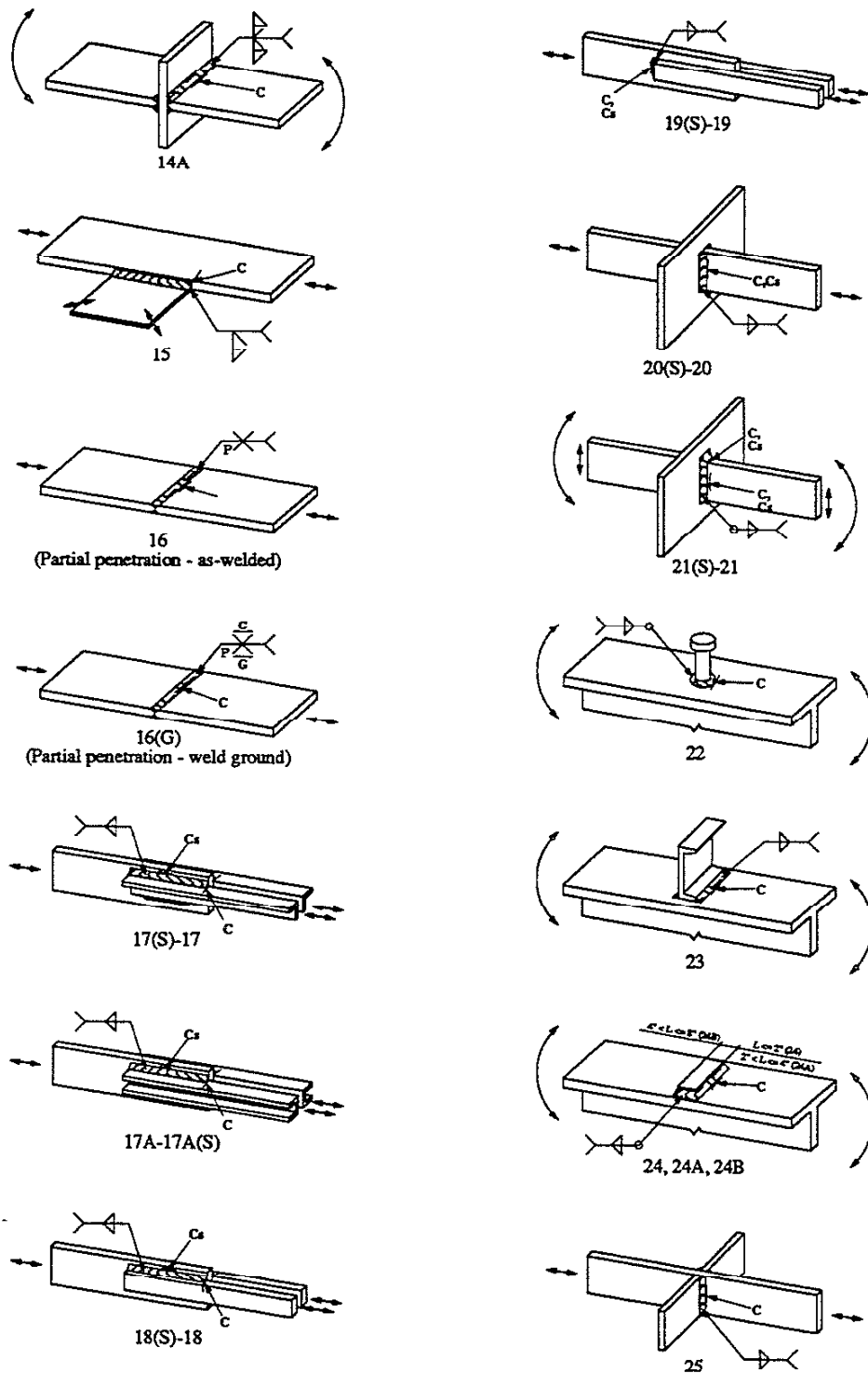


Fig. A1.1 (cont.) The structural details contained in the UTUC database.

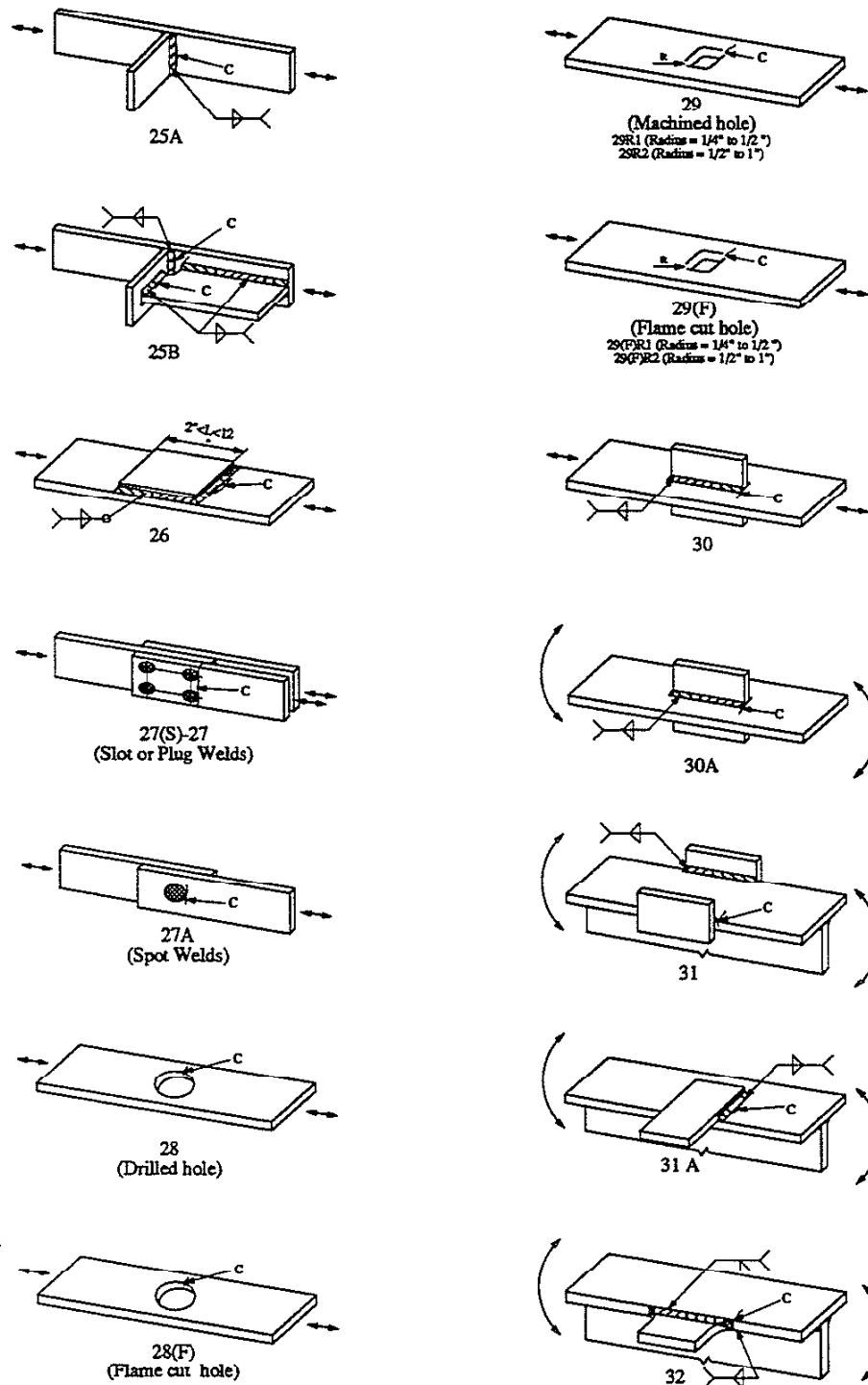


Fig. A1.1 (cont.) The structural details contained in the UIUC database.

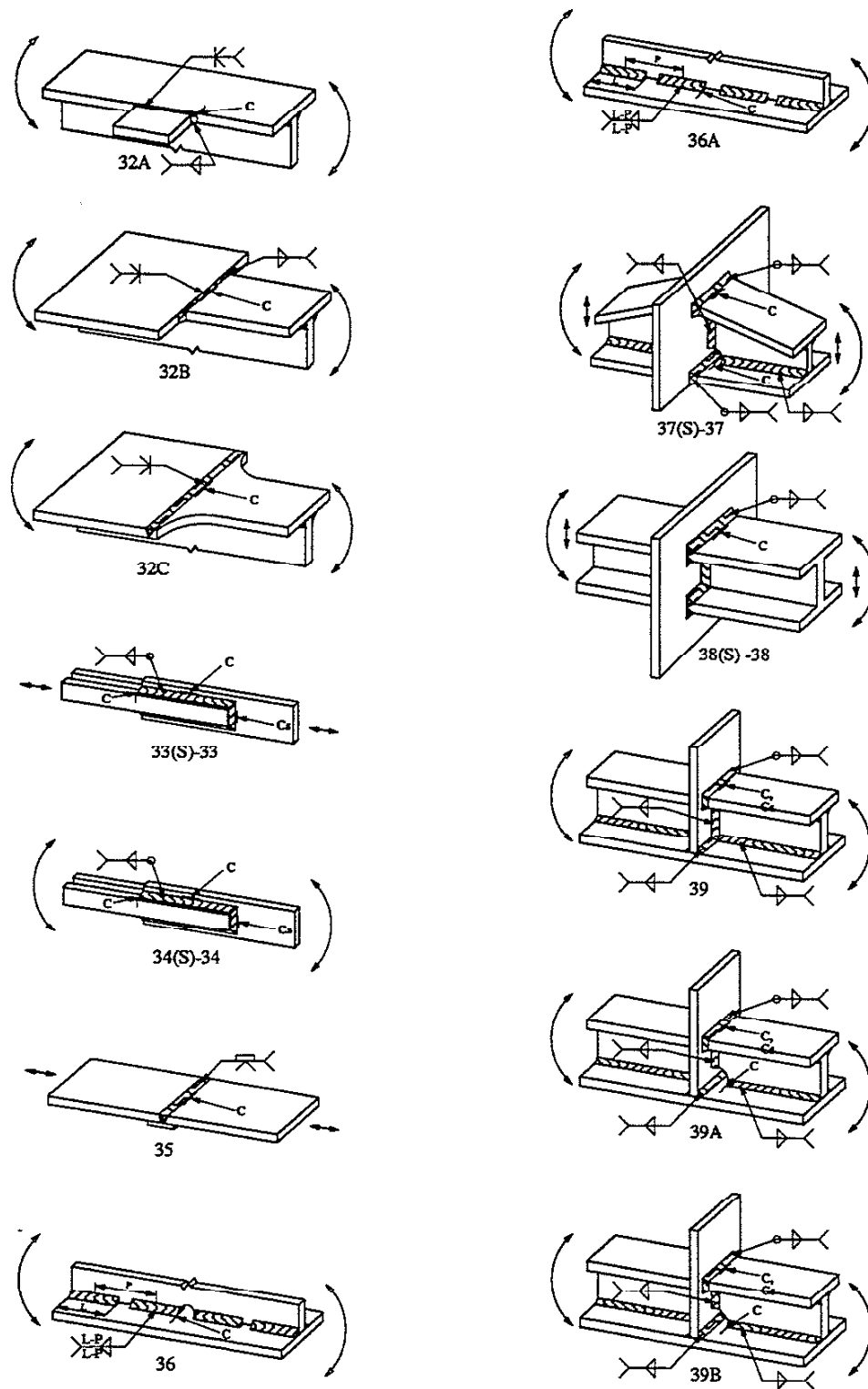


Fig. A1.1 (cont.) The structural details contained in the UIUC database.

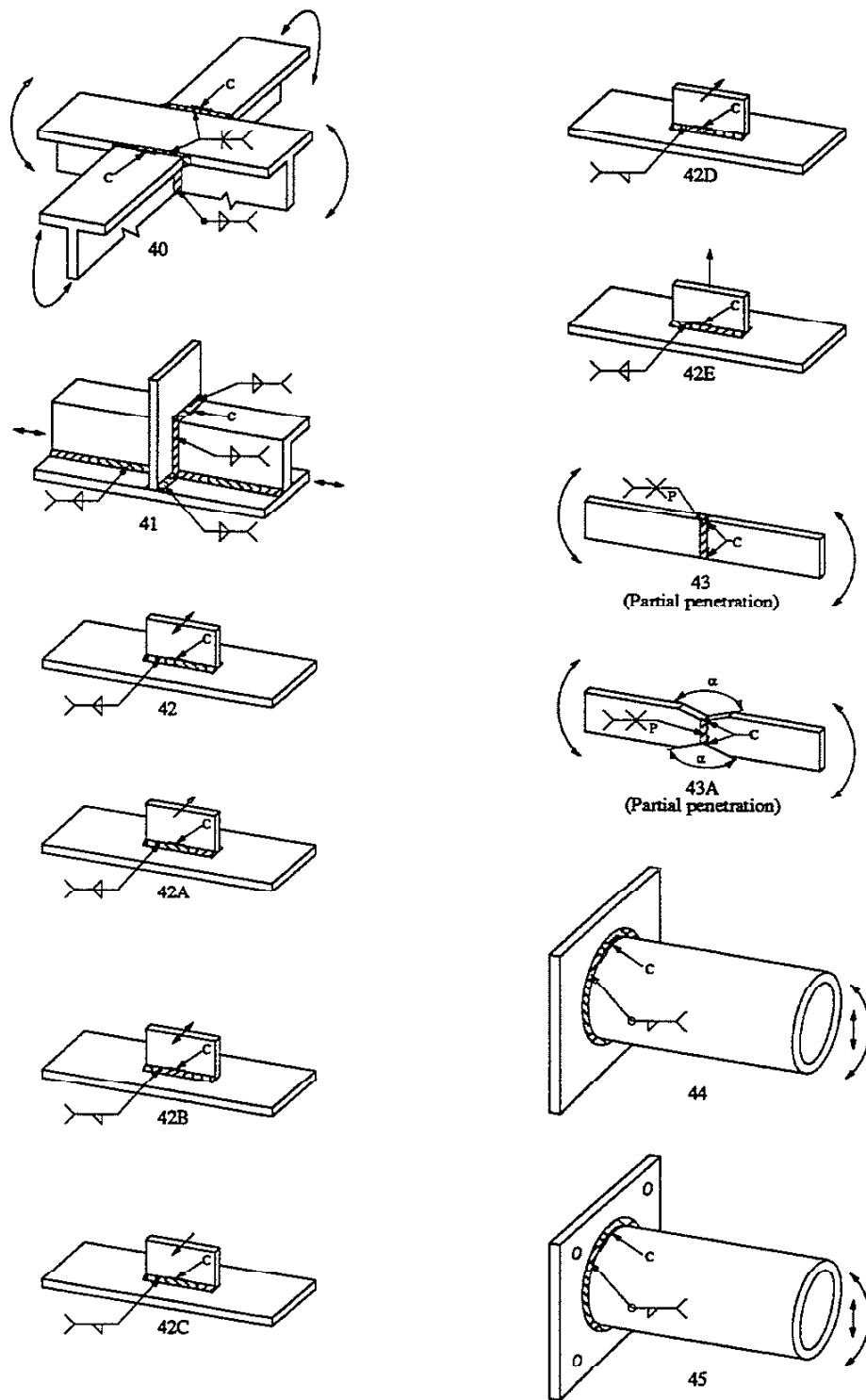


Fig. A1.1 (cont.) The structural details contained in the UTUC database.

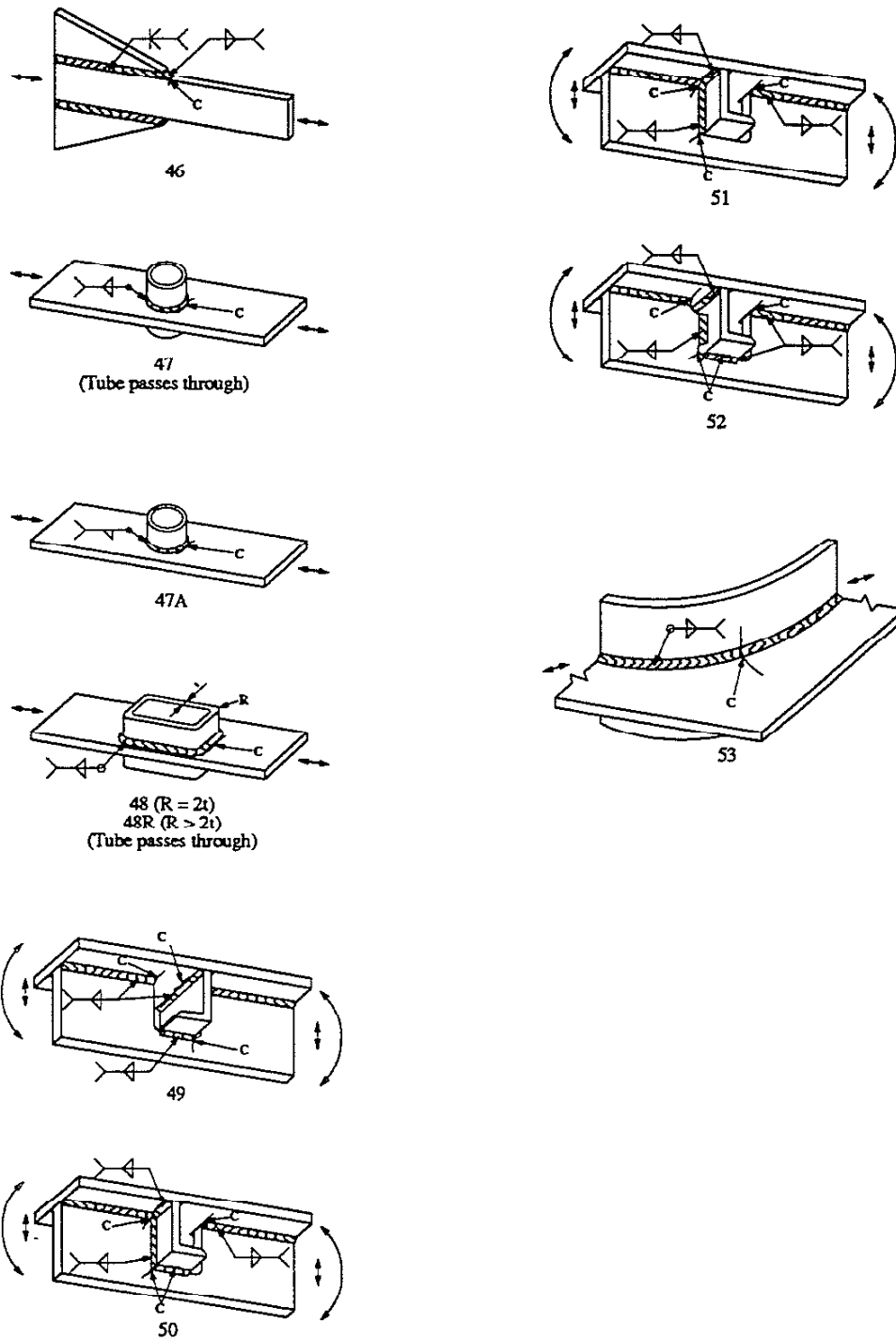


Fig. A1.1 (cont.) The structural details contained in the UIUC database.

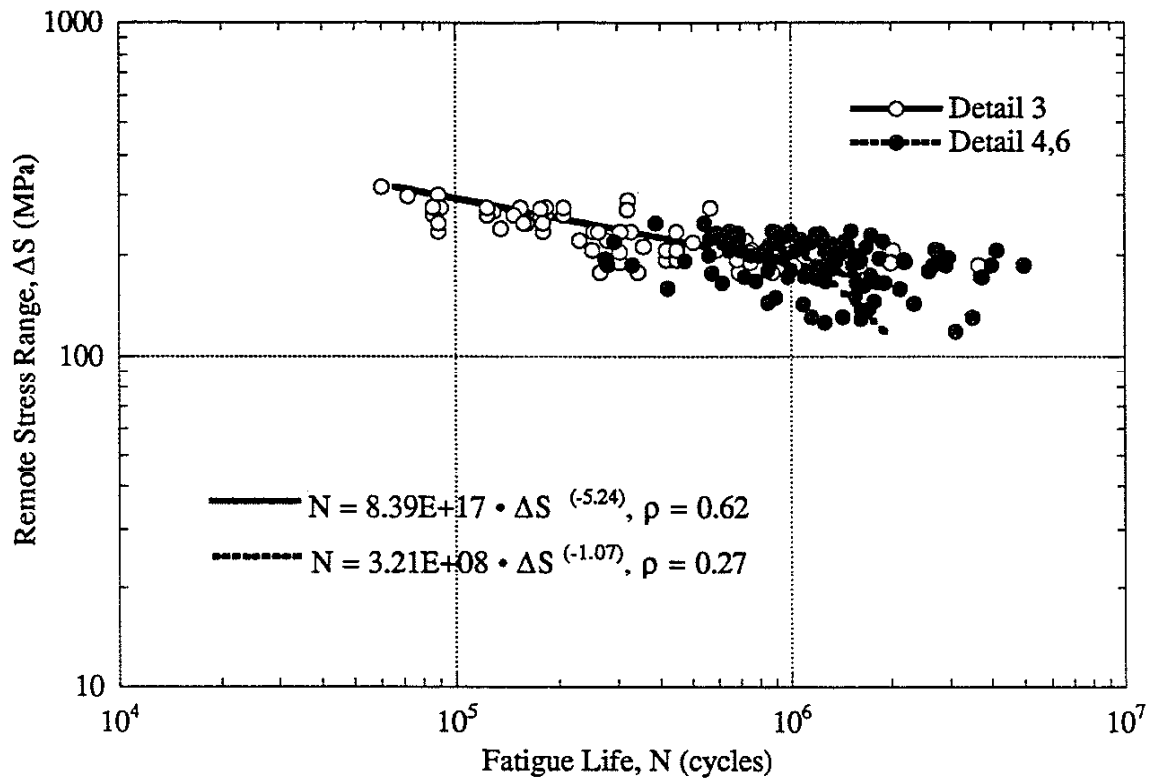


Fig. A1.2a S-N data for weld details with sites of fatigue crack initiation at a weld ripple - R

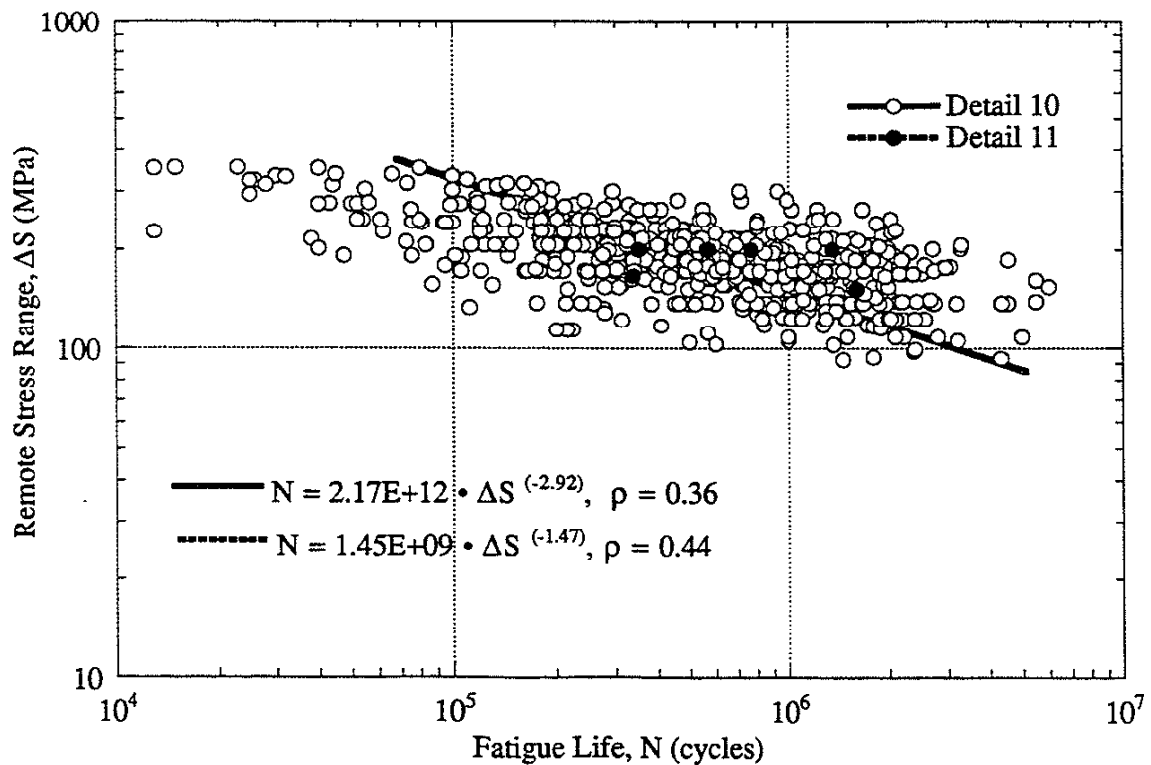


Fig. A1.2b S-N data for weld details with sites of fatigue crack initiation at toes of transversely loaded groove welds- G.

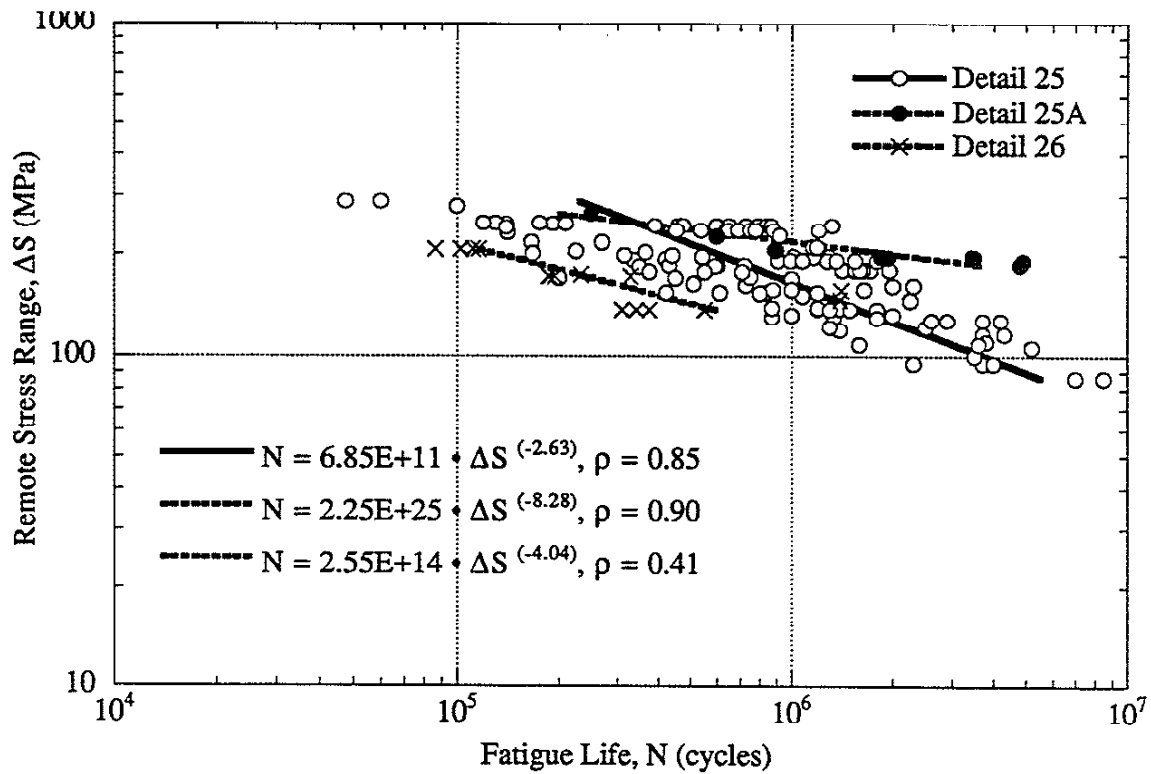


Fig. A1.2c S-N data for weld details with sites of fatigue crack initiation at toes of transversely loaded fillet welds- F.

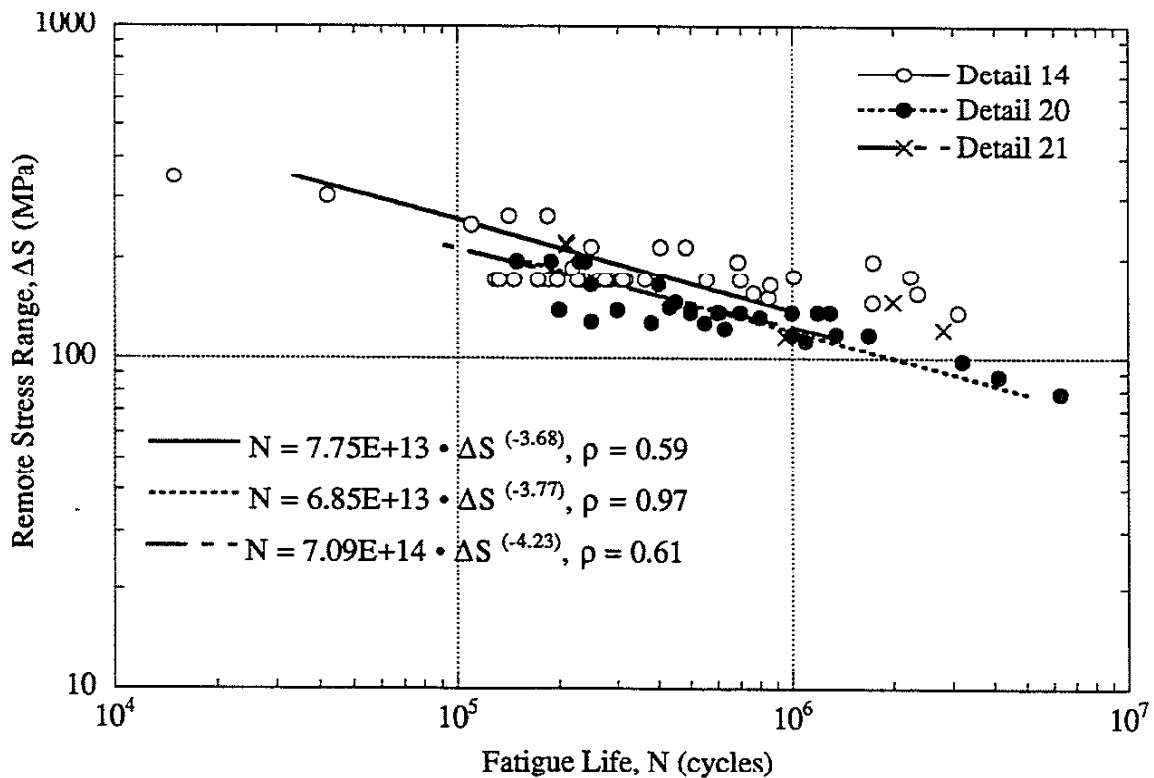


Fig. A1.2d S-N data for weld details with sites of fatigue crack initiation at toes of transversely loaded load-carrying fillet welds- F.

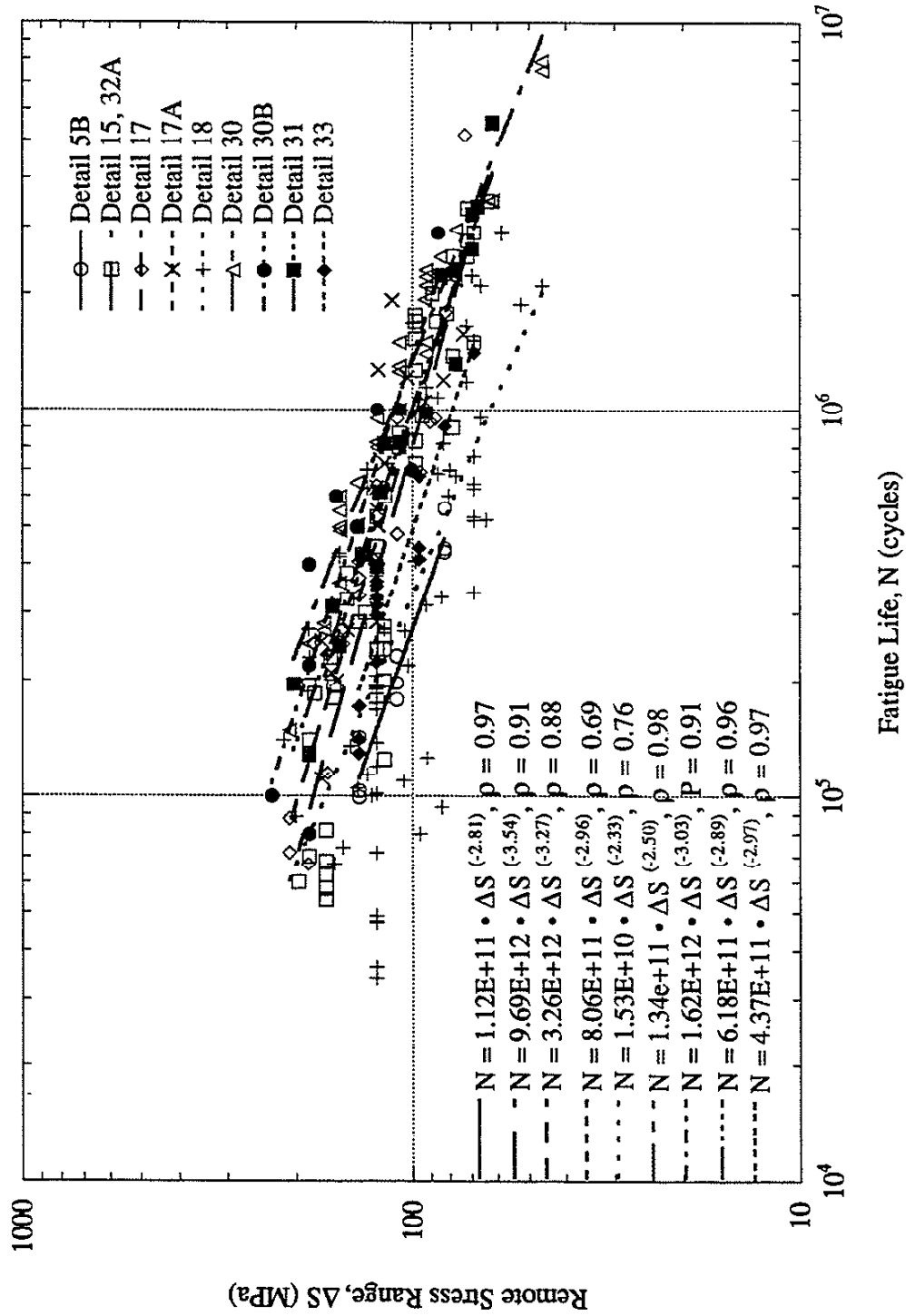


Fig. A1.2e S-N data for weld details with sites of fatigue crack initiation at fillet weld terminations- T.

APPENDIX 2: STRESS INTENSITY FACTOR FOR WELDMENTS

A2.1 WELD GEOMETRY CORRECTION FACTOR (M_K)

Solutions for the stress intensity factor of standard specimens are readily available. Unfortunately, solutions are not readily available for weldments. A problem arises in dealing with the nonuniformity of the stress field at the structural detail. In order to account for the presence of the weld geometry, the stress intensity factor for a plain plate with no weld is modified by the weld geometry correction factor (M_K) as follows:

$$K_{\text{weld}} = M_K Y S \sqrt{\pi a}.$$

where:

- K_{weld} = Stress intensity factor for the weldment
- M_K = Weld geometry correction factor
- Y = Geometry correction factor
- S = Applied remote stress
- a = Crack length

A2.2 THE SUPERPOSITION METHOD

Albrecht et al. [25] developed a simple superposition method which allows for the rapid calculation of stress intensity factors. Hobbacher [26] simplified their formula yielding:

$$K = \sqrt{\pi a} \frac{2}{\pi} \int_0^a \frac{S(y)}{\sqrt{(a^2 - y^2)}} dy$$

and therefore,

$$M_K = \frac{2}{\pi} \int_0^a \frac{K_t(y)}{\sqrt{(a^2 - y^2)}} dy$$

In order to calculate M_K , the stress concentration factor $K_t(y)$ along the anticipated crack path needs to be determined. The determination of $K_t(y)$ is usually found using FEM analysis. The advantage of using the superposition method is that only one mesh of the uncracked geometry

is needed instead of several FEM analyses requiring crack tip remeshing for each crack length. The stress intensity for the plain plate (K_{pp}) is commonly calculated using the results of Newman and Raju [31] for semi-elliptical surface cracks.

The stresses along the anticipated crack path should be used in the superposition method. The crack path is expected to start from the weld toe location since pre-existent defects are assumed to be present there. Albrecht et al. [25] used the stresses perpendicular to the vertical path down from the weld toe in the determination of M_{Ks} . Using these stresses is very simple and allows for the efficient calculation of M_{Ks} . Unfortunately, the crack path is not straight but curved and grows perpendicular to the direction of maximum principal stress. Therefore, Smith et al. [23] modified the calculation of M_{Ks} by using the maximum principal stresses on the vertical path inward from the weld toe. Smith et al. [23] justified this practice by noting that they found no significant difference between the maximum principal stresses at probable crack tip locations and those locations on the vertical path.

Other researchers [33, 34] have evaluated M_K from another location. They found that the location of maximum stress in the weld toe region does not occur at the weld toe but up the weld toe radius a small distance. Therefore, cracks will initiate and propagate from this "peak" location where the maximum principal stress in the entire weld toe region is highest. Determining M_K from the peak location is contradictory to the concept that the fatigue life of weldments consists of only the propagation of pre-existent defects found at the weld toe. Pre-existent defects may be eliminated by the use of post-weld improvement techniques or by just simply better welding procedures.

APPENDIX 3: VERIFICATION OF THE SUPERPOSITION METHOD

As mentioned in Chapter 1, M_K has usually been evaluated along a crack path perpendicular to the applied load and inward from the weld toe (vertical path from the weld toe in this study), and the calculation of K_{weld} ($M_{Ks} \cdot K_{pp}$) has been based on the readily available solutions for stress intensity factor for surface cracks in plain plate (K_{pp}) determined for straight cracks which are perpendicular (vertical) to the applied load. However, the crack paths for the specimens tested were observed to be curved and not straight; therefore, M_K should be evaluated along this curved path. However, the accuracy of determining M_K along such curved crack paths using the superposition method and using the model for K_{pp} based on cracks perpendicular to the applied load should be questioned.

A pilot study was first undertaken in which the longitudinal attachment was modeled in 2 dimensions (2-D) to verify the use of the superposition method as it has been traditionally used along the vertical path. Then, a pilot study was undertaken in which the longitudinal attachment was modeled in 2-D to determine the crack path emanating from the weld toe and to determine the best method of estimating M_K with the superposition method for this crack path.

A3.1 VERTICAL CRACK PATH

A pilot study was undertaken modeling the longitudinal attachment in 2-D to verify the accuracy of the superposition method in estimating the weld geometry correction factor (M_K) for cracks along the vertical path. The dimensions and loading conditions used in the 2-D FEM analysis can be seen in Fig. A3.1. A 2-D FEM analysis of the uncracked geometry was conducted, and the stresses perpendicular to the vertical path inward from the weld toe were used in the superposition method to determine M_{Ks} ; see Fig. A3.2 and Table A3.1.

In order to determine the stress intensity factor for the weld modeling the cracked geometry ($K_{weld CG}$), crack tip elements¹ were inserted in the 2-D FEM models. A typical mesh of the 2-D FEM model with a crack can be seen in Fig A3.3. The weld geometry correction factor for the cracked geometry ($M_{K CG}$) was then determined by normalizing $K_{weld CG}$ with the stress intensity factor of the plain plate (K_{pp}): see Fig. A3.1.2 and Table A3.1.1. K_{pp} was determined using the solutions of Newman and Raju [31] for semi-elliptical surface cracks.

¹ The crack tip elements were created in Pro/MECHANICA STRUCTURE. The first row of elements were modeled to be 1/20th of the crack length in size.

As can be seen from Table A3.1, M_{Ks} and M_{KCG} are similar with a maximum difference of 11% at a/T values of around 0.02 - 0.05. M_{Ks} slightly overestimates M_{KCG} and is therefore conservative. Only as the crack length approaches the mid-thickness of the plate is it unconservative, but at those crack lengths the fatigue life is almost over. Fatigue crack propagation lives (N_p) were calculated using the weld geometry correction factors determined for the crack geometry and from the superposition method for different initial crack lengths: see Fig. A3.2. The differences in the N_p were found to be insignificant at both of the initial crack lengths investigated.

These differences between M_{Ks} and M_{KCG} are larger than those found by Smith [45] who found a maximum difference of 6% at a/T values of around 0.20 - 0.25. Smith modeled a transverse non-load-carrying fillet welded attachment (transverse attachment) without the lack of penetration (LOP). The transverse attachment is not exactly the geometry studied here but in 2-D the details are similar. Since the LOP was modeled in the analysis performed above, the longitudinal attachment was re-evaluated without the LOP to see if the differences between M_{Ks} and M_{KCG} would decrease. The 2-D results without the LOP are plotted in Fig. A3.4 and listed in Table A3.2. A maximum difference of approximately 6% was found and the observed differences between M_{Ks} and M_{KCG} are in better agreement with the results of Smith. Once again, the differences in the resulting fatigue crack propagation lives were found to be insignificant: see Fig. A3.1.4.

A3.2 SUPERPOSITION METHOD FOR CURVED CRACK PATHS

The accuracy of determining M_K along curved crack paths using the superposition method and using the model for K_{pp} based on cracks perpendicular to the applied load should be questioned. A pilot study was undertaken in which the longitudinal attachment was modeled in 2 dimensions (2-D) (1) to determine the crack paths emanating from the weld toe and peak stress locations and (2) to determine the best method of estimating M_K with the superposition method for these crack paths. The curved crack path will first be evaluated from cracks emanating from the location of "peak" stress location and then from the weld toe.

A3.2.1 "Peak" Stress Location

The first step was to determine the peak location from which the crack will initiate and then propagate. The 2-D FEM analysis revealed the peak location to be at a small distance around the weld toe radius and inclined at 22.5° to the vertical: see Fig. A3.5. The

crack path² was determined with the cracked geometry propagation technique [R] in which actual cracks were inserted in the 2-D FEM analyses to determine the crack path. This technique involved the following steps:

- (1) perform an FEM analysis on the uncracked geometry to determine the location of maximum principal stress in the weld toe region,
- (2) determine the direction of crack extension,
- (3) propagate the crack a small distance and remesh the model for the new geometry,
- (4) recalculate K_I and K_{II} for the new geometry, and repeat steps 2-4.

This procedure was repeated until the mid-thickness of the plate was reached. For the uncracked geometry (initiation for this technique), the direction of crack extension (ϕ) was determined by:

$$\tan(2\phi) = \frac{2 * S_{xy}}{(S_{xx} - S_{yy})}$$

For the cracked geometry the maximum circumferential stress criterion proposed by Sih [32] was used to determine ϕ .

$$K_I \sin\phi + K_{II}(3 \cos\phi - 1) = 0$$

The resulting curved crack path generated from the cracked geometry can be seen in Fig. A3.5.

The weld geometry correction factor for the cracked geometry ($M_{K_{CG}}$) was then determined by normalizing $K_{weld CG}$ along the curved crack path with the stress intensity factor of the plain plate (K_{pp}): Fig. A3.6. In addition, $M_{K_{CG}}$ was determined along the "slanted path" (crack path perpendicular to the maximum principal stress direction at the peak location) and plotted in Fig. A3.6. It can be seen from Fig. A3.1.6 that there is no difference in $M_{K_{CG}}$ whether it is determined along the curved or slanted path.

The weld geometry correction factor was then calculated using the superposition method (M_{K_S}) by first projecting the maximum principal stresses determined from the

² Another technique termed the uncracked geometry propagation technique in which a fictitious crack is assumed to initiate at the peak location and follow the path perpendicular to the maximum principal stresses in the uncracked geometry. The resulting curved crack path determined using the uncracked geometry propagation technique was similar to that found using the cracked geometry propagation technique. Any differences between the two different techniques were insignificant.

uncracked geometry along the curved and slanted crack paths³ to an equivalent vertical crack path prior to performing calculations according to Thurlbeck et al. [34]: see Fig. A3.7. No difference in M_{K_S} is seen whether it is calculated along the curved or slanted path. Since the results are similar along the curved and slanted paths and in order to simplify the comparisons, it was decided to continue the analysis with only the results on the slanted path.

M_{K_S} and $M_{K_{CG}}$ determined along the slanted path were then compared in Fig. A3.8. It can be seen that the superposition method slightly overestimates M_K but does an overall good job in estimating $M_{K_{CG}}$. Therefore, the superposition method should be used to calculate M_K by first projecting the stresses to an equivalent vertical crack path. In addition, all calculations from the peak location can be performed along the well defined slanted path, since no difference was seen between M_K determined along the curved or slanted paths.

A3.2.2 Weld Toe

The first step was to determine the crack path from the toe location. The crack path was determined using the techniques described in the previous section. The resulting curved crack path emanating from the weld toe can be seen in Fig. A3.5.

The weld geometry correction factor for the cracked geometry ($M_{K_{CG}}$) was then determined by normalizing $K_{weld\ CG}$ along the curved crack path with the stress intensity factor of the plain plate (K_{pp}): Fig. A3.9. In addition, $M_{K_{CG}}$ was determined along the vertical path inward from the toe and plotted in Fig. A3.9. It can be seen that $M_{K_{CG}}$ is slightly greater along the curved path and should be considered.

The weld geometry correction factor was then calculated using the superposition method (M_{K_S}) by first projecting the maximum principal stresses determined from the uncracked geometry along the curved path to an equivalent vertical path prior to performing calculations: see Fig. A3.10. M_{K_S} was then calculated using the perpendicular stresses and maximum principal stresses along the vertical path: see Fig. A3.10. Using the maximum principal stresses along the vertical path approximates the use of the maximum principal stresses along the curved path very well and in agreement with the assumption of Smith et al. [R] for a/T values less than 0.1. The use of the maximum principal stresses as opposed to the use of the perpendicular stresses gives M_{K_S} with slightly larger values.

The solutions for M_{K_S} obtained above were then compared with $M_{K_{CG}}$ in Fig. A3.11. It can be seen that all of the solutions of the superposition method do a good job in

³ Using the maximum principal stresses along the slanted path is technically incorrect but will allow for an easily defined crack path from which the stresses can be read. The maximum principal stresses found along the slanted path are similar to the maximum principal stresses found along the curved path.

estimating M_k . The use of the well-defined vertical path allows for the most convenient determination of stresses using FEM, and the use of the maximum principal stresses is preferred by the writer. Therefore, it was decided that all further calculations using the superposition method in this study from the toe location will be performed using the maximum principal stresses along the vertical path inward from the toe.

Table A3.1 Comparison of the calculated and modeled stress intensity factors for the vertical crack path determined by a 2-D FEM analysis with an LOP.

a (mm)	a/T	M_{Ks}	M_{KCG}	% difference in M_K
0.0254	0.002	2.20	2.06	6.8
0.0635	0.005	2.14	1.99	7.5
0.254	0.02	1.92	1.73	11.0
0.635	0.05	1.62	1.46	11.0
2.54	0.2	1.14	1.14	0.0
6.35	0.5	0.94	0.95	-1.1

Table A3.2 Comparison of the calculated and modeled stress intensity factors for the vertical crack path determined by 2-D FEM analysis without an LOP.

a (mm)	a/T	M_{Ks}	M_{KCG}	% difference in M_K
0.0254	0.002	2.05	2.02	1.5
0.0635	0.005	1.99	1.95	2.1
0.254	0.02	1.79	1.69	5.9
0.635	0.05	1.52	1.43	6.3
2.54	0.2	1.11	1.10	1.0
6.35	0.5	0.95	0.94	1.1

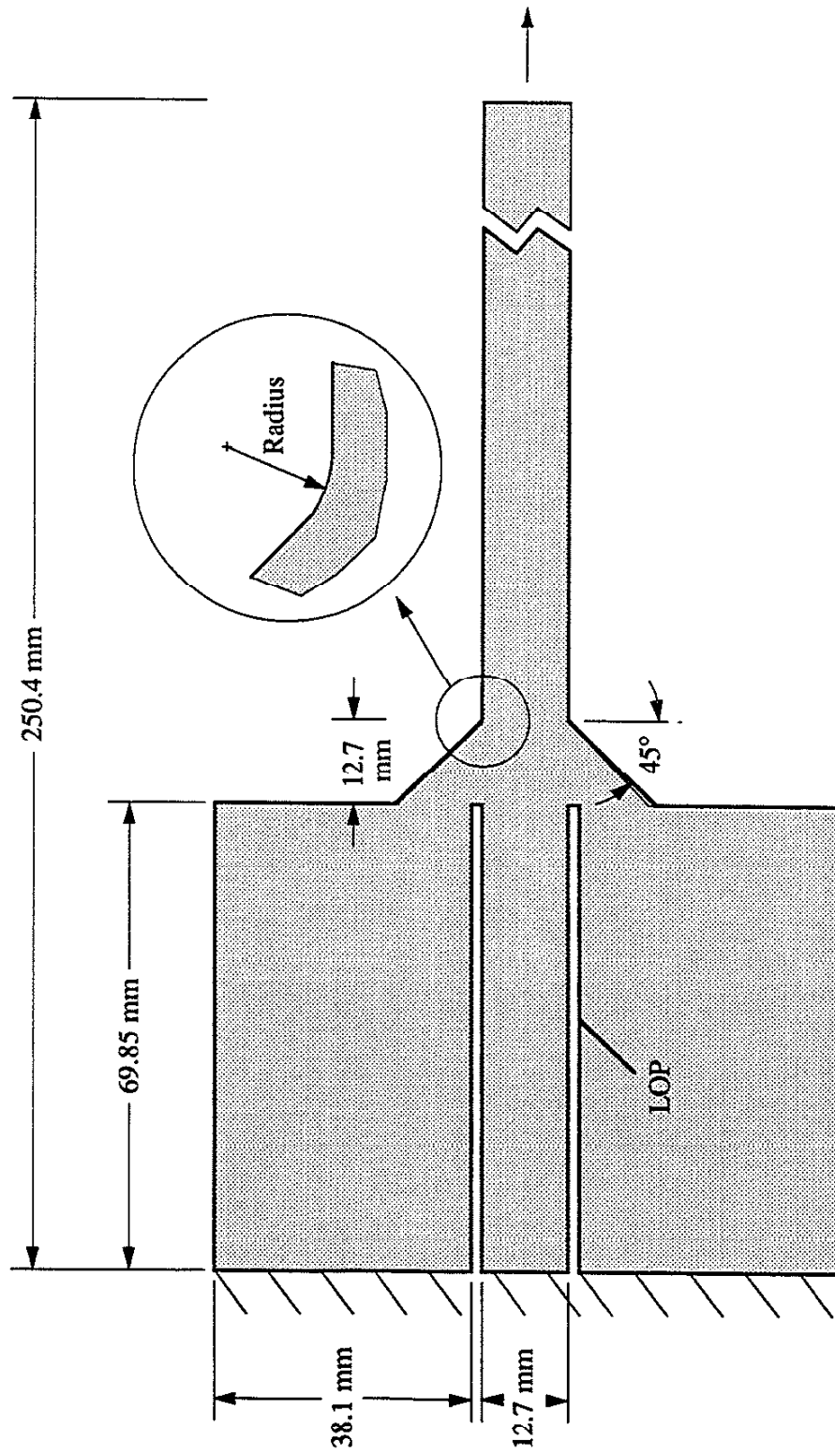
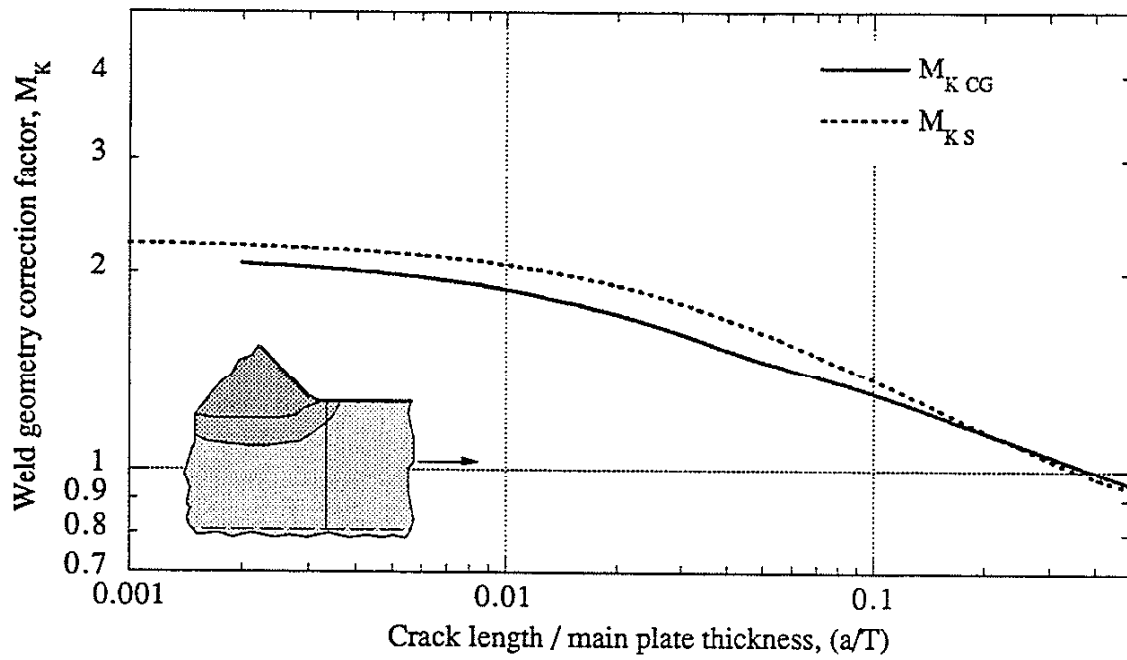
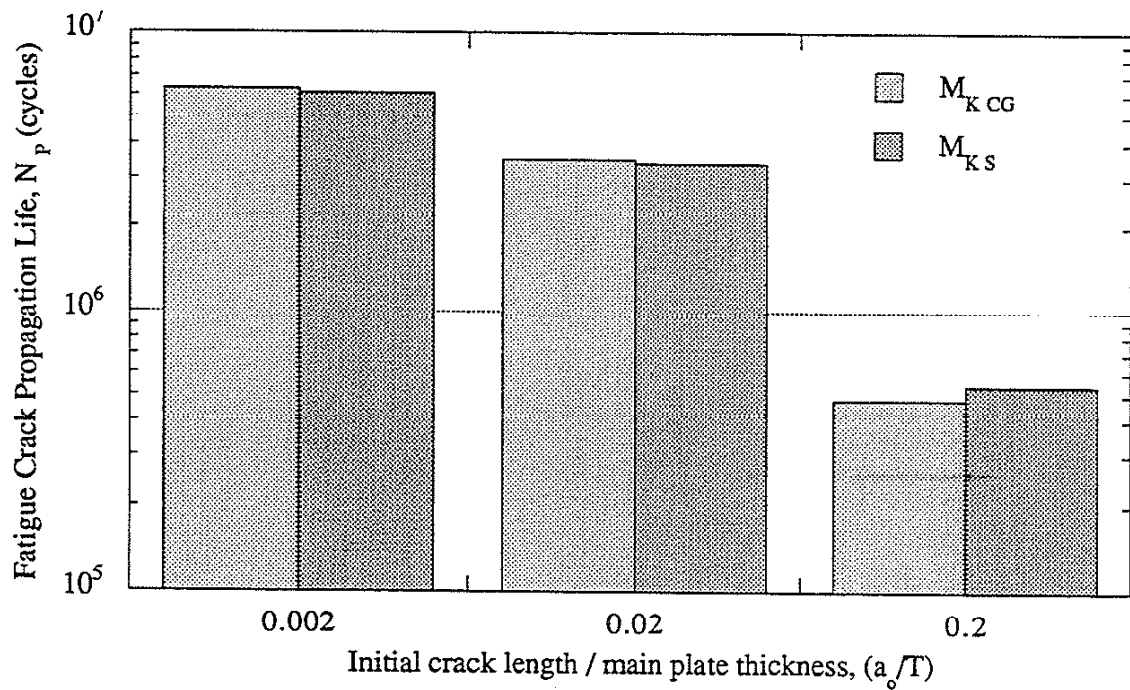


Fig. A3.1 The dimensions and loading conditions used in the 2-D FEM analyses.



(a)



(b)

Fig. A3.2 The accuracy of the superposition method in estimating (a) the weld geometry correction factor and (b) the fatigue crack propagation lives of longitudinal attachments. ($\Delta S = 100$ MPa)

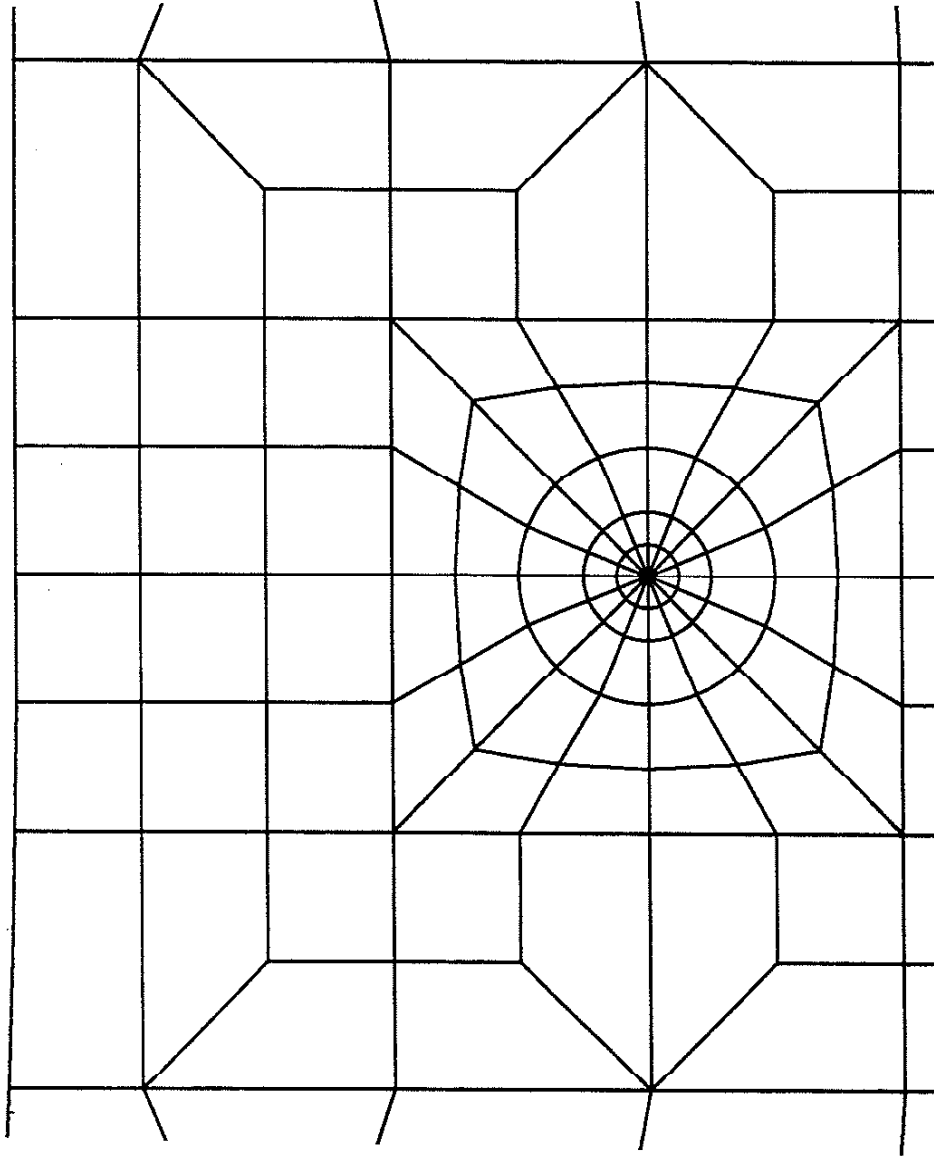
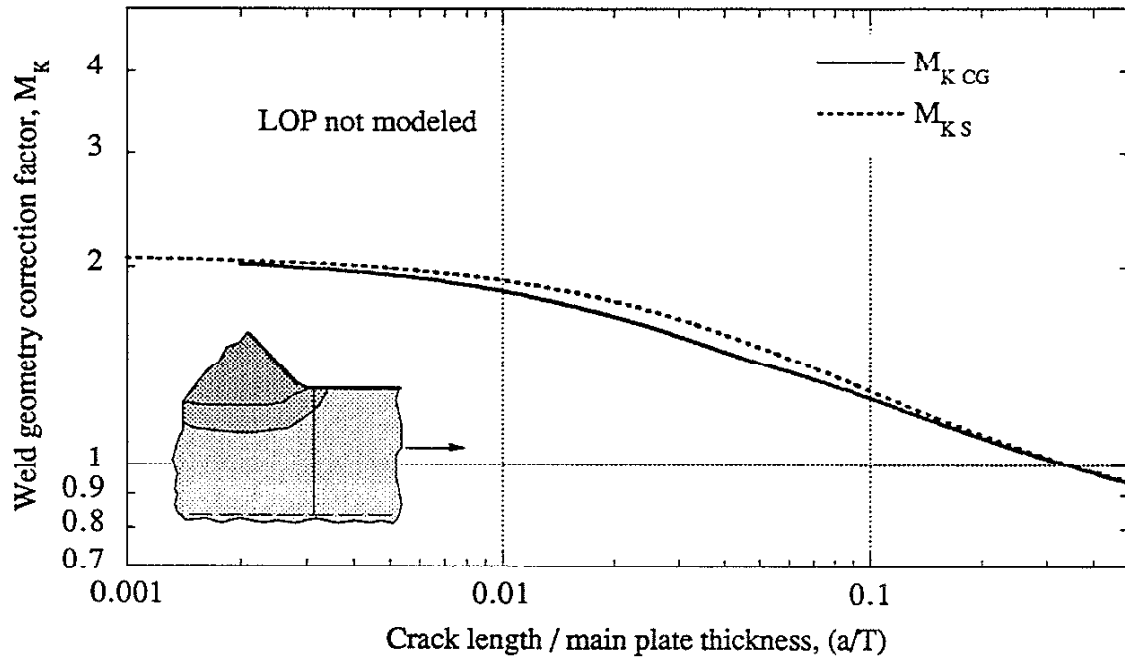
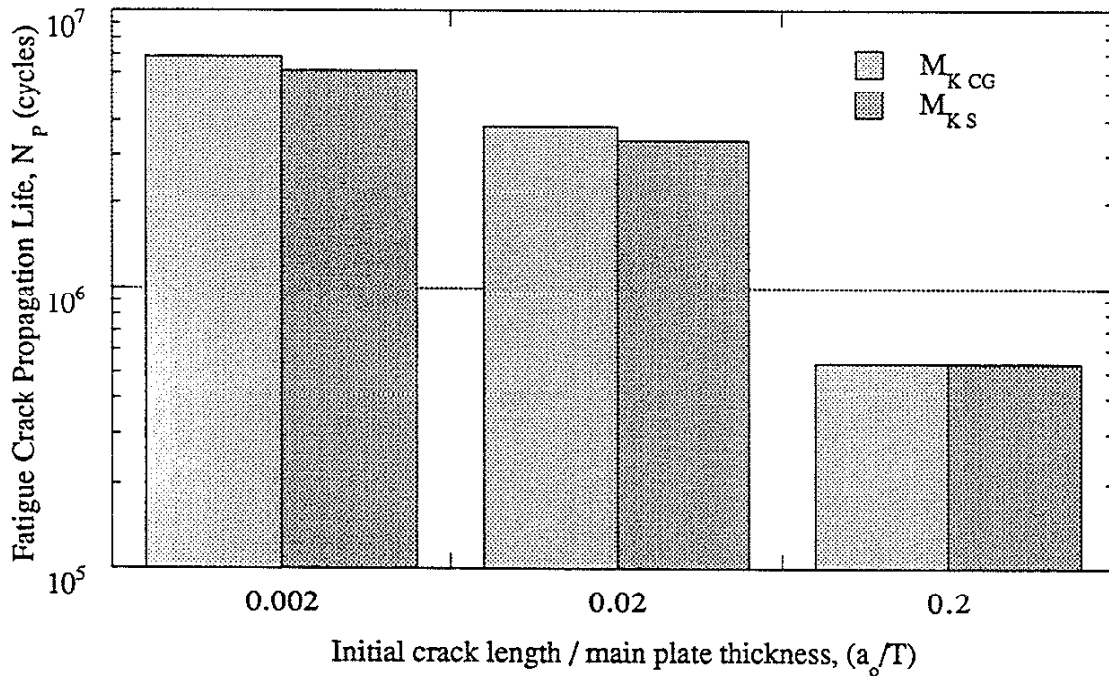


Fig. A3.3 Typical mesh of a crack using 2-D FEM analysis.



(a)



(b)

Fig. A3.4 The accuracy of the superposition method in estimating (a) the weld geometry correction factor and (b) the fatigue crack propagation lives of longitudinal attachments modeld without an LOP. ($\Delta S = 100$ MPa)

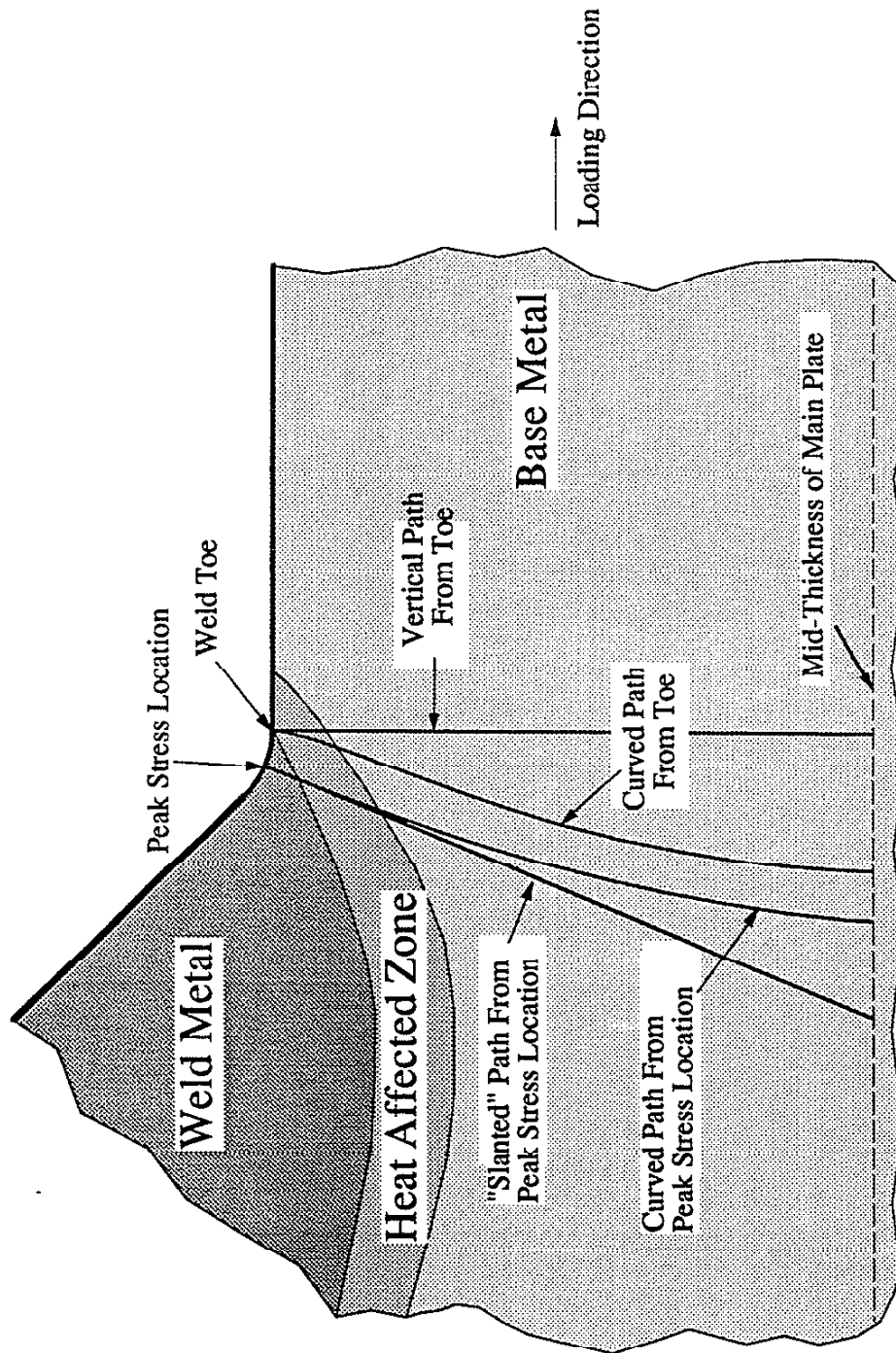


Fig. A3.5 The fatigue crack growth paths determined for a longitudinal attachment with 2-D FEM analyses.

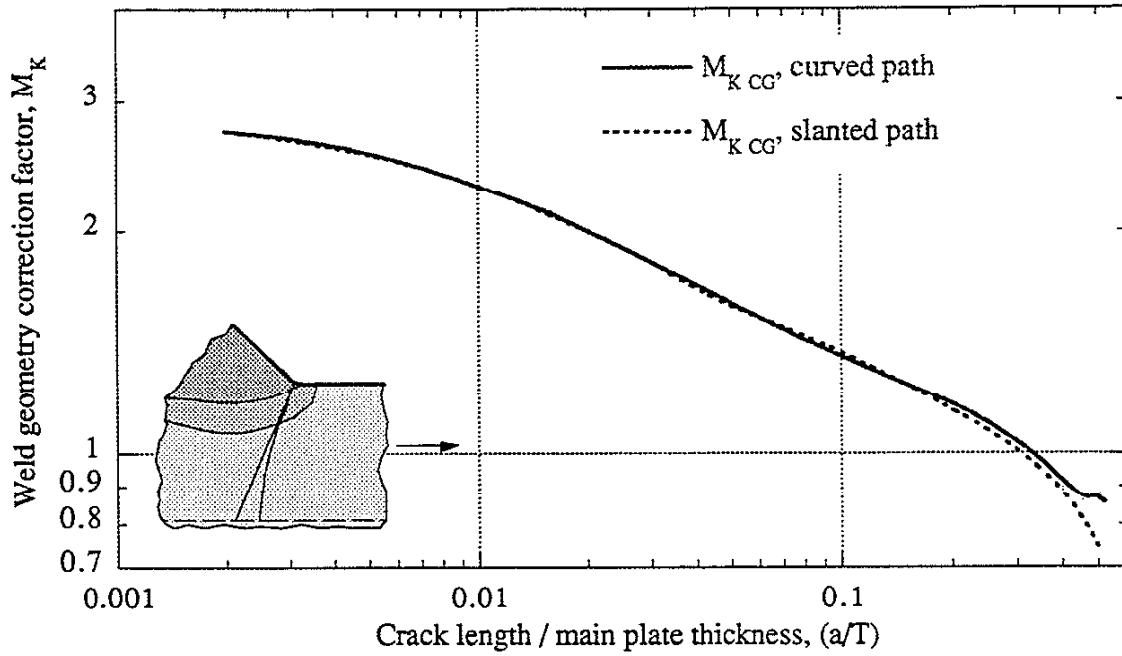


Fig. A3.6 The weld geometry correction factor determined from the cracked geometry along the curved and slanted paths emanating from the peak location.

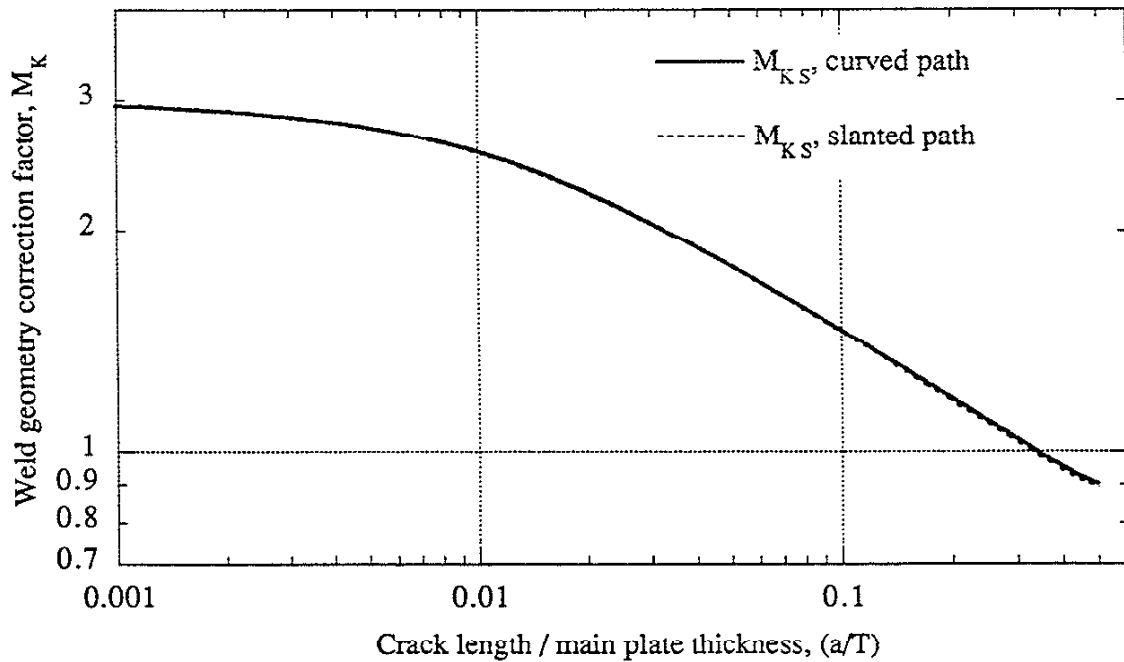
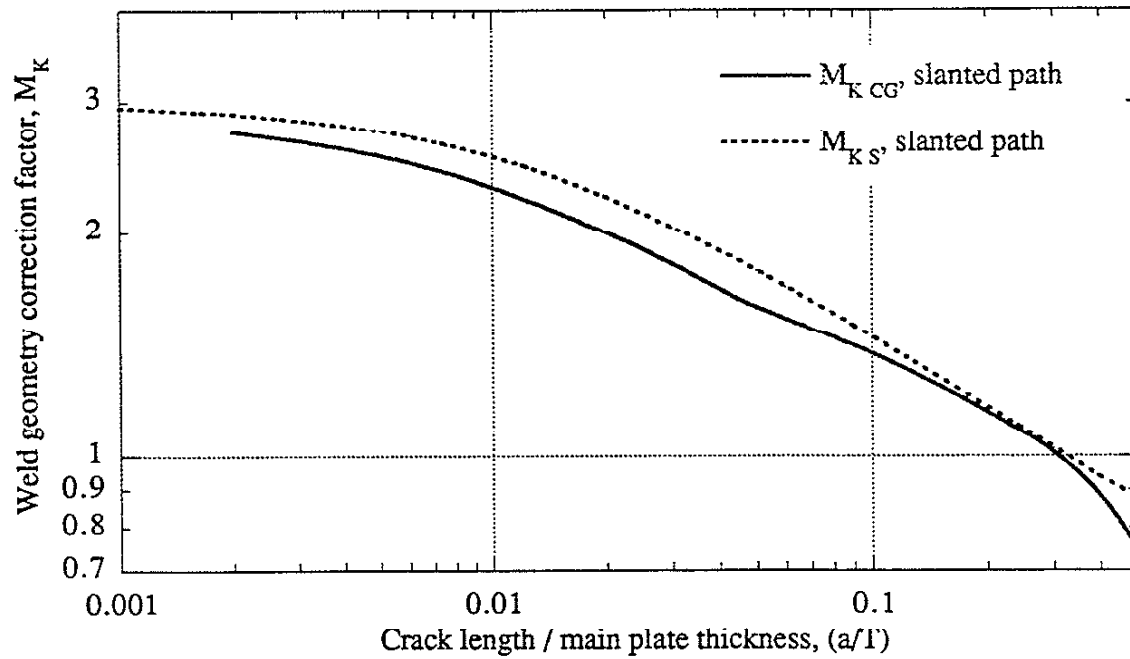
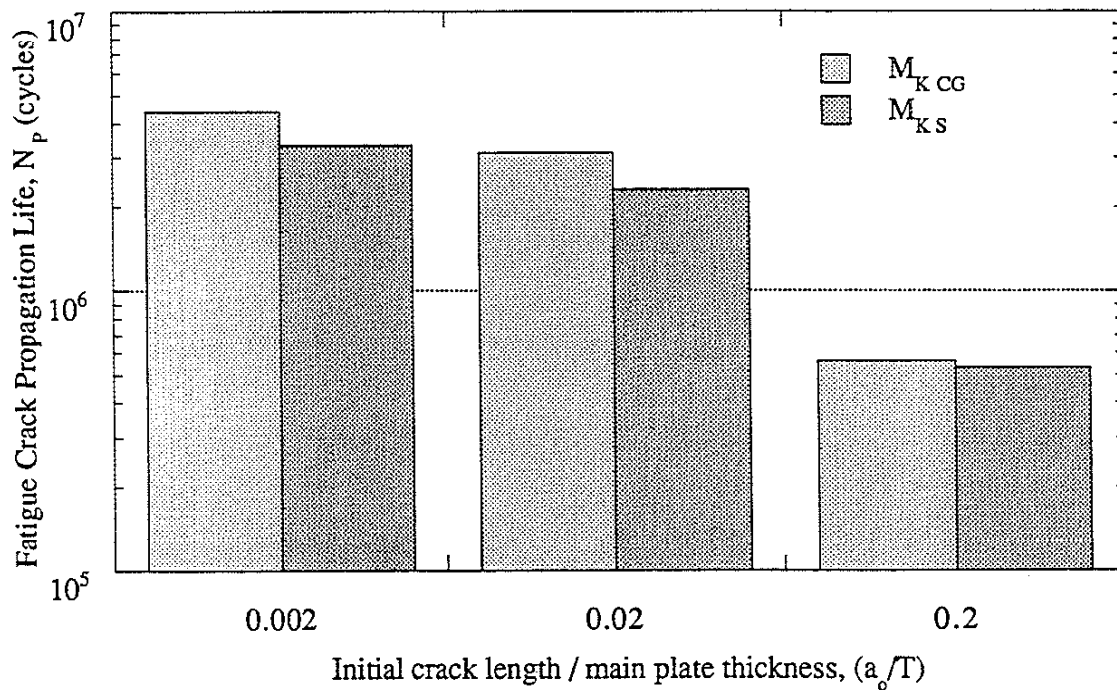


Fig. A3.7 The weld geometry correction factor calculated using the superposition method by projecting the maximum principal stresses along the curved and slanted paths to an equivalent vertical path.



(a)



(b)

Fig. A3.8 The accuracy of the superposition method in estimating (a) the weld geometry correction factor and (b) the fatigue crack propagation lives of longitudinal attachments along the slanted path. ($\Delta S = 100$ MPa)

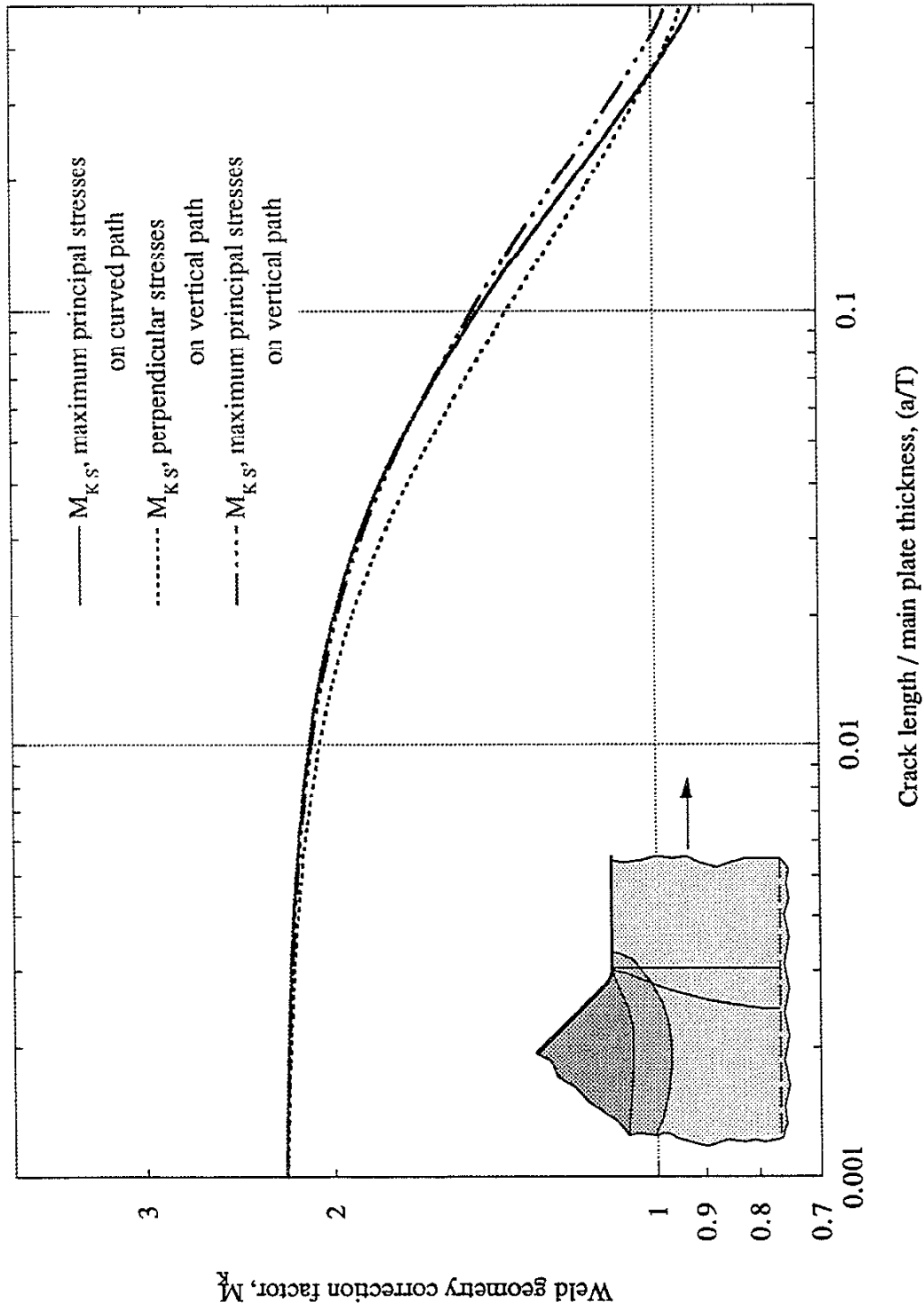
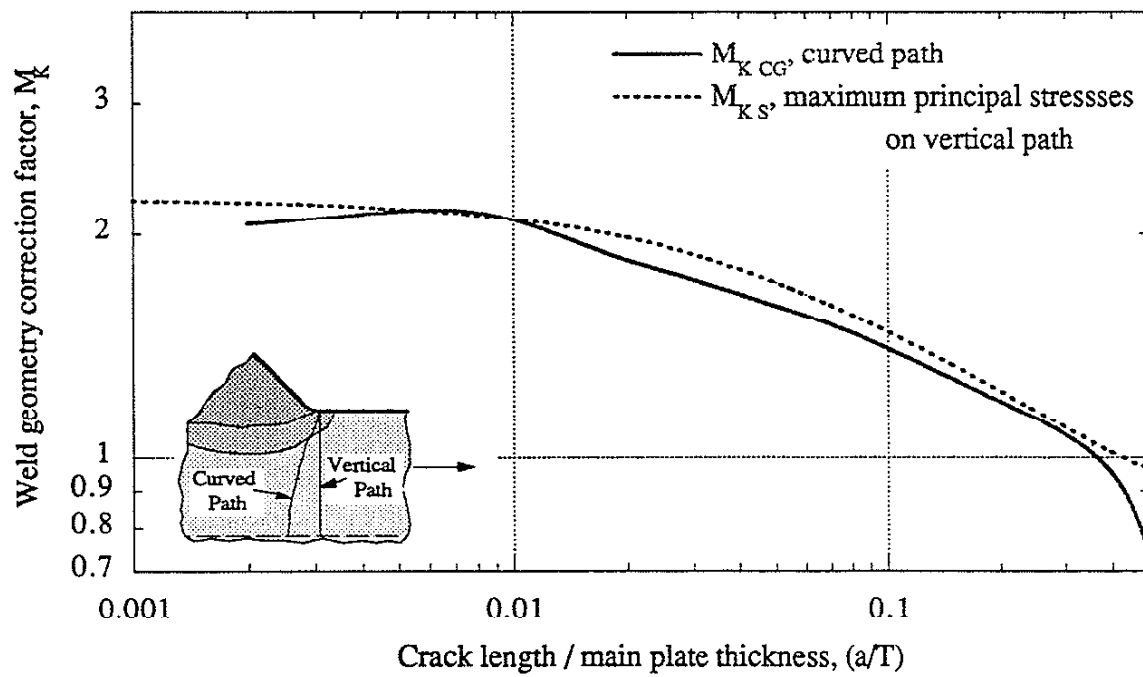
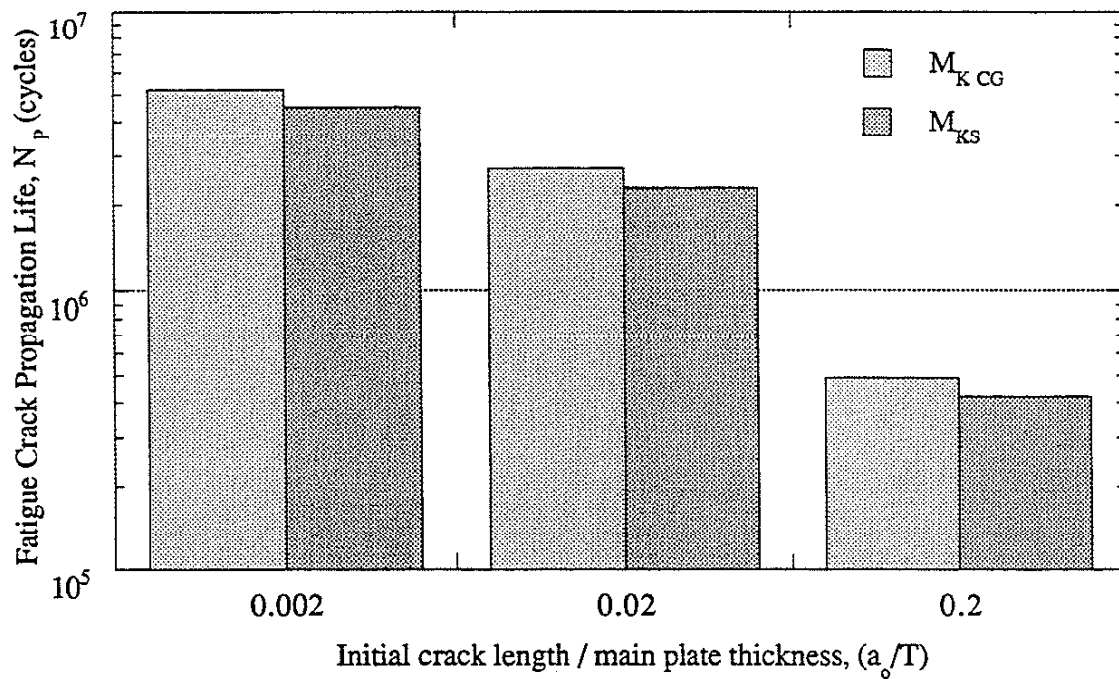


Fig. A3.9 The weld geometry correction factor calculated using the superposition method for cracks emanating from the weld toe location.



(a)



(b)

Fig. A3.10 The accuracy of the superposition method in estimating (a) the weld geometry correction factor and (b) the fatigue crack propagation lives of longitudinal attachments along the curved path from the weld toe. ($\Delta S = 100$ MPa)

APPENDIX 4: EVALUATION OF THE SUPERPOSITION METHOD IN ESTIMATING M_K FOR GEOMETRIES WITH COLD-LAP DEFECTS

The crack path emanating from a cold-lap defect is not straight but curved and grows perpendicular to the direction of maximum principal stress; therefore, M_K should be evaluated along this curved path. However, the accuracy of determining M_K along such curved crack paths using the superposition method and using the model for K_{pp} based on cracks perpendicular to the applied load should be questioned. A pilot study was undertaken in which the longitudinal attachment was modeled in 2 dimensions (2-D) to determine the crack path emanating from the root of the cold lap and to determine the best method of estimating $M_{K\ CG}$ with the superposition method for this crack path.

The weld geometry correction factor for the cracked geometry ($M_{K\ CG}$) was determined along the curved crack path by normalizing $K_{weld\ CG}$ by K_{pp} : see Fig. A4.1. In addition, $M_{K\ CG}$ was determined along the vertical path and plotted in Fig. A4.1. It can be seen that $M_{K\ CG}$ is similar whether it is determined along the curved or vertical crack path.

$M_{K\ s}$ was calculated using the maximum principal stresses along the curved crack path (Fig. 7.2) and plotted with $M_{K\ CG}$ in Fig. A4.2. There is good agreement between $M_{K\ s}$ and $M_{K\ CG}$. Then, the perpendicular stresses along the vertical path were used to calculate $M_{K\ s}$ and compared with $M_{K\ CG}$ in Fig. A4.2. This method estimates $M_{K\ CG}$ well for long crack lengths, but for very short crack lengths use of the perpendicular stresses along the vertical path underestimates $M_{K\ CG}$. Finally, $M_{K\ s}$ was calculated using the maximum principal stresses along the easily defined vertical crack path and plotted with $M_{K\ CG}$ in Fig. A4.2. Use of the maximum principal stresses along the vertical path in the superposition method tend to slightly overestimate M_K .

Regardless of the stresses used in the superposition method, $M_{K\ s}$ estimates $M_{K\ CG}$ for the weld detail well. The use of the well-defined vertical path allows for the most convenient determination of stresses using FEM, and the use of the maximum principal stresses is preferred by the author. Therefore, it was decided that all further calculations using the superposition method in this study from a cold-lap defect will be performed using the maximum principal stresses along the vertical path.

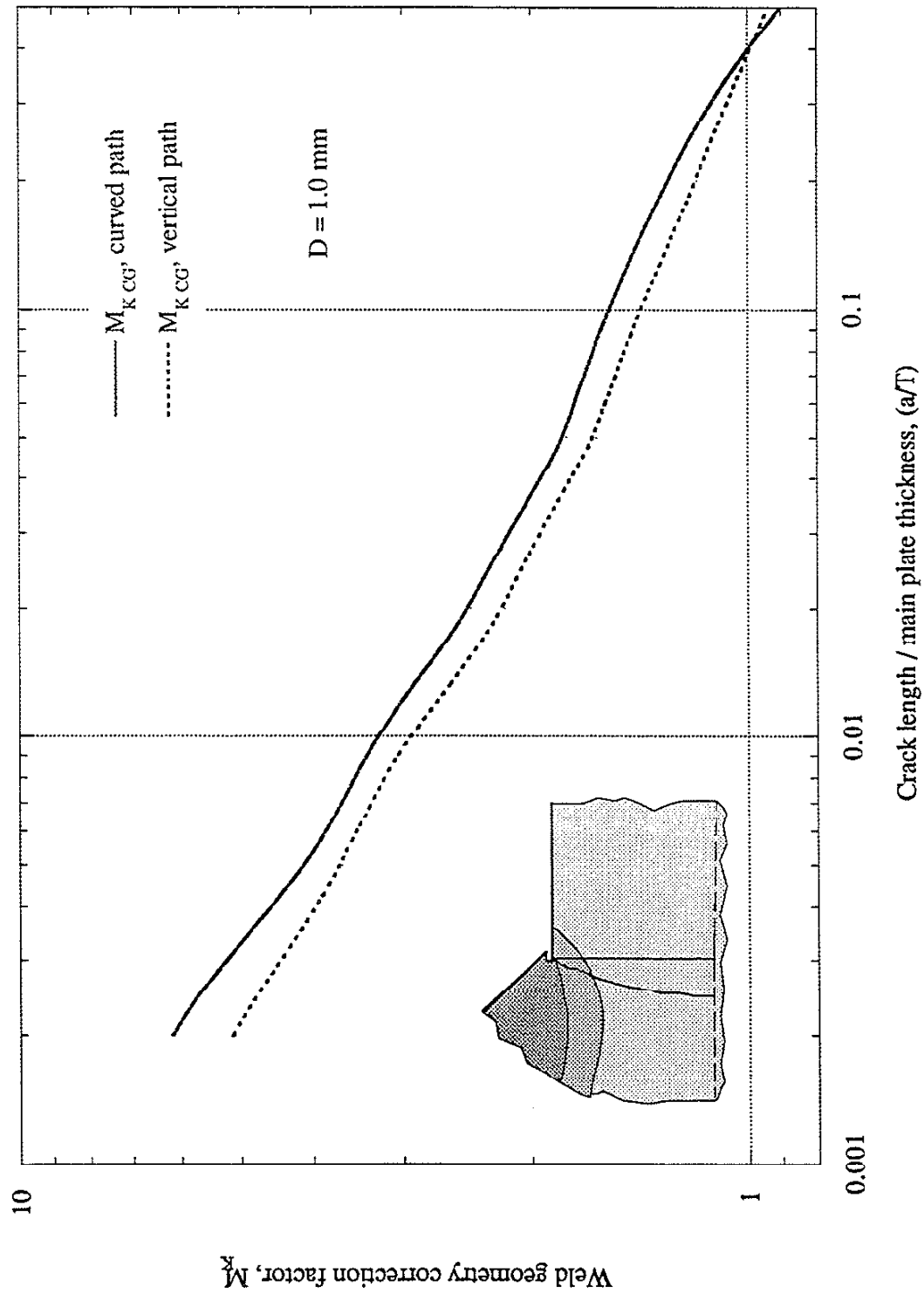


Fig. A4.1 Comparison of the weld geometry correction factors determined using cracked geometry along the vertical and curved crack paths .

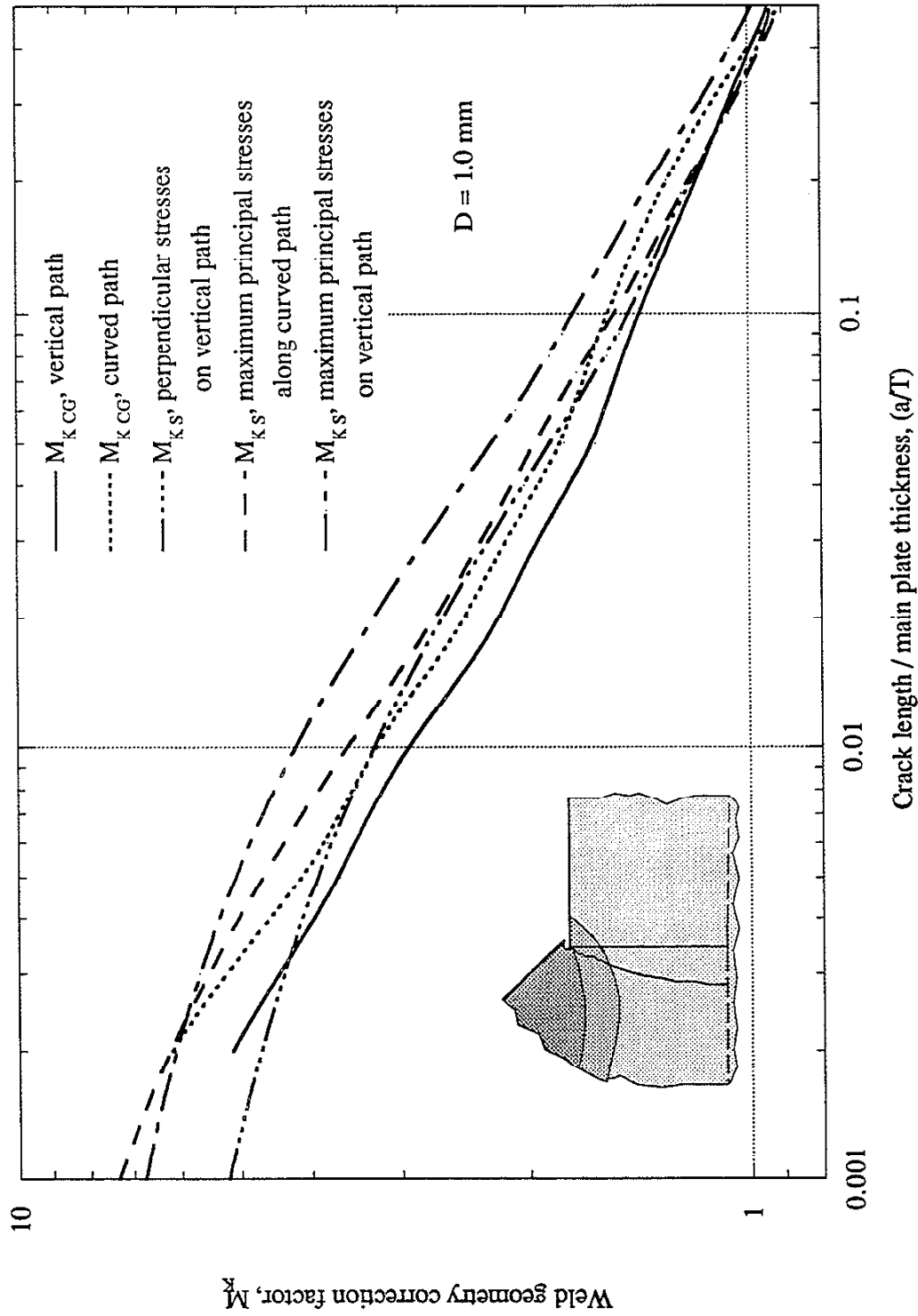


Fig. A4.2 The accuracy of the superposition method in estimating the weld geometry correction factor for cracks growing from a cold-lap defect.

REFERENCES

1. Munse, W. H., Wilbur, T. W., Telalian, M. L., Nicol, K., and Wilson, K., "Fatigue Characterization of Fabricated Ship Details for Design," Ship Structure Committee Report SSC-318, Washington D.C, 1983.
2. Gurney, T. R., "Fatigue of Welded Structures," The Welding Institute, Cambridge University Press, Cambridge, 1979.
3. Gurney, T. R., "The Influence of Residual Stresses on the Fatigue Strength of Plates with Fillet Welded Attachments," British Welding Association Research Report No. D8/3/59, 1959. (British Welding Journal, vol. 7, no. 6, 1960, pp. 415-431).
4. Gurney, T. R., and Trepka, L. N., "The Influence of Local Heating on Fatigue Behaviour of Welded Specimens," British Welding Association Research Report, 1959, pp. 468-497. (British Welding Journal, vol. 6, no. 10, 1959, pp. 491-497).
5. Gurney, T. R., "Fatigue Strength of Fillet Welded Joints in Steel," British Welding Journal, 1960, pp. 178-187.
6. Gurney, T. R., "Fatigue Tests on Butt and Fillet Welded Joints in Mild and High Tensile Structural Steels," British Welding Research Association Report No. D7/6/60, 1962. (British Welding Journal, vol. 9, no. 11, 1962, pp. 614-620).
7. Gurney, T. R., "Further Fatigue Tests on Mild Steel Specimens with Artificially Induced Residual Stresses," British Welding Journal, vol. 9, no. 11, 1962, pp. 609-613.
8. Gurney, T. R., "Some Fatigue Tests on Fillet Welded Mild and High Tensile Steel Specimens in the As-Welded and Normalised Conditions," British Welding Journal, 1966, pp. 648-651.
9. Harrison, J. D., "Further Fatigue Tests on Fillet Welded Specimens Subjected to Prior Overloading," BWRA Report D8/13/63, 1965.
10. Harrison, J. D., "Further Techniques For Improving the Fatigue Strength of Welded Joints," BWRA Report E/3/65, 1966.
11. Booth, G. S., and Maddox, S. J., "Influence of Various Factors on the Fatigue Strength of Steel Plates with Fillet-Welded Attachments," The Welding Institute, Abington Hall, Abington, Cambridge, 1979.
12. Maddox, S. J., "Some Aspects of the Influence of Residual Stresses on the Fatigue Behaviour of Fillet Welded Joints in Steel," The Welding Institute, Abington Hall, Abington, Cambridge, 1980.
13. Maddox, S. J., "Fatigue of Stress-Relieved Fillet Welds Under Part-Compressive Loading," The Welding Institute, 1982.
14. Knight, J. W., "Some Basic Fatigue Data For Various Types of Fillet Welded Joints in Structural Steel," Welding Research International, Volume 9, Number 3, 1979.

15. Smith, I.F.C., Muster, W. J., and Bremmen, U., "Residual Stresses and Fatigue Strength Improvement of Welded Connections," Effects of Fabrication Related Stresses, Paper 19, 1985, pp. 300-315.
16. Lieurade, H. P., "Effect of Residual Stresses and the Stress Ratio on the Fatigue Strength of Welded Components," Welding in the World, Vol. 26, No. 7/8, 1988, pp. 158-187.
17. Bogren, J., and Martinez, L. L., "Spectrum Fatigue Testing and Residual Stress Measurements on Non-Load-Carrying Fillet Welded Test Specimens," Proceedings of a Conference on Fatigue Under Spectrum Loading And in Corrosive Environments, Editor A. F. Blom, Technical University of Denmark, EMAS, ISBN 0 947817 05 0, 1993, pp. 77-90.
18. Smith, I. F. C., and Hirt, M. A., "Methods of Improving the Fatigue Strength of Welded Joints," Publication ICOM 114, ICOM - Construction Metallique, 1983.
19. Berge, S., and Eide, O. I., "Residual Stress and Stress Interaction in Fatigue Testing of Welded Joints," Residual Stress Effects in Fatigue, ASTM STP 776, American Society for Testing and Materials, 1981, pp. 115-131.
20. Satoh, K., Transactions of the Japan Welding Society, Vol. 3, No. 1, April 1972, pp. 135-142.
21. Smith, I. F. C., and Smith, R. A., "Defects and Crack Shape Development in Fillet Welded Joints," Fatigue of Engineering Materials and Structures, Vol. 5, No. 2, 1982, pp. 151-165.
22. Martinez, L. L., and Korsgen, P., "Characterization of Initial Defect Distribution and Weld Geometry in welded Fatigue Test Specimens," Proceedings of a Conference on Fatigue Under Spectrum Loading And in Corrosive Environments, Editor A. F. Blom, Technical University of Denmark, EMAS, ISBN 0 947817 05 0, 1993, pp. 3-21.
23. Smith, I. J., Smith, I. F. C., and Hurworth, S. J., "A 3-D Analysis of the Longitudinal Non-Load Carrying Fillet Welded Fatigue Specimen," The Welding Institute, Research Report, 1982.
24. Smith, I. F. C., and Gurney, T. R., "Changes in the Fatigue Life of Plates with Attachments Due to Geometrical Effects", AWS Welding Journal, Welding Research Supplement, 1986, pp. 244.s-249.s.
25. Albrecht, P., and Yamada, K., "Rapid Calculation of Stress Intensity Factors," Journal of the Structural Division Proc. ASCE 103 (2), 19, 1977, pp. 377-389.
26. Hobbacher, A., "Stress Intensity Factors of Welded Joints," Engineering Fracture Mechanics, Vol. 46, No. 2, 1993, pp. 173-182.
27. Dahle, T., and Larsson, B., "Fatigue Life Predictions of Longitudinal Non-Load-Carrying Fillet Welded Specimens Based on Current Flaw Distribution," Proceedings of a Conference on Fatigue Under Spectrum Loading And in Corrosive Environments, Editor A. F. Blom, Technical University of Denmark, EMAS, ISBN 0 947817 05 0, 1993. pp. 149-164.

28. Gray, T. G. F., and Spence, J., "Rational Welding Design," Second Edition, Butterworths & Co. Ltd., 1982.
29. Hornbach, D. J., "X-Ray Diffraction Determination of the Surface Residual Stresses in Three A36 Steel Welded Plates," Lambda Research.
30. Parametric Technology Corporation, "Pro/MECHANICA, Getting Started With Structure," Release 18.0, 1997.
31. Newman, J. C., Raju, S., "An Empirical Stress-Intensity Factor Equation For the Surface Crack," Engineering Fracture Mechanics, Vol. 15, No. 1-2, 1981, pp. 185-192.
32. Sih, G. C., "Strain-Energy-Density Factor Applied to Mixed-Mode Crack Problems," International Journal of Fracture, 10, 1974, pp. 305-320.
33. Lawrence, F. V., Ho, N. J., and Mazumdar, P. K., "Predicting Fatigue Resistance of Welds," Annual Review of Material Science, Vol. 11, 1981, pp. 402-425.
34. Thurlbeck, S. D., and Burdekin, F. M., "Effects of Geometry and Loading Variables on the Fatigue Design Curve of Tubular Joints," Welding in the World, Vol. 30, No. 7/8, 1992, pp. 189-200.
35. Chi, W-M, Deierlein, G. G., and Ingraffea, A. R., "Finite Element Fracture Mechanics Investigation of Welded Beam-Column Connections," SAC Joint Venture Task 5.3.1 of Phase II, Cornell University, 1997.
36. Fry, G. T., Texas A&M University, private communication, 1999.
37. American Welding Society, 1998, Structural Welding Code - Steels, ANSI/AWS D1.1-98.
38. Ho, N. J., and Lawrence, F. V., "Constant Amplitude and Variable Amplitude Load History Fatigue Test Results and Predictions for Cruciform and Lap Welds," Theoretical and Applied Fracture Mechanics 1, 1984, pp. 3-21.
39. Dimitrakis, S. D., Lawrence, F. V., "The Fatigue Resistance of Rim Weldments," Technical Report to Precision Inc., 1998.
40. Verreman, Y., and Nie, B., "Short Crack Fatigue Propagation at Fillet Welds," International Conference on Performance of Dynamically Loaded Welded Structures, IIW 50th Annual Assembly Conference, 1997.
41. Monahan, C. C., "Early Fatigue Crack Growth at Welds," Topics in Engineering, Volume 26, Computational Mechanics Publications, 1995.
42. Dimitrakis, S. D., and Lawrence, F. V., "Fatigue Design of Complex, Ship Structure Weldments", Report to the Consulting Naval Architects, University of Illinois at Urbana-Champaign, 1994.
43. Bell, R., and Vosikovsky, O., "Fatigue Life Prediction of Welded Joints for Offshore Structures Under Variable Amplitude Loading," OMAE, Volume III-B, Materials Engineering, 1991.

44. Otegui, J. L., Mohaupt, U. H., and Burns, D.J., "Effect of Weld Process on early Growth of Fatigue Cracks in Steel T Joints," *International Journal of Fatigue*, 1991, pp. 45-58.
45. Smith, I. J., 1980, "High Order Elements and Fatigue Crack Growth", *Proceedings of the 2nd International Conference on Numerical Methods in Fracture Mechanics*, pp. 583-598.

VITA

Stamati D. Dimitrakis was born on December, 18 1999 in Summit, New Jersey. He was raised in North Brunswick, New Jersey. He attended Lehigh University and received his bachelors degree in civil engineering in 1992. In the fall of 1992, he enrolled in the civil engineering program at the University of Illinois. He conducted research for the American Petroleum Institute on the S-N curves for tubular joints. He received his masters degree in 1994. He continued his research on the fatigue of weldments and completed his doctoral degree in 1999.